AN ABSTRACT OF THE DISSERTATION OF

Michael Austin Garland for the degree of Doctor of Philosophy in Toxicology presented on June 14, 2019.

Title: Transcriptomic Approaches for Discovering Regenerative and Developmental Regulatory Networks in Zebrafish

Abstract approved:

_____

Robert L. Tanguay

Zebrafish are capable of fully regenerating organs and tissue such as their caudal fin, which is similar to a human regrowing an arm or a leg. In contrast, most mammals including humans have a greatly reduced capacity for wound healing. The ability of zebrafish to undergo this regenerative process, called epimorphic regeneration, hinges on the capacity to form a blastema at the wound site. The blastema quickly recapitulates the developmental processes involved in complex tissue formation to restore lost or damaged tissue. One key mechanism for inducing blastema formation is global repression of genes involved in tissue differentiation and maintenance.

Induction of repressive factors, such as microRNAs (miRNAs), are involved in reprogramming cells during epimorphic regeneration. The upstream mechanism by which

zebrafish undergo epimorphic regeneration remains elusive. Furthermore, while focus is shifting toward regulatory RNAs such as miRNAs, the full complement of their repressive activities is unknown. We took a transcriptomics approach to investigating epimorphic regeneration and fin development. Parallel sequencing of total RNA and small RNA samples was performed on regenerating fin tissue at 1 day post-amputation (dpa). Most miRNAs had increased expression, consistent with global repression of genes involved in cell specialization during de-differentiation. We identified predicted interactions between miRNAs and genes involved in transcriptional regulation, chromatin modification, and developmental signaling. miR-146a and miR-146b are anti-inflammatory miRNAs that were predicted to target *eya4*, which is involved in chromatin remodeling and innate immunity. miR-132-3p and miR-21 were predicted to cooperate in repression Bone morphogenic protein (BMP) signaling antagonists. Depletion of miR-489 and miR-92b-3p were predicted to be involved in expression of cell cycle regulators *mycn* and *foxm1*, as well as other transcription factors associated with regeneration. We also identified Hedgehog and Scatter factor signaling as possibly targets of miRNAs regulation during regeneration.

Next, we performed microarray analysis on tissue exposed to the glucocorticoid beclomethasone diproprionate (BDP). We identified *cripto-1* as a highly upregulated gene flowing BDP exposure. Morpholino oligo knockdown of *cripto-1* permitted regeneration during BDP exposure. We were able to phenocopy the effects of BDP exposure by exposing zebrafish to an Activin signaling inhibitor, SB431542. Promoter analysis identified binding sites for genes that were differentially expressed in our data.

BDP exposure of murine embryonic stem cells confirmed that glucocorticoid-mediated induction of *cripto-1* is conserved in mammals.

Finally, we investigated a unique caudal fin duplication, called x-fin, resulting from embryonic exposure an exogenous ligand of the aryl hydrocarbon receptor (AHR), benzo[k]fluoranthene (BkF). We determined that the phenotype is Ahr2-dependent. We also determined that it is independent of hepatic metabolism using a hepatocyte ablation model. RNA seq analysis of trunk tissue at four time points of revealed that BMP and Fibroblast growth factor (FGF) ligands were robustly induced. Enrichment analysis revealed similarities to fin regeneration processes as well as inflammation. Altogether, we leveraged transcriptomics as a useful tool for identifying mechanisms associated with tissue regeneration and development.

TRANSCRIPTOMIC APPROACHES FOR DISCOVERING REGENERATIVE AND
DEVELOPMENTAL REGULATORY NETWORKS IN ZEBRAFISH

by
Michael Austin Garland

A DISSERTATION

submitted to

Oregon State University

in partial fulfillment of
the requirements for the
degree of

Doctor of Philosophy

Presented June 14, 2019
Commencement June 2020

Doctor of Philosophy dissertation of Michael Austin Garland presented on June 14, 2019.

APPROVED:

_____

Major Professor, representing Toxicology

_____

Head of the Department of Environmental and Molecular Toxicology

_____

Dean of the Graduate School

I understand that my dissertation will become part of the permanent collection of Oregon State University libraries. My signature below authorizes release of my dissertation to any reader upon request

_____

Michael Austin Garland, Author

CONTRIBUTION OF AUTHORS

In all chapters, Dr. Robert Tanguay contributed to intellectual formulation, writing, and study design.

Chapter 2: Michael Garland analyzed and interpreted the data, and prepared the manuscript. Jill Franzosa conceived the experimental design. Cheryl Dunham, Chris Sullivan, Jason Wendler, and Joseph Brown contributed to the RNA read processing and differential expression. Susan Tilton provided bioinformatics support.

Chapter 3: Michael Garland performed bioinformatic analysis, interpreted results, and prepared the manuscript. Sumitra Sengupta designed/performed laboratory experiments and bioinformatics analysis, and prepared the manuscript. Lijoy Mathew performed laboratory experiments and provided editorial comments. Lisa Truong provided editorial comments. Jane La Du assisted with microinjections. Esther de Jong and Aldert Piersma performed the embryonic stem cell experiments.

Chapter 4: Michael Garland and Mitra Geier designed/performed laboratory experiments and prepared the manuscript. Sean Bugel contributed to experimental design and provided editorial comments. Cheryl Dunham, Joseph Brown, and Susan Tilton provided bioinformatics support.

TABLE OF CONTENTS

TABLE OF CONTENTS (Continued)

TABLE OF CONTENTS (Continued)

LIST OF FIGURES

LIST OF TABLES

TRANSCRIPTOMIC APPROACHES FOR DISCOVERING REGENERATIVE AND
DEVELOPMENTAL REGULATORY NETWORKS IN ZEBRAFISH

CHAPTER 1 – INTRODUCTION

The ability of certain vertebrates, such as fish, to fully regenerate lost tissue has been of great interest for centuries [1]. Only with recent technological advancements have we been able to start characterizing the molecular dynamics associated with tissue regeneration. In particular, high-throughput measuring of transcriptomic data have allowed a more unbiased look into the molecular underpinnings of tissue regeneration. This dissertation aims to advance our understanding of epimorphic tissue regeneration and limb induction through transcriptomic and computational approaches. This introduction will briefly discuss how vertebrate limbs are formed, our current understanding of how epimorphic regeneration takes place, and how advances in transcriptomic technologies have facilitated our knowledge of this process. Genes and their respective products will be referred to using zebrafish nomenclature except where otherwise noted.

Vertebrate limb development

Complex tissue regeneration includes an ontological process that recapitulates development of the injured or lost tissue. Our focus is on limb development and regeneration. We note, however, that regeneration of other tissues proceeds similarly to limb regeneration.

A review by Capdevila and Belmonte (2001) provides an overview of the basic molecular mechanisms of limb induction [2]. Prior to embryonic limb bud formation, the positional identity of the limb field (*i.e.*, the location of the presumptive limb) is specified through a combination of interactions mediated by tissues derived from opposing germ layers (*i.e.*, ectoderm *vs* mesoderm). The limb field consists of cells occupying a particular space in the lateral plate mesoderm. Hox genes, which are expressed in response to retinoic acid signaling [3], control the signals specifying the limb bud precursor [4].

Growth and development of the limb bud relies on continued tissue-tissue interactions, particularly epithelial-mesenchymal interactions between the apical ectodermal ridge (AER) and the mesoderm [2]. Two of the most upstream pathways in limb development, Wnt/β-Catenin and Fibroblast growth factor (FGF) signaling, regulate each other through these interactions. Transforming growth factor beta (TGF-β) ligands, including Bone morphogenic proteins (BMPs), are among the other signaling factors secreted by neighboring tissues. During outgrowth, Hox genes control proximal-distal patterning while Hedgehog signaling (mediated by *sonic hedgehog*) defines the zone of polarizing activity (ZPA) involved in anterior-posterior patterning [2].

Ectodermal cells of the limb bud are induced to form the AER by *radical fringe*, a mediator of Notch signaling [5]. The AER is an important signaling structure that mediates dorsal-ventral patterning. Wnt10a and its transducer, LEF1, are involved in generating the AER [6], which itself secrets Wnts and FGFs. Interactions between the

mesenchyme, AER, and ZPA continue to facilitate distal outgrowth, with tissues differentiating into skin, muscle, bone, cartilage, vasculature, and other structures [2].

Notably, certain situations arise where an embryo can develop an ectopic limb or appendage. A classic example is the addition of exogenous retinoic acid (RA) to the lateral plate mesoderm of an embryo during development [7]. RA induces expression of *sonic hedgehog* (*shh*), leading to the induction of a new ZPA from which a limb bud forms [8]. In zebrafish, loss-of-function mutations in either Wnt or BMP antagonists (through *sfrp* and *chrdn*, respectively) result in caudal fin duplications during development [9]. In *sfrp* mutants, the caudal fin consists of three caudal fin folds equidistant to one another. In the *chrdn* mutants, there are four fin folds, with two ectopically positioned lateral to the normal fin folds. The outcomes from these mutations highlight the

Zebrafish and Epimorphic regeneration

Zebrafish are an excellent model for studying both development and regeneration. They have the capacity to regenerate several tissue types including fin, heart, retina, optic nerve, spinal cord, liver, and sensory hairs [10]. Their ease of husbandry, small size, fecundity, transparent larvae, short generation time, and genetic tractability make them suitable for many different experimental approaches. In addition, larvae are suitable for fin fold regeneration experiments at 48 hours post-fertilization and fully restore their fins

by 72 hours post-amputation (hpa). This makes zebrafish larvae particularly useful for transient knockdown experiments (as opposed to complete knockout approaches). Knockdown approaches, such as targeted morpholino oligos (MOs), may be required for interrogating the role of certain genes since those involved in development and regeneration are often required for embryonic and larval survival [10].

In addition to zebrafish, certain "lower" vertebrates are capable of fully regenerating lost appendages and organs as adults. The process by which these regenerating vertebrates restore tissue is called epimorphic regeneration [10]. The hallmark feature of this process is the de-differentiation of damaged mesenchymal tissue into a mass of pluripotent stem cells called a blastema. This structure can grow out and differentiate to restore lost tissues. Four stages of epimorphic regeneration include: 1) epithelialization; 2) blastema formation 3) regenerative outgrowth; and 4) termination of regeneration [10]. Similar to limb bud development, blastema formation relies on epithelial-mesenchymal interactions between the mesenchyme and ectoderm. Epithelialization is therefore a critical process for epimorphic regeneration. The wound epithelium develops into the apical epithelial cap (AEC) in a nerve-dependent fashion [11]. The AEC is analogous to the AER during limb bud development and serves a similar purpose in directing the underlying mesenchyme with secreted signals [12].

The most upstream signals known to initiate epimorphic regeneration include *wnt10a* and *fgf20a* [13, 14], which cooperate to induce the blastema. Signaling of *wnt10a*, which is expressed in the distal portion of the blastema, is transduced by *lef1*,

which is expressed in the basement membrane separating the blastema and AEC. FGF ligands are secreted from the AEC to the blastema, where FGF receptors are expressed [15]. As FGF and Wnt signaling take effect, induction of other signaling pathways involved in epithelial-mesenchymal interactions are activated. The most upstream pathways include TGF-β/Activin [16], BMP[17], Insulin-like growth factor [18], and Notch [19]. Retinoic acid also has an early role in establishing the blastema [20].

Evidence suggests that *wnt10a* may be activated by prostaglandin E_2 (PGE_2) after injury [21]. At least in mammalian neural tissue, PGE_2 is produced by COX2 from arachidonic acid following stimulation by interleukin 1-β (Il-1β) [22]. Notably, transient inflammation mediated Il-1β is required for zebrafish larval fin fold regeneration [23], indicating that at least a mild inflammatory response must take place during blastema formation. It is unclear whether Il-1β-mediated induction of PGE_2 is the molecular initiating event leading to epimorphic regeneration. It is important to note that inflammation is also associated with reduced healing capacity and fibrotic scarring [24]. This further demonstrates the need for tightly coordinated and balanced signaling events during epimorphic regeneration.

By 30 hours post-amputation, the mesenchymal tissue expresses Msx genes, which are the classical biomarkers of the blastema [25]. Epithelial-mesenchymal interactions continue after the blastema forms, culminating in the restoration of skin, muscle, bone, cartilage, blood vessels, and other tissues, just as in limb development. The regenerative process in adult zebrafish takes approximately 2-3 weeks [10].

Repression of gene expression by miRNAs

Cellular de-differentiation into a multipotent state involves widespread repression of gene expression. Maintenance of DNA methylation state as well as histone methylation/acetylation/phosphorylation state have been observe during epimorphic regeneration and involve genes associated with the Polycomb group (PcG) and Trithorax group (TrxG) [26, 27]. Another mechanism of quick repression involves the induction and depletion of microRNAs (miRNAs). These are short (approximately 22 nucleotides) RNAs that bind to the 3' untranslated regions (UTRs) of target genes, provided that a complementary sequence is present and available for binding [28].

Three mechanisms of miRNA-mediated post-transcriptional repression include: 1) cleavage of the target by RNA-induced silencing complex (RISC); 2) blocking translation of the target; and 3) deadenylation of the target's poly-A tail [28]. Typically cleavage happens when there is near-perfect complementarity of the binding site [28]. However, several factors can affect miRNA targeting efficiency besides the presence/absence of a complementary sequences. These include: octamer *versus* septamer binding sites [29]; presence and distance of other binding sites on the same 3'-UTR [30] [31]; AU content of the 3'-UTR[32]; distance from the 3'-UTR [33]; among others [29].

A high-throughput microarray study on the differential expression of miRNAs during zebrafish fin regeneration demonstrated robust fold changes [34]. It also demonstrated that *dicer*, which processes precursor miRNAs into mature miRNAs, is required for regeneration, indicating that transcriptional repression via miRNA biogenesis

is a key mechanism for blastema induction. Similarly, depletion of miRNAs in an FGF receptor-dependent manner was also required for regeneration [35].

In order to ascertain the role of a miRNA, target prediction tools have emerged that allow identification of potential miRNA targets. Three such databases include MicroCosm [36], MicroRNA [37], and TargetScan [29]. These account for sequence complementarity as well as some of the other predictive factors mentioned above. miRNA target analysis has been used to identify some key interactions during zebrafish regeneration. For example, predictive targeting software was able to predict that depletion of miR-203 is important for Wnt signaling via *lef1* [34], and depletion of miR-133 is necessary for expression of the FGF target, *mps1 [35]*.

Transcriptomics approaches for investigating regeneration

Previous studies into the molecular mechanisms of epimorphic regeneration were based on *a priori* knowledge of genes involved in limb development. This approach led to the discovery of Msx genes as biomarkers for blastema induction [25]. Other approaches involved forward genetics approaches such as random mutagenesis screening for non-regenerating mutants. This approach was used to discover *fgf20a* as an essential upstream factor at the onset of epimorphic regeneration [14]. Additional approaches, such as chemical genetic screening, have been utilized. The reasoning behind this approach is that chemicals inhibiting regeneration do so by perturbing a specific critical pathway

[38]. Amphibians [39] and teleosts [40] have been employed for these types of experiments. Larval zebrafish are particularly useful this method due to their amenability to high-throughput screening [38].

The implementation of microarray technology permitted a more robust interrogation of transcriptional changes. Coupled with genome sequencing, this allowed researchers to investigate the expression of potentially thousands of genes rather than rely on forward or backward genetic approaches [41]. In microarray analyses, RNA samples could be hybridized to a chip containing an oligomer probe consisting of the complementary sequence of a given RNA [42]. Fluorescent labels allowed visualization of the RNA abundance changes in a treatment or condition relative to a control group [43]. However, quantification of these changes was not always accurate, and qPCR would be needed to validate the results [44].

Microarrays have been used in several experiments involving fin regeneration, either by comparing regenerate to non-regenerate tissue [17] or by involving a second factor, such as chemical treatment [45] or transgenic effect [35]. They also permitted the high-throughput analysis of microRNA (miRNA) [34]. However, a comprehensive anti-correlated expression analysis of miRNA-mRNA interactions would be difficult with a miRNA microarray, since predicted targets would need to be validated for presence in the tissue as well as for anti-correlated expression change.

RNA sequencing is a method that involves de novo synthesis of small (30-300 bases, depending on the platform) reads based on sample input. It has robust alignment

and quantification quality. Because of its excellent track record for generating (relatively) clean downstream data and its effectiveness at characterizing transcriptomes, qPCR validation is regarded as unnecessary [46]. Furthermore, with decreased cost of use, it is more feasible to conduct miRNA-mRNA sequencing for the purpose of anti-correlated expression analyses. Such studies on the regenerating appendages of various organisms have already been conducted [47], however, focus has remained on processes after blastema formation.

Dissertation objective

The goal of this dissertation is to identify novel signaling and regulatory mechanisms involved in the induction of blastema formation. We focused on performing high-throughput transcriptomic analysis of presumptive blastema tissue (1 day post-amputation in zebrafish fins) as a discovery approach. In Chapter 2, we performed RNA sequencing for the purpose of generating a comprehensive and (relatively) unbiased sense of the transcriptomic landscape leading up to blastema formation. We also sought to identify anti-correlated miRNA-mRNA interactions using parallel sequencing. In Chapter 3, we sought to understand the mechanism of how induction of the glucocorticoid receptor with a particular class of glucocorticoid ligands (specifically, beclomethasone dipropionate) can impair fin regeneration. In Chapter 4, we used RNA sequencing to identify potential mechanisms by which a class of polycyclic aromatic hydrocarbons (PAHs; specifically benzofluoranthenes) can induce fin duplication during development.

CHAPTER 2 – PARALLEL SEQUENCING PREDICTS NOVEL REGULATORY MIRNA-MRNA INTERACTIONS DURING BLASTEMA FORMATION IN ZEBRAFISH

Abstract

During epimorphic regeneration, regulation of differential gene expression by microRNAs (miRNAs) is required for blastema induction. However, most miRNA-target interactions remain largely unknown. Here we performed parallel RNA and small RNA sequencing of regenerating adult zebrafish fin tissue at 1 day post-amputation (dpa). Small and total RNA samples were derived from the same bioreplicates, permitting miRNA-target predictions based on anti-correlated expression patterns. We presented a comprehensive survey of the mRNA transcriptome following by miRNA analysis, including Gene Ontology (GO) analysis and MetaCore enrichment analysis. We used the Bioinformatics Resource Manager to generate a list of high confidence predictions of zebrafish miRNA-target interactions in MicroCosm and TargetScan. We identified predicted regulation of Hox genes by miR-132-3p, miR-21, and miR-223. miR-21 was predicted to facilitate Wnt signaling through repressing *wif1*. Anti-inflammatory miR-146a and miR-146b were predicted to cooperate in repression of *eya4*, which regulates chromatin remodeling and immune response. miR-489 and miR-92-3p, which decreased expression, were predicted to regulate the expression of key transcription factors induced during blastema formation such as *foxm1*, *mycn*, *sox11b*, *sall1* paralogs, and AP-1 subunits. BMP signaling via *bmp7a* and hedgehog signaling via *ihhb* may be promoted by miRNA-mediated repression of their signaling antagonists *nog* and *hhip*, respectively. We identified fish-specific miRs (miR-724 and miR-727-3p) that also had deceased expression and were predicted to target the upstream regeneration factor *fgf20a*. This computational analysis predicts several key molecular interactions that will guide future

studies on the mechanism(s) of blastema induction, including new epithelial-

mesenchymal interactions mediated by hedgehog and scatter factor signaling.

Introduction

A grand challenge facing the life sciences is advancing regenerative medicine. The

promise of stem cell-related therapies has generated much interest in recent decades for

understanding how certain vertebrates are capable of regenerating complex structures and

organs throughout adulthood [48]. Model vertebrates capable of fully regenerating lost or

damaged structures as adults include different species of fish [49], amphibians [50],

lizards [51], and to a much lesser extent, rodents [52]. Most mammals lose this ability

almost entirely during development or shortly after birth [53], and general wound healing

capacity continues to decrease through aging [54].

There are two major modes of regeneration: proliferative *versus* epimorphic

regeneration. In the former process, cells enter the cell cycle and rapidly proliferate to

heal or restore tissue. Adult mammals rely almost exclusively on this mode of wound

healing in organs such as the skin and liver [55]. On the other hand, epimorphic

regeneration involves the dedifferentiation of damaged mesenchymal tissue into a mass

of multipotent stem cells called a blastema, and is the process utilized by capable species

when complex tissue is damaged [10]. Four major stages of epimorphic regeneration

include: 1) epithelialization; 2) blastema formation; 3) outgrowth and differentiation; and

4) termination. The blastema is highly proliferative, and during outgrowth it recapitulates

developmental processes as it differentiates into the tissue that was previously lost. The formation and development of the blastema relies on signaling from an apical epithelial cap (AEC) derived from wound epidermis as well as signals derived from nerve tissue [10].

While fundamentally different, these two modes of wound healing share common characteristics at their onset including epithelialization, proliferation, and inflammation [10, 56]. A key distinguishing factor between epimorphic regenerators *versus* non-regenerators is the degree of inflammation—in mammals including humans, damaged tissue becomes highly inflamed which results in fibrotic scarring. In contrast, inflammation is attenuated during epimorphic regeneration. This is thought to prevent fibrosis and allow cells to generate an extracellular matrix (ECM) enriched in fibronectin and hyaluronan that supports regenerative signaling and migration [57, 58].

Epimorphic regeneration is understood to involve epithelial-mesenchymal interactions that lead to blastema formation. Some of the major upstream signaling pathways that facilitate these interactions include Wnt, Fibroblast growth factor (FGF), Epidermal growth factor (EGF), Transforming growth factor beta (TGF-β), Insulin-like growth factor (IGF), and chemokine signaling. Several of these pathways are involved in the epithelial-mesenchymal interactions required for blastema formation [10]. To enter a developmental state, cells rely on repressive mechanisms that prevent expression of genes that define the differentiated state. One such mechanism, commonly referred to as epigenetic modification, involves DNA methyltransferases that can add methyl groups directly to DNA bases (typically cytosine) in the promoter regions of genes and prevent

transcription [59]. Another mechanism is through post-translationally modifying histone proteins through the addition or removal of acetyl, methyl, or phosphoryl groups. One such complex, Polycomb Repressive Complex 2 (PRC2), plays a major role in repression by silencing transcription factors involved in differentiation such as those in the Hox family [60]. Finally, another method of repression is through microRNAs (miRNAs), which have a 17-23 base pair sequence complementing the 3' untranslated region (UTR) of target transcripts [34]. miRNAs guide the RNA-induced silencing complex (RISC) to the target mRNA and represses gene expression by cleaving mRNA, deadenylating the poly-A tail, and blocking translation. Both induction and depletion of miRNAs are required for appropriate epithelial-mesenchymal signaling and fin regeneration in general [34].

Emerging biotechnologies have allowed researches to better characterize molecular dynamics during complex processes. In particular, high-throughput sequencing technologies have provided the means for de novo sequencing of entire transcriptomes, including small RNAs [61]. The underlying assumption of miRNA-mediated regulation of gene expression is that miRNA-target expression changes are anti-correlated [62]. Previous microarray studies have successfully utilized anti-correlation analyses involving miRNAs to identify miRNA-target interactions that are critical for regeneration [35].

Here, we present a parallel RNA-small RNA sequencing approach to identify the expression patterns of both mRNAs and small RNAs specifically to identify processes leading to blastema formation in adult zebrafish. While similar work has been performed in regenerate fins at 4 days post-amputation (dpa) [47], our approach investigated

regeneration at 1 dpa in order to characterize the molecular dynamics preceding blastema formation. We simultaneously performed parallel sequencing on juvenile (4 week old) and geriatric (2+ year old) zebrafish, which can also undergo epimorphic regeneration. These samples represented similar but different epimorphic regeneration systems and were used only as a biological validation measure. We surveyed thousands of genes encoding both the classical regenerative signaling pathways as well as genes that are novel to blastema formation. We then performed high-throughput target prediction analysis using anti-correlated miRNA-target expression patterns to identify novel regulatory functions of miRNAs.

Methods

Zebrafish husbandry and fin amputations

Wild-type zebrafish (AB strain) were raised and maintained on a recirculating water system (28 ± 1 ℃) in water supplemented with Instant Ocean salts at the Sinnhuber Aquatic Research Laboratory (SARL), Oregon State University (Corvallis, OR, USA). Animals were kept on a 14:10 h light:dark photoperiod and maintained at a density of 10 animals/gallon in 50-gallon tanks. All rearing, husbandry, and experiments were performed in accordance with Institutional Animal Care and Use Committee (IACUC) protocols (Animal Care and Use Protocol 4095).

Zebrafish from 4 month old (adult), 4 week old (juvenile), and 2+ year old (geriatric) age cohorts were used for regeneration experiments. Surgical amputations

were performed on fish anesthetized in tricaine (MS-222) by resecting fin tissue immediately anterior to the lepidotrichial bifurcation. Amputated tissue was stored in RNAlater® (Invitrogen, Carlsbad, CA). This tissue was used as the control condition, 0 days post-amputation (dpa). There were three biological replicates, each consisting of fins from n = 10 animals, with the exception of the juvenile cohort which had replicates consisting of n = 100 animals due to their smaller size. Fish recovered in tricaine-free water, and 24 h later were subject to amputation of regenerate tissue at the amputation plane.

RNA isolation and sequencing

Total RNA was isolated using miRNEasy Kits (Qiagen, Basel, Switzerland). Six µg of total RNA (100 ng/µL) for each of the 18 samples were provided to the Genomics Core of Lerner Research Institute (Cleveland, Ohio) for Illumina® RNA-Sequencing library preparation and processing. Three µg Total RNA from each sample was prepared for 78-bp single-end RNA-Sequencing using the Illumina® (San Diego, CA) TruSeq RNA sample preparation kit. Samples were bar-coded to multiplex 3 samples per lane, with each lane including one juvenile, adult and geriatric sample and run on an Illumina® (San Diego, CA) Genome Analyzer IIx.

Bioinformatics

Sequencing FASTQ data were filtered according to Illumina quality scores using htseq-qa [63]. Total RNA read alignment to the Ensembl GRCz10 (build 90) zebrafish genome was performed using HISAT2 [64]. Preprocessing and estimated gene counts

was performed using htseq-count [63]. Gene expression analysis was performed in RStudio [65] using the edgeR quasi-likelihood pipeline [66] with Bioconductor [67]. Only genes with an average of 15 counts per million in three samples were considered for further analysis. Regular log normalization was used to correct for heteroscedasticity.

Ensembl biomaRt [68] was used to for gene annotation and the Bioinformatics Resource Manager [69] was used to identify human orthologs for those not detected with biomaRt. Principal components analysis was performed using the base R package *stat* and was visualized using the *ggplot* [70], *ggthemes* [71], and *ggrepel* [72]. Genes with the greatest magnitude of differential expression across samples were identified using MatrixStats [73]. The transformed count values of these genes were scaled by their Z-score. Unsupervised hierarchical clustering was performed using *ComplexHeatmap [74]*.

Small RNA was quality processed as described above and aligned to the zebrafish miRbase (v22) database [36]. Read alignment and quantification was performed using miRDeep2 [75]. Annotated miRNAs were analyzed for differential expression as described above.

Gene Ontology (GO) term enrichment analysis was performed using the Gene Ontology Consortium website (http://geneontology.org/) [76, 77]. MetaCore (Clarivate Analytics) analysis was performed using human gene orthologs and a background consisting of all annotated genes that were mapped to the genome.

Results

Differential expression of total RNA

We performed differential expression using the edgeR quasi-likelihood pipeline. Adult gene expression data were filtered by finding the genes that commonly increased or decreased expression in all three cohorts (Adult, Juvenile, and Geriatric). Of these common changes, only differentially expressed genes (DEGs) having log_2FC (FC) of > 1.0 were considered for further analysis.

We identified a total of 4288 DEGs of which 1982 increased and 2306 decreased expression. DEGs consisted of 12 biotypes (Table 1). Most of belonged to *protein_coding* (mRNA), which consisted of 1929 that increased and 2306 that decreased expression. *lincRNA* had the second most abundance of which 34 increased and 59 decreased expression. The rest of the biotypes each had fewer than 20 total genes and consisted of *processed_transcript*, *unprocessed_pseudogene*, *antisense_RNA*, *snoRNA*, *miRNA*, *Mt_tRNA*, *processed pseudogene*, *sense_overlapping*, *TEC* (To be Experimentally Confirmed), and *transcribed_unprocessed_pseudogene*. All snoRNAs and miRNAs had increased abundance. The miRNAs belonged to mir-21 precursors.

The 500 DEGs with the greatest change in magnitude of expression in adults (that also had common differential expression in Juvenile and Geriatric cohorts) were used for heat map and principal component analysis (PCA) clustering. Unsupervised bi-hierarchical clustering demonstrated two general clusters of control *versus* regenerate conditions (Figure 1). Consistent with these observations, PCA demonstrated tight clustering between control and regenerate samples along both PC1 (x-axis, 50%) and PC2 (y-axis, 34%) with their respective conditions (Figure 2). Differential expression

analysis of total RNA from the Juvenile and Geriatric cohorts is beyond on the scope and purpose of this study and were not further considered.

Differential mRNA abundance overview

We first characterized the changes in the mRNA transcriptome at 1 dpa. Developmental and regulatory signaling pathways were analyzed by identifying known ligands, receptors, and associated genes based on their gene ontology (GO) terms. We then performed pathway and transcription factor target enrichment analysis using PANTHER classification and MetaCore software.

Enrichment analysis - GO terms

To identify the biological processes represented in our differential expression data, we performed gene ontology (GO) analysis on DEG sets with either increased or decreased expression. GO term enrichment based on PANTHER classification was queried using the Gene Ontology Consortium's GO Enrichment Analysis tool. We focused our analysis on GO terms related to biological processes. Term enrichment was considered significant if it had an FDR-adjusted p-value < 0.05, and rankings were determined based on fold enrichment.

There were 344 enriched GO terms among DEGs that had increased expression, most of which were related to cell proliferation. The top 10 enriched GO terms included six meiotic/mitotic-related terms, three related to transcription, and one related to isoprenoid metabolism (*polyprenol metabolic process*). (Table 2) GO terms relating to

other biological processes included, *proteasomal ubiquitin-independent protein catabolic process*; *proteasome assembly*; *ribosome biogenesis*; *protein refolding*; and *mitochondrial translation*.

Among DEGs with decreased expression there were 77 enriched GO terms. These were primarily associated with development and signaling. The top GO term was associated with collagen crosslinking (*peptidyl-lysine oxidation*) while the rest of the top 10 were associated with chondrocyte or cartilage development (e.g. *growth plate cartilage chondrocyte morphogenesis*) (Table 3). Other processes with significant enrichment included: *cell-matrix adhesion*; *organ growth*; *negative regulation of axon guidance*; *response to growth factor*; and *neurogenesis*.

Enrichment analysis: MetaCore Process network

MetaCore provides tools for biological systems analysis based on curated data available from the literature. To supplement our GO term enrichment analysis, we used MetaCore to identify enrichment in MetaCore Process Networks and transcription factor targets. Genes that were converted to human orthologs by biomaRt [68] and the Bioinformatics Resource Manager (BRM) [69] were uploaded to MetaCore for analysis.

We performed Process Network enrichment analysis separately on DEG sets with either increased or decreased expression as done previously with GO term enrichment. Enrichments were considered significant if they had an FDR-adjusted p-value < 0.05. We used the network building tool for each significantly enriched Process Network to attempt identification of DEGs that are upstream or central to the network.

DEGs with increased expression were enriched for 15 Process Networks (Table 3). We grouped these networks into five categories: cell cycle; transcription/translation; immunity; DNA repair; and proteostasis. We sought to determine some of the upstream regulators of these processes by building the respective network in MetaCore (not shown). *CDK1* and its activator *CDKN1C* were central to cell cycle networks, as were the cyclins *CCNA2* and *CCNB1*. *MET* was identified as an upstream regulator of *Cell cycle_Mitosis*, while *IGF2* and *FOXM1* were regulators of *Cell cycle_G2-M*. Key immunity regulators were *STAT1* and *RALA*, while regulators of DNA repair included *RAD51* and *BLM*. *Translation_Translation in mitochondria* was modulated primarily by large (MRPL) and small (MRPS) ribosomal subunits. Transcription was primarily enriched with DEGs associated with ribonucleoproteins and RNA splicing factors such as *MAGOH*.

There were six enriched Process Networks among DEGs with decreased expression (Table 4). Four were associated with cell matrix (*Cell adhesion_Cell-matrix interactions*, *Proteolysis_ECM remodeling*, *Cell adhesion_Platelet-endothelium-leucocyte interactions*, *Proteolysis_Connective tissue degradation*) while two were associated with cartilage and bone remodeling (*Development_Cartilage development*, *Development_Ossification and bone remodeling*). DEGs within cell matrix-related networked included MMPs and their regulators such as *MMP2*, *MMP7*, *TIMP2*, and *TIMP4*. Networks associated with chondrogenesis and osteogenesis were regulated by several TGF-β superfamily members, including BMPs and their receptors. *SMAD6*, *SOX5*, *SOX9*, *RUNX3*, among other DEGs were specific to cartilage development, while

IGF1, *FGF18*, *FGFR1*, *DLL1*, *DLL4*, and *SP7* were among those specific to bone development.

Gene expression data overview

We conducted a broad survey of the DEGs by categorizing them based on GO term associations and known roles in development. A list of DEGs with absolute fold change > 2 is listed on Table A.1.

Developmental signaling

We classified DEGs involved in signaling by first identifying their association with 11 known major developmental pathways: Fibroblast growth factor (FGF), Wnt, Retinoic acid (RA), Transforming growth factor beta (TGF-β)/Activin, Bone morphogenic protein (BMP), Hedgehog (Hh), Insulin-like growth factor (IGF), Notch, Chemokine, Ephrin (Eph), and Scatter factor (SF). The SF category includes semaphorins and plexins because of their ability to crosstalk with and transactivate the SF receptor (*met*). We identified 151 DEGs associated with these pathways, of which 43 (28%) had increased and 109 (72%) had decreased expression. This included several ligands, receptors, and for certain pathways, downstream targets and signal modulators. The functions of DEGs lacking gene symbol descriptions were assessed using their GO terms.

We found a moderate to strong increase in the expression of certain ligands associated with developmental signaling: *fgf20a* (FGF signaling, 3.2-fold); *wnt10a* (Wnt signaling, 1.8-fold); *hbegfa* (EGF signaling, 2.0-fold); *inhbaa* and *inhbab* (TGF-β/Activin

signaling, 3.0- and 2.3-fold); *bmp7a* (BMP signaling, 4.4-fold); *igf2b* (IGF signaling 2.7-fold); *jag1a* (Notch signaling, 4.5-fold); *cxcl12b* (Chemokine signaling, 2.8-fold); and *efna3b* (Eph signaling, 2.1-fold). The rate-limiting enzyme for RA production, *aldh1a2*, increased by 3.3-fold. We identified additional ligands for FGF, TGF-β/Activin, Chemokine, and Eph signaling that increased expression. *CU633855.1*, which encodes a probable secreted frizzled-related protein, had increased expression. Three Eph receptors, *epha2a*, *epha7*, and *epha4*, increased expression by 2.6-, 2.6-, and 2.1-fold, respectively. The SF receptor, *met*, increased expression by 2.8-fold. Of particular note was the robust increased expression of *ihhb* (Hh signaling, 3.5-fold), whose involvement in blastema induction is novel.

The most amount of DEGs that decreased expression were associated with FGF, Wnt, TGF-β, BMP, and Chemokine signaling. Notably, the BMP antagonizer *nog1* decreased expression by 5.6-fold, while its paralog *nog3* decreased by 1.5-fold. The FGF antagonist *spry2* decreased expression by 1.5-fold, while the Hh antagonist *hhip* decreased by 1.7-fold. *bmp7b*, *aldh1a3*, *jag1b* and *cxcl12a*, whose paralogs had increased expression, each respectively decreased expression by 1.6-, 1.3-, 1.2-, and 2.3-fold.

Chromatin and DNA modifiers

The chromatin and DNA modifier category include histones and enzymes that post-translationally modify or chaperone histones. It also includes DEGs that regulate DNA methylation. We identified 61 modifiers that were differentially expressed, and in contrast to previous DEG categories, there were several more modifiers that increased

(89 DEGs) rather than decreased (13 DEGs) expression. Chromatin modifiers included DEGs associated with the Polycomb group (PcG), Switch/sucrose non-fermentable (SWI/SNF) related, and High mobility group (HMG) remodeling factors. There were also several methyltransferases that were differentially expressed. The DEGs with the greatest increased *versus* decreased expression was *ruvbl2* (2.2-fold) and *tox2* (2.0-fold), respectively. Notably, two subunits (*pcgf6* and *phc2a*) of the Polycomb repressive complex 1 (PRC1) and two subunits (*ezh2* and *suz12a*) of the Polycomb repressive complex 2 (PRC2) had increased expression. One PRC1-related Chromobox (Cbx) gene, *cbx2*, had decreased expression. A non-PcG Cbx gene, *cbx3*, conversely had increased expression. Additionally, we identified five SWI/SNF related chromatin remodelers. Four (*smarcad1a*, *smarca5*, *smarca4a*, *smarcc1a*) had increased expression, in contrast to *smarca2* which decreased expression. Two histone deacetylase (HDAC) DEGs, *hdac1* and *hdac5*, respectively increased and decreased expression by 1.1-fold. We also identified two Chromobox (Cbx) genes, *cbx3* and *cbx2*, which increased by 1.1-fold and decreased 1.2-fold, respectively.

Given the role of PRC2 during tissue regeneration, we performed an interactions analysis by building a DEG network using MetaCore. To identify the repressive activities of PRC2, we extracted interactions between its differentially expressed subunits (*ezh2* and *suz12*) and DEGs that decreased expression. We identified several

Transcription factors

We classified a total of 194 DEGs as transcription factors (TFs). There were 63 TFs that increased expression including several involved in development, wound healing, immune response, and cell cycle control. *bhlha9* (*fingerin*) had the greatest increased expression of over 5.7-fold. Other TFs were associated with an immune/inflammatory response including *si:dkey-23i12.7* (predicted to share homology with *batf2*), *runx1*, *CABZ01102124.1* (a possible *runx1* paralog), and *stat1*, all of which increased over 3-fold. Two neural-related TFs, *nkx6.2* and *sox11a*, increased by over 4.7- and 3.8-fold, respectively. Two paralogous transcriptional repressors, *sall1a* and *sall1b*, respectively increased expression by 1.1- and 3.9-fold. AP-1 subunits *fosl1b*, *junba*, *fosl2*, and *junbb* all had increased expression over 2-fold. *foxm1*, a master regulator of cell cycle induction, increased expression over 3.5-fold, while the Wnt-responsive *mycn* increased by 1.2-fold. Other notable TFs included *wt1b*, *homeza*, *vezf1*, *lhx2b*, *lef1*, *rb1*, *klf12a*, and *smad1*.

Similar to the developmental signaling DEGs, the majority of differentially expressed TFs (131 DEGs) had decreased expression. Several of these were developmental regulators representing Hox, Dlx, Sox, and Fox gene families. In total we identified seven Hox genes (*hoxb3a*, *hoxc13a*, *hoxc12b*, *hoxc3a*, *hoxc13b*, *hoxa4a*, *hoxa9b*), three Dlx genes (*dlx1a*, *dlx2b*, *dlx6a*), six Sox genes (*sox12*, *sox3*, *sox13*, *sox5*, *sox8b*, *sox9a*), and nine Fox genes (*foxn1*, *foxq1b*, *foxl1*, *foxp2*, *foxd2*, *foxo3*, *foxo4*, *foxd1*, *foxo3a*). Two paralogs that regulate endothelial development, *epas1a* and *epas1b*, had decreased expression, with *epas1a* decreased over 3.3-fold. *scxa*, a TF that maintains

tendon and ligament tissues, decreased by over 2.6-fold. *sall3*, a probable TF involved in DNA methylation, decreased by approximately 1.8-fold.

Transcription factor target enrichment

To supplement TF gene expression data, we used MetaCore to identify TFs that had an enriched number of predicted or validated targets in our data (subsequently referred to as "enriched TFs"). We considered TFs to be enriched for targets if they had an enrichment p-value < 5.00E-03. Using this approach, we identified 18 enriched TFs of which nine each had increased and decreased expression (Table 6). Enriched TFs were ranked according to their z-scores. Five enriched TFs with increased expression were regulators of cell proliferation: SP3 ($z = 7.0$), MYCN ($z = 6.5$), FOXM1 ($z = 5.8$), E2F3 ($z = 4.6$), and E2F8 ($z = 3.3$). CEBPZ ($z = 4.3$) is a regulator of the cell stress response, and the interferon IRF8 ($z = 3.0$) is an immune regulator. LHX2 ($z = 3.8$) is a regulator of wound healing.

Enriched TFs with decreased expression were associated with various processes. The proto-oncogenic AP-1 subunit, JUN ($z = 6.4$), had the greatest enrichment among TFs with decreased expression. The glucocorticoid receptor (GR) NR3C1 ($z = 4.8$) is involved in immunity and the inflammatory response to injury. SOX9 ($z = 3.8$) is a mesodermal TF involved in differentiation of cartilage and skeletal development. EPAS1 ($z = 3.4$) regulates development of tubular systems such as blood vessels. SMAD3 ($z = 3.5$) is a transducer of TGF-β/Activin signaling. SOX3 ($z = 2.8$) regulates neural differentiation.

Other growth factors, cytokines, and hormones

We identified the differential expression of other DEGs including 18 related to growth factor (GF) signaling, 24 related to cytokine signaling, and 69 related to hormone signaling. Of these, 31 had increased expression while 80 had decreased expression. GFs with increased expression included *pgfb*, *mdka*, and *gfer*. Several GFs associated with nervous system development, including *gdnfa*, *ntf3*, *ptn*, *mdkb* (paralog of *mdka*), *bdnf*, and *ngfa* had decreased expression. The connective tissue GF *ctgfa* also had decreased expression. Among cytokine-related DEGs, *il11a* and *il11b* had strongly increased expression of 7.4- and 5.9-fold, respectively. *lifrb* and *il6st*, which cooperate to regulate pluripotency, respectively increased expression by 2.4- and 2.0-fold. Two Tumor necrosis factor (TNF) receptors and one TNF ligand had increased expression, and three TNF ligands had decreased expression. Several endothelin-related DEGs were also differentially expressed. While one endothelin receptor (*ednrbb*) increased expression by over 6.3-fold, three other receptors (*ednraa*, *ednrba*, *ednrab*) and one ligand (*edn2*) had decreased expression. Two peptide hormones, *lepb* and *uts2a*, strongly increased expression by 9.6- and 9.0-fold, respectively. *uts2r*, the cognate receptor for *uts2a*, had decreased expression. *dio1*, which modulates thyroid hormone activation in peripheral tissues, also had decreased expression. We also identified differential expression of several cytochrome p450 (CYP) DEGs, many of which were associated with steroid metabolism. *cyp2aa7* and *cyp20a1* were the only CYPs with increased expression.

Other GPCR, PTK, and STK signaling proteins

We identified several other signaling-related DEGs that were not directly associated with previously mentioned pathways or cell cycle/apoptosis. We chose to focus the rest of the signaling analysis on 238 DEGs related to other G protein-coupled receptors (GPCRs), protein tyrosine kinases (RTKs), and serine/threonine kinases (STKs). We identified 171 GPCR-related, 16 RTK-related, and 51 serine/threonine kinase-related DEGs. Of these, 70 had increased expression while 117 had decreased expression. All five Ras superfamily members (Ras, Rho, Ran, Rab, and Arf) were represented among the GPCRs. *eras*, which is present in stem cells but not differentiated cells, increased expression by 1.3-fold. There were 14 differentially expressed adhesion GPCRs, all of which had decreased expression except for *adgrb1b*, which increased by over 4.6-fold. Among RTKs that increased expression were *ptk2aa* and *tec*. RTKs with decreased expression included *blk*, *ltk*, *alk*, and *fyna*.

STKs included dual-specificity phosphatases (DUSPs), MAP kinases (MAPKs), and various others. Three DUSPSs each increased and decreased expression, with *dusp13a* having an increased expression of over 6.9-fold. *dusp3a* decreased expression by 2.5-fold. *sgk2*, which regulates ion channels and transporters, increased expression by 4.7-fold. Two MAPKs increased while three decreased expression, with *mapk4* increasing by 1.6-fold and *map2k6* decreased by 1.2-fold.

Extracellular matrix modulation

We identified 231 DEGs involved in extracellular matrix (ECM) composition or remodeling, of which 60 had increased expression and 171 had decreased expression. DEGs associated with structural composition included jacalin, collagen, keratin, hyaluronan, fibronectin, integrin, matrix metallopeptidase (MMP), among others. The jacalins *jac2* and *jac4* increased expression by 11.9- and 7.0-fold, respectively, while *jac1* decreased by 2.1-fold. There was increased expression of the collagen gene *col8a1a* by 6.0-fold, while 15 different DEGs *(col2a1b*, *col4a1*, *col4a2*, *col4a6*, *col5a3b*, *col5a2b*, *col8a1b*, *col8a2*, *col9a3*, *col10a1a*, *col10a1b*, *col11a1a*, *col11a1b*, *col11a2*, *col18a1b*) had decreased expression. The fibronectin paralogs *fn1a* and *fn1b* both increased expression by at least 3.7-fold. *has1*, which synthesizes hyaluronan, increased expression by 4.3-fold. We identified eight integrins: *itga5*, *itgb8*, and *itgb1a* had increased expression, while *itgb1b.1*, *itga1*, *itgb3a*, *itga10*, *itga11a* had decreased expression.

MMPs that had increased expression included *mmp13a*, *mmp25b*, *mmp9*, and *mmp14b*, the former two of which increased expression over 3.2-fold. MMPs having decreased expression were *mmp30*, *mmp23bb*, *mmp2*, *mmp28*, *mmp17a*, and *mmp20a*, the latter of which had decreased expression over 4.3-fold. The metallopeptidase inhibitor *timp2b* increased expression over 5.5-fold, while its paralog *timp2a* along with *timp4.3* decreased expression. Four lysine oxidase (LOX) family members involved in collagen and elastin crosslinking, *loxl1*, *loxl3a*, *loxl3b*, and *loxl4*, each had decreased expression.

Cell cycle and apoptosis

We identified 164 DEGs that were associated with the cell cycle and apoptosis. Of these, 116 DEGs had increased and 48 had decreased expression. Cell cycle-related DEGs included cyclins and cyclin-dependent kinases (CDKs). All five differentially expressed cyclins (*ccna2*, *ccnb1*, *ccne2*, *ccnjl*, *ccnk*) had increased expression, with the mitotic entry cyclin *ccnb1* having the highest (4.1-fold) and the transcription-regulating cyclin *ccnk* having the lowest (1.2-fold). Three CDKs (*ckd1*, *cdk2*, *cdk8*), the first two being promoters of mitotic entry, had increased expression. Three other CDKs (*cdk15*, *cdk19*, *cdkl1*) had decreased expression, as did the CDK inhibitor *cdkn1bb*. *aurka* and *aurkb*, which regulate mitotic spindle assembly, had increased expression.

DEGs involved in apoptotic signaling included both positive and negative regulators of apoptosis. *birc5a* (survivin), a negative regulator, increased expression by 3.0-fold. Three positive regulators involved in binding BCL-2, *bnip3*, *bbc3*, and *bada*, decreased expression by 3.1-, 2.7-, and 1.1-fold, respectively. *ppp1r13bb*, which regulates apoptosis via p53 and is a negative cell cycle regulator, also decreased expression. There were some DEGs that were negative regulators of apoptosis and had decreased expression, such as *uacaa*.

Proteostasis

We identified several DEGs associated with proteostasis, which includes those involved in proteolysis, ribogenesis, and protein chaperoning. In total there were 185 DEGs associated with proteolysis, 110 involved in ribogenesis, and 59 molecular chaperones. In proteolysis, 100 DEGs had increased expression while 85 had decreased

expression. Proteolytic DEGs consisted of proteasome subunits, various proteases such as metallopeptidases and serine-type peptidases, and enzymes involved in ubiquitination. There were 37 proteasome subunits, all of which increased expression. Additionally, the proteasome maturation protein (*pomp*) and the proteasome lid unit, *split hand/foot malformation* (*shfm1*), both increased expression by 1.5- and 1.0-fold, respectively.

Not including proteasome subunits, 26 enzymes involved in ubiquitination had increased expression, while 30 had decreased expression. Four enzymes involved in sumoylation (*sae1*, *sumo3b*, *uba2*, *desi2*) had increased expression. DEGs that decreased expression included six calpains, various peptidases, and enzymes involved in ubiquitination. *si:ch211-202f3.4*, which encodes a calpain orthologous to human *CAPN4*, had the greatest decreased expression at 4.2-fold.

Consistent with the observed enrichment results, 108 out of 110 DEGs associated with ribogenesis had increased expression. Only two (*nsa2* and *rsl24d1*) had decreased expression. we identified 45 DEGs encoding proteins specific to mitoribosome assembly. Other SEGs that increased expression included *ppan*, *wdr75*, *surf6*, *noc2l*, *bms1*, and *wdr12*. Two polymerases, *polr1c* and *polr1d*, transcribe genes encoding ribosomal RNA precursors. Three components of the PeBoW complex (*pes*, *bop1*, *wdr12*), which coordinates ribogenesis with the cell cycle, were also present. We also identified three DEGs (*fam118b*, *nop10*, *coil*) involved in Cajal body organization. Chaperones that increased abundance included multiple endoplasmic reticulum (ER)-related DEGs such as *pdia6*, *calr3b*, and *uggt2*.

Analysis of miRNAs

We focused our small RNA analysis on miRNAs using miRDeep2. Annotated miRNAs were subject to differential expression analysis using EdgeR and subsequently used to identify miRNA-mRNA interactions.

Differential expression of annotated miRNAs

We performed differential expression of mature miRNA reads using EdgeR [66]. miRDeep2 maps annotated mature miRNA reads to their precursor genes. The differential expression was based on the mapping of mature miRNAs to respective precursors. As with the RNA seq data, we filtered our miRNA list by considering only those mature miRNAs that had significant differential expression in all three age cohorts.

We identified a total of 44 differentially expressed mature miRNAs that were processed from 47 unique precursors. There were 35 mature miRNAs that increased expression (Table 7) and 9 that decreased expression (Table 8). Cross-referencing data with miRbase revealed 30 human orthologs. miRNAs without human orthologs included piscine-specific miRNAs such as miR-738, miR-722, miR-724, and miR-727-3p. The majority of miRNAs were associated with only one precursor gene, although several were associated with two precursors. Two let-7 family members, let-7c and let-7d, were each derived from four precursors.

miRNAs with the greatest increased expression included those with previously described effects that promote wound healing. miR-132-5p, miR-132-3p, miR-21, miR-

212-5p, miR-212-3p, and miR-31 all increased expression over 2.0-fold. miR-146a, a regulator of skin inflammation [78], and miR-19d-5p similarly increased expression over 2.0-fold. Three miRNAs (miR-132-3p, miR-21, miR-212-3p) increased expression by over 4.0-fold from each precursor. The piscine miR-738 increased expression by over 3.6-fold. Each precursor from let-7c and let-7d (four let-7 precursors in total) increased expression by over 1.6-fold. Of the nine precursors that decreased expression, there were three precursors that changed by approximately 1.0-fold or greater. This included two piscine miRNAs (miR-727-3p and miR-724). The two miRNAs with human orthologs that had the greatest magnitudes of differential expression were miR-489 and miR-92b-3p, which changed expression by 1.2- and 0.9-fold, respectively.

miRNA-mRNA interactome analysis

To create an interactome of anti-correlated interactions between miRNAs and mRNAs that we found in our data, we used BRM's miRNA Targets tool to generate a ranked list of high-confidence miRNA targets [69]. We sought to identify predicted interactions between miRNAs that increased expression and mRNAs that decreased expression (termed repressive interactions) and interactions of the inverse expression pattern (termed derepressive interactions). Of the four databases that BRM uses to generate target lists, only two (MicroCosm and TargetScan) were compatible with zebrafish data. MicroCosm [36] uses a p-value system to rank interactions, while TargetScan [29] uses a percentile system with higher scores indicating higher rankings. We considered interactions to be high confidence if they met one of three criteria: 1)

prediction by both databases, 2) prediction by MicroCosm with a score of $p < 0.01$; or 3) prediction by TargetScan with a weighted context++ score ≥ 50.

Using these parameters, we identified a large degree of multiplicity with a total of 4982 interactions. Of these, 3597 interactions were repressive while 1385 were derepressive. Among repressive interactions, there were 145 identified by both databases, while MicroCosm reported 193 and TargetScan reported 3259 interactions that were not commonly identified. Among derepressive interactions, there were 62 common to both databases, while MicroCosm and TargetScan identified 114 and 1209 that were not common, respectively. MicroCosm predicted interactions involving the same miRNAs as TargetScan, plus seven others. The data indicate strong multiplicity (number of targets per miRNA) and cooperativity (number of common targets). Given the vast number of interactions, we focused our analysis on those predicted by both databases (Tables 8-9) and some high-confidence interactions predicted by only one database.

miRNAs are predicted to target chromatin remodelers and developmental regulators

By generating miRNA-mRNA interactomes, we found several predicted interactions involving the developmental and regenerative signaling DEGs that were described above. Among repressive interactions (Figure 3), three Hox genes were predicted targets of highly upregulated miRNAs (*hoxd3a* by miR-132-p, *hoxa4a* by miR-21, and *hox3ca* by miR-223). In addition to *hoxd3a*, miR-132-3p was predicted to interact with multiple other developmental DEGs including *bmper*, *tgfb3*, *dll4*, *sox5*. Additional targets included the PRC1 subunit *cbx2* and the chromatin remodeler *prbm1*. miR-21 was

predicted to repress a validated human target, the tumor suppressor *pdcd4*, as well as an inhibitor of Wnt signaling, *wif1*. miR-223 was predicted to repress *sat1b*, a recruiter of chromatin remodelers, as well as repress *sox3* cooperatively with miR-722. miR-146a and miR-146b were predicted to cooperatively repress *eya4*, a putatively oncogenic phosphatase involved in regulating phosphorylation of the DNA repair histone H2ax [79]. miR-31 was predicted to target *fgfr*, *itgb1b.1*, *runx3*, as well as *arid6* in cooperation with miR-21.

There were fewer predicted derepressive interactions in our data and we observed little cooperativity between miRNAs (Figure 4). miR-489 was predicted to target the proteasome subunit *psmc2*, a key regulator of proteostasis affecting the cell cycle [80], as well as other enzymatic DEGs. miR-92b-3p was predicted to target the mitochondrial chaperone *hspa9*, which is required for fin regeneration [81]. Other predicted targets were the ribogenesis factor *bms1*, cathepsin L (*ctsla*), and twist neighbor (*twistnb*). Among the predicted targets of miR-727-3p were a subunit of a chaperone complex involved in telomere maintenance (*cct7*) [82], a Nodal signaling antagonist (*ncl1*), and a chemokine receptor involved in regulating angiogenesis (*cmklr1*) [83].

Single database predictions

We identified thousands of potential miRNA-mRNA interactions that passed our high confidence threshold in addition to those described above. Many of the target DEGs with the highest predicted interaction scores are involved in the upstream regenerative processes that we previously outlined. Here were briefly summarize these select, high-

ranked interactions (Table A.2) with a primary focus on miRNAs with the greatest

magnitude of differential expression.

Wnt signaling. miR-21, in addition to targeting *wif1*, was also predicted to target

other Wnt antagonists including the neurodevelopmental gene *ndrg2* as well as *dkk2*.

miR-132-3p was predicted to target *rspo1*, a positive regulator of Wnt. miR-146a and

miR-146b were predicted to cooperate in repression of positive Wnt regulators *dvl1b* and

dixdc1. Decreased expression of miR-92b-3p may be involved permitting expression of

csrp1a, which promotes cell motility in cooperation with noncanonical Wnt signaling

[84].

FGF signaling. miR-21 and miR-31 were predicted to cooperate in the repression

of *fgfr1b*, while miR-21 alone was predicted to target *fgfr1a*. Although we only

considered MicroCosm and TargetScan results, MiRTarBase (a database of validated

interactions) returned a single result of miR-21 interacting with *spry2* (not shown). miR-

132-3p was predicted to target the *fgf10b*. Notably, miR-724 was predicted to interact

with the upstream regenerative factor *fgf20a* with a TargetScan score of 100.

EGF signaling. miR-21 and miR-132-3p were predicted to cooperate in targeting

the tyrosine kinase *ptk2bb*, which is associated with Alzheimer's disease [85]. miR-21

was also predicted to target cd248a, while miR-132-3p was also predicted to target

efemp1, *tob1a*, and *scube1*.

TGF-β signaling. miR-132-5p and miR-132-3p were predicted to target *tgfb3* and *smad3a*, respectively. miR-92b-3p was precited to target *activin-βa* (*inhbaa*), and miR-489 was predicted to target *tgfb2*.

BMP signaling. miR-21 and miR-132-3p were respectively predicted to interact with the BMP signaling antagonists *bmper* and *nog1*. miR-489 was predicted to target *lemd3*, another negative regulator of BMP.

Hh signaling. Both miR-146a and miR-146b were predicted to cooperate in repressing the hedgehog signaling antagonist *hhip*.

IGF signaling. miR-21 was predicted to target *htra4*, while miR-132-3p was predicted to target *kazald3* and *igfbp2a*. miR-92b-3p was predicted to interact with the upstream ligand *igf2b*.

Chemokine signaling. *cxcl12a* was predicted to be cooperatively targeted by miR-31 and miR-132-3p.

Eph signaling. *eph3a* was predicted to be cooperatively targeted by miR-21 and miR-132-3p, while *eph4b* was predicted to be targeted by miR-31 and miR-132-3p.

SF signaling. Six semophorins were predicted to be regulated by miR-132-3p, miR-146a, miR-146b, miR-21, miR-31, and miR-92b-3p.

Histone and DNA modifiers. miR-21 and miR-31 were predicted to cooperatively repress *smarca2*, while miR-31 was also predicted to target *tox2*. miR-146a and miR-146b were predicted to cooperatively target *hdac5*. miR-489 was predicted to interact with *gatad1*, *prmt3*, and *topl1*, while miR-92b-3p was predicted to target *prmt1*.

Transcription factors. There were hundreds of notable predicted miRNA interactions with transcription factor transcripts. Some of these included: cooperative targeting of *dlx1a* by miR-21 and miR-31; cooperative targeting of *e2f3* by miR-489 and miR-92b-3p; targeting of *epas1* paralogs by miR-132-3p and miR-21; targeting of *foxm1, sall1b,* and *vezf1a* by miR-92b-3p; and targeting of *mycn*, *sall1a*, and *sp3a* by *miR-489*.

Miscellaneous signaling. This category includes DEGs related to GPCR and PTK signaling DEGs that did not fit into the above signaling categories. Some miRNA-GPCR transcript interactions included cooperative targeting of *adgrg1* by miR-21 and miR-31, as well as *eras* and *rala* by miR-489. PTK-related interactions included targeting of *aatkb* by miR-132-3p and *tie1* by miR-21.

Other growth factors, hormones, and cytokines. Some of the various predicted interactions of miRNAs with DEGs in this category included targeting of *dio1*, *il2rb*,

stat4, and *utsr2* by miR-132-3p; *ntf3* by miR-31; *ptn* by miR-21; and *m17* (*il6st*) by miR-489. The prostaglandin E2 receptor, *ptger1*, was predicted to be targeted by miR-132-3p.

Cell cycle and apoptosis. miR-21 was predicted to target *bnip3la*, while miR-132-3p was predicted to target *bnip3*. miR-31 was a predicted repressor of c*dc14ab*. miR-92b-3p was predicted to target *bub1bb*, *ccnjl*, and *cdk1*. miR-489 was predicted to target *cdk2*.

Proteostasis. The proteasome maturation protein (*pomp*) gene was precited to be targeted by miR-92b-3p. The ribogenesis factor *bop1* and the mitochondrial chaperone *hspa9* were predicted to be targeted by miR-489.

Extracellular matrix. miR-489 and miR-92b-3p were predicted to cooperatively target adam15 and respectively target *fn1a* and *fn1b*. miR-92b-3p was also predicted to target frem2a, itga5, and itgb8, while miR-489 was predicted to additionally target with the hyaluronan-interacting gene, hapln1a. Other hyaluronan-related genes, *bcan* and *itih5*, were predicted targets of mir-132-3p, as were *col8a2* and *tgfbi*. miR-31 was predicted to interact with *col11a1a*, *dpt*, *glipr2*, *itgb1a*, and *itgb1b.1*.

Discussion

Epimorphic regeneration involves a rapid shift from differentiated tissue to the multipotent blastema [10]. This involves quickly repressing transcriptional programs

involved in the maintenance of differentiated tissue. One way that cells achieve this is through globally repressing gene expression using chromatin modifiers such as the Polycomb repressive complex 2 (PCR2) [60]. Another way is through the rapid induction and depletion of microRNAs (miRNAs), which is required for epimorphic regeneration [86]. Here we performed parallel total RNA and small RNA sequencing using RNA on regenerate tissue from the same samples at 24 hours post-amputation (hpa), just prior to blastema formation. Our approach allowed for robust anti-correlation expression analysis and miRNA target prediction using the Bioinformatics Resource Manager (BRM) [69], which allows high-throughput miRNA target prediction using for miRNA databases (only MicroCosm and TargetScan were compatible with zebrafish data). Using this method, we were able to broadly characterize the transcriptional landscape to predict some of the most salient targets involved in blastema induction. Similar anti-correlated expression analyses have been highly successful in identifying miRNA-mRNA interactions [35, 47]. Filtering the differentially expression gene (DEG) list through two other age-based fin regeneration models increased the confidence in our results. We note that, for technical reasons, sample sizes differed between juvenile (n = 100) versus adult and geriatric (n = 10) cohorts. While analysis of the juvenile cohort may have more statistical power, our cohort comparisons were focused on DEGs that had false discovery rate-adjusted significance regardless of the magnitude of fold change. Other studies have utilized this comparative approach with smaller sample sizes even between different species [47].

Several of the miRNAs with the greatest changes in expression were those that have been previously identified during regeneration, such as miR-21 [87], miR-31[35],

miR-92b-3p [35], and miR-489 [88]. The full complement of their mRNA targets remains to be elucidated and are worth further investigation. Among the miRNAs with the greatest increase was miR-21, which is ubiquitous in regenerating tissue. Regarded as an oncomiR [89], it is believed to promote cellular stemness through targeting *tgfbr2* [47] and preventing apoptosis by targeting *pdcd4 [90]*. It likely serves a similar function in zebrafish. Another known target predicted target of miR-21 is *sprouty 2* (*spry2*) [91], an FGF signaling involved in regulating the epithelial-mesenchymal interactions during tooth [92] and lung [93] development. We identified *spry2* as having decreased expression in our data, and was the only interaction predicted by miRTarBase. Furthermore, we identified *wif1*, a Wnt signaling antagonist, as a high-confidence target of miR-21. These results indicate that miR-21 likely facilitate blastema induction by promoting signaling mediated by both *fgf20a* and *wnt10a*, which are two of the most upstream processes that initiate epimorphic regeneration.

While Wnt and FGF signaling ligands are highly expressed, we also observed decreased expression of genes that positively regulate their transduction. *rspo1*, which, promotes Wnt signaling, was predicted to be repressed by miR-132-3p. We previously reported that increased expression of *rspo1* mediated through the Aryl hydrocarbon receptor (AHR) caused inappropriate Wnt signaling and prevented blastema formation in zebrafish larvae [45]. It follows that these upstream signaling pathways must be tightly controlled for regeneration to proceed normally. miRNAs seem excellent candidates to fill this regulatory role. Additionally, miR-21 was predicted to cooperate with miR-31 in

repressing *fgfr1b*, suggesting that miR-21 may also contribute to balanced signaling to prevent inappropriate FGF signaling.

Both complementary mature miR-132s are newly described for blastema formation but have previously described roles in mammalian skin injury through its effect on inflammation [94] as well as epithelial-stromal interactions during mammary gland development [95]. Of these complementary miRNAs, miR-132-3p was predicted to target chromatin-modifying DEGs such as *cbx2* and *prbm1*, indicating an important role in defining the chromatin state of regenerate cells. It was also predicted to modulate ligands and antagonists of Notch, Transforming growth factor beta (TGF-β), Bone morphogenic protein (BMP), and Ephrin (Eph) signaling, suggesting it also is involved in tissue patterning during blastema formation. Another notable target of miR-132-3p was *nog1*, a BMP antagonist that decreased expression by over 5.6-fold. The induction of *bmp7a* along with evidence of mesenchymal Smad1/5/8 phosphorylation [17] suggests a key role for BMP signaling that miR-132-3p may facilitate.

miR-146a and miR-146b are also novel blastema miRNAs but have received much attention for their ability to promote healing by negatively regulating inflammation [78]. We predicted they cooperate to repress *eya4*, which itself is involved in chromatin remodeling to mediate innate immunity [79]. This could represent an avenue through which inflammation is modulated to promote blastema induction. Furthermore, their anti-inflammatory regulation is thought to prevent inflammation in endothelial cells through regulating Il-1β signaling [96]. Strong decreased expression of endothelin receptors, in addition to decreased expression of the endothelial transcription factors (TFs) *epas1a* and

epas1b which MetaCore identified in target enrichment analysis, underscores the rapid vascular dedifferentiation in blastema induction. This is further supported by induction of *vezf1a*, which is restricted to endothelial precursor cells [97]. miR-146a and miR-146b may contribute to vascular dedifferentiation through their cooperative effects on *eya4*.

Although there were fewer miRNAs that decreased expression and the fold changes were less robust, miRNA depletion is vital for epimorphic regeneration. Depletion of miRNAs at the onset of regeneration, including miR-92b-3p, was previously demonstrated to be an FGF receptor-dependent process [35]. miR-489 and miR-92b-3p were among those having the greatest decreased expression in our data. They were predicted to target key transcription factors including the oncogenic factors *mycn* and *foxm1* (respectively), which MetaCore identified as having target enrichment. *mycn* promotes cell cycle entry [98] as well as ribogenesis and protein synthesis [99], and its decreased expression is associated with cellular differentiation [100]. *foxm1* is highly expressed in embryonic tissue and promotes cell proliferation as well as fildelity of genetic replication [101]. FoxM1 can also "reprogram" cells through transcription of *hells*, which alters DNA methylation state into one that mimics head and neck squamous cell carcinoma [102]. We observed increased expression of *hells*, suggesting a similar mechanism during regeneration. FoxM1 also transcribes and forms a positive feedback loop with the Scatter factor (SF) receptor *met* [103], which also increased expression. During mouse embryogenesis, *met* facilitates movement of myogenic precursor cells to the limb bud [104]. *met* is typically expressed in epithelia [105], and consistent with its expression is the scattered, disorganized characteristic of the wound epidermis [106].

Regulation of semaphorins by miRNAs might also regulate the migration activity mediated by *met* [107]. Its expression during regeneration likely represents another mode of epithelial-mesenchymal signaling during blastema induction that requires further characterization [108]. Thus, FoxM1 may facilitate patterning of the blastema through multiple mechanisms, and its robust expression may depend on FGF-dependent depletion of miR-92b-3p.

miR-92-3p depletion may also facilitate induction of *sall1b*, another TF that is highly induced in blastemas [17]. miR-489 depletion may also facilitate increased expression of *sp3a*, a osteogenic TF [109] that MetaCore analysis indicated as having the greatest target enrichment. miR-489 was additionally predicted to target *coil*, indicating that it may be involved in the formation of Cajal bodies associated with telomere maintenance and self-renewal [110, 111]. Both miR-489 and miR-92b-3p may also promote extracellular matrix dynamics conducive to regeneration by derepression of fibronectin paralogs *fn1a* and *fn1b [112]*. miR-489 may promote dedifferentiation through its targeting of *eras*, a G protein-coupled receptor (GPCR) associated with growth in embryonic stem cells [113].

Notable among our findings was increased expression of the Hedgehog (Hh) ligand, *indian hedgehog b* (*ihhb*). While the role of Hh signaling (via *sonic hedgehog*) has been described for regenerative outgrowth, to our knowledge it has never been associated with blastema induction to our knowledge. During vertebrate development, *ihh* is expressed in epithelial tissues [114]. It activates Gli transcription factors post-translationally in mesenchyme through interactions with Patched/Smoothened receptors

[115]. Its role in epithelial-mesenchymal interactions during development suggests a similarly important function in blastema induction. A downstream target of Hh signaling is *foxm1* [116], suggesting that Hh signaling drives the FoxM1/Met positive feedback loop leading to robust proliferation of cells. miR-146a and miR-146b were predicted to cooperate in repressing the Hh antagonist, *hedgehog interacting protein* (*hhip*), adding yet another layer of complexity to miRNA control over epimorphic regeneration.

Conclusion

Using a parallel total RNA-small RNA sequencing approach, we identified novel miRNA-mRNA interactions as well as novel miRNAs involved in regeneration during blastema formation. In addition to discovering predicted interactions of miRNAs with transcripts involved in cellular differentiation, we also identified a predicted role for miRNAs in regulating the innate immune response. Thus, the role of miRNAs during regeneration is likely to control several facets of the regenerative response to injury, including attenuation of the inflammatory response. Our results provide several clear paths toward advancing our understanding of blastema induction. Some of these include demonstrating the necessity of the differential expression of particular miRNAs during regeneration; demonstrating *bona fide* interactions between miRNAs and their target mRNAs; and co-localization of transcripts involved in anti-correlated miRNA-mRNA expression patterns.

Funding

Table 2.1 Summary list RNA biotypes that commonly changed expression in regenerate fin tissue at 1 day post-amputation in Juvenile (4-week old), Adult (4-month old), and Geriatric (2+ year-old) zebrafish cohorts with a minimum absolute $\log_2$-fold change of 1.

Biotype	Increased expression	Decreased expression	Total
protein_coding	1929	2204	4133
lincRNA	34	59	93
processed_transcript	10	19	29
unprocessed_pseudogene	1	13	14
antisense_RNA	1	7	8
snoRNA	4	0	4
miRNA	2	0	2
Mt_tRNA	0	1	1
processed pseudogene	0	1	1
sense_overlapping	0	1	1
TEC	1	0	1
transcribed_unprocessed_pseudogene	0	1	1
Total	1982	2306	4288

Table 2.2 Top 10 significantly enriched Gene Ontology (GO) terms in genes that commonly increased expression in regenerate fin tissue at 1 day post-amputation in Juvenile (4-week old), Adult (4-month old, and Geriatric (2+ year-old) zebrafish cohorts with a minimum absolute $\log_2$-fold change of 1. Terms are ranked according to their fold enrichment.

PANTHER GO Biological Process	Fold enrichment	FDR p-values
meiotic sister chromatid cohesion, centromeric (GO:0051754)	4	4
positive regulation of RNA polymerase II transcriptional preinitiation complex assembly (GO:0045899)	5	5
centromeric sister chromatid cohesion (GO:0070601)	6	5
regulation of RNA polymerase II transcriptional preinitiation complex assembly (GO:0045898)	6	5
meiotic sister chromatid segregation (GO:0045144)	5	4
polyprenol metabolic process (GO:0016093)	5	4
meiotic sister chromatid cohesion (GO:0051177)	5	4
regulation of helicase activity (GO:0051095)	5	4
positive regulation of transcription initiation from RNA polymerase II promoter (GO:0060261)	7	5
anaphase-promoting complex-dependent catabolic process (GO:0031145)	7	5

Table 2.3 Top 10 significantly enriched Gene Ontology (GO) terms in genes that commonly decreased expression in regenerate fin tissue at 1 day post-amputation in Juvenile (4-week old), Adult (4-month old), and Geriatric (2+ year-old) zebrafish cohorts with a minimum absolute log2-fold change of 1. Terms are ranked according to their fold enrichment.

PANTHER GO Biological Process	Fold enrichment	FDR p-values
peptidyl-lysine oxidation (GO:0018057)	10	6
chondrocyte development involved in endochondral bone morphogenesis (GO:0003433)	20	10
growth plate cartilage chondrocyte morphogenesis (GO:0003429)	20	10
chondrocyte morphogenesis involved in endochondral bone morphogenesis (GO:0003414)	20	10
growth plate cartilage chondrocyte differentiation (GO:0003418)	21	10
chondrocyte differentiation involved in endochondral bone morphogenesis (GO:0003413)	21	10
chondrocyte morphogenesis (GO:0090171)	22	10
growth plate cartilage morphogenesis (GO:0003422)	24	10
growth plate cartilage development (GO:0003417)	26	10
endochondral bone growth (GO:0003416)	26	10

Table 2.4 All significantly enriched MetaCore process networks in genes that commonly increased expression in regenerate fin tissue at 1 day post-amputation in Juvenile (4-week old), Adult (4-month old, and Geriatric (2+ year-old) zebrafish cohorts with a minimum absolute $\log_2$-fold change of 1.

MetaCore Process networks	FDR p-value
Translation_Translation in mitochondria	1.144E-18
Cell cycle_Core	3.764E-13
Cell cycle_Mitosis	2.368E-09
Cell cycle_S phase	1.473E-08
Transcription_mRNA processing	2.174E-07
Cytoskeleton_Spindle microtubules	1.229E-06
Immune response_Antigen presentation	2.546E-06
Immune response_Phagosome in antigen presentation	2.223E-05
DNA damage_DBS repair	3.699E-04
Cell cycle_G2-M	7.136E-04
Proteolysis_Ubiquitin-proteasomal proteolysis	8.719E-04
Cell cycle_G1-S	8.103E-03
Protein folding_Folding in normal condition	1.085E-02
DNA damage_MMR repair	3.615E-02
Cell cycle_Meiosis	4.519E-02

Table 2.5. All significantly enriched MetaCore process networks in genes that commonly decreased expression in regenerate fin tissue at 1 day post-amputation in Juvenile (4-week old), Adult (4-month old), and Geriatric (2+ year-old) zebrafish cohorts with a minimum absolute log2-fold change of 1.

MetaCore Process networks	FDR p-value
Cell adhesion_Cell-matrix interactions	6.717E-12
Proteolysis_ECM remodeling	9.612E-05
Development_Cartilage development	2.124E-04
Development_Ossification and bone remodeling	2.178E-03
Cell adhesion_Platelet-endothelium-leucocyte interactions	7.971E-03
Proteolysis_Connective tissue degradation	1.973E-02

Table 2.6. Transcription factors identified by MetaCore as having target enrichment among genes that commonly changed expression in regenerate fin tissue at 1 day post-amputation in Juvenile (4-week old), Adult (4-month old), and Geriatric (2+ year-old) zebrafish cohorts with a minimum absolute log2-fold change of 1.

TF	Z-score	p-value
SP3	7.021	1.51E-11
MYCN	6.462	1.20E-10
JUN	6.393	4.40E-10
FOXM1	5.804	1.88E-08
NR3C1	4.829	1.57E-06
E2F3	4.631	7.54E-06
CEBPZ	4.343	3.49E-05
SOX9	3.836	8.93E-05
LHX2	3.827	1.51E-04
SMAD3	3.505	4.33E-04
EPAS1	3.382	7.27E-04
E2F8	3.319	1.66E-03
TCF7L2	3.301	6.13E-04
IRF8	3.057	1.80E-03
SP7	2.878	6.53E-03
SOX3	2.813	4.88E-03
ATF3	2.659	6.12E-03
DBP	2.619	6.22E-03

Table 2.7 Differentially expressed miRNAs that had increased expression in regenerate fin tissue at 1 day post-amputation in Juvenile (4-week old), Adult (4-month old), and Geriatric (2+ year-old) zebrafish cohorts.

miRNA (zebrafish)	miRNA (human)	precursor	log$_2$FC	FDR
dre-miR-132-5p	hsa-miR-132-5p	dre-mir-132-1	4.079857	9.56E-13
dre-miR-212-3p	hsa-miR-212-3p	dre-mir-212	4.078762	7.28E-10
		dre-mir-212-2	4.078762	7.28E-10
dre-miR-21	hsa-miR-21	dre-mir-21-1	4.011847	1.78E-08
		dre-mir-21-2	4.010892	1.78E-08
dre-miR-212-5p	hsa-miR-212-5p	dre-mir-212-2	3.777476	8.89E-10
		dre-mir-212	3.777476	8.89E-10
dre-miR-738		dre-mir-738	3.612288	1.75E-07
dre-miR-132-3p	hsa-miR-132-3p	dre-mir-132-2	3.386618	4.41E-10
		dre-mir-132-1	3.380934	4.29E-10
dre-miR-19d-5p		dre-mir-19d	2.782201	0.000175
dre-miR-31	hsa-miR-31	dre-mir-31	2.627882	8.13E-06
dre-miR-146a	hsa-miR-146a-5p	dre-mir-146a	2.224112	3.58E-06
dre-miR-125b-2-3p	hsa-miR-125b-2-3p	dre-mir-125b-2	1.965866	3.32E-05
dre-miR-223	hsa-miR-223-5p	dre-mir-223	1.91777	3.58E-06
dre-miR-25-5p	hsa-25-5p	dre-mir-25	1.877833	6.82E-08
dre-miR-146b	hsa-miR-146b-5p	dre-mir-146b	1.832812	3.58E-06
dre-miR-15a-3p	hsa-miR-15a-3p	dre-mir-15a-1	1.822516	8.54E-07
dre-let-7c-3p	hsa-let-7c-3p	dre-let-7d-1	1.669845	3.58E-06
		dre-let-7d-2	1.669845	3.58E-06
		dre-let-7c-1	1.649774	3.58E-06
		dre-let-7c-2	1.649774	3.58E-06
dre-let-7d-3p	hsa-let-7d-3p	dre-let-7d-1	1.669845	3.58E-06
		dre-let-7d-2	1.669845	3.58E-06
		dre-let-7c-1	1.649774	3.58E-06
		dre-let-7c-2	1.649774	3.58E-06
dre-miR-92a-2-5p	hsa-miR-92a-2-5p	dre-mir-92a-2	1.616941	1.46E-05
dre-miR-181a-3p	hsa-miR-181a-3p	dre-mir-181a-1	1.584647	1.23E-05
dre-miR-92a-5p		dre-mir-92a-1	1.57723	1.62E-06
dre-miR-18b-3p	hsa-miR-18b-3p	dre-mir-18b	1.283873	0.001407
dre-miR-200b-5p	hsa-miR-200b-5p	dre-mir-200b	1.170947	0.000365
dre-miR-1788-3p		dre-mir-1788	1.126458	0.00025
dre-miR-125b-3-3p		dre-mir-125b-3	1.103805	5.31E-05
dre-miR-221-5p	hsa-miR-221-5p	dre-mir-221	0.991074	0.000141
dre-miR-222a-3p		dre-mir-222a	0.986703	3.97E-05
dre-miR-221-3p	hsa-miR-221-3p	dre-mir-221	0.896528	1.96E-06
dre-miR-193a-3p	hsa-miR-193a-3p	dre-mir-193a-1	0.787613	0.021087
		dre-mir-193a-2	0.787613	0.021087
dre-miR-17a-3p		dre-mir-17a-1	0.78043	0.020498
dre-miR-17a-2-3p		dre-mir-17a-2	0.763227	0.026962
dre-miR-107a-5p		dre-mir-107a	0.714514	0.002185
dre-miR-722		dre-mir-722	0.648292	0.007507
dre-miR-200c-5p	hsa-miR-200c-5p	dre-mir-200c	0.648108	0.000323
dre-miR-20a-3p	hsa-miR-20a-3p	dre-mir-20a	0.62748	0.008327
dre-miR-20b-5p	hsa-miR-20b-5p	dre-mir-20b	0.339757	0.006294
dre-miR-17a-5p		dre-mir-17a-2	0.27675	0.020109
		dre-mir-17a-1	0.276689	0.020176

Table 2.8. Differentially expressed miRNAs that had decreased expression in regenerate fin tissue at 1 day post-amputation in Juvenile (4-week old), Adult (4-month old), and Geriatric (2+ year-old) zebrafish cohorts.

miRNA (zebrafish)	miRNA (human)	precursor	log$_2$FC	FDR
dre-miR-727-3p		dre-mir-727	-2.46078	0.000287
dre-miR-489	hsa-miR-489	dre-mir-489	-1.16533	0.000398
dre-miR-724		dre-mir-724	-0.9544	0.008517
dre-miR-92b-3p	hsa-miR-92b-3p	dre-mir-92b	-0.87067	3.30E-06
dre-miR-190a	hsa-miR-190a-5p	dre-mir-190a	-0.64161	0.001845
dre-miR-130c-5p		dre-mir-130c-1	-0.46982	0.003336
		dre-mir-130c-2	-0.47412	0.003657
dre-miR-145-5p	hsa-miR-145-5p	dre-mir-145	-0.41907	0.003657
dre-miR-203b-5p	hsa-miR-203b-5p	dre-mir-203b	-0.38751	0.00737
dre-miR-203a-5p	hsa-miR-203a-5p	dre-mir-203a	-0.37474	0.010173

Table 2.9. Anti-correlated miRNA-mRNA interactions between miRNAs that increased expression and mRNAs that decreased expression in regenerate fin tissue at 1 day post-amputation in Juvenile (4-week old), Adult (4-month old), and Geriatric (2+ year-old) zebrafish cohorts. MC: MicroCosm p-value score. TS: TargetScan percentile score.

miRNA	Symbol	MC	TS
miR-17a-5p	PDE3B	1.76E-09	76
miR-21	pdcd4b	1.07E-08	95
miR-132-3p	sox5	3.46E-07	95
miR-21	glcci1	7.94E-07	89
miR-222a-3p	nt5e	2.24E-05	83
miR-221-3p	slc6a4a	9.81E-05	90
miR-221-3p	npl	1.76E-04	83
miR-17a-5p	mmp2	1.98E-04	89
miR-20b-5p	pthlha	2.48E-04	99
miR-221-3p	lhx9	2.84E-04	61
miR-132-3p	pck1	2.86E-04	76
miR-146a	atp1a1b	2.95E-04	100
miR-146b	atp1a1b	2.95E-04	100
miR-132-3p	dll4	3.01E-04	72
miR-31	uros	3.72E-04	99
miR-146a	arhgap27l	4.17E-04	90
miR-146b	arhgap27l	4.17E-04	89
miR-222a-3p	ypel1	4.28E-04	85
miR-146a	scarb1	4.70E-04	66
miR-31	SLC9A3R2 (1 of many)	5.48E-04	85
miR-20b-5p	mmp2	7.60E-04	89
miR-146a	tspan12	7.60E-04	79
miR-146b	tspan12	7.60E-04	72
miR-17a-5p	map3k5	7.63E-04	88
miR-17a-5p	sar1ab	8.56E-04	80
miR-17a-5p	pthlha	9.03E-04	99
miR-146a	lamb4	9.35E-04	68
miR-146b	lamb4	9.35E-04	66
miR-20b-5p	sar1ab	1.35E-03	80
miR-132-3p	elovl6l	1.53E-03	99
miR-222a-3p	metrn	1.81E-03	73
miR-132-3p	cbx2	1.82E-03	74
miR-222a-3p	lhx9	1.84E-03	66
miR-17a-5p	sgcb	2.11E-03	97
miR-193a-3p	ache	2.79E-03	78
miR-31	arid6	2.92E-03	90
miR-223	hoxc3a	2.96E-03	63
miR-722	lrtm2a	3.17E-03	66
miR-20b-5p	sgcb	3.23E-03	97
miR-722	slc7a1	3.28E-03	25
miR-132-3p	adamts6	3.42E-03	72
miR-21	prss35	3.51E-03	83
miR-132-3p	eef2k	3.68E-03	98
miR-222a-3p	rnf11a	3.68E-03	81
miR-221-3p	pah	3.83E-03	87
miR-17a-5p	ache	3.94E-03	87
miR-17a-5p	ppm1k	4.19E-03	78
miR-722	rgn	4.32E-03	99
miR-146a	peli2	4.56E-03	61
miR-146b	peli2	4.56E-03	56
miR-221-3p	nt5e	4.71E-03	80
miR-222a-3p	slc6a4a	4.73E-03	88
miR-722	cpamd8	4.92E-03	46
miR-132-3p	bmper	4.96E-03	88
miR-20b-5p	map3k5	5.16E-03	90
miR-221-3p	metrn	5.23E-03	77
miR-146a	rab40c	5.28E-03	26
miR-146b	rab40c	5.28E-03	26
miR-222a-3p	pah	5.95E-03	84
miR-132-3p	pbrm1	5.96E-03	71

Table 2.9 (continued)

miRNA	Symbol	MC	TS
miR-221-3p	si:dkey-180p18.9	6.13E-03	93
miR-17a-5p	tgfbr2b	6.79E-03	97
miR-31	thy1	7.00E-03	97
miR-21	arid6	7.45E-03	90
miR-222a-3p	phf2	7.45E-03	54
miR-21	wif1	7.55E-03	89
miR-223	anos1a	7.59E-03	96
miR-31	itgb1b.1	7.61E-03	74
miR-193a-3p	satb2	7.87E-03	78
miR-21	ptgdsb.1	8.06E-03	88
miR-17a-5p	abat	8.51E-03	30
miR-17a-5p	nt5e	8.59E-03	90
miR-223	satb1b	8.66E-03	91
miR-146a	nrxn2a	8.78E-03	31
miR-146a	gpm6ba	8.84E-03	85
miR-31	cyp1c1	8.92E-03	91
miR-31	slc51a	8.96E-03	88
miR-146a	eya4	9.29E-03	89
miR-146b	eya4	9.29E-03	89
miR-146a	heca	9.77E-03	91
miR-132-3p	dcun1d4	1.17E-02	58
miR-223	vim	1.20E-02	97
miR-20b-5p	nt5e	1.46E-02	90
miR-193a-3p	zbtb47a	1.52E-02	26
miR-146b	gpm6ba	1.60E-02	85
miR-722	rem1	1.61E-02	96
miR-722	hoxc13a	1.72E-02	83
miR-132-3p	zgc:113229	1.79E-02	99
miR-132-3p	dhrs13b	1.97E-02	99
miR-222a-3p	pmaip1	1.99E-02	88
miR-146a	slco1c1	2.02E-02	87
miR-223	uros	2.04E-02	69
miR-146b	heca	2.17E-02	91
miR-21	zgc:77439	2.23E-02	79
miR-223	slc20a1a	2.30E-02	88
miR-132-3p	ampd2b	2.39E-02	58
miR-221-3p	gng7	2.40E-02	55
miR-221-3p	myom3	2.44E-02	90
miR-21	il15	2.49E-02	93
miR-221-3p	cdkn1bb	2.57E-02	99
miR-21	sesn1	2.57E-02	97
miR-722	slco1c1	2.59E-02	76
miR-20b-5p	ache	2.71E-02	87
miR-222a-3p	zfp36l2	2.75E-02	85
miR-132-3p	thy1	2.84E-02	90
miR-222a-3p	myom3	2.92E-02	89
miR-21	zgc:110353	2.94E-02	97
miR-722	spry2	2.98E-02	82
miR-17a-5p	apol1	2.98E-02	77
miR-223	mhc2dbb	3.21E-02	96
miR-193a-3p	xkrx	3.29E-02	41
miR-132-3p	arg2	3.32E-02	69
miR-223	itih5	3.34E-02	71
miR-132-3p	edil3a	3.40E-02	27
miR-132-3p	anxa13l	3.42E-02	98
miR-132-3p	il15	3.50E-02	98
miR-222a-3p	npl	3.51E-02	80
miR-132-3p	tgfb3	3.53E-02	87
miR-222a-3p	flot1a	3.54E-02	94
miR-722	cx34.4	3.59E-02	14

Table 2.9 (continued)

miRNA	Symbol	MC	TS
miR-146a	atf7b	3.64E-02	48
miR-738	rbl2	3.74E-02	70
miR-223	sox3	3.92E-02	92
miR-722	cpa6	3.97E-02	92
miR-17a-5p	elnb	4.09E-02	90
miR-31	fgfr4	4.20E-02	93
miR-132-3p	slc7a1	4.21E-02	28
miR-21	rgs4	4.22E-02	81
miR-222a-3p	gng7	4.25E-02	60
miR-21	hoxa4a	4.25E-02	91
miR-722	enpp5	4.29E-02	54
miR-146a	casz1	4.29E-02	73
miR-31	runx3	4.30E-02	70
miR-193a-3p	zgc:158868	4.38E-02	65
miR-132-3p	hoxd3a	4.40E-02	85
miR-193a-3p	alpl	4.55E-02	86
miR-20b-5p	sec14l1	4.67E-02	100
miR-20b-5p	CABZ01074398.1	4.67E-02	100
miR-20b-5p	zgc:153952	4.72E-02	83
miR-20b-5p	apol1	4.78E-02	77
miR-221-3p	nhsb	4.79E-02	87
miR-738	elnb	4.80E-02	87
miR-722	sox3	4.84E-02	98
miR-722	zgc:114045	4.84E-02	86
miR-20b-5p	elnb	4.98E-02	91

Table 2.10. Anti-correlated miRNA-mRNA interactions between miRNAs that decreased expression and mRNAs that increased expression in regenerate fin tissue at 1 day post-amputation in Juvenile (4-week old), Adult (4-month old), and Geriatric (2+ year-old) zebrafish cohorts. . MC: MicroCosm p-value score. TS: TargetScan percentile score.

miRNA	Symbol	MC	TS
miR-92b-3p	gap43	9.33E-05	100
miR-92b-3p	krt18	1.69E-02	80
miR-92b-3p	kif23	2.86E-02	95
miR-190a	mad2l1	4.80E-04	88
miR-724	cdc20	2.12E-03	69
miR-727-3p	cmklr1	4.85E-02	67
miR-727-3p	qars	1.73E-02	91
miR-145-5p	bcs1l	5.84E-03	84
miR-489	nol6	1.65E-03	99
miR-724	nol6	1.88E-03	92
miR-724	ppih	4.27E-03	98
miR-145-5p	wnt10a	8.36E-03	64
miR-724	anxa2a	2.96E-02	94
miR-145-5p	anxa2a	3.32E-04	64
miR-489	rtca	5.79E-03	72
miR-145-5p	utp15	5.37E-03	96
miR-92b-3p	smpd2b	3.52E-03	95
miR-145-5p	calr	1.24E-03	67
miR-92b-3p	mcfd2	2.27E-03	79
miR-92b-3p	cdt1	6.44E-05	99
miR-145-5p	ergic3	8.73E-03	88
miR-724	lap3	4.62E-02	51
miR-145-5p	apex1	4.35E-03	83
miR-92b-3p	dclre1a	8.03E-03	89
miR-92b-3p	g3bp1	1.59E-03	58
miR-92b-3p	bms1	4.18E-04	72
miR-92b-3p	hspa9	5.66E-03	93
miR-489	psmc2	2.93E-03	77
miR-92b-3p	mcm7	5.39E-03	69
miR-727-3p	ctsz	1.33E-03	92
miR-92b-3p	lrpap1	5.26E-04	84
miR-724	adrm1	3.41E-02	54
miR-145-5p	cd63	3.50E-02	88
miR-145-5p	cpsf3	4.80E-02	67
miR-727-3p	ctsla	6.33E-03	93
miR-92b-3p	ctsla	3.36E-02	84
miR-92b-3p	st6galnac	4.21E-02	98
miR-92b-3p	acat2	5.85E-04	93
miR-145-5p	pgd	2.76E-03	46
miR-489	alg3	8.15E-03	32
miR-727-3p	cct7	2.96E-02	88
miR-724	carm1	4.38E-02	57
miR-145-5p	ptp4a1	6.36E-03	82
miR-92b-3p	twistnb	7.09E-04	58
miR-489	cad	3.08E-04	83
miR-724	nono	3.92E-02	91
miR-727-3p	kdelr2b	1.33E-03	86
miR-724	tfg	4.27E-03	100
miR-145-5p	slc30a7	5.76E-04	84
miR-92b-3p	bet1	2.32E-02	97
miR-489	ndufab1b	1.50E-02	92
miR-190a	hsd17b10	2.23E-02	79
miR-727-3p	copb1	3.34E-03	30
miR-92b-3p	sec23ip	1.33E-02	81
miR-724	mad1l1	6.34E-03	48
miR-727-3p	wdr3	2.09E-03	89
miR-145-5p	clptm1	7.46E-05	72
miR-145-5p	aars	2.50E-02	79
miR-727-3p	ncl1	3.87E-02	87
miR-145-5p	hnrpl	2.83E-03	85
miR-92b-3p	rrbp1b	3.17E-02	88
miR-92b-3p	kifap3b	1.13E-03	96
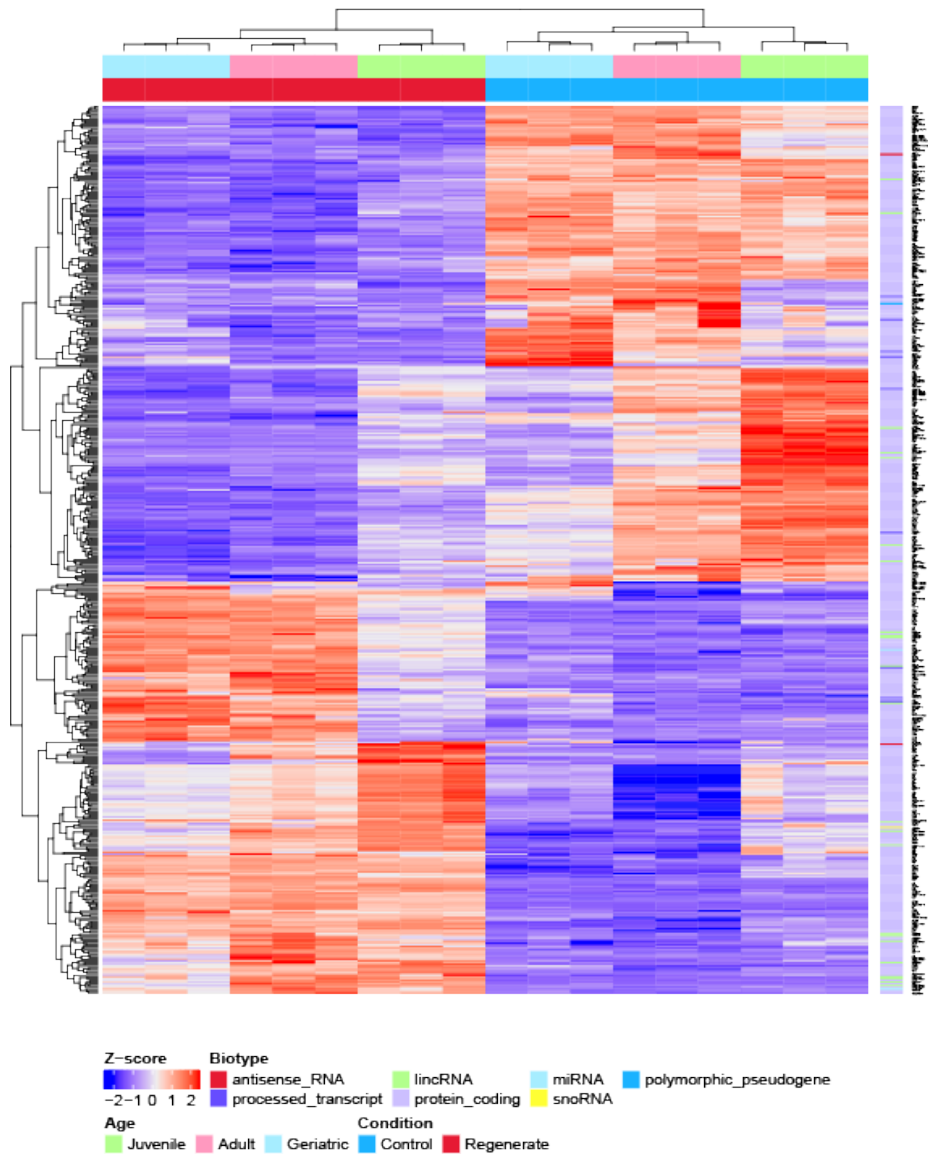
Figure 2.1. Unsupervised hierarchical clustering of the 500 genes with the greatest experimental magnitude change relative to the control group in regenerate fin tissue at 1 day post-amputation. Includes Juvenile (4-week old), Adult (4-month old) and Geriatric (2+ year-old) zebrafish cohorts. Color within the heat map indicates distance from average gene counts across all samples, with blue indicating lower than average expression and red indicating higher than average expression. Color above the heat map indicates age (Juvenile, Adult, or Geriatric) and condition (Control or Regenerate).
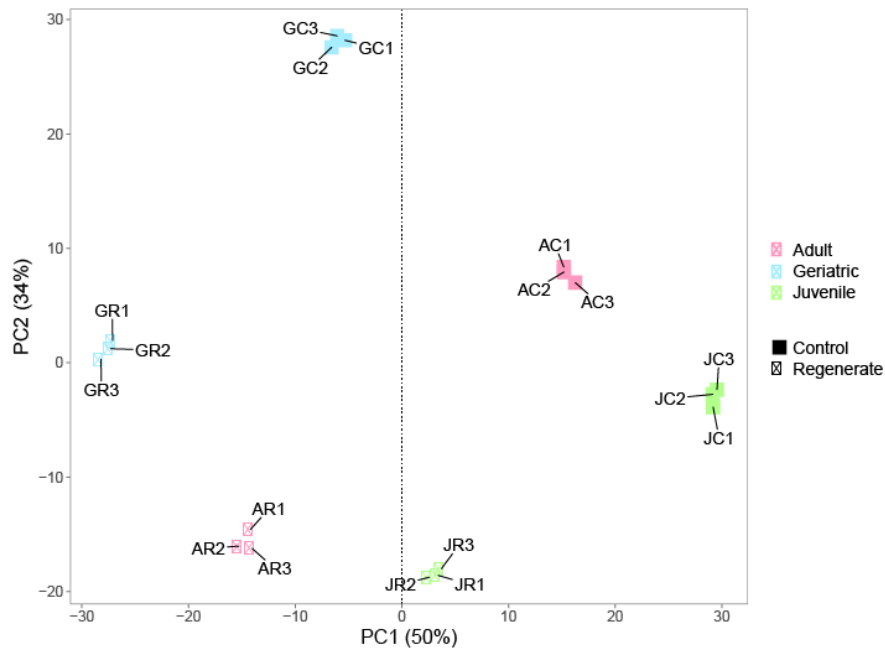
Figure 2.2. Principal components analysis of samples from Regenerate and Control fin tissue at 1 day post-amputation. Samples include Juvenile (4-week old), Adult (4-month old) and Geriatric (2+ year-old) zebrafish cohorts. Color represents age cohort while full vs. empty squares indicate Control vs. Regenerate conditions.
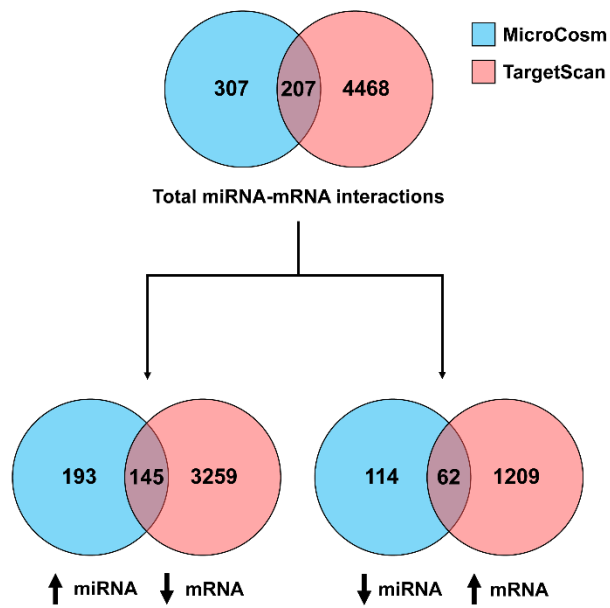
Figure 2.3. Venn diagram of the predicted miRNA-mRNA interactions. All interactions met one of three criteria: 1) prediction by both databases, 2) prediction by MicroCosm with a score of p < 0.01; or 3) prediction by TargetScan with a weighted context++ score ≥ 50.

Figure 2.4. Network of predicted miRNA-mRNA interactions between miRNAs that increased expression and mRNAs that decreased expression in regenerate fin tissue (1 day post-amputation). Only interactions that were predicted by both MicroCosm and TargetScan were included. Yellow indicates increased expression; blue indicated decreased expression.
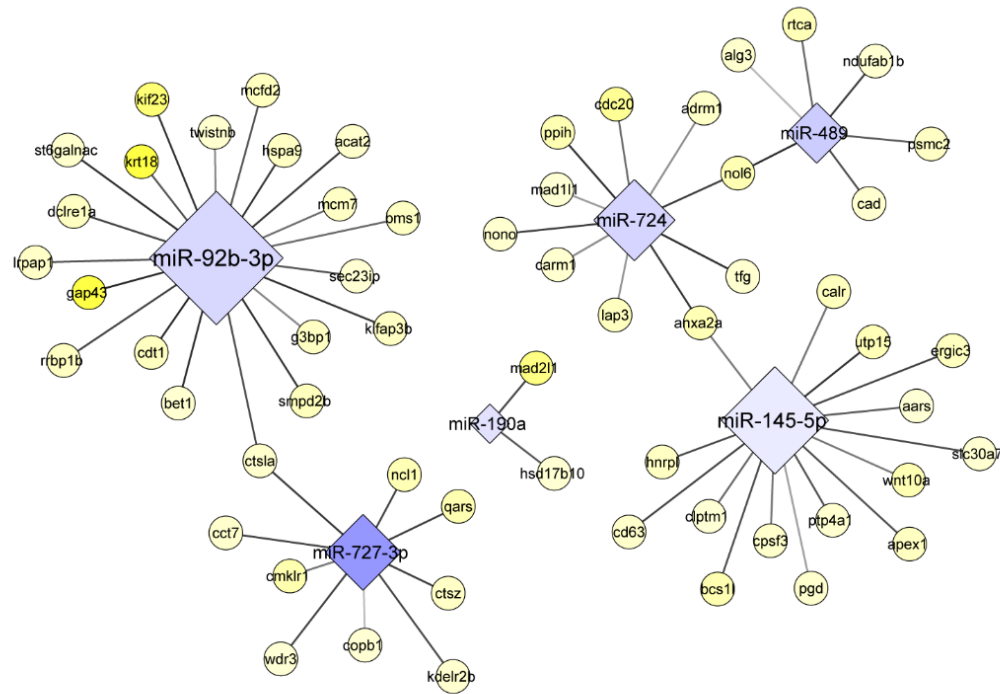
Figure 2.5. Network of predicted miRNA-mRNA interactions between miRNAs that decreased expression and mRNAs that increased expression in regenerate fin tissue (1 day post-amputation). Only interactions that were predicted by MicroCosm and TargetScan were included. Yellow indicates increased expression; blue indicated decreased expression.

CHAPTER 3 – GLUCOCORTICOID RECEPTOR-DEPENDENT INDUCTION OF CRIPTO-1 (ONE-EYED PINHEAD) INHIBITS ZEBRAFISH CAUDAL FIN REGENERATION

Michael A. Garland[†], Sumitra Sengupta[†], Lijoy K Mathew, Lisa Truong, Aldert H. Piersma, Jane La Du, and Robert L Tanguay

Abstract

We previously used a chemical genetics approach with the larval zebrafish to identify small molecule inhibitors of tissue regeneration. This led to the discovery that glucocorticoids (GC) block early stages of tissue regeneration by the inappropriate activation of the glucocorticoid receptor (GR). We performed a microarray analysis to identify the changes in gene expression associated with beclomethasone dipropionate (BDP) exposure during epimorphic fin regeneration. Oncofetal *cripto-1* showed > eight-fold increased expression in BDP-treated regenerates. We hypothesized that the mis-expression of *cripto-1* was essential for BDP to block regeneration. Expression of *cripto-1* was not elevated in GR morphants in the presence of BDP indicating that *cripto-1* induction was GR-dependent. Partial translational suppression of Cripto-1 in the presence of BDP restored tissue regeneration. Retinoic acid exposure prevented increased *cripto-1* expression and permitted regeneration in the presence of BDP. We demonstrated that BDP exposure increased *cripto-1* expression in mouse embryonic stem cells and that regulation of *cripto-1* by GCs is conserved in mammals.

Introduction

Some vertebrates, such as zebrafish (Danio rerio), have the capacity to fully restore complex tissues such as limbs, appendages, and organs in a process called epimorphic regeneration. Zebrafish caudal fin regeneration is a useful model of this

process for several reasons including the fast restoration of resected fin tissue (2-3 weeks), tractability of the zebrafish genome, high survival rate, and ease of husbandry, observation, and data acquisition [1, 2]. The deterministic mechanism(s) leading to epimorphic regeneration versus scarring is unknown, but it is understood that regeneration is divided into four major phases: wound healing, blastema formation, regenerative outgrowth, and termination. Each phase requires a tightly coordinated sequence of molecular events involving several signaling pathways. Fibroblast growth factor, Wnt, Activin, and others are among the first activated pathways following injury [1, 3]. During wound healing, epithelial cells migrate to form a wound epidermis from which the apical epithelial cap (AEC) is derived. Epithelial-mesenchymal interactions involving the AEC cause the underlying mesenchyme to dedifferentiate into a multipotent mass of cells called a blastema. Once established, the blastema undergoes rapid proliferation and differentiation to restore all damaged or lost structures. This process terminates once the damaged tissue is fully regenerated to its original structure [1].

Like adults, larval zebrafish also undergo epimorphic regeneration following fin amputation, and the molecular and structural processes are fundamentally similar [2, 4, 5]. Larval fin regeneration offers several advantages over adults, the most notable being rapid rate of regeneration (3 days), amenability to transient knockdown of gene expression using antisense repression, and small size of the organism. These characteristics make the larval regeneration model amenable to high-throughput screening of chemicals that can modulate epimorphic regeneration [6]. This chemical

genetics approach is guided by the hypothesis that compounds inhibiting regeneration do so by perturbing specific signaling events required for the regenerative process. This makes chemical genetics a useful tool for providing mechanistic insight into regeneration. Likewise, such a screen could also identify novel effects of chemicals within the regenerative framework [6]. For example, we previously used this larval regeneration approach to identify a novel link between Wnt and Aryl hydrocarbon receptor signaling via R-spondin 1 [7].

We previously performed a blinded screen of a 2000-member library of FDA-approved chemicals to identify compounds that modulate larval zebrafish fin regeneration [6]. Among the chemical classes inhibiting regeneration was glucocorticoids (GCs). GCs modulate several biological processes including energy metabolism, immunity, development, and wound healing [8-12]. Endogenous GCs such as cortisol and exogenous GCs such as dexamethasone act primarily through the glucocorticoid receptor (GR), a nuclear receptor that can potentially transactivate or transrepress thousands of genes [8].

Beclomethasone dipropionate (BDP) had the greatest potency to inhibit regeneration and this inhibition was GR-dependent. This BDP regenerative inhibition, however, was independent of anti-inflammatory effects on neutrophil and macrophage recruitment to the wound site. Finally, the inhibitory effects of BDP occurred within a narrow 4 h critical window following amputation indicating that the upstream GR target was present during the early stages of regeneration [6]. We performed microarray

analysis (unpublished until now) on regenerating caudal fins exposed to BDP and discovered that BDP increased the expression of the oncofetal gene *cripto-1*, also known as *one-eyed pinhead* (*oep*) in zebrafish and *teratoma-derived growth factor 1* (*tdgf1*) in humans. Using qRT-PCR, we found that GR activity (based on *anxa1b* repression) was similar between GCs that inhibited or permitted regeneration [13]. Those that inhibited regeneration had increased cripto-1 expression similar to BDP, whereas those that permitted regeneration did not increase cripto-1 expression.

In vertebrates, cripto-1 is a required co-factor in Nodal signaling as well as an antagonist of Activin signaling [14-16]. The importance of functional cripto-1 in zebrafish development was demonstrated in oep loss-of-function mutants, which developed cyclopia and died as larvae due to impaired Nodal signaling [17]. Antisense knockdown of *cripto-1* expression using translation-blocking MOs produced identical effects [18]. As an oncogene controlling cellular stemness, *cripto-1* is expressed in various cancer types [19] and modulation of its expression could be a desirable therapeutic strategy. In human and murine teratocarcinoma cells, *cripto-1* expression is downregulated in response to compounds that induce cellular differentiation such as retinoic acid [20], indicating that its expression can be influenced by chemical exposure.

Increased abundance of Cripto-1 in regenerating tissue could potentially interfere with critical regenerative pathways such as Activin [15]. We therefore hypothesized that BDP inhibited regeneration by modulating the expression of a gene (*cripto-1*) that other GCs do not. In the current study, we present the original microarray data demonstrating

that BDP increased the expression of *cripto-1*. We then conclusively demonstrate that a GR-dependent increase in *cripto-1* expression following BDP exposure was responsible for inhibited zebrafish fin regeneration, and that the effect of BDP on *cripto-1* expression is conserved in murine stem cells.

Materials and Methods

Ethics statement

All experiments were performed according to the recommendations in the Guide for the Care and Use of Laboratory Animals of the National Institutes of Health. The Oregon State University Institutional Animal Care and Use Committee reviewed and approved the animal care and use protocols (internal approval number 3903). Tricaine mesylate (MS-222) was used to anesthetize animals during the amputation procedures, and every effort was implemented to curtail pain and suffering.

Chemical exposures

All chemical exposures started at 2 days post-fertilization (dpf) immediately following fin amputation. Static exposure to beclomethasone dipropionate (BDP) (Sigma; $\geq$ 99% pure) was performed at a final concentration of 1 µM using 0.1% DMSO (vehicle). Static exposure to SB431542 (Sigma; $\geq$ 98% pure) was performed at a final concentration of 100 µM. Others have reported the use of < 100 µM SB431542 [3] in adult zebrafish and our most recent data (not shown) indicate that 50 µM is sufficient to

inhibit fin regeneration in the larval model. Exposure to all-trans retinoic acid (RA) (Sigma; $\geq$ 98%) was performed at a concentration of 0.1 µM for 8 h followed by static co-exposure to a lower RA concentration of 0.01 µM as well as BDP at a final concentration of 1 µM. Dimethyl sulfoxide (DMSO) was used to prepare all chemical stocks.

Zebrafish embryos and larvae

Standard husbandry procedures were used for all embryos [21]. Microarray experiments were performed using AB strain embryos, while Tropical 5D strain embryos were used to validate the response to beclomethasone dipropionate (BDP) in subsequent experiments. Excluding microarray and qRT-PCR procedures (described below), a sample size of n = 12 was used for all experiments. Caudal fin amputations were performed according to previously described procedures [6, 22, 23].

Fin RNA isolation

Larvae were subject to caudal fin amputation at 2 dpf and were immediately exposed to either 1 µM BDP or vehicle control (0.1% DMSO) as described above. The regenerating fin tissues were amputated a second time at 24 hours post-amputation (hpa) and collected for total RNA extraction using the RNAqueous Micro kit (Ambion). Each biological replicate consisted of pooled fin tissue from 150 larvae, and each treatment consisted of three replicates. The quality and quantity of isolated total RNA was determined using UV absorbance analysis. Electropherogram patterns were analyzed for

degradation and ribosomal RNA abundance using the 2100 Bioanalyzer and RNA 6000

Nano chips (Agilent Technologies).

Affymetrix microarray processing

Microarray preparation and processing were performed for the Affymetrix

platform at the Center for Genome Research and Biocomputing (CGRB), Oregon State

University. Single-stranded cDNA was synthesized using 100 ng total RNA from larval

regenerating fin tissue (AB strain) with Superscript II reverse transcriptase and T7-

(dT)24 primer (Invitrogen). A second round of cDNA synthesis was performed to

generate double-stranded cDNA. This cDNA template was used for generating

biotinylated cRNA using biotin-conjugated pseudouridine and T7 polymerase

(Affymetrix). Following quantification, 10 µg of the purified and fragmented biotinylated

cRNA was hybridized to zebrafish genome arrays (Zebrafish430_2) as specified in the

Affymetrix GeneChip Expression Analysis Technical Manual (7010201 Rev.5).

Affymetrix Scanner 3000 was used to scan arrays. Each array was visualized to screen

for non-specific signals from debris, scratches, or other artefacts. Microarray experiments

were certified under Minimum Information About a Microarray Experiment (MIAME)

standards.

Genespring software (Agilent Technologies) was used to analyze Affymetrix CEL

files generated from the microarray. Background signal was removed using gene chip-

robust multiarray processing. Each transcript was normalized based on median signal

thus allowing comparisons to be made between arrays on a relative scale for each gene.

To identify significant ($p < 0.05$) differential expression of genes following BDP exposure, one-way analysis of variance (ANOVA) assuming equal variance was performed comparing BDP- and DMSO-treated experimental groups. Further analysis focused primarily on genes that had differential expression of at least 2-fold. These genes were annotated by comparing sequence similarity of the respective Affymetrix probe set with known mammalian proteins based on the Sanger database (http://www.sanger.ac.uk/Projects/D_rerio/). Annotation was confirmed using the Genbank and Ensembl (http://uswest.ensembl.org/Danio_rerio/Info/Index) databases. Raw data were uploaded to the National Center for Biotechnology Information (NCBI) Gene Expression Omnibus (GEO) under the accession number GSE10766. A heatmap of bi-hierarchical clusters were generated using MultiExperiment Viewer (MEV) from which a gene list was created. Human orthologs of these genes were identified using ZFIN (https://zfin.org/) and Ensembl databases.

Quantitative real time reverse transcriptase polymerase chain reaction (qRT PCR)

As previously described, total RNA was isolated from larval regenerating fin tissue exposed to either 1 µM BDP or 0.1% DMSO. Biological replicates consisted of pooled fin samples of n = 60 with three replicates per experimental group. cDNA was generated from 1 µg total RNA using Superscript II (Life Technologies) and oligo(dT) primers. qRT-PCR was performed using gene-specific primers (Table B.6) in the Opticon 2 real time PCR detection system (MJ Research) with the SYBR green qPCR kit (Finnzymes). Samples were normalized to endogenous β-actin quantity. Formation of the anticipated PCR products was verified using agarose gel electrophoresis and melt curve

analysis. Sigmastat software (Systat Software) was used to identify statistically
significant differences in mRNA abundance by one-way ANOVA with Tukey's post-hoc
test ($p < 0.05$) on log10-transformed data.

Oligonucleotides

Primers were designed according to Affymetrix probe target sequences and are
listed in Table B.6. Forward and antisense reverse primers are prefixed with F and R,
respectively.

In situ hybridization

Localization of transcripts within larvae at 24 hpa was performed using in situ
hybridization according to published methods. Probes for dlx5a, mvp, smarca4, and ilf2
were generously gifted by Atsushi Kawakami (Tokyo Institute of Technology,
Yokahama, Japan).

Morpholinos

Knockdown of Cripto-1 and the glucocorticoid receptor (GR) was performed
using morpholino oligos (MOs) (Gene Tools) that blocked the translation start site of
cripto-1 and the splice junction of exons 7 and 8 of the GR. Both the cripto-1 MO (5'
GCCAATAAACTCCAAAACAACTCGA 3') [18] and the GR MO (5' -
CGGAACCCTAAAATACATGAAGCAG - 3') [6] were fluorescein tagged and targeted
zebrafish-specific transcript sequences. MO controls consisted of a standard MO control
sequence (5' CTCTTACCTCAGTTACAATTTATA 3'). MOs were reconstituted to a
stock concentration of 3 mM in 1x Danieau's solution (58 mM NaCl, 0.7 mM KCl, 0.4

mM MgSO4, 0.6 mM Ca(NO3)2, 5 mM HEPES, pH 7.6). 1-4 cell stage embryos were injected with either 1.2 mM cripto-1 MO or 3 mM GR MO, and controls were injected with a matching concentration of standard control MO. Uniform distribution of morpholino was evaluated at 1 dpf by screening for fluorescence using a GFP filter. Morphant larvae underwent caudal fin amputation as previously described and then were statically exposed to 1 µM BDP or 0.1% DMSO. Larvae were grown out to 3 days post-amputation (dpa) as previously described in standard regeneration protocols [6].

Embryonic stem cell (eSC) treatment

Murine D3 embryonic stem cells (eSCs) (ATCC, Rockville, MD) were sustained in Dulbecco's modified Eagle's medium (Invitrogen, Breda, The Netherlands) at 37°C and 5% CO2. Cells were routinely subcultured every 2-3 days. Medium was supplemented with 20% heat inactivated fetal calf serum (Hyclone, Thermo-Fisher Scientific, Etten-Leur, The Netherlands), 2 mM glutamine (Invitrogen), 50 U/ml penicillin (Invitrogen), 50 µg/ml streptomycin (Invitrogen), 1% non-essential amino acids (Invitrogen), and 0.1 mM β-mercaptoethanol (Sigma-Aldrich, Zwijndrecht, The Netherlands). Pluripotency was maintained by addition of murine leukemia inhibitory factor (mLIF) (Chemicon, Amsterdam, The Netherlands) to cell cultures at a final concentration of 1000 U/mL [24]. D3 eSCs were induced to differentiate into cardiac cells using routine culture medium (without mLIF) as previously described. On culture day 0, 20 µL of eSC suspension (3.75×10^4 cells/mL) was translocated to the inner side of the lid of a 10 cm Petri dish (Greiner) containing 5 mL of PBS. eSCs were incubated in a humidified atmosphere at 37°C and 5% CO2. The resultant embryoid bodies (EBs)

were transferred to bacteriological Petri dishes (Greiner). The differentiation cultures were exposed from culture day 3 onward to BDP and retinoic acid (Fluka, Buchs, Switzerland). Two parallel cultures were performed for each of the compounds. After 24 hours of exposure (culture day 4), EBs from one culture were collected and directly stored in RNA Protect at -20°C to stabilize RNA (Qiagen, Venlo, The Netherlands).

Promoter analysis

The promoters of zebrafish, mouse, and human cripto-1 were analyzed for transcription factor binding sites using MatInspector release professional 8.4.1 (Genomatix Software Suite v3.10) [25]. The genomic region 3000 bp upstream of the zebrafish (GRCz11), mouse (GRCm38.p6), and human (GRCh38.p12) cripto-1 transcriptional start sites were retrieved using Ensembl (release 95). These sequences were input into MatInspector and analyzed for general core promoter element and vertebrate element matrices from Matrix Library 11.0. The core/matrix similarity thresholds were set at 0.75/optimized.

Results

Gene expression analysis identified cripto-1 as a potential GR target in regenerating tissue.

To identify the early gene expression changes associated with the inhibition, we performed global gene expression analysis in the regenerating fin tissue exposed to

vehicle (0.1% DMSO) or 1 µM BDP. Only genes that were at least 2-fold differentially expressed in comparison to the control were considered (Fig. 3.1).

The heat map illustrated two major clusters of differentially expressed mRNAs. Statistical significance determined by one-way ANOVA revealed 169 transcripts with greater than a 2-fold change (p < 0.05) (Table B.1). These transcripts were analyzed based on sequence homology and further grouped by function (Table B1). Most of the transcripts were involved in wound healing, extracellular matrix (ECM) remodeling and metabolism. Other known GR target genes such as gilz [26] and fkbp506 [27] were also significantly affected (Fig. 3.2). Notably, cripto-1 was expressed 8.5-fold higher in the regenerating fin tissue upon BDP exposure (Table B.1). qRT-PCR analysis confirmed this induction in the regenerating fin tissue as well as in the whole embryo (Fig. 3.2).

Activin signaling is important for larval caudal fin regeneration.

As a first step to understand the downstream effectors of activated GR, we explored the role of Activin signaling specifically for larval tissue regeneration. SB431542 is a specific inhibitor of endogenous Activin and Transforming growth factor beta (TGF-β) signaling [117-119]. Exposure of amputated larvae to 100 µM SB431542 from 0 to 72 hours post-amputation (hpa) completely impaired regeneration producing the characteristic "V" shape observed in BDP-exposed larvae (Fig. 3.3a). Regeneration was characterized by the expression of specific transcripts in the wound epithelium and blastema. Comparative *in situ* analysis between BDP- and SB431542-exposed fish revealed loss of *dlx5a* expression in the wound epithelium, signifying absence of apical

epithelial cap [17, 120]. Moreover, the expression of *raldh2*, *mvp*, *junbl*, *smarca4*, *wnt10a*, and *ilf2* in the blastemal cells were similarly misexpressed in BDP- and SB431542-exposed larvae compared to control animals. Exposure to SB431542 did not change *cripto-1* expression (Fig. 3c).

GR-mediated misregulation of cripto-1 is required for inhibition of regeneration.

An initial goal was to determine if *cripto-1* induction is GR dependent. Quantitative analysis of *cripto-1* transcript in GR-MO injected larvae (morphants) exposed to BDP showed significantly reduced *cripto-1* expression compared to control morphants exposed to BDP (Fig. 3.4a). When BDP exposure was initiated immediately after amputation (0 hpa), *cripto-1* expression was significantly induced by 1 dpa. When BDP exposure was initiated after the 4-hour window (4 hpa), *cripto-1* expression was not induced by 1 dpa (Fig 3.4b).

Cripto-1 is required for the BDP-inhibition of fin regeneration.

To determine the role of *cripto-1* in regeneration, we utilized a *cripto-1* translation blocking morpholino. When Cripto-1 expression was completely repressed, larvae exhibited the one eyed pinhead phenotype (Fig. 3.5a), and lethality by 5 dpf (days post fertilization) [121]. To avoid lethality, we injected 2-4 cell-staged embryos with reduced volumes of fluorescein tagged morpholino. The morphants were screened for uniform fluorescence at 24 hpf, and both control and *cripto-1* morphants were exposed to vehicle and BDP following amputation at 2 dpf. The transient antisense repression allowed us to avoid lethality and show that the regenerative response was completely

abrogated in control morphants exposed to BDP. *cripto-1* morphants exposed only to vehicle were able to regenerate except for the presence of a characteristic notch on the fin (Fig. 3.5b). In nearly 80% of the *cripto-1* morphants exposed to BDP, regeneration progressed similar to the untreated control larvae (Fig. 3.5b). BDP exposure did not block regeneration when Cripto-1 levels were repressed.

Suppression of cripto-1 by retinoic acid rescues BDP-inhibited regeneration.

We used RA treatment to transiently suppress *cripto-1* expression. Analysis of *cripto-1* expression in whole embryos exposed to 0.1 and 0.01 µM RA at 1 dpa, revealed concentration-dependent suppression of *cripto-1* expression (Fig. 3.6a). Co-exposure to BDP and 0.01 µM RA did not rescue regeneration. An extended exposure to RA > 0.01 µM inhibited regeneration (data not shown). Pre-exposure of 2 dpf larvae to 0.1 µM RA for 8 hours prior to amputation, then co-exposure to BDP and 0.01 µM RA post-amputation was tested. RA pre-exposure alone did not affect regeneration, but RA pre-exposure followed by co-exposure to 0.01 µM RA during the BDP treatment rescued regeneration in approximately 75% of amputated larvae. RA exposure reduced BDP-induced *cripto-1* expression down to the baseline level of vehicle control larvae (Fig. 3.6b). The presence of *dlx5a* and *junbl* in co-exposed larvae suggested normal regenerative signaling (Fig. 3.6c), and the animals completed fin regeneration similar to the controls (Fig. 3.6d).

BDP induces cripto-1 expression in mouse embryonic stem cells.

To understand whether the regulatory role of GR activation is conserved in other biological systems, we analyzed the expression of *cripto-1* in mouse embryonic stem cells (eSCs). BDP exposure at 1 μM for 24 h induced *cripto-1* expression in differentiating mouse eSCs, indicating that activated GR can modulate *cripto-1* expression across species (Fig. 3.7). We also observed RA suppression of *cripto-1* expression in mouse eSCs.

To identify possible conserved transcriptional mechanisms of *cripto-1* induction, we performed promoter analysis of the zebrafish, mouse, and human *cripto-1* promoters 3000 bp upstream of the transcriptional start site. Using a list (Table B.2) of differentially expressed transcription factors (TFs) from the microarray data plus the GR, we searched a database of predicted response elements in the zebrafish, mouse, and human promoter regions. Only the TFs having predicted response elements in all three species were considered for further analysis (Tables S3-S5). We found predicted repressive glucocorticoid response elements (GREs) in the *cripto-1* promoter. We also identified potential binding sites for ISL1, HMX3, POU3F3, MYT1, MAFK, EN1, and MYBL2.

Discussion

Understanding tissue regeneration requires having the critical signaling targets in hand to experimentally manipulate and assemble a mechanism. In a microarray analysis, we found that exposure to beclomethasone dipropionate (BDP) severely inhibited

zebrafish's natural capacity for regeneration of amputated caudal fin tissue, and that the inhibition was closely accompanied by strong induction of the *cripto-1* transcript. This induction following BDP exposure was also observed in a separate study [122]. Cripto-1 is an evolutionarily conserved regulator of cell function and proliferation [123]. Preventing *cripto-1* induction with either retinoic acid (RA) exposure or antisense knockdown rescued fin regeneration in the presence of BDP. This demonstrated that induction of *cripto-1* was required for BDP to block fin regeneration. The regenerative block and increased expression of *cripto-1* were glucocorticoid receptor (GR)-dependent, indicating that modulation of *cripto-1* expression occurred downstream of the GR. *cripto-1* was induced when BDP exposure occurred within 4 h of fin amputation, correlating with the 4 h critical window previously established for BDP-mediated disruption of regeneration [40]. These results, along with previous work, demonstrate a novel link between the GR and *cripto-1* induction, and that inappropriate activation of the GR blocks fin regeneration in a *cripto-1*-dependent manner. Importantly, we further demonstrated that glucocorticoid (GC)-mediated expression of *cripto-1* is conserved in mammals.

During vertebrate development, Cripto-1 functions primarily as a required co-factor for Transforming growth factor beta (TGF-β) signaling, specifically for Nodal signaling [124]. During gastrulation, Cripto-1-dependent Nodal signaling at the primitive streak facilitates epithelial-to-mesenchymal transition (EMT) and regulates cell migration, allowing the embryo to form multiple tissue layers [125, 126]. As an oncofetal gene, *cripto-1* is expressed during development but largely absent in adult tissues except

during tumorigenesis or carcinogenesis [123]. It is overexpressed in triple negative breast cancer, colon carcinoma, squamous cell carcinoma, lung adenocarcinoma among several others [127-130]. Cripto-1 promotes tumor cell survival, proliferation, and migration by interacting with proteins that affect signaling pathways beyond TGF-β [131]. There is no evidence to our knowledge that *cripto-1* expression is endogenously modulated by the GR during development or carcinogenesis.

We showed that *cripto-1* expression increased in larval fin tissue if zebrafish were exposed to BDP within four hours of amputation. After 4 hpf, the fin tissue may undergo a change that no longer supports GR-dependent induction of *cripto-1*. Notably, the lack of increased *dlx5a* expression demonstrated that BDP exposure prevented formation of the apical epithelial cap (AEC), despite formation of the wound epithelium [40]. Several signaling pathways are active prior to and after AEC formation including Fibroblast growth factor (FGF), Wnt, RA, and Activin/Transforming growth factor beta (TGF-β) [15, 16, 132]. Previous work in adult zebrafish has shown that epimorphic fin regeneration requires TGF-β/Activin signaling within the first day of regeneration [16]. By inhibiting type I receptors using SB431541, we demonstrated that TGF-β/Activin signaling is also required during the early stages of larval fin regeneration.

Given our results and Cripto-1's known role of antagonizing Activin, we conjectured that increased expression of *cripto-1* following BDP exposure prevents fin regeneration by a similar mechanism. The identical expression patterns of AEC and blastema markers in the fin tissue exposed to BDP and SB431542 suggested disrupted

Activin signaling in BDP-exposed larvae. Since Cripto-1 suppressed Activin signaling in multiple cell types by binding Activin ligands at the protein level [133-137], we expect that inhibition of Activin signaling has no effect on *cripto-1* transcription. This was demonstrated to be the case in our model, indicating that *cripto-1* is upstream of Activin signaling.

Cripto-1 is a pleiotropic protein that could also interfere with other signaling pathways including Wnt (canonical and planar cell polarity pathways) [138, 139], c-Src [140], and Notch [141]. Graphical summaries of these interactions can be found in reviews such as Strizzi et al. (2005) [139], Nagaoka et al. (2012) [142], and Klauzinska et al. (2014) [131]. Additionally, a recent proteomic analysis of the Cripto-1 interactome identified 51 Cripto-1 binding proteins from human epithelial cells including regulators of extracellular exosomes, myosin II complexes, and the cytoskeleton. The myosin II activity was shown to regulate subcellular localization of Cripto-1 in epithelial and mesenchymal stem cell populations and to function cooperatively with zebrafish Cripto-1 to promote caudal fin regeneration [143]. Although we were unable to localize *cripto-1* expression in the fin, these new data suggest that Cripto-1 may be expressed in both epithelial and mesenchymal cells following BDP exposure. Furthermore, their study identified an intrinsic role for increased *cripto-1* expression during the outgrowth phase of regeneration, which may explain why *oep* morphants had notched fins following regeneration. The impacts of increased *cripto-1* expression during the initiation of fin regeneration appear quite complex.

Since RA co-exposure rescues fin regeneration, and *raldh2* is not detectable by ISH at 1 dpa following BDP exposure, Cripto-1 likely acts upstream of *raldh2* induction and normal RA signaling [20]. We did not observe any chemical precipitation during BDP and RA co-exposures. Since RA concentrations greater than 0.01 μM during the pre-exposure did not result in a higher incidence of regeneration, the uptake of BDP by the animals was likely not affected by the presence of RA in the media. In human teratocarcinoma cells, the addition of exogenous RA to cell culture induces germ cell nuclear factor which directly represses *cripto-1* expression [144]. It is possible that this mechanism occurs in the regenerating zebrafish fin during BDP and RA co-exposure. However, RA co-exposure also rescues regeneration when fish are exposed to FGF and ERK1/2 signaling inhibitors [20]. Its rescuing effect on regeneration might therefore not be specific for its effect on *cripto-1* induction. Another possibility is that RA co-exposure could be "overriding" Cripto-1's effect on upstream pathways by stimulating downstream signaling events mediated by RA.

We show conclusively for the first time that activation of the GR by BDP (and other specific GCs) is sufficient to increase *cripto-1* expression to levels that exert physiological consequence *in vivo*. *cripto-1* induction would seem an important conserved signaling step between taxa. We note that differences have been observed in xenobiotic responses between murine and non-human primate eSCs [145], indicating that further work is needed to demonstrate a link between *cripto-1* induction and the GR in humans. If this response is conserved in humans, it would have implications for therapeutic GC treatment whether for immunosuppression or cancer treatment.

Modulation of Cripto-1 expression via the GR could be useful in the laboratory setting. For example, *cripto-1* induction promotes cardiomyogenesis whereas suppression promotes neural differentiation [146, 147]. Certain GCs may be useful for directing cell fate commitment *in vitro*. Considering the importance of Cripto-1 in ES cells, development, cancer, and regenerative medicine, GCs have the potential to offer novel modes of manipulating Cripto-1 for therapeutic benefit.
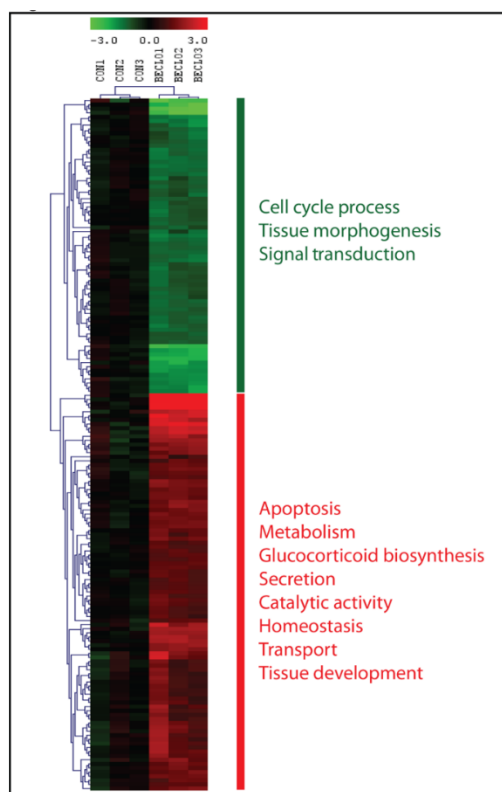
Figure 3.1 Gene expression changes in larval regenerating fin tissue after exposure to BDP. Heat map demonstrates bi-hierarchical clustering of 169 statistically significant (p < 0.05) transcripts that are at least two-fold differentially expressed.
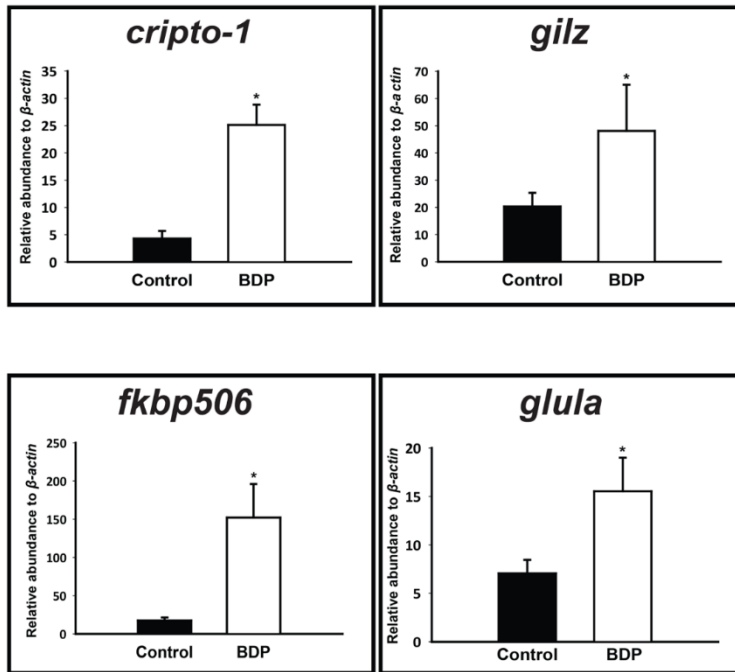
Figure 3.2 qRT-PCR analysis of BDP-enhanced transcripts in DMSO or BDP treated larval fin tissue at 1 dpa. The expression of cripto-1, gilz, fkbp506, and glula following beclomethasone dipropionate (BDP) exposure at one day post-amputation (dpa) are illustrated as relative abundance to β-actin mRNA levels. Gene specific primers were used to quantify mRNAs using real time qRT-PCR. Data presented as mean ± SEM (n = 3). One-way ANOVA was conducted to determine differences in expression. Asterisks indicate significant difference between vehicle and treatment ($p < 0.05$).
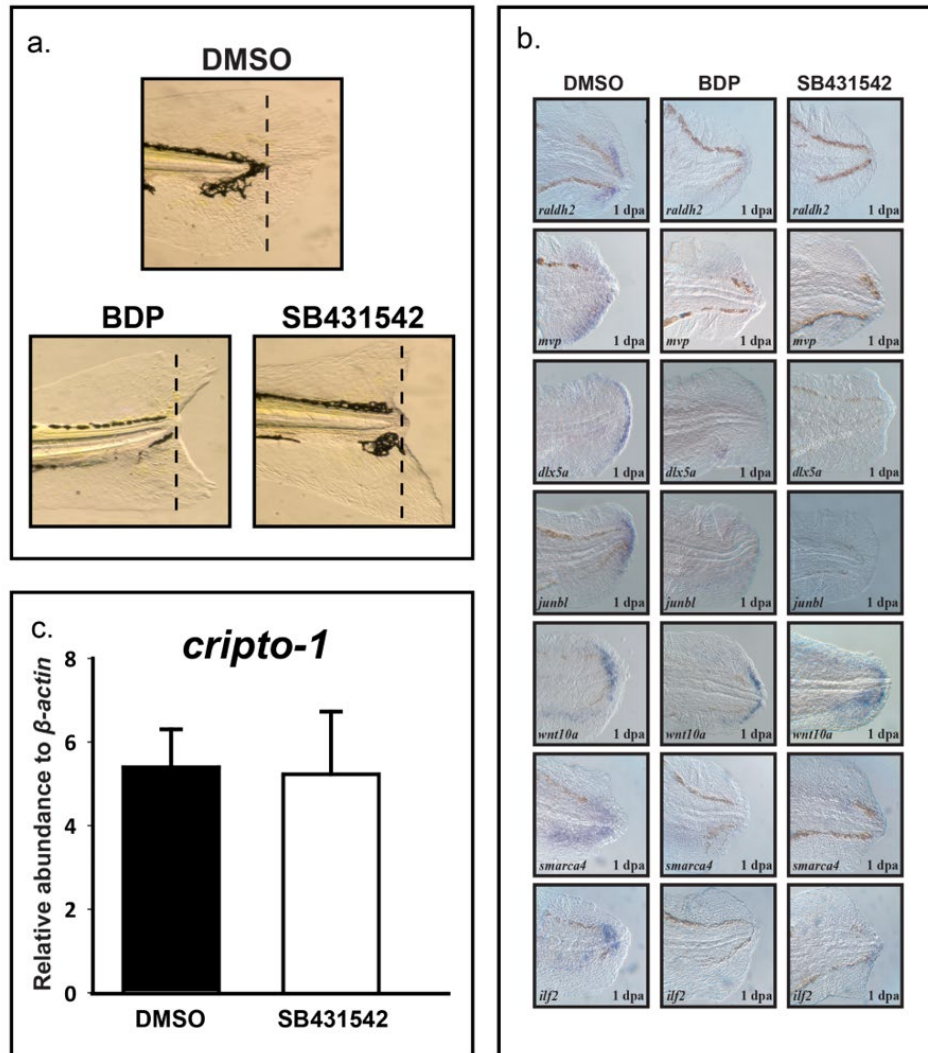
Figure 3.3 BDP and SB431542 impact larval regeneration. a) Caudal fins of 2 dpf (days post-fertilization) larvae were amputated and exposed to vehicle (0.1% DMSO), 1 µM beclomethasone dipropionate (BDP), or 100 µM SB431542. Regenerative progression was evaluated and pictures were taken at 3 dpa (days post-amputation). b) *In situ* localization of *dlx5a*, *junbl*, *wnt10a*, *ilf2*, *smarca4*, *raldh2* and *mvp* in larvae exposed to BDP and SB431542 demonstrated a similar expression pattern. c) Exposure to SB431542 did not significantly alter expression of *cripto-1*.
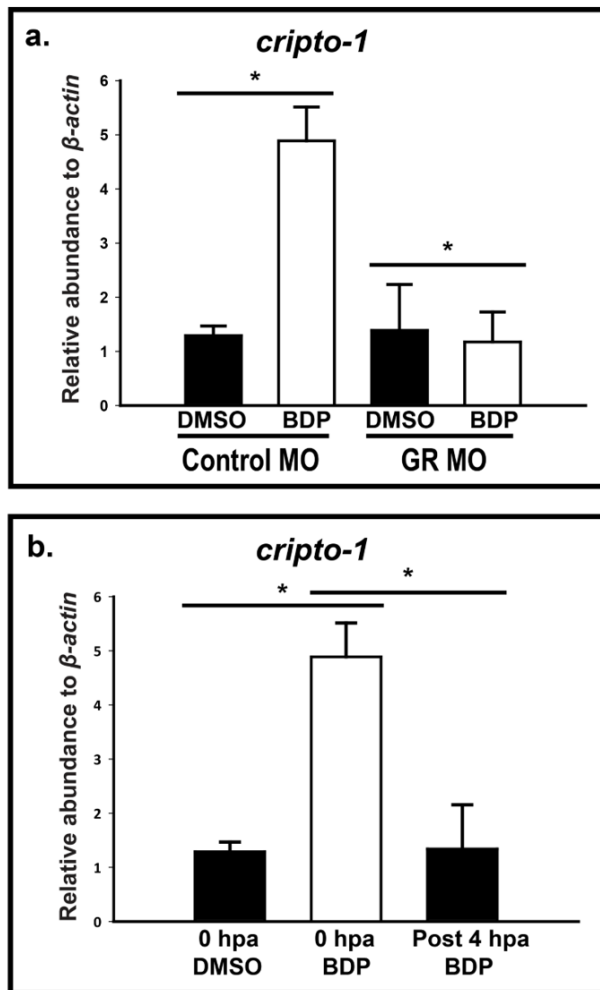
Figure 3.2 Inappropriate GR activation during early stages of regeneration leads to induced *cripto-1* expression. a) Glucocorticoid receptor (GR) splice variant morpholino oligo (MO) transiently knocked down GR compared to standard control MO-injected embryos. The amputated control and GR morphants were exposed to DMSO or beclomethasone dipropionate (BDP). The abundance of *cripto-1* transcript estimated by qRT-PCR at 1 day post-amputation (dpa) in the whole embryo indicate significantly reduced expression in the BDP exposed morphants. The respective values represent the mean ± SEM and the asterisks indicate statistical significance (One-way ANOVA, n = 3, p < 0.05). b) 2 days post-fertilization (dpf) embryos were amputated and exposed to three different groups; DMSO at 0 hours post-amputation (hpa), BDP at 0 hpa and BDP post 4 hpa. The expression of *cripto-1* was evaluated in whole embryos at 1 dpa. cripto-1 expression was significantly up-regulated when exposed at 0 hpa, but BDP exposure didn't induce *cripto-1* when exposed after 4 hpa. The respective values represent the mean ± SEM and the asterisks indicate statistical significance (One-way ANOVA, n = 3, p < 0.05).

a.

b.
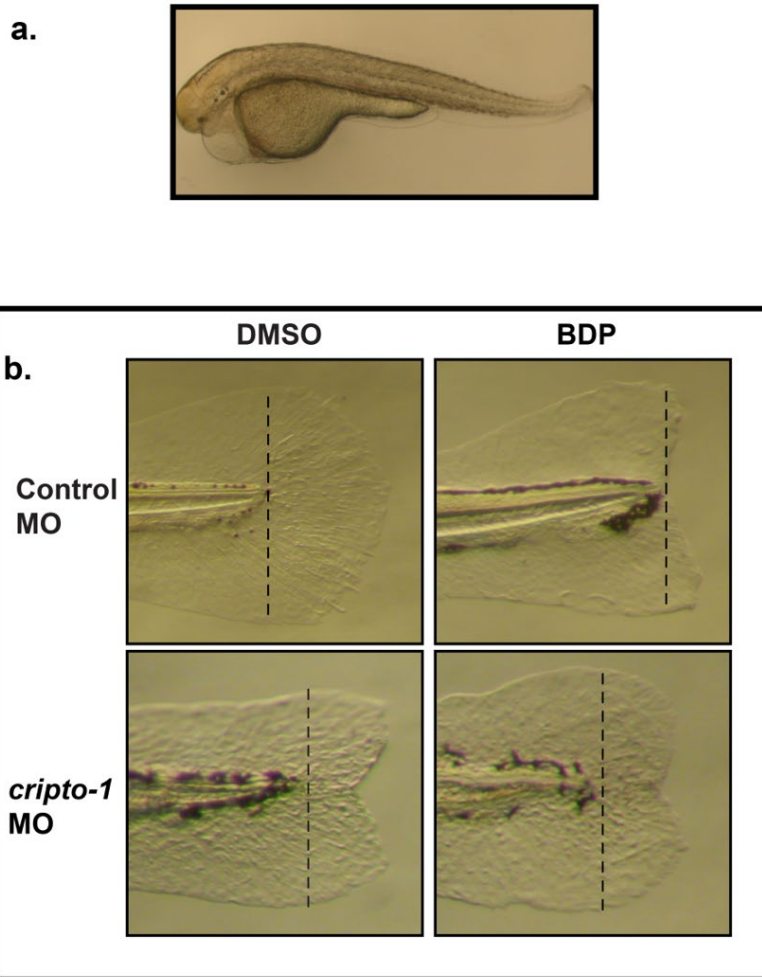
Figure 3.3 Partial antisense repression of Cripto-1 rescues inhibition of regeneration by BDP. a) Translation-blocking *cripto-1* morpholino oligo (MO) transiently knocked down Cripto-1. The morphants developed the characteristic one-eyed pinhead phenotype by 2 days post-fertilization (dpf). b) The control and *cripto-1* morphants were exposed to DMSO or beclomethasone dipropionate (BDP) at 2 dpf following amputation. The dotted lines mark the plane of amputation. Regenerative progression was evaluated and pictures were taken at 3 days post-amputation (dpa). In each replicated experiment approximately 80% of the *cripto-1* morphants were resistant to inhibition of regeneration by BDP exposure.
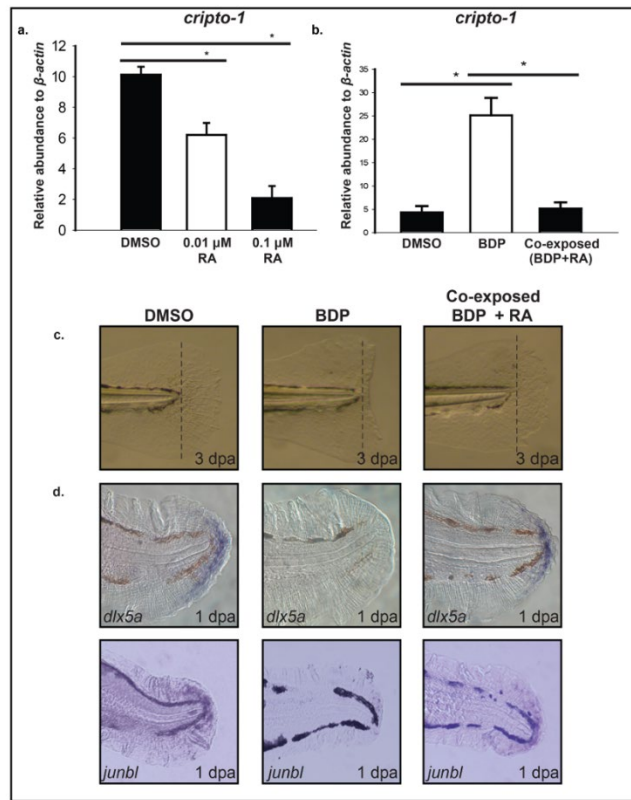
Figure 3.4 Retinoic acid exposure suppress *cripto-1* expression in the fin tissue and rescues BDP impaired regeneration. a) Caudal fin of 2 days post-fertilization (dpf) embryos were amputated and exposed to DMSO or either 0.01 μM or 0.1 μM retinoic acid (RA). The abundance of cripto-1 was estimated in the regenerating fin tissues. The expression of cripto-1 was significantly reduced in a concentration-dependent manner compared to the control. The respective values represent the mean ± SEM and the asterisks indicate statistical significance (One-way ANOVA, n = 3, p < 0.05). b.) 2 dpf larvae were exposed to 0.1 μM RA for 8 hours followed by amputation and co-exposure with 0.01 μM RA and DMSO or beclomethasone dipropionate (BDP). The abundance of cripto-1 was evaluated at 1 day post-amputation (dpa) in the regenerating fin tissue by qRT-PCR. Co-exposure with RA significantly suppressed cripto-1 expression compared to BDP exposure. The respective values represent the mean ± SEM and the asterisks indicate statistical significance (One-way ANOVA, n = 3). c). Amputated 2 dpf larvae pre-exposed with 0.1 μM RA were exposed to DMSO, BDP or co exposed with BDP and 0.01 μM RA. Regenerative progression was monitored and pictures were taken at 3 dpa. In each replicated experiment regeneration was restored in approximately 75% embryos co exposed to BDP and RA compared to BDP alone. d) In situ localization of dlx5a and junbl in the regenerating fin tissue at 1 dpa demonstrated restoration of regeneration markers in the caudal fin of larvae co-exposed with BDP and RA.
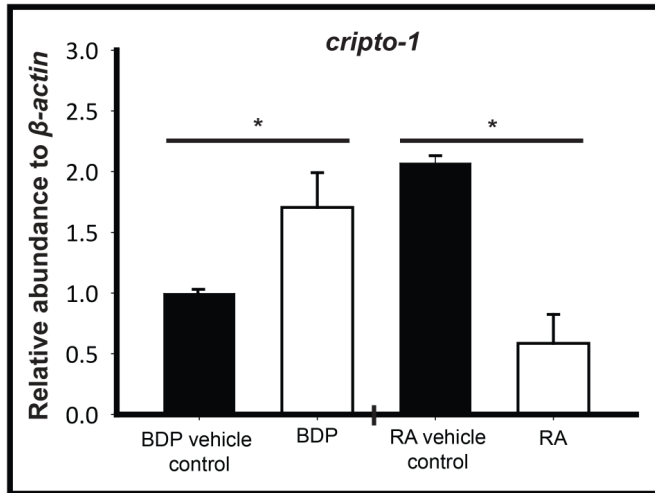
Figure 3.5 BDP induces *cripto-1* expression in the mouse embryonic stem cells. Embryoid bodies cultured from mouse D3 embryonic stem cells were exposed to beclomethasone dipropionate (BDP). The relative abundance of cripto-1 was quantified by qRT-PCR. Exposure to 1 µM BDP significantly induced while retinoic acid (RA) exposure suppressed cripto-1 expression. The respective values represent the mean ± SEM and the asterisks indicate statistical significance compared to the respective vehicle controls (One-way ANOVA on ranks, n = 3, p < 0.05).

CHAPTER 4 – BENZOFLUORANTHENES PRODUCE ECTOPIC FIN DEVELOPMENT IN LARVAL ZEBRAFISH REVEALING COMPLEXITY OF AHR-DEPENDENT PAH ACTIVITY

Michael A. Garland, Mitra C. Geier, Sean M. Bugel, Cheryl L. Dunham, Joe Brown,

Susan Tilton, Robert L. Tanguay

Abstract

The aryl hydrocarbon receptor (AHR) mediates developmental toxicity of several xenobiotic classes including polycyclic aromatic hydrocarbons (PAHs). Using embryonic zebrafish, we previously identified four PAHs that caused a novel phenotype among AHR ligands – growth of a lateral, duplicate caudal fin. The window of sensitivity to the most potent inducer of this phenotype, benzo[k]fluoranthene (BkF), was prior to 36 hours post-fertilization (hpf), although the phenotype was not manifest until 60 hpf. Ahr2-dependency was demonstrated using morpholino knockdown. Hepatocyte ablation demonstrated that metabolism of BkF in the liver is not required for the phenotype. RNA sequencing was performed on distal trunk tissue from BkF-exposed animals collected at 48, 60, 72, and 96 hpf. Across all time points, genes associated with AHR activation, limb development, and tissue patterning had increased expression. Genes encoding fibroblast growth factor and bone morphogenic protein ligands, along with retinaldehyde dehydrogenase, were prominently upregulated. GO term analysis revealed that genes with increased expression were enriched for mesoderm development and fin regeneration pathways, while genes with decreased expression were enriched for Wnt signaling and neuronal development. MetaCore (Clarivate Analytics) systems analysis revealed enrichment of pro-inflammatory Th17-derived cytokines in response to BkF exposure. R-SMADs, AP-1, and LEF1 were predicted to regulate expression of an enriched number of gene targets across all time points. Our results demonstrate a novel aspect of AHR biology that advances our understanding of AHR-mediated developmental toxicity.

Introduction

The aryl hydrocarbon receptor (AHR) is a basic helix-loop-helix ligand-activated transcription factor that is highly conserved among vertebrates and known to be activated by many xenobiotics from natural and anthropogenic sources [1]. A wide range of environmental chemicals interact with the AHR, including dioxins, furans, dioxin-like PCBs, PAHs, flavonoids, and organochlorines [2-4]. Once bound to a ligand, chaperone proteins dissociate and the ligand-bound AHR translocates to the nucleus and dimerizes with the AHR nuclear translocator (ARNT). In the nucleus, the ligand-AHR–ARNT complex binds to xenobiotic response elements, which leads to both the upregulation and downregulation of a variety of gene targets (e.g. cytochrome P450 1A), and interactions with downstream pathways [5]. This includes genes in pathways that play important roles in cardiovascular systems, reproduction, immune regulation, oxidative stress responses, and development [6-10]. The repertoire of known biological effects downstream of AHR activation is diverse. Our understanding of how diverse xenobiotic ligands can seem to similarly activate the same AHR but lead to such diverse outcomes is not well understood.

AHR mediated developmental toxicity has been mainly characterized for the prototypical ligand 2,3,7,8-tetrachlorodibenzo-p-dioxin (TCDD), and includes phenotypic craniofacial malformations and cardiovascular dysfunction [11, 12]. Many effects and resulting phenotypes are often similar for other AHR ligands, including polycyclic aromatic hydrocarbons (PAHs), which elicit developmental toxicity [13-18]. PAHs are

common environmental pollutants, comprised of two or more fused aromatic rings, and can be petrogenic (formed in petroleum) and/or pyrogenic (formed through incomplete combustion of organic material). Exposure to PAHs during development has been correlated with an increase in neurobehavioral disorders [19-21], obesity [22, 23], decreased intelligence [19, 24], reproductive effects [25], and decreased birth weight and size [26-28]. Similar to other AHR ligands, developmental PAH exposure can result in a variety of effects, though toxicity is similar to the developmental effects of TCDD including cardiovascular toxicity and oxidative stress [17, 29-31]Thus, PAHs provide an environmentally salient opportunity to explore a large range of ligand-AHR bioactivities and identify the transcriptional and proteomic patterns that underlie them.

The zebrafish is an ideal model for rapidly evaluating developmental toxicity of environmental toxicants, and useful for linking adverse outcomes and unique phenotypes with initiating molecular events to define chemical bioactivity and mechanisms of effect [32]. Zebrafish have been used extensively to study AHR related mechanisms for developmental effects of TCDD [12, 33], and the ability of adult and larval zebrafish to regenerate removed caudal fin tissue has been useful for interrogating downstream pathways mediated by AHR [34, 35]. Higher vertebrates have a single AHR gene, while a genome-wide duplication event in zebrafish resulted in 3 co-orthologs: Ahr1a, Ahr1b, and Ahr2. Ahr2 is primarily associated with TCDD induced developmental toxicity and demonstrated to mediate toxicity of several PAHs similar to the mammalian AHR [16, 36, 37]. The developmental toxicity of some PAHs is Ahr1a dependent [38], while the function of Ahr1b is still unknown although it has similar binding affinities as Ahr2 [39].

AHR-dependent developmental toxicity in zebrafish is canonically characterized by pericardial and yolk sac edema, and craniofacial malformations.

Previously, we performed a large comparative study of developmental toxicity associated with 123 PAHs and derivatives [40]. Unexpectedly, exposure to four different PAHs resulted in development of an ectopic caudal fin perpendicular to the normal caudal fin. These four PAHs were, in order of most to least potent nominal EC20 values: benzo[k]fluoranthene (BkF), dibenzo[b,k]fluoranthene, dibenzo[a,h]anthracene, and benzo[j]fluoranthene (Table 1). Caudal fin duplication has been previously reported in zebrafish mutants that have increased Wnt and bone morphogenic protein (BMP) [41], while exogenous addition of retinoic acid (RA) is sufficient to induce ectopic limb formation in other vertebrates [42]. In the present study, we investigated the etiology of the ectopic fin phenotype through the critical window of sensitivity to (BkF), dependence on AHR orthologue by antisense knockdown, and transcriptional changes and molecular pathways involved. Here we demonstrate that: 1) BkF-induced caudal fin duplication is Ahr2-dependent; 2) the development of the liver is not required for the phenotype; and 3) BkF alters the expression of several genes involved in limb bud formation.

Methods

Chemicals

PAH chemical structures are shown in Table 1. Analytical grade standards of benzo[j]fluoranthene (98.1%, CAS: 205-82-3), benzo[k]fluoranthene (100%, CAS: 207-08-9), and dibenzo[a,h]anthracene (99%, CAS: 53-70-3) were obtained from AccuStandard (New Haven, CT, USA), and dibenzo[b,k]fluoranthene (unknown purity, CAS: 205-97-0) was obtained from Chiron AS(Trondheim, Norway). Stock solutions of benzo[j]fluoranthene and benzo[k]fluoranthene were prepared in 100% DMSO at 10 mM, while solubility limits required dibenzo[b,k]fluoranthene and dibenzo[a,h]anthracene to be prepared at 1 mM. Tricaine mesylate (MS-222, 95%, CAS: 886-86-2) was obtained from Tocris Biosciences (Minneapolis, MN). DMSO (99.9%, CAS: 67-68-5) was obtained from Avantor Performance Materials (Center Valley, PA).

Zebrafish Husbandry and Developmental Exposures

Tropical 5D zebrafish were maintained at the Sinnhuber Aquatic Research Laboratory (SARL) at Oregon State University (Corvallis, OR, USA) according to Institutional Animal Care and Use Committee (IACUC) protocols. Adult zebrafish were raised in densities of ~500 animals/50-gallon tank at $28 \pm 1°C$ under a 14:10 hour light/dark cycle in recirculating filtered water supplemented with Instant Ocean salts. Spawning funnels were placed in tanks the night prior, and the following morning embryos were collected, staged, and maintained in an incubator at $28 \pm 1°C$ [43]. Embryonic and larval zebrafish to be euthanized were overdosed with tricane at concentrations exceeding 300-400 mg/L.

Chorions were enzymatically removed with pronase at 4 hours post-fertilization (hpf) using a custom automated dechorionator as previously described, and at 6 hpf embryos were placed one per well in round bottom 96-well plates prefilled with 100 µL embryo medium using an automated embryo placement system [44]. A Hewlett Packard D300e chemical dispenser was used to dispense 100% DMSO dissolved stocks into 2 replicate exposure plates. Final DMSO concentrations were normalized to 1% (vol/vol), and gently shaken by the chemical dispenser during dispensing. Plates were sealed with Parafilm to minimize evaporation, wrapped in foil to minimize light exposure, and shaken overnight at 235 rpm on an orbital shaker at $28 \pm 1°C$ to enhance solution uniformity [45]. Embryos were kept in a $28 \pm 1°C$ incubator for the duration of the 5 day study.

Aqueous exposures were either static throughout development or staggered to determine the developmental window of susceptibility (Figure 1A). For static exposures, embryos were exposed from 6 hpf until 120 hpf. For window of susceptibility and morpholino studies, a single concentration of 3µM benzo[k]fluoranthene was used which corresponded to an EC100 value. For RNAseq studies, the exposure concentration was 12 µM, which ensured robust induction of the phenotype in 100% of the animals.

Morpholino Microinjections

Embryos were injected at the single cell stage with a fluorescein-tagged translation-blocking morpholino targeting Ahr2, splice-blocking morpholinos targeting Ahr1a or Ahr1b, or a standard nonsense control purchased from Gene Tools (Philomath,

Oregon) (Table 2). Injection volume was ~2 nL. Fertilized, normally developing embryos were screened for morpholino incorporation at 4 hpf by fluorescence microscopy, and dechorionated by hand. Embryos with evenly incorporated morpholino were exposed to benzo[k]fluoranthene as described above.

Immunohistochemistry

Immunohistochemistry (IHC) of cytochrome P450, family 1, subfamily A (Cyp1A) protein localization was performed as previously described [35]. Two replicates of eight larvae at 5 dpf each were euthanized with tricaine and fixed overnight in 4% paraformaldehyde at 4°C. Fixed embryos were permeablized 10 minutes on ice in 0.005% trypsin, rinsed with PBS+Tween 20 (PBST) and post-fixed in 4% paraformaldehyde for 10 minutes. Larvae were blocked with 10% normal goat serum (NGS) in PBS+0.5% Triton X-100 (PBSTx) for 1 hour at RT and incubated overnight in the mouse anti-fish Cyp1A monoclonal primary antibody (Biosense Laboratories, Bergen, Norway) (1:500) in 1% NGS. Larvae were washed in PBST and incubated for 2 hours in secondary antibody (Fluor 594 goat anti-mouse, IgG). Eight embryos per treatment group were assessed by epi-fluorescence microscopy using a Zeiss Axiovert 200 M or Keyence BZ-X700 microscope with 10× and 20× objectives for the presence or absence of fluorescence in specific tissues.

Hepatic ablation

Hepatocyte ablation studies were conducted using Tg(l-fabp:CFP-NTR)s891 (background strain TL) [46]. Transgenic embryos from in-crossed homozygous adults

were collected from small group spawns. At 6 hpf, dechorionated embryos were hand-

loaded into 96-well plates containing either 2 mM MTZ or vehicle (0.2% DMSO).

Immediately after loading, half of all MTZ- and vehicle-exposed animals were exposed

to 12 uM BkF, and all wells were normalized to a final concentration of 1% DMSO,

using a Hewlett-Packard Digital Dispenser. At 5 dpf, animals were screened for hepatic

ablation by presence/absence of hepatic tissue fluorescence using a Zeiss ASDF

fluorescence microscope with a green fluorescent protein (GFP) filter. Animals were then

evaluated for mortality and ectopic caudal fin phenotype. Hepatic fluorescence imaging

was performed using a Keyence BZ-X700 fluorescence microscope with a GFP filter.

Tissue Isolation

To collect caudal fin tissue, larval zebrafish were anesthetized in tricaine and the

trunk was removed at the proximal end of the ventral pigment gap using a glass

microdissection blade. Trunk tissue was collected at 48, 60, 72, and 96 hpf, pooling 50

animals per replicate at each time point. Collected tissue was immediately placed into

RNAzol® RT (Molecular Research Center, Inc., Cincinnati, OH) and frozen at -80°C

until isolation.

RNA Isolation and Sequencing

Four biological replicates per treatment of total RNA were isolated from fin tissue

samples using the Zymo Direct-zol RNA MiniPrep kit (Irvine, CA). Embryos were

homogenized in 500 μl RNAzol RT with 0.5 mm zirconium oxide beads using a bullet

blender (Next Advance, Averill Park, NY) for 3 min at speed 8. Samples were stored at

−80°C until RNA isolation. Total RNA was extracted according to the manufacturer's protocols. The optional in-column DNase I digestion step was performed for the RNAseq samples. Total RNA concentration and was determined on a SynergyMX spectrophotometer using a Gen5 Take3 sample holder (BioTek Instruments, Inc., Winooski, VT).

RNA samples were placed in a 96-well RT-PCR plate and shipped overnight on dry ice to the University of Wisconsin-Madison Biotechnology Center (Madison, WI) for library preparation and sequencing. RNA integrity was determined using the Agilent 2100 Bioanalyzer. Samples were prepared using the Illumina TruSeq Stranded mRNA Library Prep Kit. Libraries were randomized across 4 lanes and sequenced with 100bp single-end reads using the Illumina HiSeq 2500. Sequence files were transferred to the Pacific Northwest National Laboratory for analysis.

RNAseq Analysis

Sequences were filtered based on Illumina quality scores and analyzed for quality using FastQC analytical software (Babraham Bioinformatics). Read ends were trimmed using Trimmomatic [47] to exclude low-quality sequences. Salmon's quasi-mapping alignment method [48] was used to map reads to Danio rerio Zv9 ENSEMBL transcripts. Transcript abundances were aggregated to gene level counts using tximport [49]. Normalization and differential expression across statistical contrasts was performed using DESeq2 [50] on genes with at least 10 counts in at least 3 samples.

Ensembl BioMart [51]was used to create the transcript-to-gene mapping key required for tximport to estimate gene expression levels (http://mar2015.archive.ensembl.org/biomart/martview, Ensembl Genes 79, Zv9 via Bioconductor [52] package biomaRt [53]). For clustering analyses, regular-log transformation was applied to the relative gene counts in order to correct for the heteroscedasticity inherent in RNAseq data [54]. Principle components analysis was performed in RStudio [55] using the base R [56] package, stat, and visualized with ggplot2 [57], ggthemes [58], and ggrepel [59]. MatrixStats [60] was used to identify genes that varied most in their expression across samples. Transformed count values of selected genes were scaled by Z-score, and heat maps with bidirectional, hierarchical clustering were produced using ComplexHeatmap [61]. For images of the top 50 significant differentially expressed genes (DEGs), a DEG list for each comparison ($p <$ 0.05) was sorted based on either the Benjamini-Hochberg method of false discovery rate (FDR) at 5% or absolute log2FC (fold change), and the top 50 genes (or all DEGs in cases with fewer than 50) from each ordered gene list were combined to create a master list of top combined DEGs.

All statistical analysis was performed using custom code developed in R [55]. GO term enrichment analysis was performed on separate upregulated and downregulated differentially expressed gene sets using topGO [62]. Excluding terms with fewer than 30 significantly differentially expressed transcripts (FDR-adjusted p-value ≤ 0.05), the 15 terms with the lowest p-value were selected from each time point and cross referenced to identify other time points for which that term was significant. The GO term heat map was

generated using the Broad Institute's online tool Morpheus

(https://software.broadinstitute.org/morpheus). Venn diagrams were created using Venny

2.1.0 [63].

For the MetaCore enrichment analysis, D. rerio Ensembl gene IDs were converted

to their orthologous human Ensembl IDs and gene symbols using the Bioinformatics

Resource Manager v2.3 (BRM) with Ensembl release 91 [64]. Transcription factor target

enrichment analysis was performed for each time point using genes that having a log2-

fold change ≥ 1. Gene targets were identified using MetaCore's network building tool

based on direct interactions. Interactome figures were generated by importing the direct

interactions data into Cytoscape v3.7.1.

Results and Discussion

We previously identified a duplicate caudal fin-like phenotype, nicknamed "x-

fin," in a developmental toxicity screen of 123 polycyclic aromatic hydrocarbons (PAHs)

and PAH derivatives using embryonic zebrafish exposed at 6 hours post-fertilization

(hpf) [148]. The x-fin phenotype is characterized by a secondary fin perpendicular to the

normal caudal fin, along each lateral face of the distal trunk, and accompanied by

hyperpigmentation at the caudal peduncle (Figure 1). Four PAHs elicited x-fin:

benzo[k]fluoranthene (BkF), benzo[j]fluorathene, dibenzo[b,k]fluoranthene, and

dibenzo[a,h]anthracene (Table 1). These are relatively high molecular weight, 5-6 ringed

parent PAHs. BkF was the most potent inducer of x-fin with an EC_{20} of 0.5 μM. We selected BkF as the representative compound in all subsequent experiments due to its potency and ability to produce 100% prevalence of the phenotype. Aside from the caudal fin duplication and, in some cases, protruding pectoral fins, zebrafish embryos exposed to ≤ 50 μM BkF were morphologically normal.

During developmental exposure to BkF, caudal fins appeared morphologically normal until between 60 and 72 hpf, during which a fold emerged laterally from the center of the caudal fin that extended in both directions along the proximo-distal axis over time. By 96 hpf, all animals exhibited the x-fin phenotype, which then continued to grow in proportion to the growth of the normal caudal fin.

X-fin phenotype is dependent on early stage exposure

BkF caused the x-fin phenotype within discrete developmental windows (Figure 2). The window of exposure that maximally elicited the x-fin phenotype was 12-36 hpf. Exposures started after 48 hpf did not elicit the phenotype, and shorter exposure durations did not fully recapitulate the percent effect observed in our static 6 – 120 hpf screening protocol.

X-fin phenotype is AHR-dependent

As previously reported [148], exposure to BkF induced unusual skin and neuromast expression of Cyp1A at 120 hpf, which indicated elevated AHR signaling. Transient antisense knockdown of each zebrafish AHR isoform (Ahr1a, Ahr1b, and Ahr2) using morpholino oligos (MOs) was used to test AHR dependency. Control

morphants exposed to 3 μM BkF exhibited 100% prevalence of the x-fin phenotype, knockdown of Ahr1a resulted in 91.7% prevalence (Figure 3), knockdown of Ahr1b resulted in 66.7% of morphants displaying a qualitatively less severe version of the phenotype, and knockdown of Ahr2 completely prevented development of the x-fin phenotype (0% prevalence). Concordant with these results, knockdown of Ahr1a and Ahr1b did not alter the pattern of Cyp1a expression in response to BkF, but knockdown of Ahr2 eliminated expression of Cyp1A in skin, but not the neuromasts (Figure 4).

X-fin phenotype is independent of hepatogenesis

AHR activation induces transcription of phase I metabolic enzymes, and for PAHs in particular this often leads to bioactivation [149]. The differentiation of hepatic tissue approximates the window of sensitivity to BkF [150]. Given the AHR dependency of the x-fin phenotype, we sought to determine whether hepatic function was necessary to produce the x-fin phenotype. One method involves knocking in a bacterial nitroreductase gene with a tissue-specific promoter [151]. Embryos from these animals would be exposed to the pro-drug metronidazole (MTZ), which nitroreductase metabolizes into a bioactive cytotoxin. Using homozygous Tg(*l-fabp:CFP-NTR*)[s891] embryos, we conditionally ablated hepatocytes by static exposure to 2 mM MTZ from 6 – 120 hpf in two separate experiments. No adverse effects were detected as a result of MTZ treatment. Hepatic ablation of MTZ-treated animals was confirmed at 5 dpf using fluorescence microscopy.

Animals that were not treated with BkF did not have the x-fin phenotype regardless of MTZ treatment (Figure 5). Conversely, all animals treated with BkF had the x-fin phenotype, except for one MTZ-treated animal in the Plate 1 experiment (Table 3). This information allowed us to conclude that hepatic metabolism of BkF is not required for x-fin induction during BkF treatment.

Global gene expression

To investigate global changes in the transcriptome that corresponded to development of the x-fin phenotype, we collected tissue samples of the distal trunk region just below the pigment gap in animals exposed to BkF (12 µM to ensure 100% prevalence) or vehicle (1% DMSO). To capture the changes in gene expression prior to and during emergence of the phenotype, we collected tissue at four time points: 48, 60, 72, and 96 hpf. Principal components analysis (PCA) indicated strong separation of chemical treatment along PC1 (x-axis, 37%), while separation between time points occurred along PC2 (y-axis, 26%) with a clearer separation in BkF-treated animals compared to vehicle-treated animals (Figure C1).

A total of 11,215 unique differentially expressed genes (DEGs; FDR-adjusted p-value < 0.05) were identified across all time points. The number of DEGs increased relative to each time point: at 48 hpf, 3753 DEGs; at 60 hpf, 5558 DEGs; at 72 hpf, 7052 DEGs; and at 96 hpf, 7991 DEGs. Of all the identified DEGs, 20.3% were shared across all time points (Figure 6). The 60 and 72 hpf time points shared the greatest number of DEGs and 48 and 96 hpf shared the fewest. Each pairwise comparison had at least 30%

of their DEGs in common. A table for each respective of all DEGs age that had a fold change > 2.0 is available in Tables C1-4.

Hierarchical clustering of the top 50 DEGs with the greatest change in magnitude of expression indicated clear separation between BkF- and vehicle-treated animals (Figure 7). Across all time points, the most upregulated DEGs in response to BkF were cytochrome P450s associated with canonical AHR activation (*cyp1a*, *cyp1b1*, *cyp1b2*, *cyp1c2*, *cyb5a*), with log$_2$-fold changes > 7 at each time point. These results are consistent with other PAHs with AHR dependent effects [152]. The most downregulated genes were related to keratin filament construction (*zgc:158846*, *krtt1c19e*), with fold changes > 2 at each time point. Other canonical AHR activation responses included upregulation of phase I and II metabolic genes and AHR repressors (e.g. *ugt1b1*, *cyb5a*, *foxq1a*, *gstp2*, and *ahrrb*), and downregulation of *sox9b*.

Cell fate, differentiation and limb development

At 48 hpf, before the x-fin was manifest, significant increases in cell fate and differentiation related genes were observed in BkF treated samples. Transcripts of cell fate regulators *sox14* and *prdm14* each showed 2.4-fold upregulation [153, 154], and differentiation regulator *fosl2* showed a 2-fold upregulation. Mesodermal differentiation gene *msgn1* [155] and epithelium development gene *pkhd1l1* [156] showed significantly increased expression, consistent with the additional skin structures needed for formation of the x-fin. At 60 hpf these gene changes were still maintained with the addition of a 2.3-fold increase in hand2 transcript, a gene involved in limb development [157].

Changes in expression of several genes related to dorsal-ventral patterning and limb development were observed. At 60 hpf, when the phenotype visibly began, expression of homeobox gene *dlx4b*, known to control dorsoventral patterning of zebrafish pharyngeal arches [158], increased 2-fold in the caudal region. At 72 hpf, when the phenotype was still developing, *dlx4b* expression was still > 2-fold higher in BkF exposed animals than in controls. The functionally redundant homeobox genes *vox* and *vent*, previously shown to control dorsoventral patterning in zebrafish, were upregulated >2-fold and 0.75-fold, respectively by 72 hpf [159]. At 72 hpf *osr1* and *osr2*, genes involved in limb bud formation [160], were downregulated 2.6- and 1.4-fold, respectively. By 96 hpf, when x-fin had fully developed, these up and down regulations were no longer observed.

Tissue remodeling and growth

Growth processes were largely stimulated at 48 hpf. *aldh1a3*, which synthesizes retinoic acid (RA) [161], showed > 3-fold increase in expression, respectively. Cell growth inhibitor *osgn1* [162] transcript showed a 2-fold downregulation. Transcription of fibroblast growth factors *fgf7*, *fgf20a*, and *fgf22*, and bone morphogenetic proteins *bmp8a* and *bmp16* was significantly upregulated. Though some previously mentioned upregulated transcripts are associated with increased *fgf8* expression (*vox* and *aldh1a2*) [163, 164], the *fgf8* transcript was not affected at 48 hpf and downregulated at 60, 72, and 96 hpf. This was accompanied by upregulation of bone morphogenetic protein antagonist *grem2*, implicated in tissue patterning [165]. Matrix metalloproteinases (MMPs) are involved in wound healing and organogenesis and act by enabling cell migration [166]. MMP inducer *nuak1* [167] had a 2.8-fold increase in expression at 48 hpf following

exposure to BkF, suggesting that extracellular matrix breakdown and cell migration were part of x-fin formation. R-spondin transcript *rspo1*, a positive regulator of canonical Wnt signaling, [168], was significantly upregulated by BkF at 48 hpf. These genes were similarly differentially expressed at 60 hpf.

chordin (*dino*) and *sizzled* (*mes*) are antagonists of BMP and Wnt signaling, respectively. Loss-of-function mutations in these genes has been reported to result in fin duplication, with *dino* mutants having four caudal fin folds and *mes* mutants having three fin folds [9]. This would suggest that inappropriate propagation of BMP or Wnt signaling is sufficient to induce fin duplication. We did not identify differential expression of these genes in our data, however, the presence of four caudal fin folds in BkF-treated fish suggests that inappropriate BMP signaling is involved. The strong induction of *bmp8a*, which can induce downstream activation of both Smad2/3 (TGF-β/Activin) and Smad1/5/8 (BMP) transcription factors [169], is consistent with this observation.

GO Term Pathway Analysis

Gene ontology (GO) enrichment analysis was used to identify the 15 most upregulated and downregulated processes in each time point, which were then cross-referenced for significance across each of the other time points (Figure 8). The most significantly enriched upregulated GO term across all time points was *cellular response to xenobiotic stimulus*, which mostly contains cytochrome P450s and other phase I metabolism enzymes. This response is consistent both with a typical AHR activation response, and the Cyp1A expression pattern observed in the IHC images. Several other

GO terms related to xenobiotic response were also significantly altered across all four time points, including upregulation of response to stress and response to external stimulus, and downregulation of oxidation-reduction processes. Processes related to cell redox homeostasis were upregulated in all but the 48 hpf time point. This is consistent with an increase in oxidative stress following the initiation of PAH phase I metabolism at 48 hpf [170, 171],

Several GO terms related to DNA and RNA functional processes were downregulated in the caudal fin with exposure to BkF, primarily at 72 and 96 hpf. Translation was downregulated at 72 hpf, including elongation and formation of the translation preinitiation complex. As might be expected with BkF, a long-known mutagen [172], the mitotic DNA damage checkpoint, which helps ensure DNA damage has been adequately repaired before cell division, was downregulated. Additionally, DNA biosynthesis was downregulated in all time points except 48 hpf.

Several other processes that have previously been identified as downstream effects of AHR were differentially expressed. As previously reported for other PAHs that activate AHR [152], ion transport was differentially regulated when exposed to BkF. ATP hydrolysis coupled proton transport and zinc II ion transmembrane transport were significantly upregulated processes in all four time points, while cellular calcium ion homeostasis was significantly downregulated at 96 hpf. As would be expected due to the observed increased pigmentation at the caudal peduncle at 120 hpf, the cellular pigmentation GO term was significantly upregulated at 60 and 72 hpf. This response may

be similar to previous work demonstrating AHR ligands stimulate human melanocytes [173].

Multiple signaling pathways were significantly downregulated in response to BkF exposure, all with known roles in axis formation, cell differentiation, apoptosis, or cell growth regulation. Wnt signaling, which has documented roles in vertebrate anterior-posterior and dorsoventral axes formation, was downregulated in all four time points [174] [175]. The integrin-mediated signaling pathway, which regulates cell survival, apoptosis, proliferation and differentiation [176], was also downregulated across all 4 time points. At 48 hpf, the adenylate cyclase-modulating G-protein coupled receptor signaling pathway was downregulated. The JNK cascade, which is modulated by G-protein coupled receptors [177], was also downregulated at 48, 60 and 96 hpf. These pathways together control apoptosis and cell growth pathways that could contribute to the development of the x-wing phenotype. Finally, Notch signaling, which controls anterior-posterior polarity during somitogenesis [178], embryo polarity, and mesoderm, cell fate, and left-right asymmetry determination [179] was significantly downregulated at 96 hpf. Notably, the Wnt and Notch signaling pathways are known to be involved in fin regeneration in a spatiotemporal dependent manner [180]. Despite these pathways being downregulated, fin regeneration processes overall were observed to be significantly upregulated in all 4 time points.

As might be expected with differential expression of the Notch, Wnt, G-protein coupled receptor, and integrin-regulated signaling pathways, processes involving cell

fate, adhesion and migration were similarly differentially regulated. Regulation of cell fate specification and cell-cell adhesion were upregulated across all four time points, suggesting an overall decrease in these processes. However, cell fate commitment involved in formation of primary germ layer was also upregulated at all time points. This, combined with the observed upregulation of mesodermal cell differentiation and mesoderm and mesenchyme development, also observed during regenerative fin growth, suggested that an increase in cell proliferation, migration and differentiation is integral to fin regeneration-like tissue growth.

Several processes related to neuronal development in general, and lateral line development specifically, were enriched in the GO term analysis. Hair cell differentiation was downregulated across all four time points along with the sensory hair cell development involved in the formation of posterior lateral line neuromasts. This is in agreement with the observed downregulation in all but the 48 hpf time point of processes related to the differentiation of the inner ear receptor cell, which is another sensory hair cell structure. Notably, cilium assembly, which is required for development of the cilium of hair cells, was upregulated at 60 and 72 hpf. Embryonic camera-type eye morphogenesis was downregulated across all four time points, while retina morphogenesis was upregulated across all four time points. Other, more general neuronal processes were differentially regulated with exposure to BkF, including the downregulation of axonogenesis, brain development, and neuron fate specification. Wnt and notch signaling pathways have been implicated in nervous system effects [181, 182], and could be partially responsible for these effects.

The GO term enrichment analysis suggests that Wnt, FGF, and Notch signaling mediate an increase in proliferation and tissue remodeling in the caudal fin similar but not identical to that observed in epimorphic fin regeneration. It is plausible that modulation of these processes leads to the structural duplication of the caudal fin.

MetaCore Systems Analysis

MetaCore software (Clarivate Analytics) provides analytical tools for biological systems data using manually curated information from the literature. We used MetaCore to identify enriched process networks, predict transcription factor activity, and build a network of direct gene interactions. To make the data compatible with MetaCore, zebrafish Ensembl gene IDs were converted to their orthologous human Ensembl IDs and gene symbols using the Bioinformatics Resource Manager (BRM) [183]. Of all 21,604 unique DEGs, BRM converted 12,765 (59%) to human orthologs to generate the background gene list. At each time point, BRM converted the following numbers of DEGs to their human orthologs: at 48 hpf, 2939/3753 (78%) genes; at 60 hpf, 4434/5663 (80%); at 72 hpf, 5663/7052 (80%); and at 96 hpf, 6339/7991 (79%).

Process network analysis predicts inflammation and decreased neurodevelopment

MetaCore can identify significantly enriched (FDR-adjusted p-value ≤ 0.05) processes in systems data using proprietary gene annotations similar to GO enrichment analysis. We performed process network analysis separately on up- and down-regulated DEGs (Table 4). Across all four time points, inflammatory processes were enriched among DEGs with increased expression. At 48 hpf there was enrichment of

Inflammation_Complement system and *Inflammation_Innate inflammatory response*. By 60 hpf, enrichment of inflammatory processes was expanded to include *Inflammation_Kallikrein-kinin system* and *Immune response_Th17-derived cytokines*. Most of these processes had sustained enrichment through 96 hpf.

AHR can modulate inflammation as well as direct the priming of T cells into either anti-inflammatory T_{reg}s or pro-inflammatory Th17 cells [184]. Enrichment of the *Immune response_Th17-derived cytokines* pathway suggests the latter process where inflammation might occur directly as a result of AHR activation. Whether inflammation is related to the x-fin phenotype remains unknown. Since inflammation is an important first step in fin regeneration [185], it is possible that AHR-mediated inflammation induced an aberrant wound healing response that resulted in the growth of a duplicate caudal fin. The GO term enrichment of fin regeneration-related pathway suggests this may a possibility.

The other enriched process networks were consistent with wound healing. Cell adhesion and proteolytic processes were enriched at most time points (similar results were observed in the GO term enrichment), while blood coagulation was enriched starting at 60 hpf. By 96 hpf, *Signal transduction_Leptin signaling*, which regulates wound healing [186], and *Development_EMT_Regulation of epithelial-to-mesenchymal transition*, were both enriched. At the same time point, DEGs with decreased expression were enriched for *Development_Neurogenesis in general*, *Development_Skeletal muscle development*, and *Development_Cartilage development*. This suggests BkF-exposed

animals are unable to appropriately develop lateral line and mesoderm-derived tissues in the trunk. Notably, these processes are Wnt-dependent and may be explained by decreased expression of Wnt ligands [187, 188].

Transcription factors with enriched target genes control wound healing and development

We used MetaCore's transcription factor (TF) enrichment tool to identify TFs whose number of target genes are enriched in our differential expression data (hereafter referred to as enriched TFs). Across all time points, MetaCore identified 52 unique TFs that were significantly ($p \leq 0.05$) enriched, including 23 that increased expression and 29 that decreased expression (Table 5).

Overall, enriched TFs with increased expression were primarily associated with developmental processes and inflammation. Consistent with AHR activation, the negative-feedback regulator AHRR was enriched at all time points. Similarly, the developmental TFs FOSL1, LEF1, JUNB, and FOSL2 had early and sustained target enrichment. These TFs are part of the AP-1 complex, which is involved in and fin regeneration [189]. By 96 hpf, several developmental TFs had target enrichment including those involved in limb morphogenesis (HAND2, TBX2, SHOX2, and DLX3) [157, 190-192]. BCL6, which controls T follicular helper cell development [193], along with the pro-inflammatory NFATC2, were both enriched at 60 and 72 hpf. These two enrichments are consistent with the process network enrichment of inflammation mediated by Th17 cells. A marker of neuronal injury, ATF3, was enriched at 72 and 96 hpf [194].

Enriched TFs that decreased expression were similarly associated with development and inflammation, but there were several others having roles in neuronal development or axis specification. The metabolic regulator PPARA had an enrichment of targets at 48 and 60 hpf. Starting at 60 hpf, enriched TFs involved in neuronal development were identified among those having decreased expression. TCF4, which initiates neuronal differentiation [195], was enriched at 60 and 72 hpf. By 96 hpf, several TFs involved in neuronal development were enriched including POU3F3, ASCL1, ZIC1, PAX6, PROX1, TLX3, IRX3, ISL1, OLIG2, MYT1, ATOH1, and FOXP2. There were also enriched TFs involved in antero-posterior (A-P) axis specification (HOXA2, HOXB8, and HOXA1), mesoderm development (MEOX1 and MYOD1), and limb patterning (LMX1 and SIX2).

Network analysis predicts possible paths to fin duplication

We sought to integrate the above data into a visual network and identify possible pathways leading to fin duplication. Our focus was on the 48 hpf interactome. MetaCore's "Build Network" tool was used to identify direct interactions between enriched TFs and DEGs. These predicted interactions are based on manual curation of the literature. Because *bmp8a* was prominently upregulated and can activate both TGF-β and BMP receptors, we included Smad2/3 and Smad1/5/8 in our analysis. Data were imported into Cytoscape [196] to visualize the network.

MetaCore identified a direct interaction between AHR and aldh1a3. Previous work has shown a direct link between AHR activation and *aldh1a3* induction [197], and

the same induction might be present in our model. AHR was also predicted to interact with the prostaglandin synthesizing gene, *ptgs2* (*cox2*), which may lead to inflammation and the downstream synthesis of the pro-regeneration prostanoid, prostaglandin E2 [198]. Smad2/3 and Smad1/5/8 were predicted to interact with several notable genes in our data including TFs involved in limb development (*lef1*, *dlx3*, and *prdm12*). AP-1 subunits were predicted to be involved in prdm1 induction, also involved in limb formation [199]. *fgf7* was predicted to be regulated by Junb and Smad1/5/8. We identified one degree of separation between AHR, Smad 2/3, Smad1/5/8, and Lef1 through the chemokine receptor *cxcr4*.

Based on our network analysis, we conjecture the involvement of multiple pathways that lead to fin duplication (Figure 10). One possibility is that BkF requires bioactivation via metabolic genes induced by AHR (e.g., Cyp genes). This mechanism of involving secondary metabolite formation has been well established for AHR-mediated toxicity. Although we ruled out metabolism in hepatocytes as being necessary for fin duplication, the observed induction of metabolic enzymes (e.g. Cyp1a) in the skin and neuromasts could play a role. Second, AHR is predicted to directly increase expression of *retinaldehyde dehydrogenase 3* (*aldh1a3*), thereby increasing the local concentration of RA. Exogenous RA is highly teratogenic and sufficient to induce ectopic appendage development. Another possibility is the induction of metabolic enzymes that bioactivate BkF into an active metabolite. Next, induction of *bmp8a* through an unknown pathway could activate TGF-β and BMP receptors, leading to phosphorylation of their respective R-Smad targets, Smad2/3 and Smad1/5/8. Our interactome analysis predicts that

Smad1/5/8, presumably phosphorylated due to increased bmp8a expression, could

cooperate with Lef1 to induce expression of *dlx3*, which is expressed in the distal tip of

limbs during zebrafish and mouse development. Given that Wnt signaling is overall

decreased in our samples, it is more likely that Lef1 serves to transduce TGF-β or BMP

signaling. Downstream induction of AP-1 subunit were also predicted to regulate

expression of prdm1, which has been observed during fin regeneration.

Conclusions
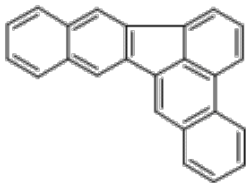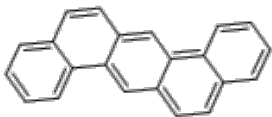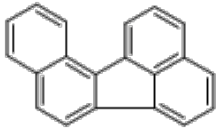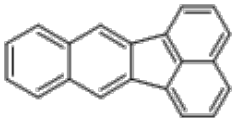
We identified four PAHs that elicited a unique AHR-dependent ectopic caudal fin

during limb development accompanied by skin hyperpigmentation. For BkF we

demonstrated that the phenotype was Ahr2-dependent. Other than Cyp1A induction, the

morphology responses the 4 PAHs were dissimilar to phenotypes typical of

developmental exposure to other xenobiotic Ahr2 ligands (i.e. pericardial edema and

craniofacial malformations) aside from induction of. Transcriptome responses suggested

that signaling via several pathways was required for the x-fin phenotype, chief among

them FGF, BMP, Notch, and fin regeneration. The structural similarity of our phenotype

to the fin duplication in *chordin* mutants suggests a role for BMP signaling. A predicted

direct interaction of the AHR with *aldh1a3* also indicates a role for RA signaling. Thus,

our data suggest the possibility of crosstalk between AHR and BMP/RA signaling. We

also note that MetaCore identified an inflammatory signature in our gene expression data,

including inflammation mediated by Th17 cells. Combined with enrichment of fin

regeneration genes, this also suggests the possibility of an aberrant wound healing response.

We compared our 48 hpf sequencing data to that of sequencing data from 48 hpf whole embryos exposed to different PAHs [200]. In that study, embryos exposed to BkF and benzo[j]fluoranthene had significantly increased expression of *dlx3* compared to embryos exposed to six other PAHs. As *dlx3* is a target of Smad1/5/8 *via* BMP signaling (and of Lef1, through which BMP cooperates with Wnt [201]), this adds further evidence that BkF facilitates AHR-BMP crosstalk. Future work should seek a complete mechanism of how benzofluoranthenes and structurally related PAHs appear to interact with the AHR differently than most xenobiotics, including potential binding and spatiotemporal activation differences. This unusual signaling in response to common PAHs suggests that our canonical models of xenobiotic AHR signaling still only describe a small part of the complex signaling that can occur.

Table 4.1 Structures and EC_{20} values of four PAHs identified with x-fin phenotype.

PAH	Structure	EC_{20} (μM)
Dibenzo[b,k]fluoranthene		3.5
Dibenzo[a,h]anthracene		3.6
Benzo[j]fluoranthene		7.3
Benzo[k]fluoranthene (BkF)		0.5

Table 4.2 Morpholino oligo (MO) sequences and injection concentrations for the standard control MO as well as *ahr2*, *ahr1a*, and *ahr1b* MOs.

Morpholino	Sequence	Concentration
Control	5'CCTCTTACCTCAGTTACAATTTATA3'	1 mM
ahr2	5'CTTTTGAAGTGACTTTTGGCCCGCA3'	1 mM
ahr1a	5'ACACAGTCGTCCATGATTACTTTGC3'	1.5 mM
ahr1b	5'ACACAGTCGTCCATGATTACTTTGC3'	0.75 mM

Table 4.3 Mortality and X-fin prevalence observed in Tg(*l-fabp*:*CFP-NTR*)[s891] larvae at 120 hpf following a static embryonic exposure to either 12 μM BkF, 2 mM metronidazole, both, or neither (1% DMSO). Hepatic ablation (+MTZ treatments) had no discernable effect on the induction of X-fin following BkF exposure, nor on overall mortality.

Treatment	Plate 1		Plate 2	
	Mortality	**X-fin**	**Mortality**	**X-fin**
(-) MTZ (-) BkF	0/24	0/24	1/24	0/24
(-) MTZ (+) BkF	2/24	22/24	2/24	22/24
(+) MTZ (-) BkF	1/24	0/24	1/24	0/24
(+) MTZ (+) BkF	0/24	23/24	1/24	23/24

Table 4.4 MetaCore Process network analysis of differentially expressed genes with log$_2$FC > 1.0 in larvae exposed to 12 µM BkF vs 1% DMSO at various time points: (a) 48 hfp; (b). 60 hpf; (c) 72 hpf; (d) 96 hpf.

Upregulated genes			Downregulated genes		
(a) 48 hpf					
Process network	FDR	Ratio	Process network	FDR	Ratio
Inflammation_Complement system	4.06e-07	9/26	Cell adhesion_Cell-matrix interactions	6.75e-04	13/132
Inflammation_Innate inflammatory response	7.28E-04	10/79	Cell adhesion_Integrin priming	8.82e-03	7/53
			Neurophysiological process_Transmission of nerve impulse	4.54e-02	9/118
(b) 60 hpf					
Process network	FDR	Ratio	Process network	FDR	Ratio
Inflammation_Complement system	5.56e-07	10/26	Cell adhesion_Cell-matrix interactions	6.75E-04	13/132
Cell adhesion_Platelet-endothelium-leucocyte interactions	3.359E-05	15/97	Cell adhesion_Integrin priming	8.82E-03	7/53
Blood coagulation	1.147-3	9/49	Neurophysiological process_Transmission of nerve impulse	4.54E-02	9/118
Inflammation_Innate inflammatory response	1.648e-3	11/79			
Proteolysis_ECM remodeling	2.115e-3	8/44			
Inflammation_Kallikrein-kinin system	3.153e-3	10/74			
Cell adhesion_Cell-matrix interactions	2.352e-2	12/132			
Proteolysis_Connective tissue degradation	2.352e-2	8/67			
Immune response_Th17-derived cytokines	2.352e-2	6/39			
(c) 72 hpf					
Process network	FDR	Ratio	Process network	FDR	Ratio
Proteolysis_ECM remodeling	2.44E-06	13/44	Cell adhesion_Cell-matrix interactions	9.76E-04	19/132
Inflammation_Complement system	3.343e-6	10/26	Cell adhesion_Amyloid proteins	9.119e-3	17/137
Cell adhesion_Platelet-endothelium-leucocyte interactions	1.178e-4	16/97	Proteolysis_Connective tissue degradation	9.119e-3	11/67
Proteolysis_Connective tissue degradation	7.087e-4	12/67	Transport_Potassium transport	2.002e-2	13/100
Cell adhesion_Cell-matrix interactions	1.043e-3	17/132			
Blood coagulation	4.329e-3	9/49			
Inflammation_Kallikrein-kinin system	2.145e-2	10/74			
Inflammation_Innate inflammatory response	3.126e-2	10/79			

Table 4.4 (continued)

Upregulated genes			Downregulated genes		
Process network	**FDR**	**Ratio**	**Process network**	**FDR**	**Ratio**
(d) 96 hpf					
Inflammation_Complement system	1.83E-03	8/26	Development_Neurogenesis in general	3.55E-11	36/140
Proteolysis_ECM remodeling	1.826e-3	10/44	Cell adhesion_Cell-matrix interactions	6.175e-3	21/132
Inflammation_Kallikrein-kinin system	6.612e-3	12/74	Muscle contraction	6.175e-3	16/87
Proteolysis_Connective tissue degradation	7.527e-3	11/67	Cell adhesion_Amyloid proteins	6.731e-3	21/137
Inflammation_Innate inflammatory response	7.527e-3	12/79	Development_Skeletal muscle development	1.678e-2	17/110
Immune response_Th17-derived cytokines	7.840e-3	8/39	Transport_Calcium transport	1.678e-2	18/120
Cell adhesion_Cell-matrix interactions	7.840e-3	16/132	Development_Cartilage development	3.398e-2	10/52
Signal transduction_Leptin signaling	1.008e-2	9/52			
Reproduction_Gonadotropin regulation	1.008e-2	13/99			
Development_EMT_Regulation of epithelial-to-mesenchymal transition	1.090e-2	17/154			

Table 4.5 MetaCore transcription factor target enrichment analysis of differentially expressed genes with log2FC > 1.0 in larvae exposed to 12 μM BkF vs 1% DMSO at various time points: (a) 48 hfp; (b). 60 hpf; (c) 72 hpf; (d) 96 hpf. The p-values generated by the enrichment analysis are calculated using a hypergeometric distribution and represent the probability that the observed ratio of connections with a particular transcription factor would occur in our data by chance. The z-score is a measure of how saturated the number of connections is for a particular transcription factor based on our data set.

| Enriched	z-score	p-value	Enriched	z-score	p-value
(a) 48 hpf			**(d) 96 hpf**		
AHRR	8.0	1.39E-04	FOSL2	9.3	3.27E-12
FOSL2	3.6	3.44E-03	LEF1	8.3	1.54E-11
FOSL1	4.3	4.44E-04	FOSL1	8.1	7.80E-11
JUNB	3.7	1.94E-03	CEBPB	7.6	1.21E-11
LEF1	4.1	5.14E-04	FOS	7.0	1.13E-09
PPARA	3.5	2.32E-03	AHRR	6.6	5.05E-05
			JUNB	6.2	2.22E-07
(b) 60 hpf			ASCL1	5.9	4.85E-07
AHRR	8.9	5.32E-06	PPARG	5.5	8.76E-07
JUNB	7.0	6.76E-08	JUND	5.4	1.23E-06
TCF4	3.3	8.50E-03	GATA4	5.1	4.29E-06
FOSL2	4.9	1.17E-04	FOXQ1	5.1	1.74E-04
NFATC2	5.3	1.87E-05	HOXB8	4.8	2.25E-03
FOSL1	5.2	2.13E-05	SIX2	4.7	9.57E-05
LEF1	5.5	6.90E-06	OLIG2	4.6	4.47E-05
PPARA	2.7	9.76E-03	ISL1	4.5	6.12E-05
BCL6	3.3	2.05E-03	LMX1B	4.4	1.27E-03
TCF4	2.6	8.63E-03	KLF2	4.4	3.53E-04
			FOXF1	4.3	4.57E-04
(c) 72 hpf			ZIC1	4.2	2.68E-03
AHRR	7.4	2.09E-05	PAX6	4.2	1.25E-04
FOSL2	6.1	1.52E-06	FOXA1	4.1	1.33E-04
NFAT5	3.4	7.37E-03	MAL	3.9	1.65E-03
TCF4	4.0	1.71E-03	IRX3	3.9	3.07E-03
JUNB	7.2	1.20E-08	FOSB	3.7	1.51E-03
FOSL1	5.7	2.69E-06	MYOD1	3.7	7.15E-04
FOXF1	3.1	8.07E-03	BCL11B	3.7	1.21E-03
NFATC2	4.9	3.07E-05	KLF13	3.7	9.88E-03
LEF1	5.5	3.57E-06	SHOX2	3.7	9.88E-03
ZBTB16	3.4	3.47E-03	MEOX1	3.6	2.02E-02
PBX1	3.3	2.10E-03	HOXA1	3.6	2.02E-02
BCL6	4.6	2.62E-05	ATOH1	3.6	1.39E-03
PPARA	2.9	5.37E-03	MAFB	3.5	1.88E-03
ATF3	3.0	3.90E-03	MYT1	3.3	1.03E-02
TCF4	2.9	3.27E-03	NR4A1	3.3	3.55E-03
			TLX3	3.3	1.62E-02
			TBX2	3.2	8.19E-03
			MYB	3.2	2.81E-03
			ATF3	3.0	3.51E-03
			HOXA2	3.0	2.91E-03
			POU3F3	2.9	1.28E-02
			FOXP2	2.8	5.42E-03
			HAND2	2.7	1.34E-02
			DLX3	2.7	1.89E-02
			PROX1	2.5	1.67E-02
			VIT	2.4	1.71E-02
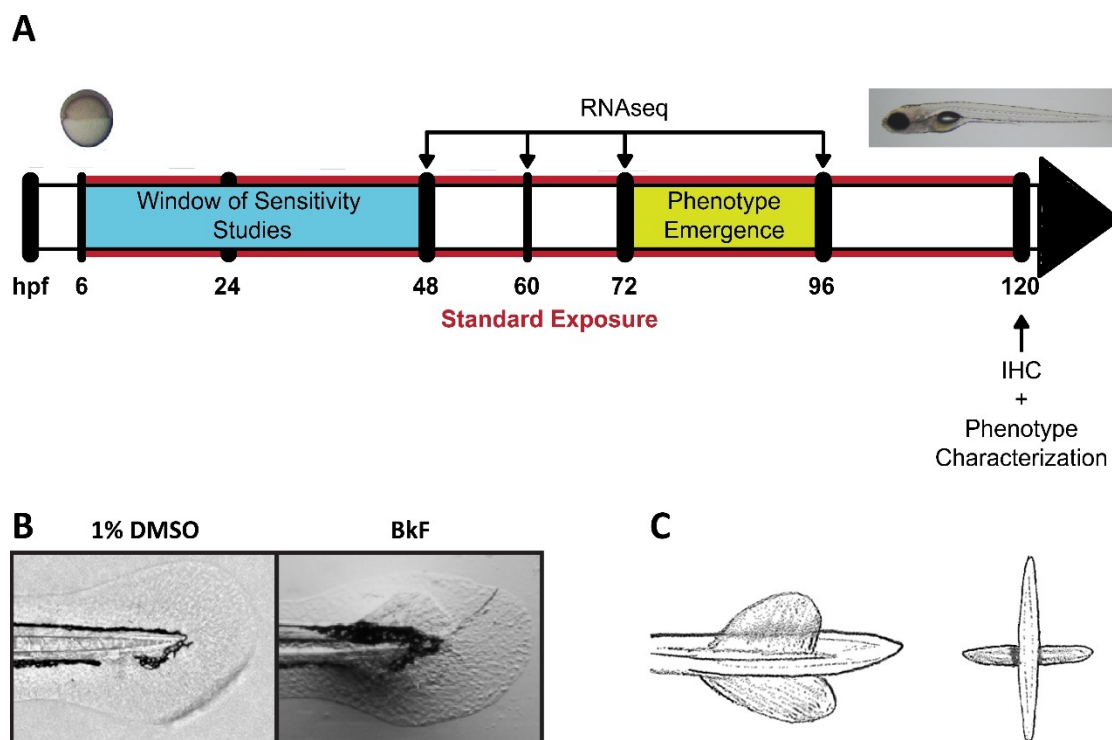
Figure 4.1 Exposure study paradigm and representative images of x-fin caudal fin phenotype. A) Study paradigm. B) Example of x-fin phenotype following exposure to 12 μM BkF. C) Artist's rendering of dorsal and posterior views of x-fin phenotype.
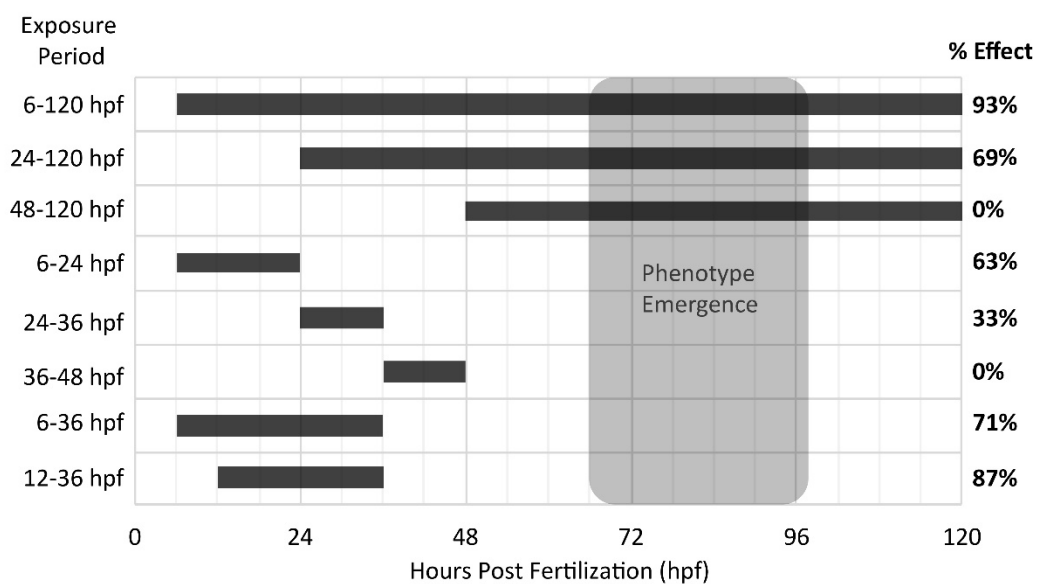
Figure 4.2 Critical window of sensitivity studies. Percent effect (out of n = 16) indicates the prevalence of the x-wing phenotype for the windowed exposure period indicated by the black bars. Grey phenotype emergence box indicates when the visible phenotype emerges.

CO MO + 1% DMSO   **CO MO + BkF**

AHR1A MO + BkF   **AHR1B MO + BkF**   **AHR2 MO + BkF**
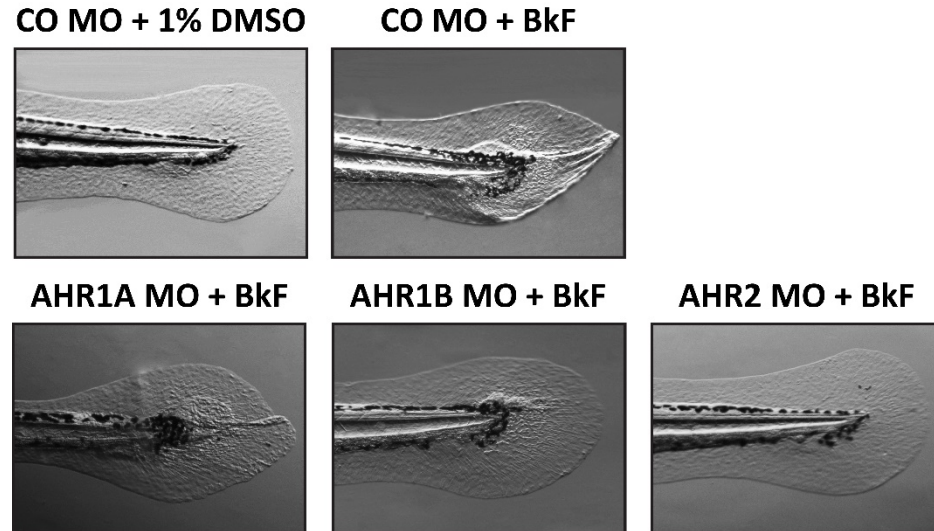
Figure 4.3 Brightfield representative images of caudal fins of BkF- or DMSO-treated animals at 5 days post-fertilization (dpf). Pictured are control, *ahr1a*, *ahr1b*, or *ahr2* morphants (n = 16 per treatment.)
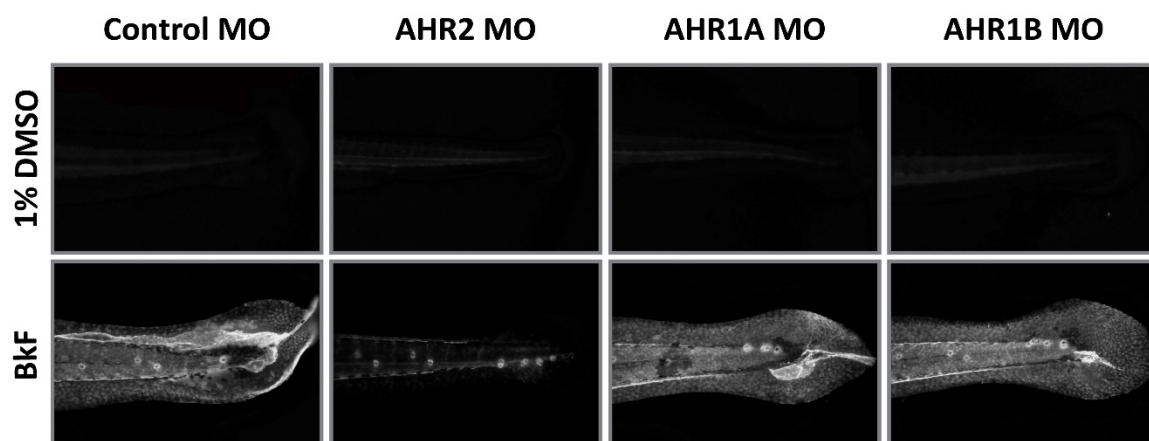
Figure 4.4 Cyp1a expression patterns related to 3 μm BkF or 1% DMSO exposure (n = 16 per treatment). Skin expression is Ahr2 dependent but expression in neuromasts was not dependent for any AHR isoform.
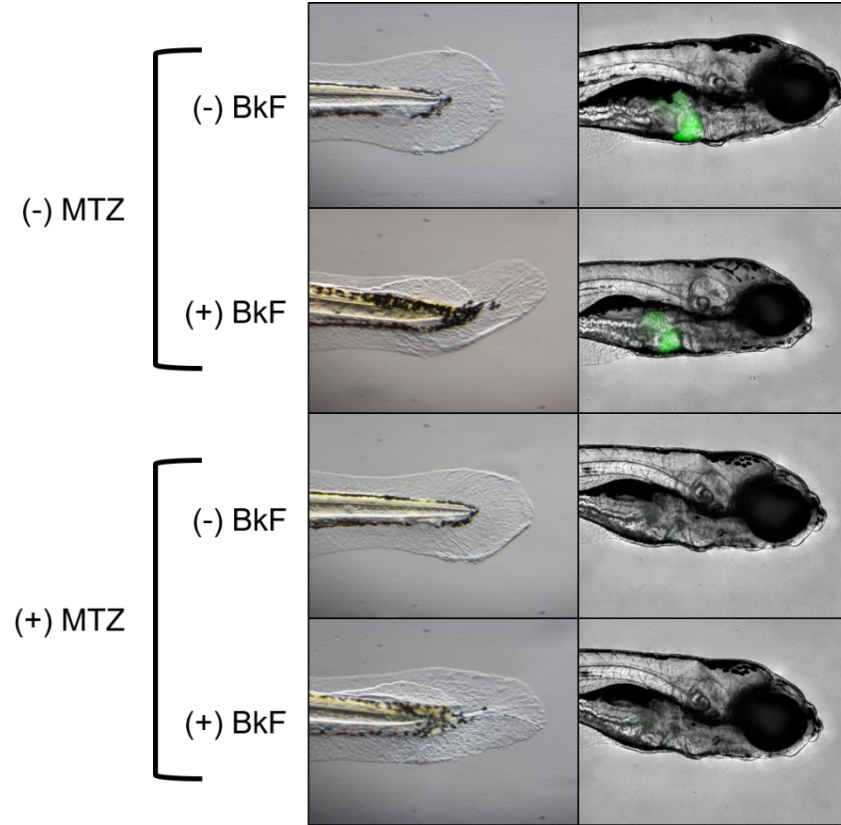
Figure 4.5 Hepatic ablation of Tg(*l-fabp:CFP-NTR*)[s891] larvae at 120 hpf follow static embryonic exposure to 12 μM BkF, 2 mM MTZ, both, or neither (1% DMSO). The trunk and head belong to the same individual for each respective treatment. The X-fin phenotype is visible in 12 μM
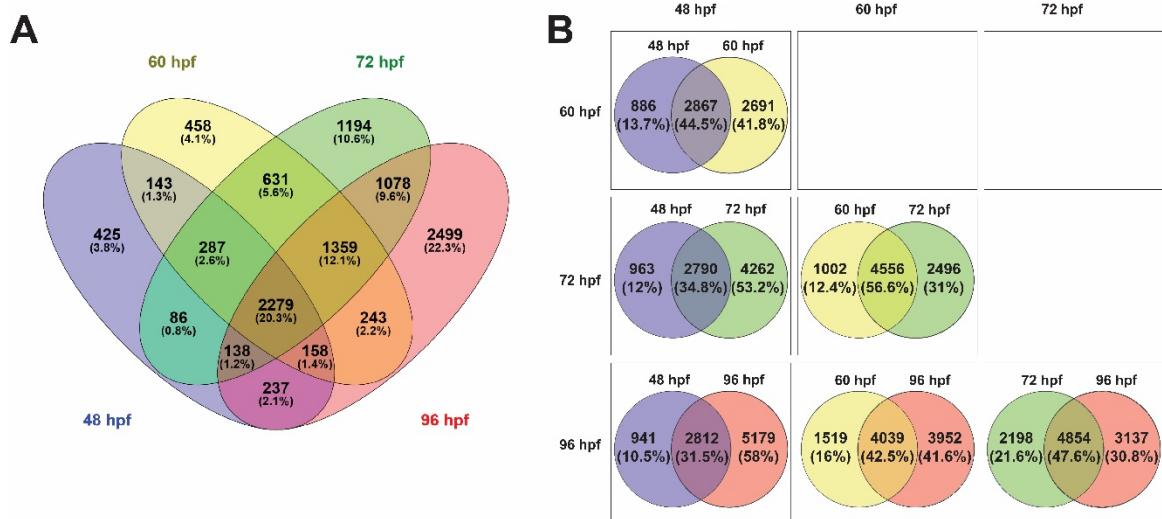
Figure 4.6 Venn diagrams of differentially expressed genes (adjusted p-value < 0.05) in animals exposed to benzo[k]fluoranthene or DMSO. A) Across all four time points. B) Pairwise comparisons.
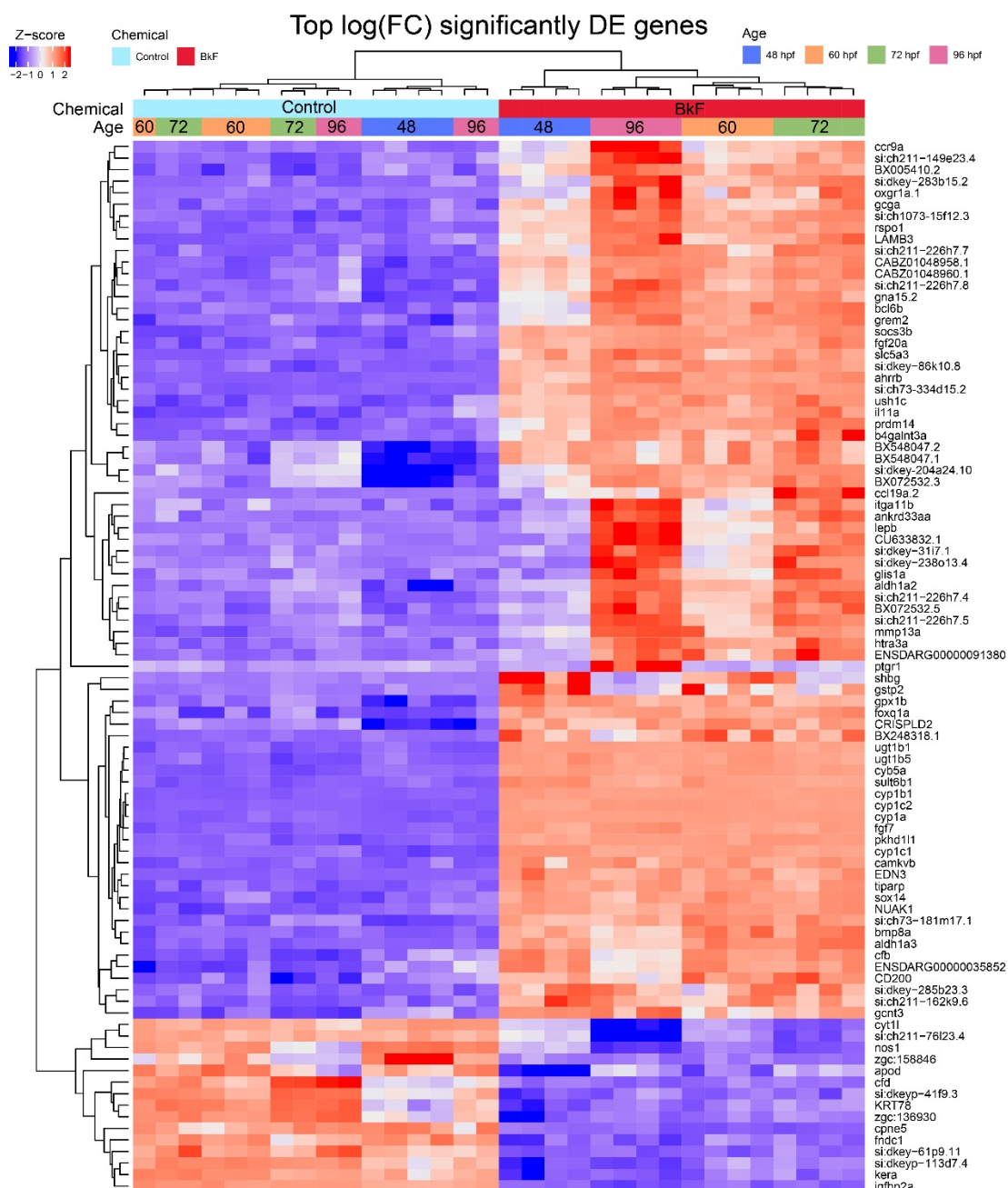
Figure 4.7 Heat map of 50 transcripts with highest fold changes of expression in distal trunk tissue following exposure to benzo[k]fluoranthene (BkF) across four time points, hierarchically clustered based on treatment, age, and gene. Color indicates distance from average gene counts across all samples, with blue indicating lower than average expression and red indicating higher than average expression.
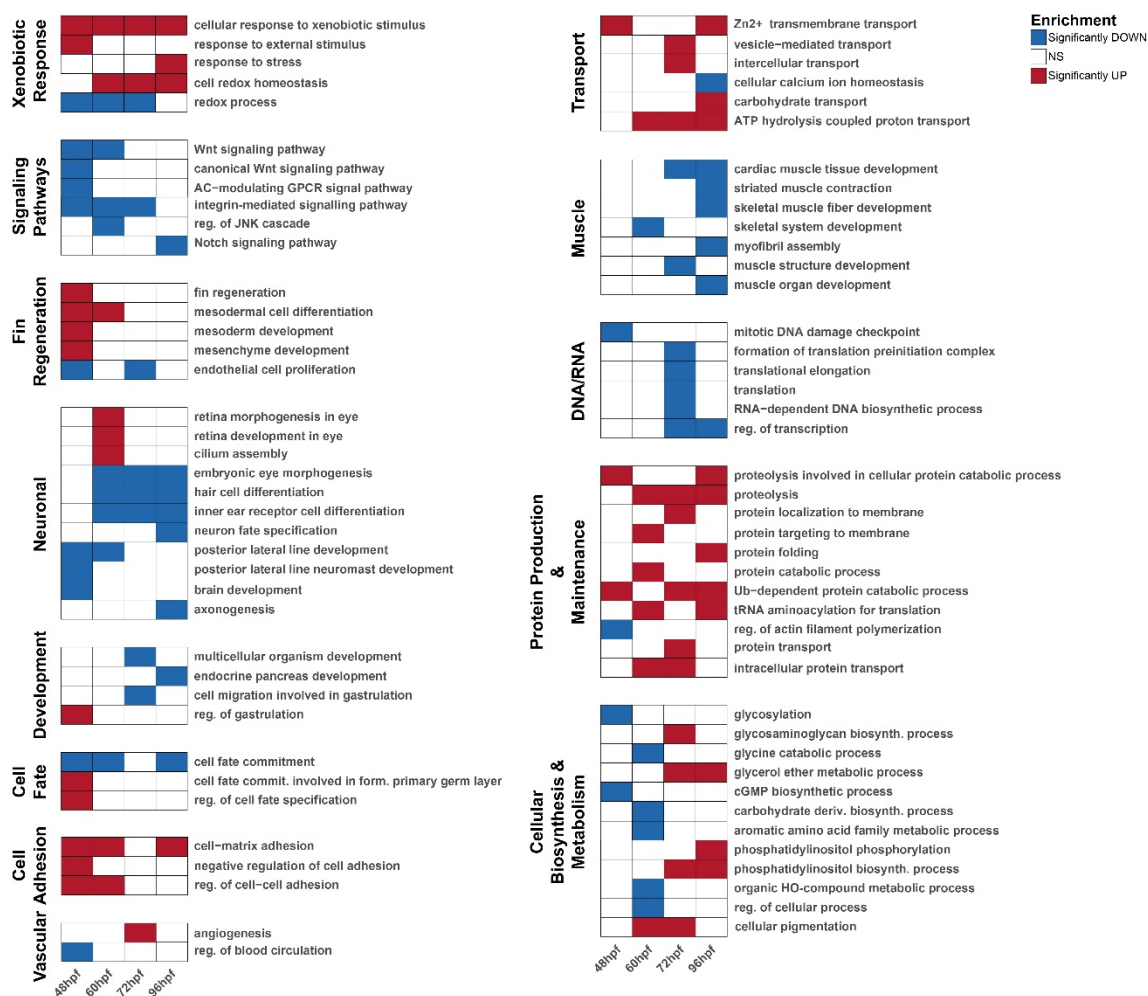
Figure 4.8 Heat map of significant (p ≤ 0.05) Gene Ontology (GO) term enrichments across four time points in distal trunk tissue following exposure to benzo[k]fluoranthene (BkF). Red indicates significantly enriched processes among upregulated genes, blue indicates significantly enriched processes among downregulated genes, and white indicates processes that were not significantly enriched at the given time point.
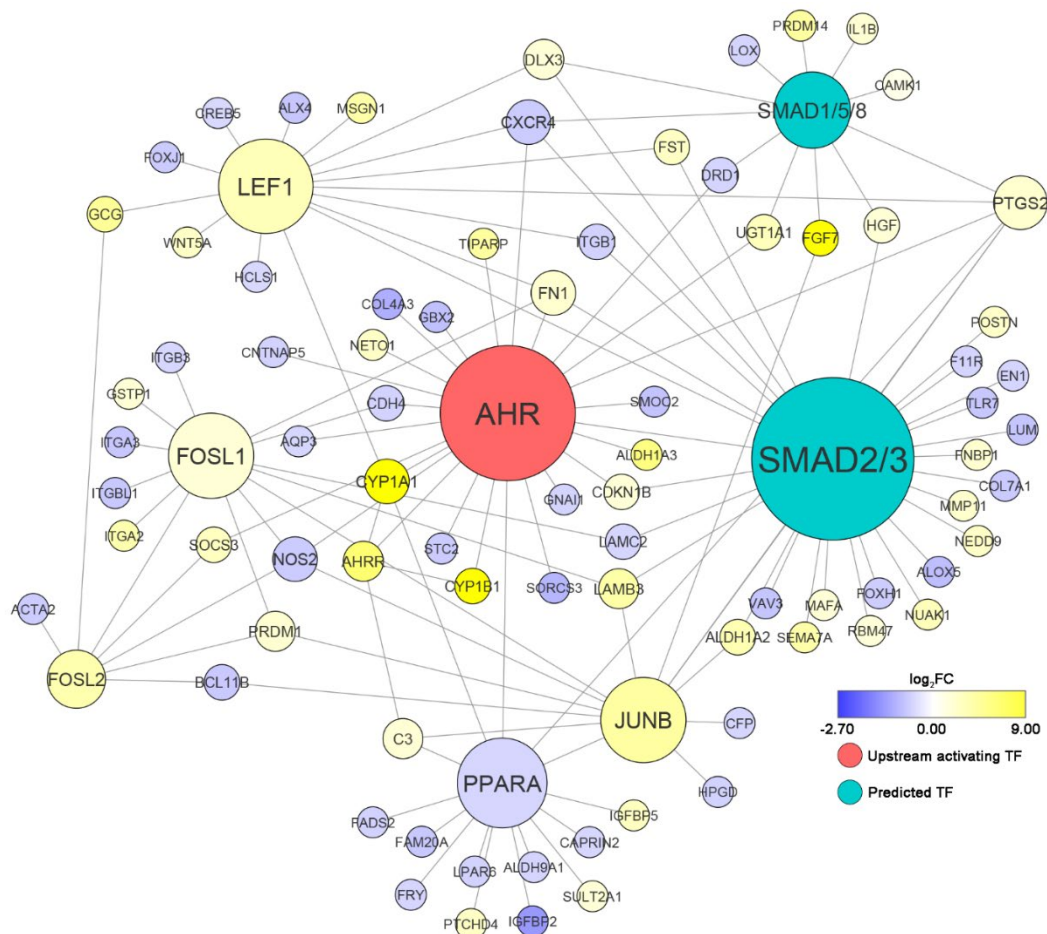
Figure 4.9. Interactome of enriched and predicted active transcription factors (TFs) and their target interactions at 48 hours post-fertilization following BkF exposure, as indicated by MetaCore. Log$_2$FC is displayed as a gradient increased from blue to yellow. The upstream activated TF (AHR) is red and the TFs that are hypothesized to be activated are teal. Size reflects the number of interactions.
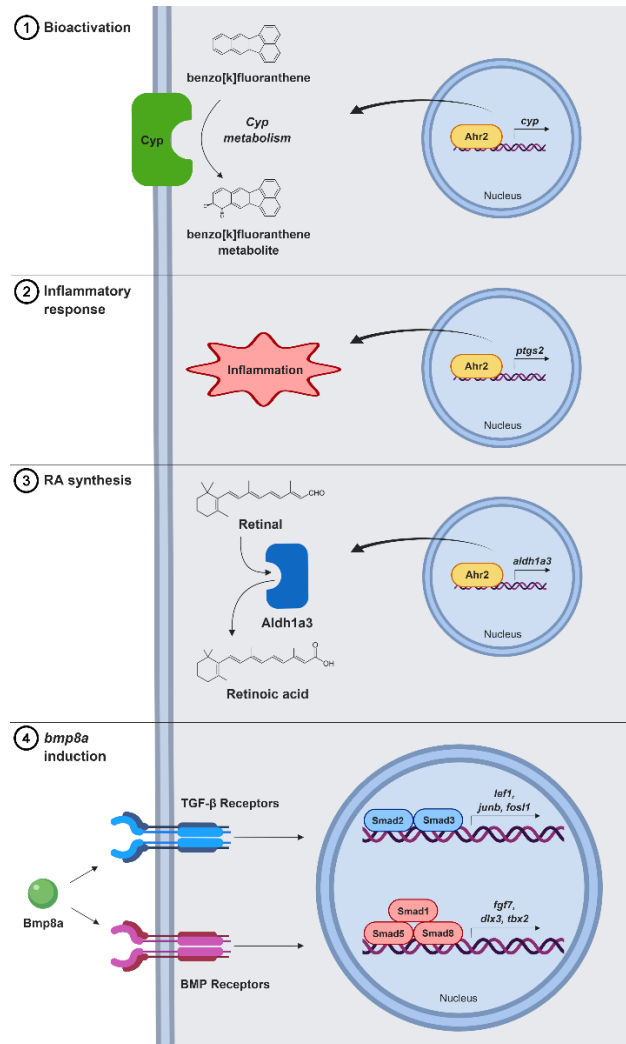
Figure 4.10. Illustration of four hypothesized mechanisms that could potentially induce the X-fin phenotype following AHR activation based on RNA sequencing data. (1) BkF could be bioactivated into a metabolite following Cyp induction. (2) BkF-bound Ahr2 may induce inflammation, possibly through induction of *ptgs2* (*cox2*), and cause an aberrant regenerative response. (3) BkF-bound Ahr2 could direct induce expression of aldh1a3, resulting in retinoic acid synthesis. (4) Through an unknown pathway, BkF-bound Ahr2 could activate BMP signaling via induction of *bmp8a*, resulting in X-fin. (Made in ©BioRender - biorender.com)

CHAPTER 5 – DISCUSSION

Epimorphic regeneration is a complex process involving a tightly coordinated sequence of events that starts with wounded tissue and ends with a near-perfect replacement of lost tissue [10]. In this process, damaged tissue undergoes limited dedifferentiation into a mass of multipotent stem cells called a blastema. Induction of the blastema involves epithelial-mesenchymal signaling between the wound epidermis and stump tissue, which rapidly transform into the apical epithelial cap (AEC) and blastema [10]. Compared to other vertebrates such as certain fish, amphibians, and lizards, the ability of mammals to regenerate tissue is severely impaired. Interestingly, mammals including humans do have a very limited capacity for epimorphic regeneration. This ability is strongest during fetal development and is retained very briefly after birth, but it quickly diminishes [202]. In some cases, adult humans are capable of regenerating finger tips, but only if the injury is distal to the nail matrix. This demonstrates that adult mammals have the innate capacity to undergo epimorphic regeneration similar to "lower" vertebrates, but for unknown reasons, this ability is locked away.

The primary aim of this dissertation was to advance our understanding of how zebrafish are capable of undergoing epimorphic fin regeneration by analyzing the regenerate transcriptome. In Chapter 2, we took a computational approach to interrogating epimorphic regeneration. Our goal was to identify miRNAs that are differentially expressed during the induction of the fin blastema. We performed parallel sequencing of total and small RNA derived from presumptive blastema tissue at 1 day post-amputation (dpa). At this point, the blastema has yet to form as indicated by the

absence of increased expression of Msx gene family members, which are the classical

blastema biomarkers. We started out analysis by broadly characterizing the

transcriptomic landscape by identifying enriched processes, key transcription factors, and

general changes in gene expression. This analysis was comprehensive because few

studies have fully explored the regenerate transcriptome, especially prior to blastema

formation. Since we used a *de novo* sequencing approach, we could potentially identify

new signaling pathways that have been overlooked. We then identified differentially

expressed microRNAs and performed an anti-correlated miRNA-mRNA expression

analysis. Using predictive databases, we discovered thousands of potential interactions

that were stringently filtered based on prediction scores. Among these predictions were

the miRNA targeting of novel transcription factors, chromatin remodelers, and signaling

genes. We identified a fish-specific miRNA, miR-724, that was predicted to target *fgf20a*

with a score of 100 from TargetScan, indicating extremely high confidence. We also

discovered evidence that Scatter factor signaling (through *met* and semaphorins) and

Hedgehog signaling (through *ihhb*) are upstream of blastema induction, and their

activities may also be regulated by miRNAs. These may represent a novel paradigm in

epithelial-mesenchymal signaling that has previously been overlooked. *foxm1* and *mycn*,

which control the cell cycle and proliferation, were also predicted to be miRNA targets.

Finally, we demonstrated that miRNAs such as miR-146a and mR-146b could mediate

inflammation and promote regeneration by targeting *eya4*.

In Chapter 3, we used a microarray to discover the mechanism behind impaired

larval fin regeneration following exposure to glucocorticoids (GCs). Notably, this was

independent of inflammation as previously demonstrated [40]. We discovered that activation of the glucocorticoid receptor (GR) by beclomethasone dipropionate (BFP) induced expression of an oncofetal gene, *cripto-1* (*one-eyed pinhead*). Outside of our lab, induction of *cripto-1* by the GR has never been demonstrated. We used a transient knockdown approach by injecting embryos with a morpholino oligo (MO) targeting *cripto-1*. We found that this was sufficient to permit regeneration in the presence of BDP. We performed an analysis of the *cripto-1* promoter, and while we did not identify a transactivation binding site for the GR, we did find binding sites for several transcription factors that increased expression in the microarray. This study demonstrated that the GR is capable of inducing expression of an oncofetal gene. We also showed that cripto-1 may play an important role during the early stages of regeneration and that perturbing its expression can have adverse effects.

This dissertation also sought to understand how chemical exposure to an environmental pollutant could induce appendage duplication during development. Chapter 4 involved characterizing the role of the aryl hydrocarbon receptor (AHR) in duplicate caudal fin phenotype we nicknamed x-fin. As its name suggests, zebrafish exposed to benzo[k]fluoranthene (BkF) develop an ectopic caudal fin lateral to the normally developing fin. Given the role of AHR in activating metabolism of xenobiotics, we sought to determine whether hepatic metabolism of BkF was involved. Ablation of hepatocytes using a transgenic line demonstrated that the phenotype was independent of liver metabolism. We performed RNA sequencing on trunk tissue at four different time points and discovered that BMP and FGF signaling ligands had strongly increased

expression. Enrichment analysis identified an inflammatory response, possibly mediated by Th17 cells. It also found that the fin regeneration process was enriched. We also found using MetaCore network analysis that AHR could directly increase transcription of *aldh1a3*, which synthesizes retinoic acid. While we did not fund out the exact mechanism leading to x-fin, we generated several hypotheses as to how AHR could mediate this process.

In summary, we used transcriptomics as the primary tool for interrogating zebrafish fin regeneration and aberrant development. This allowed us to identify novel regulatory signaling mechanisms involved in the early stages of blastema induction. We also characterized how xenobiotic-sensing ligands can modulate regeneration and development. The results of this dissertation provide several new directions for regenerative medicine and developmental research.

CHAPTER 6 – FUTURE DIRECTIONS

The results of this dissertation offer several different paths that subsequent research could take. The RNA sequencing data generating by Chapters 2 and 4 provide literally thousands of testable hypotheses. The chapters also outline what are likely to be the more salient hypotheses to test.

In Chapter 2, we identified several regulatory processes that have a high probability of being crucial to blastema formation. In general, ideal follow up studies would use in situ hybridization to characterize the spatiotemporal expression patterns of miRNAs and their predicted targets. CRISPR-Cas9 could be used to target miRNAs for generating loss-of-function mutants or complete removal or a miRNA gene. One caveat to such a study would be that the target miRNA may be developmentally critical or that the indel mutation would cause an unintended effect on an associated miRNA cluster. Also, presence of more than one precursor for certain miRNAs may be helpful or harmful. For example, if a miRNA is required for life, deletion of one paralog might allow the animal to survive while also impairing regeneration. Conversely, if both miRNA genes need to be knocked out, then creation of another mutant could be cumbersome especially if the target lacks ideal PAM sites.

Discovery of the Indian hedgehog (*ihhb*) prior to blastema formation suggests a novel mechanism of epithelial-mesenchymal interactions. Chemical and genetic approaches could be taken to test the hypothesis that Hedgehog signaling is required for blastema formation. Such studies could utilize cyclopamine as an inhibitor of Hedgehog

signaling and demonstrate its effect on blastema formation by using in situ hybridization of blastema and apical epithelial cap (AEC) biomarkers. Transient knockdown of *ihhb* using an MO would be a more specific approach. An even more precise approach would be to use CRISPR-Cas9 to induce an indel causing a loss-of-function mutation. Although hedgehog is a vital development pathway, functional compartmetalization of *indian hedgehog* paralogs may allow the zebrafish to survive the mutation. A mutant capable of induced overexpression of the Hedgehog antagonist *hhip* would be another way test the important of Hedgehog signaling during regeneration. Another knockdown or knockout experiment involving in miR-146a and miR-146b would be useful determine their role in mediating Hedgehog signaling via repression of *hhip*.

In Chapter 3, we identified several transcription factors that are known to be involved in neural development. Since appropriate neural function is required for regeneration at its earliest stages, and given that embryos must be exposed to BDP within 4 hours of amputation, it is possible that the GR may mediate this neural process. One follow up study might include staining acetylated β-tubulin to characterize regeneration of the caudal fin nerves following BDP exposure. Another study could utilize laser capture microscopy to specifically target nerve-enriched tissue and measure cripto-1 abundance relative to tissue with low nerve density.

In Chapter 4, we were unable to determine the exact aryl hydrocarbon receptor (AHR)-dependent mechanism leading to ectopic caudal fin formation, but we generated multiple hypothesis. As in Chapter 2, *in situ* hybridization would be a good first step for

characterizing the spatiotemporal expression patterns of key genes such as Bone morphogen protein (BMP) and Fibroblast growth factor (FGF) ligands following BkF exposure. Next, use of antibodies targeting phosphorylated Smad2/3 or Smad1/5/8 could be used to respectively determine whether Transforming growth factor beta (TGF-β) or BMP signaling have increased signaling following BkF exposure. If phosphorylation is detected, necessity could be tested by using chemical inhibitors, such as SB431542 to specifically target TGF-β and K02288 to specifically target BMP.

BIBLIOGRAPHY

1. Broussonet, M., *Observations sur la régénérations de quelques parties du corps des poissons.* Hist. d. l'Acad. Roy. des Sciences, 1786.

2. Capdevila, J. and J.C.I. Belmonte, *Patterning mechanisms controlling vertebrate limb development.* Annual Review of Cell and Developmental Biology, 2001. **17**: p. 87-132.

3. Marshall, H., et al., *Retinoids and Hox genes.* Faseb Journal, 1996. **10**(9): p. 969-978.

4. Zakany, J. and D. Duboule, *The role of Hox genes during vertebrate limb development.* Current Opinion in Genetics & Development, 2007. **17**(4): p. 359-366.

5. Laufer, E., et al., *Expression of radical fringe in limb-bud ectoderm regulates apical ectodermal ridge formation.* Nature, 1997. **386**(6623): p. 366-373.

6. Narita, T., et al., *Wnt10a is involved in AER formation during chick limb development.* Developmental Dynamics, 2005. **233**(2): p. 282-287.

7. Niederreither, K., et al., *Morphological and molecular characterization of retinoic acid-induced limb duplications in mice.* Developmental Biology, 1996. **176**(2): p. 185-198.

8. Ogura, T., et al., *Evidence that Shh cooperates with a retinoic acid inducible co-factor to establish ZPA-like activity.* Development, 1996. **122**(2): p. 537-542.

9. Hammerschmidt, M., et al., *dino and mercedes, two genes regulating dorsal development in the zebrafish embryo.* Development, 1996. **123**: p. 95-102.

10. Tal, T.L., J.A. Franzosa, and R.L. Tanguay, *Molecular signaling networks that choreograph epimorphic fin regeneration in zebrafish - a mini-review.* Gerontology, 2010. **56**(2): p. 231-40.

11. Kumar, A. and J.P. Brockes, *Nerve dependence in tissue, organ, and appendage regeneration.* Trends in Neurosciences, 2012. **35**(11): p. 691-699.

12. Satoh, A., A. Makanae, and N. Wada, *The apical ectodermal ridge (AER) can be re-induced by wounding, wnt-2b, and fgf-10 in the chicken limb bud.* Developmental Biology, 2010. **342**(2): p. 157-168.

13. Poss, K.D., J.X. Shen, and M.T. Keating, *Induction of lef1 during zebrafish fin regeneration.* Dev Dyn, 2000. **219**(2): p. 282-286.

14. Whitehead, G.G., et al., *fgf20 is essential for initiating zebrafish fin regeneration.* Science, 2005. **310**(5756): p. 1957-60.

15. Poss, K.D., et al., *Roles for Fgf signaling during zebrafish fin regeneration.* Dev Biol, 2000. **222**(2): p. 347-58.

16. Jazwinska, A., R. Badakov, and M.T. Keating, *Activin-betaA signaling is required for zebrafish fin regeneration.* Curr Biol, 2007. **17**(16): p. 1390-5.

17. Schebesta, M., et al., *Transcriptional profiling of caudal fin regeneration in zebrafish.* Sci World J, 2006. **6**: p. 38-54.

18. Chablais, F. and A. Jazwinska, *IGF signaling between blastema and wound epidermis is required for fin regeneration.* Development, 2010. **137**(6): p. 871-879.

19. Munch, J., A. Gonzalez-Rajal, and J.L. de la Pompa, *Notch regulates blastema proliferation and prevents differentiation during adult zebrafish fin regeneration.* Development, 2013. **140**(7): p. 1402-1411.

20. Mathew, L.K., et al., *Comparative expression profiling reveals an essential role for raldh2 in epimorphic regeneration.* J Biol Chem, 2009. **284**(48): p. 33642-53.

21. Goessling, W., et al., *Genetic interaction of PGE2 and Wnt signaling regulates developmental specification of stem cells and regeneration.* Cell, 2009. **136**(6): p. 1136-47.

22. Samad, T.A., et al., *Interleukin-1 beta-mediated induction of Cox-2 in the CNS contributes to inflammatory pain hypersensitivity.* Nature, 2001. **410**(6827): p. 471-475.

23. Roehl, H.H., *Linking wound response and inflammation to regeneration in the zebrafish larval fin.* International Journal of Developmental Biology, 2018. **62**(6-8): p. 473-477.

24. Mori, R., T.J. Shaw, and P. Martin, *Molecular mechanisms linking wound inflammation and fibrosis: knockdown of osteopontin leads to rapid repair and reduced scarring.* Journal of Experimental Medicine, 2008. **205**(1): p. 43-51.

25. Akimenko, M.A., et al., *Differential induction of four msx homeobox genes during fin development and regeneration in zebrafish.* Development, 1995. **121**(2): p. 347-57.

26. Stewart, S., Z.Y. Tsun, and J.C.I. Belmonte, *A histone demethylase is necessary for regeneration in zebrafish.* Proceedings of the National Academy of Sciences of the United States of America, 2009. **106**(47): p. 19889-19894.

27. Katsuyama, T. and R. Paro, *Epigenetic reprogramming during tissue regeneration.* Febs Letters, 2011. **585**(11): p. 1617-1624.

28. Bushati, N. and S.M. Cohen, *MicroRNA functions.* Annual Review of Cell and Developmental Biology, 2007. **23**: p. 175-205.

29. Agarwal, V., et al., *Predicting effective microRNA target sites in mammalian mRNAs.* Elife, 2015. **4**.

30. !!! INVALID CITATION !!! {}.

31. Nielsen, C.B., et al., *Determinants of targeting by endogenous and exogenous microRNAs and siRNAs.* Rna, 2007. **13**(11): p. 1894-1910.

32. Robins, H. and W.H. Press, *Human microRNAs target a functionally distinct population of genes with AT-rich 3 ' UTRs.* Proceedings of the National Academy of Sciences of the United States of America, 2005. **102**(43): p. 15557-15562.

33. Gaidatzis, D., et al., *Inference of miRNA targets using evolutionary conservation and pathway analysis.* Bmc Bioinformatics, 2007. **8**.

34. Thatcher, E.J., et al., *Regulation of zebrafish fin regeneration by microRNAs.* Proceedings of the National Academy of Sciences of the United States of America, 2008. **105**(47): p. 18384-18389.

35. Yin, V.P., et al., *Fgf-dependent depletion of microRNA-133 promotes appendage regeneration in zebrafish.* Genes Dev, 2008. **22**(6): p. 728-33.

36. Kozomara, A., M. Birgaoanu, and S. Griffiths-Jones, *miRBase: from microRNA sequences to function.* Nucleic Acids Research, 2019. **47**(D1): p. D155-D162.

37. Betel, D., et al., *The microRNA.org resource: targets and expression.* Nucleic Acids Research, 2008. **36**: p. D149-D153.

38. Tanguay, R.L., et al., *Regenerative pathways probed using chemical genetics in zebrafish.* Faseb Journal, 2007. **21**(5): p. A626-A627.

39. Ponomareva, L.V., et al., *Using Ambystoma mexicanum (Mexican axolotl) embryos, chemical genetics, and microarray analysis to identify signaling pathways associated with tissue regeneration.* Comparative Biochemistry and Physiology C-Toxicology & Pharmacology, 2015. **178**: p. 128-135.

40. Mathew, L.K., et al., *Unraveling tissue regeneration pathways using chemical genetics.* J Biol Chem, 2007. **282**(48): p. 35202-10.

41. Brown, P.O. and D. Botstein, *Exploring the new world of the genome with DNA microarrays.* Nature Genetics, 1999. **21**: p. 33-37.

42. Romanov, V., et al., *A critical comparison of protein microarray fabrication technologies.* Analyst, 2014. **139**(6): p. 1303-1326.

43. Barbulovic-Nad, I., et al., *Bio-microarray fabrication techniques - A review.* Critical Reviews in Biotechnology, 2006. **26**(4): p. 237-259.

44. Morey, J.S., J.C. Ryan, and F.M. Van Dolah, *Microarray validation: factors influencing correlation between oligonucleotide microarrays and real-time PCR.* Biological Procedures Online, 2006. **8**: p. 175-193.

45. Mathew, L.K., et al., *Crosstalk between AHR and Wnt signaling through R-Spondin1 impairs tissue regeneration in zebrafish.* FASEB J, 2008. **22**(8): p. 3087-96.

46. Fang, Z.D. and X.Q. Cui, *Design and validation issues in RNA-seq experiments.* Briefings in Bioinformatics, 2011. **12**(3): p. 280-287.

47. King, B.L. and V.P. Yin, *A Conserved MicroRNA Regulatory Circuit Is Differentially Controlled during Limb/Appendage Regeneration.* Plos One, 2016. **11**(6).

48. Tamura, K., S. Ohgo, and H. Yokoyama, *Limb blastema cell: A stem cell for morphological regeneration.* Development Growth & Differentiation, 2010. **52**(1): p. 89-99.

49. Akimenko, M.A., et al., *Old questions, new tools, and some answers to the mystery of fin regeneration.* Dev Dyn, 2003. **226**(2): p. 190-201.

50. Rivera-Gonzalez, G.C. and S.A. Morris, *Tracing the Origins of Axolotl Limb Regeneration.* Developmental Cell, 2018. **47**(6): p. 675-677.

51. Tokuyama, M.A., et al., *Developmental and adult-specific processes contribute to de novo neuromuscular regeneration in the lizard tail.* Developmental Biology, 2018. **433**(2): p. 287-296.

52. Maden, M., et al., *Perfect chronic skeletal muscle regeneration in adult spiny mice, Acomys cahirinus.* Scientific Reports, 2018. **8**.

53.   Seifert, A.W. and K. Muneoka, *The blastema and epimorphic regeneration in mammals.* Developmental Biology, 2018. **433**(2): p. 190-199.

54.   Conboy, I.M. and T.A. Rando, *Aging, stem cells and tissue regeneration - Lessons from muscle.* Cell Cycle, 2005. **4**(3): p. 407-410.

55.   Yanger, K., et al., *Robust cellular reprogramming occurs spontaneously during liver regeneration.* Genes & Development, 2013. **27**(7): p. 719-724.

56.   King, M.W., A.W. Neff, and A.L. Mescher, *The Developing Xenopus Limb as a Model for Studies on the Balance between Inflammation and Regeneration.* Anatomical Record-Advances in Integrative Anatomy and Evolutionary Biology, 2012. **295**(10): p. 1552-1561.

57.   Govindan, J. and M.K. Iovine, *Dynamic remodeling of the extra cellular matrix during zebrafish fin regeneration.* Gene Expression Patterns, 2015. **19**(1-2): p. 21-29.

58.   Ouyang, X.H., et al., *Hyaluronic acid synthesis is required for zebrafish tail fin regeneration.* Plos One, 2017. **12**(2).

59.   Takayama, K., et al., *Expression patterns of dnmt3aa, dnmt3ab, and dnmt4 during development and fin regeneration in zebrafish.* Gene Expression Patterns, 2014. **14**(2): p. 105-110.

60.   Dupret, B., et al., *The histone lysine methyltransferase Ezh2 is required for maintenance of the intestine integrity and for caudal fin regeneration in zebrafish.* Biochimica Et Biophysica Acta-Gene Regulatory Mechanisms, 2017. **1860**(10): p. 1079-1093.

61.   Ozsolak, F. and P.M. Milos, *RNA sequencing: advances, challenges and opportunities.* Nature Reviews Genetics, 2011. **12**(2): p. 87-98.

62.   Tal, T.L., et al., *MicroRNAs control neurobehavioral development and function in zebrafish.* FASEB J, 2012. **26**(4): p. 1452-61.

63.   Anders, S., P.T. Pyl, and W. Huber, *HTSeq--a Python framework to work with high-throughput sequencing data.* Bioinformatics, 2015. **31**(2): p. 166-9.

64.   Kim, D., B. Langmead, and S.L. Salzberg, *HISAT: a fast spliced aligner with low memory requirements.* Nat Methods, 2015. **12**(4): p. 357-60.

65.   RStudio Team, *RStudio: Integrated Development for R.* 2016, RStudio, Inc.: Boston, MA.

66.   Chen, Y., A.T. Lun, and G.K. Smyth, *From reads to genes to pathways: differential expression analysis of RNA-Seq experiments using Rsubread and the edgeR quasi-likelihood pipeline.* F1000Res, 2016. **5**: p. 1438.

67.   Anders, S., et al., *Count-based differential expression analysis of RNA sequencing data using R and Bioconductor.* Nat Protoc, 2013. **8**(9): p. 1765-86.

68.   Durinck, S., et al., *Mapping identifiers for the integration of genomic datasets with the R/Bioconductor package biomaRt.* Nat Protoc, 2009. **4**(8): p. 1184-91.

69.   Brown, J., et al., *Bioinformatics Resource Manager: a systems biology web tool for microRNA and omics data integration.* BMC Bioinformatics, 2019. **20**(1): p. 255.

70.   Wickham, H., *ggplot2: Elegant Graphics for Data Analysis*. 2016, New York: Springer-Verlag.

71.   Arnold, J.B., *ggthemes: Extra Themes, Scales and Geoms for 'ggplot2'*. 2017.

72.   Slowikowski, K., *ggrepel: Repulsive Text and Label Geoms for 'ggplot2'*. 2017.

73.   Bengtsson, H., *matrixStats: Functions that Apply to Rows and Columns of Matrices (and to Vectors)*. R package version 0.53, 2017. **1**.

74.   Gu, Z., R. Eils, and M. Schlesner, *Complex heatmaps reveal patterns and correlations in multidimensional genomic data.* Bioinformatics, 2016. **32**(18): p. 2847-9.

75.   Friedlander, M.R., et al., *miRDeep2 accurately identifies known and hundreds of novel microRNA genes in seven animal clades.* Nucleic Acids Res, 2012. **40**(1): p. 37-52.

76.   Ashburner, M., et al., *Gene ontology: tool for the unification of biology. The Gene Ontology Consortium.* Nat Genet, 2000. **25**(1): p. 25-9.

77.   Carbon, S., et al., *The Gene Ontology Resource: 20 years and still GOing strong.* Nucleic Acids Research, 2019. **47**(D1): p. D330-D338.

78.   Lee, H.M., T.S. Kim, and E.K. Jo, *MiR-146 and miR-125 in the regulation of innate immunity and inflammation.* Bmb Reports, 2016. **49**(6): p. 311-318.

79.   Krishnan, N., et al., *Dephosphorylation of the C-terminal Tyrosyl Residue of the DNA Damage-related Histone H2A.X Is Mediated by the Protein Phosphatase Eyes Absent.* Journal of Biological Chemistry, 2009. **284**(24): p. 16066-16070.

80.   Song, M.Z., et al., *PSMC2 is up-regulated in osteosarcoma and regulates osteosarcoma cell proliferation, apoptosis and migration.* Oncotarget, 2017. **8**(1): p. 933-953.

81.   Yoshinari, N., et al., *Gene expression and functional analysis of zebrafish larval fin fold regeneration.* Developmental Biology, 2009. **325**(1): p. 71-81.

82.   Freund, A., et al., *Proteostatic Control of Telomerase Function through TRiC-Mediated Folding of TCAB1.* Cell, 2014. **159**(6): p. 1389-1403.

83.   Kaur, J., et al., *Identification of chemerin receptor (ChemR23) in human endothelial cells: Chemerin-induced endothelial angiogenesis.* Biochemical and Biophysical Research Communications, 2010. **391**(4): p. 1762-1768.

84.   Miyasaka, K.Y., et al., *Csrp1 regulates dynamic cell movements of the mesendoderm and cardiac mesoderm through interactions with Dishevelled and Diversin.* Proceedings of the National Academy of Sciences of the United States of America, 2007. **104**(27): p. 11274-11279.

85.   Dourlen, P., et al., *Functional screening of Alzheimer risk loci identifies PTK2B as an in vivo modulator and early marker of Tau pathology.* Molecular Psychiatry, 2017. **22**(6): p. 874-883.

86.   Thatcher, E.J., et al., *Regulation of zebrafish fin regeneration by microRNAs.* Proc Natl Acad Sci U S A, 2008.

87.   Holman, E.C., et al., *Microarray Analysis of microRNA Expression during Axolotl Limb Regeneration.* Plos One, 2012. **7**(9).

88.   Sehm, T., et al., *miR-196 is an essential early-stage regulator of tail regeneration, upstream of key spinal cord patterning events.* Developmental Biology, 2009. **334**(2): p. 468-480.

89.   Folini, M., et al., *miR-21: an oncomir on strike in prostate cancer.* Molecular Cancer, 2010. **9**.

90.   Asangani, I.A., et al., *MicroRNA-21 (miR-21) post-transcriptionally downregulates tumor suppressor Pdcd4 and stimulates invasion, intravasation and metastasis in colorectal cancer.* Oncogene, 2008. **27**(15): p. 2128-2136.

91.   Sayed, D., et al., *MicroRNA-21 targets Sprouty2 and promotes cellular outgrowths.* Molecular Biology of the Cell, 2008. **19**(8): p. 3272-3282.

92.   Klein, O.D., et al., *Sprouty genes control diastema tooth development via bidirectional antagonism of epithelial-mesenchymal FGF signaling.* Developmental Cell, 2006. **11**(2): p. 181-190.

93.   Mailleux, A.A., et al., *Evidence that SPROUTY2 functions as an inhibitor of mouse embryonic lung growth and morphogenesis.* Mechanisms of Development, 2001. **102**(1-2): p. 81-94.

94.   Li, D.Q., et al., *MicroRNA-132 enhances transition from inflammation to proliferation during wound healing.* Journal of Clinical Investigation, 2015. **125**(8): p. 3008-3026.

95.   Ucar, A., et al., *miR-212 and miR-132 are required for epithelial stromal interactions necessary for mouse mammary gland development.* Nature Genetics, 2010. **42**(12): p. 1101-U100.

96.   Cheng, H.S., et al., *MicroRNA-146 represses endothelial activation by inhibiting pro-inflammatory pathways.* EMBO Mol Med, 2013. **5**(7): p. 1017-34.

97.   Xiong, J.W., et al., *Vezf1: A Zn finger transcription factor restricted to endothelial cells and their precursors.* Developmental Biology, 1999. **206**(2): p. 123-141.

98.   Bell, E., J. Lunec, and D.A. Tweddle, *Cell cycle regulation targets of MYCN identified by gene expression microarrays.* Cell Cycle, 2007. **6**(10): p. 1249-1256.

99.   Boon, K., et al., *N-myc enhances the expression of a large set of genes functioning in ribosome biogenesis and protein synthesis.* The EMBO journal, 2001. **20**(6): p. 1383-1393.

100.   Janardhanan, R., N.L. Banik, and S.K. Ray, *N-Myc down regulation induced differentiation, early cell cycle exit, and apoptosis in human malignant neuroblastoma cells having wild type or mutant p53.* Biochemical Pharmacology, 2009. **78**(9): p. 1105-1114.

101.   Korver, W., J. Roose, and H. Clevers, *The winged-helix transcription factor Trident is expressed in cycling cells.* Nucleic Acids Research, 1997. **25**(9): p. 1715-1719.

102.   Teh, M.T., et al., *FOXM1 Induces a Global Methylation Signature That Mimics the Cancer Epigenome in Head and Neck Squamous Cell Carcinoma.* Plos One, 2012. **7**(3).

103. Cui, J., et al., *HGF/Met and FOXM1 form a positive feedback loop and render pancreatic cancer cells resistance to Met inhibition and aggressive phenotypes.* Oncogene, 2016. **35**(36): p. 4708-4718.

104. Bladt, F., et al., *Essential Role for the C-Met Receptor in the Migration of Myogenic Precursor Cells into the Limb Bud.* Nature, 1995. **376**(6543): p. 768-771.

105. Prat, M., et al., *The Receptor Encoded by the Human C-Met Oncogene Is Expressed in Hepatocytes, Epithelial-Cells and Solid Tumors.* International Journal of Cancer, 1991. **49**(3): p. 323-328.

106. Santos-Ruiz, L., et al., *Cell proliferation during blastema formation in the regenerating teleost fin.* Developmental Dynamics, 2002. **223**(2): p. 262-272.

107. Conrotto, P., et al., *Sema4D induces angiogenesis through met recruitment by Plexin B1.* Blood, 2005. **105**(11): p. 4321-4329.

108. Rosen, E.M., S.K. Nigam, and I.D. Goldberg, *Scatter Factor and the C-Met Receptor - a Paradigm for Mesenchymal Epithelial Interaction.* Journal of Cell Biology, 1994. **127**(6): p. 1783-1787.

109. Gollner, H., et al., *Impaired ossification in mice lacking the transcription factor Sp3.* Mechanisms of Development, 2001. **106**(1-2): p. 77-83.

110. Walker, M.P., L.P. Tian, and A.G. Matera, *Reduced Viability, Fertility and Fecundity in Mice Lacking the Cajal Body Marker Protein, Coilin.* Plos One, 2009. **4**(7).

111. Vogan, J.M., et al., *Minimized human telomerase maintains telomeres and resolves endogenous roles of H/ACA proteins, TCAB1, and Cajal bodies.* Elife, 2016. **5**: p. e18221.

112. Nace, J.D. and R.A. Tassava, *Examination of Fibronectin Distribution and Its Sources in the Regenerating Newt Limb by Immunocytochemistry and in-Situ Hybridization.* Developmental Dynamics, 1995. **202**(2): p. 153-164.

113. Takahashi, K., K. Mitsui, and S. Yamanaka, *Role of ERas in promoting tumour-like properties in mouse embryonic stem cells.* Nature, 2003. **423**(6939): p. 541-545.

114. Watt, F.M., *Unexpected Hedgehog-Wnt interactions in epithelial differentiation.* Trends in Molecular Medicine, 2004. **10**(12): p. 577-580.

115. Jiang, J. and C. Hui, *Hedgehog Signaling in Development and Cancer.* Developmental Cell, 2008. **15**(6): p. 801-812.

116. Teh, M.T., et al., *FOXM1 is a downstream target of Gli1 in basal cell carcinomas.* Cancer Research, 2002. **62**(16): p. 4773-4780.

117. Callahan, J.F., et al., *Identification of novel inhibitors of the transforming growth factor beta 1 (TGF-beta 1) type 1 receptor (ALK5).* J Med Chem, 2002. **45**(5): p. 999-1001.

118. Laping, N.J., et al., *Inhibition of transforming growth factor (TGF)-beta 1-induced extracellular matrix with a novel inhibitor of the TGF-beta type I receptor kinase activity: SB-431542.* Mol Pharmacol, 2002. **62**(1): p. 58-64.

119. Inman, G.J., et al., *SB-431542 is a potent and specific inhibitor of transforming growth factor-beta superfamily type I activin receptor-like kinase (ALK) receptors ALK4, ALK5, and ALK7.* Mol Pharmacol, 2002. **62**(1): p. 65-74.

120. Kawakami, A., T. Fukazawa, and H. Takeda, *Early fin primordia of zebrafish larvae regenerate by a similar growth control mechanism with adult regeneration.* Dev Dyn, 2004. **231**(4): p. 693-9.

121. Feldman, B. and D.L. Stemple, *Morpholino phenocopies of sqt, oep, and ntl mutations.* Genesis, 2001. **30**(3): p. 175-7.

122. Chatzopoulou, A., et al., *Glucocorticoid-Induced Attenuation of the Inflammatory Response in Zebrafish.* Endocrinology, 2016. **157**(7): p. 2772-84.

123. Bianco, C., et al., *Role of Cripto-1 in stem cell maintenance and malignant progression.* Am J Pathol, 2010. **177**(2): p. 532-40.

124. Schier, A.F., *Nodal morphogens.* Cold Spring Harb Perspect Biol, 2009. **1**(5): p. a003459.

125. Rangel, M.C., et al., *Role of Cripto-1 during epithelial-to-mesenchymal transition in development and cancer.* Am J Pathol, 2012. **180**(6): p. 2188-200.

126. Zhou, X., et al., *Nodal is a novel TGF-β-like gene expressed in the mouse node during gastrulation.* Nature, 1993. **361**(6412): p. 543.

127. Rangel, M.C., et al., *Developmental signaling pathways regulating mammary stem cells and contributing to the etiology of triple-negative breast cancer.* Breast Cancer Res Treat, 2016. **156**(2): p. 211-26.

128. Bianco, C., et al., *Identification of Cripto-1 as a novel serologic marker for breast and colon cancer.* Clinical Cancer Research, 2006. **12**(17): p. 5158-5164.

129. Yoon, H.J., et al., *The role of Cripto-1 in the tumorigenesis and progression of oral squamous cell carcinoma.* Oral Oncol, 2011. **47**(11): p. 1023-31.

130. Zhang, H., et al., *Clinical significance of cripto-1 expression in lung adenocarcinoma.* Oncotarget, 2017. **8**(45): p. 79087-79098.

131. Klauzinska, M., et al., *The multifaceted role of the embryonic gene Cripto-1 in cancer, stem cells and epithelial-mesenchymal transition.* Semin Cancer Biol, 2014. **29**: p. 51-58.

132. Kawakami, Y., et al., *Wnt/beta-catenin signaling regulates vertebrate limb regeneration.* Genes Dev, 2006. **20**(23): p. 3232-7.

133. Gray, P.C., C.A. Harrison, and W. Vale, *Cripto forms a complex with activin and type II activin receptors and can block activin signaling.* Proc Natl Acad Sci U S A, 2003. **100**(9): p. 5193-8.

134. Gray, P.C., et al., *Cripto binds transforming growth factor beta (TGF-beta) and inhibits TGF-beta signaling.* Mol Cell Biol, 2006. **26**(24): p. 9268-78.

135. Shani, G., et al., *GRP78 and cripto form a complex at the cell surface and collaborate to inhibit transforming growth factor beta signaling and enhance cell growth.* Mol Cell Biol, 2008. **28**(2): p. 666-677.

136. Yeo, C. and M. Whitman, *Nodal signals to Smads through Cripto-dependent and Cripto-independent mechanisms.* Mol Cell, 2001. **7**(5): p. 949-57.

137. Kelber, J.A., et al., *Cripto is a noncompetitive activin antagonist that forms analogous signaling complexes with activin and nodal.* J Biol Chem, 2008. **283**(8): p. 4490-500.

138. Nagaoka, T., et al., *Cripto-1 enhances the canonical Wnt/β-catenin signaling pathway by binding to LRP5 and LRP6 co-receptors.* Cell Signal, 2013. **25**(1): p. 178-189.

139. Strizzi, L., et al., *Cripto-1: a multifunctional modulator during embryogenesis and oncogenesis.* Oncogene, 2005. **24**(37): p. 5731-41.

140. Bianco, C., et al., *A Nodal- and ALK4-independent signaling pathway activated by Cripto-1 through Glypican-1 and c-Src.* Cancer Res, 2003. **63**(6): p. 1192-7.

141. Watanabe, K., et al., *Enhancement of Notch receptor maturation and signaling sensitivity by Cripto-1.* J Cell Biol, 2009. **187**(3): p. 343-53.

142. Nagaoka, T., et al., *An evolving web of signaling networks regulated by Cripto-1.* Growth Factors, 2012. **30**(1): p. 13-21.

143. Hoover, M., et al., *Identification of myosin II as a cripto binding protein and regulator of cripto function in stem cells and tissue regeneration.* Biochem Biophys Res Commun, 2019. **509**(1): p. 69-75.

144. Hentschke, M., et al., *Germ cell nuclear factor is a repressor of CRIPTO-1 and CRIPTO-3.* J Biol Chem, 2006. **281**(44): p. 33497-504.

145. Walker, L., et al., *Non-human primate and rodent embryonic stem cells are differentially sensitive to embryotoxic compounds.* Toxicol Rep, 2015. **2**: p. 165-174.

146. Xu, C., et al., *Specific arrest of cardiogenesis in cultured embryonic stem cells lacking Cripto-1.* Dev Biol, 1998. **196**(2): p. 237-47.

147. Parisi, S., et al., *Nodal-dependent Cripto signaling promotes cardiomyogenesis and redirects the neural fate of embryonic stem cells.* J Cell Biol, 2003. **163**(2): p. 303-14.

148. Geier, M.C., et al., *Comparative developmental toxicity of a comprehensive suite of polycyclic aromatic hydrocarbons.* Arch Toxicol, 2018. **92**(2): p. 571-586.

149. Crowell, S.R., et al., *Preliminary physiologically based pharmacokinetic models for benzo[a]pyrene and dibenzo[def,p]chrysene in rodents.* Toxicology and Applied Pharmacology, 2011. **257**(3): p. 365-376.

150. Ober, E.A., H.A. Field, and D.Y. Stainier, *From endoderm formation to liver and pancreas development in zebrafish.* Mech Dev, 2003. **120**(1): p. 5-18.

151. Curado, S., et al., *Conditional targeted cell ablation in zebrafish: a new tool for regeneration studies.* Dev Dyn, 2007. **236**(4): p. 1025-35.

152. Goodale, B.C., et al., *Structurally distinct polycyclic aromatic hydrocarbons induce differential transcriptional responses in developing zebrafish.* Toxicol Appl Pharmacol, 2013. **272**(3): p. 656-70.

153. Julian, L.M., A.C.H. McDonald, and W.L. Stanford, *Direct reprogramming with SOX factors: masters of cell fate.* Current Opinion in Genetics & Development, 2017. **46**: p. 24-36.

154. Burton, A. and M.E. Torres-Padilla, *A Pluripotency Platform for Prdm14.* Developmental Cell, 2016. **38**(1): p. 3-5.

155. Fior, R., et al., *The differentiation and movement of presomitic mesoderm progenitor cells are controlled by Mesogenin 1.* Development, 2012. **139**(24): p. 4656-4665.

156. Nagasawa, Y., et al., *Identification and characterization of Pkhd1, the mouse orthologue of the human ARPKD gene.* Journal of the American Society of Nephrology, 2002. **13**(9).

157. Osterwalder, M., et al., *HAND2 Targets Define a Network of Transcriptional Regulators that Compartmentalize the Early Limb Bud Mesenchyme.* Developmental Cell, 2014. **31**(3): p. 345-357.

158. Talbot, J.C., S.L. Johnson, and C.B. Kimmel, *hand2 and Dlx genes specify dorsal, intermediate and ventral domains within zebrafish pharyngeal arches.* Development, 2010. **137**(15): p. 2506-2516.

159. Gilardelli, C.N., et al., *Functional and hierarchical interactions among zebrafish vox/vent homeobox genes.* Developmental Dynamics, 2004. **230**(3): p. 494-508.

160. Neto, A., N. Mercader, and J.L. Gomez-Skarmeta, *The Osr1 and Osr2 genes act in the pronephric anlage downstream of retinoic acid signaling and upstream of Wnt2b to maintain pectoral fin development.* Development, 2012. **139**(2): p. 301-11.

161. Pittlik, S., et al., *Expression of zebrafish aldh1a3 (raldh3) and absence of aldh1a1 in teleosts.* Gene Expression Patterns, 2008. **8**(3): p. 141-147.

162. Liu, M., et al., *Allele-Specific Imbalance of Oxidative Stress-Induced Growth Inhibitor 1 Associates With Progression of Hepatocellular Carcinoma.* Gastroenterology, 2014. **146**(4): p. 1084-U319.

163. Fabian, P., et al., *vox homeobox gene: a novel regulator of midbrain-hindbrain boundary development in medaka fish?* Development Genes and Evolution, 2016. **226**(2): p. 99-107.

164. Shou, S.M., et al., *HOXA13 regulates Aldh1a2 expression in the autopod to facilitate interdigital programmed cell death.* Developmental Dynamics, 2013. **242**(6): p. 687-698.

165. Yeung, C.Y.C., et al., *Gremlin-2 is a BMP antagonist that is regulated by the circadian clock.* Scientific Reports, 2014. **4**.

166. Gill, S.E. and W.C. Parks, *Metalloproteinases and their inhibitors: Regulators of wound healing.* International Journal of Biochemistry & Cell Biology, 2008. **40**(6-7): p. 1334-1347.

167. Chen, P., et al., *High NUAK1 expression correlates with poor prognosis and involved in NSCLC cells migration and invasion.* Experimental Lung Research, 2013. **39**(1): p. 9-17.

168. Jin, Y.R. and J.K. Yoon, *The R-spondin family of proteins: Emerging regulators of WNT signaling.* International Journal of Biochemistry & Cell Biology, 2012. **44**(12): p. 2278-2287.

169. Wu, F.J., et al., *BMP8A sustains spermatogenesis by activating both SMAD1/5/8 and SMAD2/3 in spermatogonia.* Science Signaling, 2017. **10**(477).

170. Goldstone, J., et al., *Identification and developmental expression of the full complement of Cytochrome P450 genes in Zebrafish.* BMC Genomics, 2010. **11**(1): p. 643.

171. Baird, W.M., Hooven Louisa A., Mahadevan, Brinda, *Carcinogenic polycyclic aromatic hydrocarbon-DNA adducts and mechanism of action.* Environmental and Molecular Mutagenesis, 2005. **45**(2-3): p. 106-114.

172. Weyand, E.H., et al., *Metabolism and Mutagenic Activity of Benzo[K]Fluoranthene and 3-Flurobenzo[K]Fluoranthene, 8-Flurobenzo[K]Fluoranthene and 9-Fluorobenzo[K]Fluoranthene.* Carcinogenesis, 1988. **9**(7): p. 1277-1281.

173. Luecke, S., et al., *The aryl hydrocarbon receptor (AHR), a novel regulator of human melanogenesis.* Pigment Cell & Melanoma Research, 2010. **23**(6): p. 828-833.

174. Ten Berge, D., et al., *Embryonic stem cells require Wnt proteins to prevent differentiation to epiblast stem cells.* Nature Cell Biology, 2011. **13**(9): p. 1070-U88.

175. Hikasa, H. and S.Y. Sokol, *Wnt Signaling in Vertebrate Axis Specification.* Cold Spring Harbor Perspectives in Biology, 2013. **5**(1).

176. Moreno-Layseca, P. and C.H. Streuli, *Signalling pathways linking integrins with cell cycle progression.* Matrix Biology, 2014. **34**: p. 144-153.

177. Gutkind, J.S., *The pathways connecting G protein-coupled receptors to the nucleus through divergent mitogen-activated protein kinase cascades.* Journal of Biological Chemistry, 1998. **273**(4): p. 1839-1842.

178. Galceran, J., et al., *LEF1-mediated regulation of Delta-like1 links Wnt and Notch signaling in somitogenesis.* Genes & Development, 2004. **18**(22): p. 2718-2723.

179. Levin, M., *Left-right asymmetry in embryonic development: a comprehensive review.* Mechanisms of Development, 2005. **122**(1): p. 3-25.

180. Wehner, D. and G. Weidinger, *Signaling networks organizing regenerative growth of the zebrafish fin.* Trends Genet, 2015. **31**(6): p. 336-43.

181. Yamaguchi, M., et al., *Histone deacetylase 1 regulates retinal neurogenesis in zebrafish by suppressing Wnt and Notch signaling pathways.* Development, 2005. **132**(13): p. 3027-3043.

182. Lie, D.C., et al., *Wnt signalling regulates adult hippocampal neurogenesis.* Nature, 2005. **437**(7063): p. 1370-1375.

183. Tilton, S.C., et al., *Bioinformatics Resource Manager v2.3: an integrated software environment for systems biology with microRNA and cross-species analysis tools.* BMC Bioinformatics, 2012. **13**(1): p. 311.

184. Hao, N. and M.L. Whitelaw, *The emerging roles of AhR in physiology and immunity.* Biochem Pharmacol, 2013. **86**(5): p. 561-70.

185. Hasegawa, T., et al., *Transient inflammatory response mediated by interleukin-1 beta is required for proper regeneration in zebrafish fin fold.* Elife, 2017. **6**.

186. Murad, A., et al., *Leptin is an autocrine/paracrine regulator of wound healing.* Faseb Journal, 2003. **17**(11): p. 1895-+.

187. Jacques, B.E., et al., *The role of Wnt/beta-catenin signaling in proliferation and regeneration of the developing basilar papilla and lateral line.* Developmental Neurobiology, 2014. **74**(4): p. 438-456.

188. Tamamura, Y., et al., *Developmental regulation of Wnt/beta-catenin signals is required for growth plate assembly, cartilage integrity, and endochondral ossification.* Journal of Biological Chemistry, 2005. **280**(19): p. 19185-19195.

189. Ishida, T., et al., *Phosphorylation of Junb family proteins by the Jun N-terminal kinase supports tissue regeneration in zebrafish.* Developmental Biology, 2010. **340**(2): p. 468-479.

190. Gibson-Brown, J.J., et al., *Involvement of T-box genes Tbx2-Tbx5 in vertebrate limb specification and development.* Development, 1998. **125**(13): p. 2499-2509.

191. Bobick, B.E. and J. Cobb, *Shox2 regulates progression through chondrogenesis in the mouse proximal limb.* Journal of Cell Science, 2012. **125**(24): p. 6071-6083.

192. Mullen, L.M., et al., *Nerve dependency of regeneration: The role of Distal-less and FGF signaling in amphibian limb regeneration.* Development, 1996. **122**(11): p. 3487-3497.

193. Nurieva, R.I., et al., *Bcl6 Mediates the Development of T Follicular Helper Cells.* Science, 2009. **325**(5943): p. 1001-1005.

194. Seijffers, R., A.J. Allchorne, and C.J. Woolf, *The transcription factor ATF-3 promotes neurite outgrowth.* Molecular and Cellular Neuroscience, 2006. **32**(1-2): p. 143-154.

195. Forrest, M.P., et al., *Knockdown of Human TCF4 Affects Multiple Signaling Pathways Involved in Cell Survival, Epithelial to Mesenchymal Transition and Neuronal Differentiation.* Plos One, 2013. **8**(8).

196. Shannon, P., et al., *Cytoscape: a software environment for integrated models of biomolecular interaction networks.* Genome Res, 2003. **13**(11): p. 2498-504.

197. Kim, S., et al., *Comparative Analysis of AhR-Mediated TCDD-Elicited Gene Expression in Human Liver Adult Stem Cells.* Toxicological Sciences, 2009. **112**(1): p. 229-244.

198. Park, J.Y., M.H. Pillinger, and S.B. Abramson, *Prostaglandin E-2 synthesis and secretion: The role of PGE(2) synthases.* Clinical Immunology, 2006. **119**(3): p. 229-240.

199. Bikoff, E.K., M.A. Morgan, and E.J. Robertson, *An expanding job description for Blimp-1/PRDM1.* Current Opinion in Genetics & Development, 2009. **19**(4): p. 379-385.

200. Shankar, P., et al., *Coupling Genome-wide Transcriptomics and Developmental Toxicity Profiles in Zebrafish to Characterize Polycyclic Aromatic Hydrocarbon (PAH) Hazard.* Int J Mol Sci, 2019. **20**(10).

201. Armenteros, T., et al., *BMP and WNT signalling cooperate through LEF1 in the neuronal specification of adult hippocampal neural stem and progenitor cells.* Scientific Reports, 2018. **8**.

202. Muneoka, K., et al., *Mammalian regeneration and regenerative medicine.* Birth Defects Research Part C: Embryo Today: Reviews, 2008. **84**(4): p. 265-280.

APPENDICES

List of Appendix Tables

List of Appendix Figures

Appendix A – Supplemental Data for Chapter 2

Table A.1 Differentially expressed genes with > 2-fold change in adult fin regenerates at 1 dpa.

genes	Symbol	logFC	FDR
ENSDARG00000105358	si:dkeyp-32g11.8	11.98	4.59E-09
ENSDARG00000092352	jac4	11.93	9.97E-11
ENSDARG00000045548	lepb	9.58	3.03E-11
ENSDARG00000073918	rnf41l	9.49	2.46E-10
ENSDARG00000023526	ggt1a	9.03	1.04E-09
ENSDARG00000053854	uts2a	8.99	4.86E-08
ENSDARG00000055705	f5	7.53	1.75E-09
ENSDARG00000037859	il11a	7.37	4.52E-11
ENSDARG00000036082	tph1b	7.06	3.02E-14
ENSDARG00000056166	jac2	6.99	3.16E-08
ENSDARG00000041382	si:dkey-283b15.2	6.94	1.58E-08
ENSDARG00000061498	dusp13a	6.93	4.71E-05
ENSDARG00000103515	vcana	6.91	3.43E-13
ENSDARG00000001452	adam8a	6.79	2.93E-15
ENSDARG00000036505	syt4	6.79	9.17E-08
ENSDARG00000055439	adamtsl7	6.70	7.45E-12
ENSDARG00000099819	sb:cb1058	6.49	7.51E-09
ENSDARG00000096664	cxl34c	6.43	3.79E-11
ENSDARG00000053498	ednrbb	6.34	7.69E-10
ENSDARG00000055527	cmn	6.34	1.98E-11
ENSDARG00000073900	fam212b	6.16	3.81E-11
ENSDARG00000077403	col8a1a	5.96	2.65E-06
ENSDARG00000058557	il11b	5.89	5.77E-09
ENSDARG00000103981	bhlha9	5.76	2.11E-09
ENSDARG00000024189	pnocb	5.68	3.62E-09
ENSDARG00000102277	lama1	5.52	2.53E-10
ENSDARG00000075261	timp2b	5.52	5.27E-12
ENSDARG00000000551	slc1a4	5.49	6.41E-08
ENSDARG00000099438	CABZ01073736.1	5.44	7.84E-08
ENSDARG00000014248	pdlim3b	5.32	8.25E-12
ENSDARG00000037415	dlgap1b	5.22	1.76E-05
ENSDARG00000086703	si:dkey-126g1.7	5.22	4.93E-12
ENSDARG00000102375	si:ch211-204c21.1	5.20	6.90E-07
ENSDARG00000099457	PTGDR2	5.11	6.57E-12
ENSDARG00000076897	CU570782.1	4.87	4.88E-07
ENSDARG00000105562	si:dkey-23i12.7	4.85	4.31E-09
ENSDARG00000078244	si:ch211-197l9.2	4.82	7.37E-15
ENSDARG00000102300	ca9	4.76	1.88E-08
ENSDARG00000074117	CCKBR (1 of many)	4.72	5.61E-06
ENSDARG00000104735	nkx6.2	4.71	3.07E-05
ENSDARG00000006598	sgk2b	4.66	1.03E-06
ENSDARG00000078529	adgrb1b	4.63	5.04E-05
ENSDARG00000053027	si:dkey-33i11.1	4.61	4.82E-09
ENSDARG00000044125	txn	4.56	9.02E-14
ENSDARG00000045051	slc16a3	4.55	1.22E-05
ENSDARG00000087646	runx1	4.54	1.51E-07
ENSDARG00000021948	tnc	4.54	4.10E-14
ENSDARG00000030289	jag1a	4.53	7.26E-12
ENSDARG00000103592	CABZ01102124.1	4.49	5.38E-08
ENSDARG00000104114	setd8b	4.49	9.79E-09
ENSDARG00000093712	CABZ01021530.1	4.48	2.15E-06
ENSDARG00000059259	pabpc4	4.42	1.20E-10
ENSDARG00000087704	gfra3	4.39	4.00E-07
ENSDARG00000068691	kctd4	4.38	8.53E-11

ENSDARG00000079296	gcga	4.38	8.22E-07
ENSDARG00000018260	bmp7a	4.36	9.03E-09
ENSDARG00000099744	gap43	4.36	1.57E-09
ENSDARG00000018404	krt18	4.35	1.71E-09
ENSDARG00000060498	tnfrsf9a	4.32	4.45E-13
ENSDARG00000002986	gda	4.28	6.04E-08
ENSDARG00000042983	has1	4.28	2.64E-11
ENSDARG00000006526	fn1b	4.24	1.47E-09
ENSDARG00000017901	tln2a	4.22	2.98E-11
ENSDARG00000090833	igfbp6b	4.21	3.43E-11
ENSDARG00000009949	fndc4b	4.17	7.81E-06
ENSDARG00000056374	noxo1b	4.17	2.58E-07
ENSDARG00000051923	ccnb1	4.12	3.28E-10
ENSDARG00000089362	grn1	4.10	6.59E-11
ENSDARG00000098327	CT573860.1	4.07	1.49E-07
ENSDARG00000077853	ttll2	4.01	1.06E-06
ENSDARG00000012395	mmp13a	3.95	2.09E-09
ENSDARG00000079373	fosl1b	3.94	1.51E-09
ENSDARG00000077811	sox11a	3.89	2.04E-09
ENSDARG00000075891	sall1b	3.88	4.42E-12
ENSDARG00000074378	junba	3.79	1.16E-12
ENSDARG00000019815	fn1a	3.74	2.01E-12
ENSDARG00000045367	tuba1b	3.74	5.11E-13
ENSDARG00000013719	gtse1	3.74	9.40E-09
ENSDARG00000058815	ihhb	3.72	8.88E-07
ENSDARG00000037142	zgc:153146	3.72	6.71E-08
ENSDARG00000014024	ms4a17a.4	3.71	2.75E-12
ENSDARG00000038066	kpna2	3.71	8.38E-13
ENSDARG00000101776	syt12	3.70	2.63E-07
ENSDARG00000054931	ppp2r5b	3.69	6.38E-05
ENSDARG00000042688	bora	3.66	7.40E-08
ENSDARG00000093098	ccl34b.8	3.66	1.83E-05
ENSDARG00000074363	TTC9	3.65	3.15E-11
ENSDARG00000090524	f2rl2	3.61	2.40E-10
ENSDARG00000039234	zgc:171579	3.61	7.08E-06
ENSDARG00000003200	foxm1	3.59	1.29E-06
ENSDARG00000077430	CLDN20 (1 of many)	3.59	6.75E-06
ENSDARG00000004932	anos1b	3.58	4.13E-13
ENSDARG00000026417	ccr12b.2	3.56	5.49E-09
ENSDARG00000037997	tubb5	3.55	2.97E-09
ENSDARG00000104801	tubb6	3.54	8.41E-08
ENSDARG00000009123	sele	3.53	3.48E-10
ENSDARG00000038278	ptgir	3.50	4.36E-09
ENSDARG00000087393	prr11	3.48	1.41E-06
ENSDARG00000023963	tpm4a	3.47	4.50E-08
ENSDARG00000096603	bmb	3.40	2.46E-07
ENSDARG00000076913	eme1	3.39	3.52E-07
ENSDARG00000031783	adcy8	3.38	6.37E-10
ENSDARG00000036721	tomm40l	3.37	4.22E-09
ENSDARG00000039062	morn4	3.36	2.09E-10
ENSDARG00000051731	faap24	3.36	3.38E-07
ENSDARG00000012485	aurka	3.35	1.14E-08
ENSDARG00000063385	cenpe	3.34	4.52E-08
ENSDARG00000096979	NPC2 (1 of many)	3.33	7.69E-12
ENSDARG00000100019	arhgap11a	3.32	1.95E-06
ENSDARG00000099265	slc7a5	3.32	1.84E-05
ENSDARG00000043004	si:dkeyp-117h8.4	3.31	5.45E-07
ENSDARG00000053493	aldh1a2	3.31	9.43E-12
ENSDARG00000062517	si:ch211-107n13.1	3.30	2.22E-10
ENSDARG00000075539	snphb	3.30	0.00021574
ENSDARG00000087554	cdk1	3.28	1.86E-07
ENSDARG00000088040	MDP1	3.28	1.75E-09
ENSDARG00000078654	tpx2	3.28	2.22E-10

ENSDARG00000102467	CABZ01056516.1	3.27	1.38E-10
ENSDARG00000043137	cdca8	3.27	2.14E-08
ENSDARG00000011094	ccna2	3.26	2.64E-08
ENSDARG00000007990	wt1b	3.25	0.00066333
ENSDARG00000105018	lrrc20	3.24	5.08E-10
ENSDARG00000076182	stat1b	3.24	2.17E-08
ENSDARG00000014943	kif23	3.23	1.04E-07
ENSDARG00000026611	socs3b	3.22	2.48E-12
ENSDARG00000007356	fgf20a	3.21	1.50E-10
ENSDARG00000025903	lgals9l1	3.20	2.64E-08
ENSDARG00000010556	mmp25b	3.20	1.09E-08
ENSDARG00000040009	palld	3.20	2.04E-13
ENSDARG00000075045	cxcl18b	3.20	1.04E-07
ENSDARG00000011141	dpysl5a	3.20	3.84E-06
ENSDARG00000040178	havcr1	3.18	1.84E-09
ENSDARG00000091150	mki67	3.17	3.27E-09
ENSDARG00000025043	trip13	3.17	3.48E-09
ENSDARG00000093622	spc24	3.16	9.94E-07
ENSDARG00000060246	slc16a6b	3.16	2.45E-06
ENSDARG00000016494	ddc	3.15	9.89E-09
ENSDARG00000092651	si:dkey-57a22.11	3.13	7.27E-06
ENSDARG00000058471	plk1	3.12	7.70E-10
ENSDARG00000090337	pprc1	3.12	3.14E-05
ENSDARG00000055632	smtnl	3.11	1.48E-09
ENSDARG00000099194	CABZ01058261.1	3.10	1.47E-09
ENSDARG00000009689	daam1b	3.07	1.06E-12
ENSDARG00000034643	fhl3a	3.07	1.16E-12
ENSDARG00000012671	inhbaa	3.04	1.64E-13
ENSDARG00000010144	plppr3a	3.03	3.10E-06
ENSDARG00000004049	marcksa	3.02	5.06E-10
ENSDARG00000069917	ska3	3.02	9.43E-07
ENSDARG00000007221	pbk	3.02	9.18E-09
ENSDARG00000032369	btbd6b	3.01	2.72E-11
ENSDARG00000090785	diaph3	3.01	2.59E-07
ENSDARG00000045932	cpeb1a	3.01	2.16E-07
ENSDARG00000011999	ybey	3.01	4.91E-06
ENSDARG00000030449	crabp2b	3.00	2.90E-12
ENSDARG00000077559	CABZ01052290.1	3.00	0.00015057
ENSDARG00000089486	cplx3b	3.00	3.16E-05
ENSDARG00000060917	anln	2.99	3.03E-08
ENSDARG00000010487	sae1	2.99	3.03E-11
ENSDARG00000045167	dlgap5	2.99	1.34E-08
ENSDARG00000015273	alpi.1	2.99	7.93E-12
ENSDARG00000077029	bub1	2.98	6.39E-08
ENSDARG00000101479	BX908782.3	2.98	5.32E-08
ENSDARG00000070239	casc5	2.98	1.27E-05
ENSDARG00000092290	si:dkeyp-26a9.2	2.98	6.74E-06
ENSDARG00000027310	lsp1	2.97	8.42E-12
ENSDARG00000016594	haus4	2.97	1.13E-07
ENSDARG00000074379	knstrn	2.97	4.86E-06
ENSDARG00000075621	birc5a	2.96	7.63E-10
ENSDARG00000032849	ndrg1a	2.95	1.50E-11
ENSDARG00000004713	mad2l1	2.93	3.41E-09
ENSDARG00000055226	slc7a7	2.93	5.83E-11
ENSDARG00000061231	tinagl1	2.92	1.28E-08
ENSDARG00000005098	zgc:86764	2.91	2.90E-08
ENSDARG00000076767	pgfb	2.91	8.06E-06
ENSDARG00000058731	slc2a6	2.89	6.89E-08
ENSDARG00000013670	hyou1	2.89	1.45E-08
ENSDARG00000063177	manf	2.89	1.18E-08
ENSDARG00000100426	fam167b	2.89	2.52E-12
ENSDARG00000076620	abhd8b	2.89	2.62E-05
ENSDARG00000057035	stoml3b	2.88	1.06E-07

ENSDARG00000069113	dbn1	2.88	1.07E-10
ENSDARG00000101060	acrc	2.87	1.74E-07
ENSDARG00000040110	kif20bb	2.87	2.11E-07
ENSDARG00000038882	smc4	2.86	1.56E-10
ENSDARG00000013476	arhgef39	2.86	8.74E-06
ENSDARG00000089563	CU633855.1	2.85	2.60E-05
ENSDARG00000020887	armc1l	2.84	3.96E-10
ENSDARG00000099371	cygb1	2.84	9.02E-14
ENSDARG00000093440	tnfaip6	2.84	9.60E-13
ENSDARG00000024488	top2a	2.83	9.09E-08
ENSDARG00000095458	si:dkey-240h12.3	2.83	1.01E-05
ENSDARG00000057099	papss1	2.82	5.46E-10
ENSDARG00000057323	e2f8	2.82	1.50E-06
ENSDARG00000019838	ugdh	2.82	4.56E-11
ENSDARG00000070903	met	2.81	1.79E-11
ENSDARG00000086550	dbf4b	2.81	2.12E-05
ENSDARG00000017739	ak5l	2.80	1.79E-06
ENSDARG00000099424	lcat	2.80	0.00044048
ENSDARG00000033587	CABZ01088134.1	2.79	5.26E-08
ENSDARG00000055100	cxcl12b	2.78	3.79E-09
ENSDARG00000093546	ms4a17a.2	2.78	2.45E-08
ENSDARG00000042221	mthfd1l	2.78	8.08E-09
ENSDARG00000058372	mcph1	2.77	0.00013644
ENSDARG00000099385	CT030188.1	2.77	8.28E-13
ENSDARG00000103907	sgol1	2.77	1.05E-07
ENSDARG00000044437	cdca5	2.75	5.00E-06
ENSDARG00000071491	nrros	2.75	1.76E-08
ENSDARG00000095807	hp	2.75	4.39E-09
ENSDARG00000052192	s1pr5b	2.75	2.58E-09
ENSDARG00000012450	vmp1	2.75	8.35E-11
ENSDARG00000021794	hmmr	2.74	8.63E-07
ENSDARG00000102202	phospho2	2.74	5.48E-08
ENSDARG00000073721	smarcad1b	2.74	2.28E-08
ENSDARG00000098647	ankdd1a	2.73	4.12E-05
ENSDARG00000078547	si:ch211-264f5.2	2.73	2.58E-05
ENSDARG00000035958	tnni2b.1	2.72	1.71E-05
ENSDARG00000005058	ncapd2	2.72	8.07E-09
ENSDARG00000071384	slc7a11	2.72	8.36E-10
ENSDARG00000102748	CABZ01074745.1	2.71	2.90E-10
ENSDARG00000011262	traip	2.71	1.04E-07
ENSDARG00000043593	rapgef1a	2.70	6.34E-08
ENSDARG00000074927	bub1bb	2.70	3.08E-07
ENSDARG00000044492	ublcp1	2.70	2.45E-07
ENSDARG00000087198	cthrc1a	2.69	2.24E-10
ENSDARG00000037640	aurkb	2.69	6.57E-08
ENSDARG00000042659	thyn1	2.68	2.40E-05
ENSDARG00000033307	igf2b	2.67	4.71E-10
ENSDARG00000086670	ice2	2.67	1.15E-09
ENSDARG00000101975	BX682558.1	2.66	1.20E-07
ENSDARG00000035435	m17	2.66	0.00036724
ENSDARG00000058992	cers2b	2.66	6.09E-12
ENSDARG00000044976	krt93	2.64	3.61E-05
ENSDARG00000022772	OSBP2 (1 of many)	2.63	1.36E-09
ENSDARG00000043798	ms4a17a.1	2.62	4.35E-11
ENSDARG00000094324	efemp2a	2.62	7.39E-13
ENSDARG00000099674	dicp3.1	2.61	7.56E-06
ENSDARG00000070109	ncapg	2.61	8.99E-08
ENSDARG00000098377	tnfrsf11b	2.61	2.52E-08
ENSDARG00000018165	depdc1a	2.60	4.11E-07
ENSDARG00000015460	racgap1	2.60	9.82E-08
ENSDARG00000097527	si:ch73-56d11.3	2.60	7.60E-11
ENSDARG00000089291	stra13	2.60	1.04E-07
ENSDARG00000054304	homeza	2.60	4.20E-10

ENSDARG00000090486	CABZ01114051.1	2.59	8.53E-11
ENSDARG00000062830	fam46d	2.59	0.00277471
ENSDARG00000017354	epha2a	2.59	9.95E-12
ENSDARG00000099304	si:ch211-51f19.1	2.59	7.98E-06
ENSDARG00000004635	epha7	2.58	3.86E-10
ENSDARG00000061468	ncaph	2.58	8.73E-07
ENSDARG00000010437	fam46c	2.58	3.79E-07
ENSDARG00000017910	pdss1	2.58	7.16E-08
ENSDARG00000035631	sdf2l1	2.58	1.56E-10
ENSDARG00000075354	espl1	2.58	8.38E-08
ENSDARG00000102185	PCDH8	2.58	9.66E-06
ENSDARG00000006353	itga5	2.57	1.25E-11
ENSDARG00000056832	exo1	2.57	8.48E-07
ENSDARG00000104765	chek1	2.57	6.38E-08
ENSDARG00000062655	ydjc	2.56	1.40E-08
ENSDARG00000014329	npm1a	2.56	1.46E-06
ENSDARG00000078125	rusc1	2.55	4.90E-08
ENSDARG00000063333	nup210	2.55	2.98E-11
ENSDARG00000071658	ywhag2	2.55	3.42E-09
ENSDARG00000041381	arntl2	2.55	4.13E-07
ENSDARG00000052617	raver1	2.55	4.98E-08
ENSDARG00000098374	FLNB	2.54	6.94E-10
ENSDARG00000042563	mis18bp1	2.54	2.65E-06
ENSDARG00000086848	atad3	2.53	4.30E-06
ENSDARG00000029071	creld2	2.53	4.59E-09
ENSDARG00000104217	gpc2	2.53	4.21E-05
ENSDARG00000015088	dnajb11	2.52	1.92E-09
ENSDARG00000076789	cx32.2	2.52	2.80E-10
ENSDARG00000037962	psmb7	2.51	3.01E-12
ENSDARG00000044562	cycsb	2.51	2.13E-06
ENSDARG00000070155	tuba8l3	2.50	7.51E-09
ENSDARG00000100741	cdc20	2.50	2.88E-09
ENSDARG00000097909	si:dkey-195m11.11	2.50	0.00014763
ENSDARG00000067608	zswim7	2.49	6.72E-06
ENSDARG00000017744	smc2	2.49	6.33E-09
ENSDARG00000086840	si:ch211-266k8.4	2.48	7.98E-06
ENSDARG00000078069	rrm2	2.48	2.24E-07
ENSDARG00000012506	rnpep	2.48	3.32E-09
ENSDARG00000045224	glipr1a	2.48	8.60E-08
ENSDARG00000008022	kif18a	2.48	4.56E-07
ENSDARG00000040623	fosl2	2.47	5.79E-07
ENSDARG00000074322	si:ch211-194m7.3	2.47	4.42E-11
ENSDARG00000042722	blnk	2.46	4.82E-09
ENSDARG00000036998	arf3b	2.46	7.24E-05
ENSDARG00000073952	slc4a7	2.45	2.60E-07
ENSDARG00000100954	wars	2.45	3.35E-09
ENSDARG00000053558	rtkn2a	2.44	6.15E-05
ENSDARG00000101010	hpdl	2.44	4.79E-06
ENSDARG00000071009	kif20ba	2.44	4.00E-07
ENSDARG00000062152	chaf1a	2.44	1.17E-11
ENSDARG00000071694	ndc80	2.44	1.14E-08
ENSDARG00000035913	yars	2.44	9.09E-08
ENSDARG00000052565	cenpi	2.43	2.03E-07
ENSDARG00000099667	snrpg	2.43	1.78E-09
ENSDARG00000056203	si:ch211-201h21.5	2.42	7.69E-06
ENSDARG00000070006	rcn1	2.42	1.01E-09
ENSDARG00000101356	CABZ01044157.1	2.41	1.24E-05
ENSDARG00000071774	eef1e1	2.41	6.38E-09
ENSDARG00000009001	pdia6	2.41	2.14E-11
ENSDARG00000091271	si:ch211-225g23.1	2.40	4.35E-07
ENSDARG00000038822	mrc1b	2.40	1.90E-07
ENSDARG00000076144	si:ch211-74m13.3	2.40	7.64E-11
ENSDARG00000040064	acp6	2.39	2.85E-07

ENSDARG00000102808	calr3b	2.39	9.35E-12
ENSDARG00000056617	rpgra	2.39	0.00020348
ENSDARG00000055365	si:dkey-25e12.3	2.39	9.30E-08
ENSDARG00000039863	lifrb	2.38	3.03E-11
ENSDARG00000027087	tgfb2	2.38	3.10E-07
ENSDARG00000098529	ccne2	2.38	1.79E-07
ENSDARG00000097351	flnbl	2.37	4.39E-11
ENSDARG00000036036	mdka	2.37	9.02E-14
ENSDARG00000005821	ncf2	2.36	1.32E-09
ENSDARG00000012044	polr3gla	2.36	5.54E-07
ENSDARG00000104659	CABZ01109604.1	2.36	2.74E-06
ENSDARG00000091692	havcr2	2.35	8.89E-06
ENSDARG00000024471	nsl1	2.35	7.36E-05
ENSDARG00000053215	me1	2.35	3.59E-05
ENSDARG00000020606	nfe2	2.35	0.00157932
ENSDARG00000053456	GK3P	2.35	6.02E-08
ENSDARG00000089892	cd44b	2.35	1.27E-07
ENSDARG00000058480	chtf18	2.35	1.18E-08
ENSDARG00000103109	chl1b	2.34	7.26E-12
ENSDARG00000086838	itga2.3	2.34	1.57E-07
ENSDARG00000032264	mybl2b	2.34	6.82E-08
ENSDARG00000054543	samsn1a	2.34	1.35E-10
ENSDARG00000024759	inhbab	2.34	2.59E-09
ENSDARG00000003570	hsp90b1	2.34	1.35E-09
ENSDARG00000016044	gins4	2.33	2.74E-09
ENSDARG00000015623	cecr1b	2.33	3.85E-06
ENSDARG00000058968	haus1	2.33	7.27E-05
ENSDARG00000004018	CHST13	2.32	5.61E-08
ENSDARG00000090396	si:cabz01074946.1	2.32	2.89E-06
ENSDARG00000098206	ptrh1	2.32	3.51E-07
ENSDARG00000036781	si:dkey-170l10.1	2.32	2.08E-06
ENSDARG00000027933	glis1b	2.32	3.90E-07
ENSDARG00000068457	tnnt3b	2.32	9.38E-07
ENSDARG00000091754	CHCHD5	2.32	0.0001519
ENSDARG00000007823	atf3	2.31	1.28E-07
ENSDARG00000073843	myo9ab	2.31	2.40E-10
ENSDARG00000014685	esco2	2.31	3.41E-07
ENSDARG00000034650	fabp7b	2.30	1.79E-08
ENSDARG00000041361	ttk	2.30	3.84E-07
ENSDARG00000056160	hspd1	2.30	4.59E-05
ENSDARG00000089404	si:dkey-24p1.7	2.30	0.00017439
ENSDARG00000063285	ube2t	2.29	4.97E-07
ENSDARG00000057100	zwilch	2.29	1.50E-08
ENSDARG00000037966	thoc6	2.29	2.58E-09
ENSDARG00000028000	pfkpa	2.29	1.75E-09
ENSDARG00000021151	ptpreb	2.29	0.00033346
ENSDARG00000057263	zgc:173729	2.28	5.24E-08
ENSDARG00000101441	lima1a	2.27	3.22E-10
ENSDARG00000095821	si:dkey-122a22.2	2.27	1.12E-09
ENSDARG00000060115	lrrn1	2.26	4.57E-09
ENSDARG00000040319	C5AR1	2.26	6.53E-06
ENSDARG00000010717	chchd10	2.26	2.37E-06
ENSDARG00000058828	ccdc51	2.26	4.05E-07
ENSDARG00000010181	asap2a	2.25	6.64E-09
ENSDARG00000100366	si:dkey-102m7.3	2.24	2.19E-08
ENSDARG00000105195	dnajc21	2.24	1.70E-07
ENSDARG00000058319	cep76	2.23	4.25E-06
ENSDARG00000043640	cenpn	2.23	3.86E-07
ENSDARG00000004754	hspa4a	2.23	3.13E-05
ENSDARG00000098774	si:zfos-741a10.3	2.23	7.11E-06
ENSDARG00000037158	rcc1	2.23	7.52E-07
ENSDARG00000024026	sdf2	2.22	4.79E-09
ENSDARG00000004576	plk4	2.22	1.04E-08

ENSDARG00000101707	si:ch211-156b7.4	2.22	6.01E-10
ENSDARG00000103854	CABZ01078593.1	2.21	6.68E-08
ENSDARG00000036164	cars	2.21	1.48E-09
ENSDARG00000011973	slc35d1a	2.20	5.04E-07
ENSDARG00000089705	CABZ01084566.2	2.20	9.11E-08
ENSDARG00000059596	clip2	2.20	4.07E-08
ENSDARG00000089626	ptges3b	2.20	4.48E-10
ENSDARG00000042539	ywhaqa	2.20	1.34E-11
ENSDARG00000097155	GDPGP1	2.20	7.04E-05
ENSDARG00000058346	sass6	2.19	1.60E-06
ENSDARG00000074790	c23h20orf24	2.19	1.75E-08
ENSDARG00000005423	pgam1a	2.19	2.35E-08
ENSDARG00000097473	zgc:113340	2.19	5.62E-06
ENSDARG00000078825	bub1ba	2.18	1.46E-05
ENSDARG00000008805	orc3	2.18	3.42E-09
ENSDARG00000055639	ruvbl2	2.18	1.43E-09
ENSDARG00000016484	dkc1	2.18	3.60E-05
ENSDARG00000098591	tubb2b	2.17	7.92E-08
ENSDARG00000092134	rad54b	2.17	1.29E-06
ENSDARG00000077309	si:ch211-209f23.6	2.17	3.31E-05
ENSDARG00000056367	mpv17l2	2.17	8.27E-07
ENSDARG00000044807	dck	2.17	4.39E-09
ENSDARG00000086337	si:dkey-102g19.3	2.17	9.04E-06
ENSDARG00000061385	haus3	2.16	1.03E-06
ENSDARG00000010445	trabd	2.16	8.09E-11
ENSDARG00000000767	spi1b	2.16	2.22E-10
ENSDARG00000038980	txndc12	2.16	2.32E-10
ENSDARG00000090904	RNF219	2.15	3.02E-05
ENSDARG00000008278	rcor2	2.15	1.25E-06
ENSDARG00000103846	hspa5	2.15	2.57E-06
ENSDARG00000023299	snu13b	2.14	2.97E-06
ENSDARG00000079497	zgc:110340	2.14	3.57E-08
ENSDARG00000090988	larsa	2.14	6.63E-09
ENSDARG00000069980	lman1	2.14	2.67E-10
ENSDARG00000099078	SLC29A2 (1 of many)	2.14	2.91E-07
ENSDARG00000077372	tfr1b	2.14	2.10E-09
ENSDARG00000026454	mis12	2.14	3.87E-07
ENSDARG00000060252	mogs	2.13	1.83E-10
ENSDARG00000012274	eif4e1c	2.13	5.15E-05
ENSDARG00000038505	polr2h	2.13	6.68E-08
ENSDARG00000033175	snrpe	2.13	8.78E-10
ENSDARG00000045254	zmp:0000000624	2.13	6.42E-07
ENSDARG00000025889	usp14	2.13	2.29E-11
ENSDARG00000061100	nars	2.12	1.15E-09
ENSDARG00000101540	fgf3	2.12	5.60E-06
ENSDARG00000074591	eda	2.12	1.49E-06
ENSDARG00000018953	gclm	2.12	5.64E-08
ENSDARG00000069909	HTRA2	2.12	7.80E-07
ENSDARG00000071294	tonsl	2.12	1.11E-07
ENSDARG00000044094	gfpt2	2.12	1.04E-09
ENSDARG00000031506	flvcr2b	2.11	4.62E-10
ENSDARG00000077339	ptrh2	2.11	1.14E-05
ENSDARG00000098508	CABZ01111958.1	2.11	0.00165421
ENSDARG00000037188	rpa2	2.11	3.03E-11
ENSDARG00000101251	ldha	2.11	4.46E-10
ENSDARG00000006029	lta4h	2.10	1.68E-10
ENSDARG00000038785	abcf2a	2.10	0.00242621
ENSDARG00000012073	kif15	2.09	2.53E-08
ENSDARG00000045628	rab34a	2.09	5.75E-08
ENSDARG00000030700	ctps1a	2.09	8.83E-05
ENSDARG00000096229	si:dkey-260c8.8	2.09	0.00017428
ENSDARG00000002445	prdm1a	2.09	1.27E-10
ENSDARG00000103137	rmi2	2.09	3.24E-05

ENSDARG00000054454	epha4a	2.09	4.38E-10
ENSDARG00000074985	aurkaip1	2.08	2.92E-08
ENSDARG00000023002	dtl	2.08	4.26E-07
ENSDARG00000045351	ccdc58	2.08	3.66E-08
ENSDARG00000010246	prmt1	2.07	1.81E-06
ENSDARG00000003693	hars	2.07	7.05E-10
ENSDARG00000100047	ergic1	2.07	2.11E-07
ENSDARG00000104773	junbb	2.07	1.04E-05
ENSDARG00000033567	fkbp1ab	2.07	9.24E-07
ENSDARG00000043865	timm9	2.07	3.15E-08
ENSDARG00000092204	ms4a17a.5	2.07	6.24E-11
ENSDARG00000098295	efna3b	2.07	1.97E-05
ENSDARG00000016375	asns	2.06	1.60E-06
ENSDARG00000008247	vezf1a	2.06	3.22E-07
ENSDARG00000060394	mtfr2	2.06	8.26E-06
ENSDARG00000015576	itprip	2.06	2.83E-08
ENSDARG00000077002	igsf3	2.06	5.03E-11
ENSDARG00000044752	p2rx4a	2.05	1.61E-05
ENSDARG00000075265	plaua	2.05	0.0008264
ENSDARG00000044114	cyb561d2	2.05	2.50E-05
ENSDARG00000011404	fen1	2.05	2.22E-09
ENSDARG00000018491	pdia4	2.05	3.62E-09
ENSDARG00000103959	pak1	2.05	7.93E-09
ENSDARG00000012215	umps	2.04	6.01E-07
ENSDARG00000031795	abcf1	2.04	6.67E-08
ENSDARG00000059308	golt1bb	2.04	9.92E-06
ENSDARG00000089213	adam15	2.04	1.69E-05
ENSDARG00000018653	acot7	2.04	8.67E-08
ENSDARG00000003142	dachc	2.04	9.96E-11
ENSDARG00000079605	prmt5	2.04	3.75E-07
ENSDARG00000023323	ywhaqb	2.04	8.00E-12
ENSDARG00000080006	tmem41b	2.03	8.61E-07
ENSDARG00000030630	mfsd2aa	2.03	7.85E-05
ENSDARG00000014106	cfl2	2.03	3.61E-10
ENSDARG00000026766	bcl2l10	2.03	5.75E-11
ENSDARG00000075121	hbegfa	2.03	1.97E-10
ENSDARG00000099374	sp9	2.03	1.39E-05
ENSDARG00000013776	thop1	2.03	1.91E-07
ENSDARG00000104903	cdkn1cb	2.03	0.00023372
ENSDARG00000024540	tspan36	2.03	9.06E-09
ENSDARG00000039020	fbxo5	2.02	0.00016323
ENSDARG00000034773	ncapd3	2.02	1.89E-06
ENSDARG00000003902	ctsl.1	2.02	0.00093856
ENSDARG00000032103	mapk6	2.01	3.60E-08
ENSDARG00000053563	ms4a17a.12	2.01	6.59E-11
ENSDARG00000103996	spdl1	2.01	1.03E-06
ENSDARG00000004937	skp2	2.00	1.58E-06
ENSDARG00000090152	anapc10	2.00	1.55E-06
ENSDARG00000104693	il6st	2.00	1.73E-09
ENSDARG00000079542	stard13a	-2.00	4.94E-09
ENSDARG00000098103	tefb	-2.00	4.25E-08
ENSDARG00000021555	park2	-2.00	5.10E-06
ENSDARG00000057671	epas1b	-2.00	0.00011984
ENSDARG00000101866	asic1b	-2.00	0.0002503
ENSDARG00000003250	pik3cd	-2.01	1.20E-06
ENSDARG00000088301	si:dkey-254e13.6	-2.01	0.0005993
ENSDARG00000053906	angpt2b	-2.01	4.58E-05
ENSDARG00000077722	ppp2r3a	-2.01	1.58E-07
ENSDARG00000103978	sh3bp5b	-2.01	1.13E-05
ENSDARG00000044048	prnpb	-2.01	5.98E-08
ENSDARG00000091540	notum1b	-2.01	3.86E-06
ENSDARG00000099978	CABZ01078427.1	-2.01	2.71E-07
ENSDARG00000090560	mfap5	-2.01	8.07E-09

ENSDARG00000104219	gpc6b	-2.01	9.45E-06
ENSDARG00000042112	dio1	-2.02	4.22E-07
ENSDARG00000040059	gbp	-2.02	1.47E-07
ENSDARG00000093024	si:ch211-213a13.2	-2.02	5.25E-05
ENSDARG00000101701	bmp5	-2.02	2.39E-07
ENSDARG00000026548	cyp2u1	-2.02	4.12E-06
ENSDARG00000093572	lamc3	-2.02	9.04E-11
ENSDARG00000104408	zgc:152774	-2.02	2.04E-08
ENSDARG00000011407	col2a1b	-2.03	5.59E-12
ENSDARG00000009087	cd74a	-2.03	1.35E-10
ENSDARG00000091209	ucp3	-2.03	0.00069064
ENSDARG00000058133	foxd2	-2.03	0.01003746
ENSDARG00000103946	si:dkey-124l13.1	-2.03	7.12E-07
ENSDARG00000105223	pmp22a	-2.03	2.71E-11
ENSDARG00000100708	jakmip3	-2.03	1.53E-06
ENSDARG00000006546	ak4	-2.04	1.37E-09
ENSDARG00000060349	wasf1	-2.04	0.00455737
ENSDARG00000045123	oplah	-2.04	5.79E-08
ENSDARG00000071015	pbxip1a	-2.04	1.67E-10
ENSDARG00000025513	dip2cb	-2.04	1.04E-09
ENSDARG00000097726	si:ch211-149e23.4	-2.04	1.59E-07
ENSDARG00000020811	efemp2b	-2.04	4.36E-09
ENSDARG00000075188	adamts10	-2.05	1.03E-10
ENSDARG00000070041	zgc:153920	-2.05	8.05E-10
ENSDARG00000074721	rassf9	-2.05	2.35E-05
ENSDARG00000021163	thrb	-2.05	5.71E-10
ENSDARG00000035819	sirt3	-2.05	7.74E-05
ENSDARG00000053484	syne2b	-2.05	1.01E-08
ENSDARG00000061994	acacb	-2.05	1.29E-05
ENSDARG00000030104	sh3bp4	-2.05	6.25E-10
ENSDARG00000071497	zic3	-2.05	8.12E-07
ENSDARG00000061436	col6a2	-2.05	3.01E-12
ENSDARG00000088505	fam217b	-2.05	1.06E-06
ENSDARG00000075930	adamts2	-2.05	1.89E-06
ENSDARG00000097483	si:ch211-213d14.2	-2.06	1.86E-07
ENSDARG00000006065	znf385b	-2.06	0.00010365
ENSDARG00000024717	selenbp1	-2.06	1.33E-09
ENSDARG00000025615	prr15la	-2.06	7.76E-06
ENSDARG00000103736	gramd2aa	-2.06	2.44E-05
ENSDARG00000079547	zbtb47b	-2.06	0.00119355
ENSDARG00000067824	cntnap3	-2.06	0.00298289
ENSDARG00000099538	si:ch211-188p14.3	-2.06	2.08E-11
ENSDARG00000091127	klf15	-2.06	7.65E-10
ENSDARG00000032820	rxfp2a	-2.07	1.61E-08
ENSDARG00000076685	wisp1b	-2.07	1.71E-08
ENSDARG00000041724	glipr2	-2.07	2.96E-07
ENSDARG00000101389	zgc:174180	-2.07	5.41E-06
ENSDARG00000079227	plekhs1	-2.07	0.018682
ENSDARG00000006202	erbb3a	-2.07	6.24E-11
ENSDARG00000096216	si:ch211-162i8.7	-2.07	1.62E-06
ENSDARG00000040911	meox2a	-2.07	2.74E-05
ENSDARG00000019365	zgc:110712	-2.08	1.70E-08
ENSDARG00000016391	calcoco1b	-2.08	1.84E-06
ENSDARG00000062855	plekhg7	-2.08	7.34E-08
ENSDARG00000099482	BX569782.1	-2.08	6.81E-06
ENSDARG00000061885	satb2	-2.08	8.48E-10
ENSDARG00000093111	si:ch211-209l18.2	-2.08	6.75E-05
ENSDARG00000044524	def6b	-2.08	1.21E-07
ENSDARG00000074715	stk17a	-2.09	2.85E-09
ENSDARG00000070625	enpp5	-2.09	0.00028463
ENSDARG00000025788	chp2	-2.09	1.09E-06
ENSDARG00000020123	adck3	-2.09	4.57E-10
ENSDARG00000030367	metrn	-2.09	1.10E-08

ENSDARG00000016538	zgc:55888	-2.09	0.00914662
ENSDARG00000054835	ugt5f1	-2.09	9.05E-07
ENSDARG00000073786	cmbl	-2.09	1.10E-09
ENSDARG00000025595	agmo	-2.09	1.21E-05
ENSDARG00000101195	cyp1c1	-2.09	4.59E-07
ENSDARG00000058048	ugt5e1	-2.10	1.61E-05
ENSDARG00000029263	hoxb3a	-2.10	0.00300051
ENSDARG00000061580	kctd7	-2.10	0.00016112
ENSDARG00000076748	ntn2	-2.10	4.95E-06
ENSDARG00000063578	DGKI	-2.11	2.95E-09
ENSDARG00000102082	nr3c2	-2.11	0.00271711
ENSDARG00000060280	pde9a	-2.11	3.57E-05
ENSDARG00000100190	si:ch211-188p14.4	-2.11	1.05E-09
ENSDARG00000011600	epha4b	-2.11	4.75E-08
ENSDARG00000011076	MREG	-2.11	8.81E-09
ENSDARG00000092162	mhc1zaa	-2.11	9.48E-08
ENSDARG00000090629	tmtops3b	-2.12	0.0001456
ENSDARG00000056502	si:ch73-334d15.4	-2.12	1.58E-08
ENSDARG00000076834	LRRC75A	-2.12	1.64E-06
ENSDARG00000086419	si:ch211-282j17.13	-2.12	2.33E-05
ENSDARG00000001950	ak1	-2.12	2.98E-11
ENSDARG00000042410	rab40b	-2.12	2.26E-07
ENSDARG00000032618	mgst1.1	-2.12	5.73E-10
ENSDARG00000059948	HS3ST6	-2.12	4.59E-06
ENSDARG00000005924	serpina10a	-2.12	6.67E-10
ENSDARG00000054050	vsig8a	-2.13	0.00010295
ENSDARG00000057353	ehbp1l1a	-2.13	4.92E-10
ENSDARG00000091006	cobl	-2.13	1.54E-08
ENSDARG00000054332	trim66	-2.13	7.28E-06
ENSDARG00000087574	nox1	-2.13	3.17E-05
ENSDARG00000092521	jac1	-2.13	1.65E-07
ENSDARG00000043531	jun	-2.13	4.88E-06
ENSDARG00000099849	ebf1a	-2.13	1.14E-07
ENSDARG00000069998	si:ch211-145b13.6	-2.13	1.11E-07
ENSDARG00000075048	lonrf1	-2.13	4.58E-06
ENSDARG00000040002	pnpla7b	-2.13	3.73E-08
ENSDARG00000052158	il23r	-2.13	3.39E-05
ENSDARG00000103167	si:dkey-245n4.2	-2.14	0.00479605
ENSDARG00000103162	CABZ01046954.1	-2.14	1.79E-07
ENSDARG00000075720	il2rb	-2.14	8.07E-06
ENSDARG00000074185	pcsk9	-2.14	4.01E-07
ENSDARG00000095833	alk	-2.14	1.96E-08
ENSDARG00000042548	tpd52l1	-2.14	1.06E-09
ENSDARG00000102585	fam160a1b	-2.14	4.16E-05
ENSDARG00000045180	acta2	-2.14	7.32E-07
ENSDARG00000101633	CABZ01050166.1	-2.14	6.44E-05
ENSDARG00000069441	lpar6b	-2.14	1.34E-06
ENSDARG00000086712	si:dkeyp-97b10.3	-2.15	2.38E-07
ENSDARG00000029952	ampd2b	-2.15	2.38E-09
ENSDARG00000092394	dcun1d4	-2.15	9.70E-10
ENSDARG00000058685	si:dkey-204a24.11	-2.15	0.00065061
ENSDARG00000063375	pter	-2.15	5.05E-07
ENSDARG00000101423	cyp2y3	-2.15	7.39E-07
ENSDARG00000061797	zgc:154006	-2.16	0.00312194
ENSDARG00000091408	mtcl1	-2.16	0.01542816
ENSDARG00000095065	si:ch211-113e8.9	-2.16	1.50E-06
ENSDARG00000045979	zgc:153704	-2.16	0.00013549
ENSDARG00000070578	edn2	-2.17	6.63E-09
ENSDARG00000053279	apln	-2.17	5.46E-10
ENSDARG00000041873	si:dkey-221h15.4	-2.17	2.77E-05
ENSDARG00000077715	GRIK3	-2.17	0.00017628
ENSDARG00000021137	adgrv1	-2.18	1.59E-08
ENSDARG00000100110	si:ch211-79g12.2	-2.18	1.08E-06

ENSDARG00000060711	sv2bb	-2.18	3.64E-06
ENSDARG00000092604	si:ch211-15j1.4	-2.18	7.53E-06
ENSDARG00000011824	pbxip1b	-2.18	7.23E-12
ENSDARG00000062402	frem1b	-2.18	3.24E-11
ENSDARG00000014646	aoc2	-2.18	2.98E-11
ENSDARG00000076011	PPM1K (1 of many)	-2.18	3.75E-06
ENSDARG00000101034	ZC3H12A	-2.18	0.00016489
ENSDARG00000040133	ackr4b	-2.18	3.91E-05
ENSDARG00000013240	zgc:172271	-2.18	2.33E-09
ENSDARG00000036186	mbpa	-2.18	3.47E-07
ENSDARG00000103713	cd248a	-2.18	3.51E-11
ENSDARG00000076402	si:ch211-196f2.7	-2.19	0.00073902
ENSDARG00000062481	mlphb	-2.19	3.09E-06
ENSDARG00000009693	llgl1	-2.19	9.00E-10
ENSDARG00000011370	fyna	-2.19	1.85E-08
ENSDARG00000097637	si:ch211-246i5.5	-2.19	1.02E-07
ENSDARG00000005814	klhl10a	-2.19	0.01948755
ENSDARG00000061762	trim108	-2.20	5.20E-10
ENSDARG00000038639	elovl6l	-2.20	3.92E-05
ENSDARG00000079738	znf219	-2.20	5.71E-10
ENSDARG00000028517	hbp1	-2.20	1.28E-05
ENSDARG00000058246	cysltr1	-2.20	7.74E-07
ENSDARG00000104126	ccpg1	-2.21	3.48E-06
ENSDARG00000103390	cacna2d2a	-2.21	2.81E-05
ENSDARG00000063032	dok6	-2.21	0.00159361
ENSDARG00000037122	TENM2	-2.21	7.54E-06
ENSDARG00000004745	lmbr1l	-2.21	1.66E-06
ENSDARG00000101980	bmper	-2.21	1.50E-06
ENSDARG00000102636	zgc:73340	-2.21	0.00344173
ENSDARG00000088048	fgf18a	-2.22	6.97E-09
ENSDARG00000061099	nfasca	-2.22	6.37E-05
ENSDARG00000105442	si:cabz01100188.1	-2.22	1.91E-11
ENSDARG00000076420	dkk2	-2.22	8.95E-06
ENSDARG00000074752	hlfa	-2.22	4.23E-10
ENSDARG00000086421	si:ch211-212k18.8	-2.22	4.74E-09
ENSDARG00000098769	slitrk6	-2.22	1.75E-09
ENSDARG00000043818	CASKIN2	-2.22	0.00015676
ENSDARG00000042133	si:dkey-51e6.1	-2.23	1.53E-06
ENSDARG00000100255	si:ch73-29l19.1	-2.23	0.00018552
ENSDARG00000076862	fam198a	-2.23	2.49E-08
ENSDARG00000071095	abi3bpb	-2.23	6.24E-09
ENSDARG00000010873	DDX17	-2.23	7.69E-12
ENSDARG00000035185	fzd9a	-2.23	3.35E-06
ENSDARG00000074508	si:dkey-28e7.3	-2.24	3.42E-05
ENSDARG00000023369	mxd	-2.24	4.99E-06
ENSDARG00000007682	ppdpfa	-2.24	3.10E-10
ENSDARG00000011170	ndrg2	-2.24	7.95E-09
ENSDARG00000098214	CABZ01072487.1	-2.24	3.32E-05
ENSDARG00000094492	si:ch211-284e13.12	-2.24	0.0041618
ENSDARG00000100159	angptl1b	-2.24	6.19E-08
ENSDARG00000091457	CABZ01072538.1	-2.24	1.53E-06
ENSDARG00000075666	tsc22d3	-2.24	6.21E-05
ENSDARG00000077188	atrnl1a	-2.25	0.00015787
ENSDARG00000022176	IGLON5	-2.25	0.02313587
ENSDARG00000006031	abat	-2.25	1.30E-06
ENSDARG00000077847	olfm2a	-2.25	9.82E-05
ENSDARG00000056979	lhx9	-2.25	1.32E-06
ENSDARG00000087599	TENM3	-2.25	0.00060651
ENSDARG00000044569	cldn19	-2.25	8.29E-09
ENSDARG00000005416	map3k5	-2.25	1.55E-10
ENSDARG00000005216	zgc:158328	-2.25	0.00025691
ENSDARG00000079698	asb13a.1	-2.25	0.00035901
ENSDARG00000095901	col18a1b	-2.25	4.34E-08

ENSDARG00000036428	EMP3 (1 of many)	-2.25	1.82E-08
ENSDARG00000032389	tspan12	-2.26	2.46E-06
ENSDARG00000009624	UTS2R	-2.26	3.28E-08
ENSDARG00000015546	alpl	-2.26	2.85E-12
ENSDARG00000061758	sh3pxd2ab	-2.26	5.03E-11
ENSDARG00000088975	si:ch211-14k19.8	-2.26	1.26E-10
ENSDARG00000017229	megf10	-2.26	1.33E-08
ENSDARG00000036102	ctdsp2	-2.27	3.12E-11
ENSDARG00000097299	FLRT2 (1 of many)	-2.27	1.11E-07
ENSDARG00000042233	fgf16	-2.27	1.03E-07
ENSDARG00000103752	DUSP26	-2.27	0.00108155
ENSDARG00000059043	ntf3	-2.27	0.00122185
ENSDARG00000078748	si:ch211-137a8.4	-2.27	2.41E-08
ENSDARG00000062817	crym	-2.27	3.06E-06
ENSDARG00000079012	cbfa2t3	-2.27	2.32E-07
ENSDARG00000074808	megf6b	-2.28	7.51E-09
ENSDARG00000042620	gstr	-2.28	1.10E-12
ENSDARG00000056087	ecrg4a	-2.28	1.79E-10
ENSDARG00000090914	si:ch211-117k10.3	-2.28	6.43E-08
ENSDARG00000101939	BX324216.3	-2.28	5.17E-05
ENSDARG00000089187	wfdc2	-2.28	6.22E-08
ENSDARG00000069415	col17a1a	-2.29	3.40E-09
ENSDARG00000089354	tspan4a	-2.29	2.09E-09
ENSDARG00000089071	ushbp1	-2.30	3.00E-06
ENSDARG00000052000	cav2	-2.30	5.11E-10
ENSDARG00000088950	sycp2	-2.30	2.31E-06
ENSDARG00000097789	pon3.2	-2.30	1.35E-06
ENSDARG00000079183	sod3b	-2.30	2.94E-10
ENSDARG00000007275	si:ch211-251b21.1	-2.31	1.26E-10
ENSDARG00000061165	slc6a4a	-2.31	2.64E-09
ENSDARG00000042336	impdh1a	-2.31	4.89E-07
ENSDARG00000095675	ccdc141	-2.31	2.39E-07
ENSDARG00000075521	cpz	-2.31	2.30E-07
ENSDARG00000103129	nid1b	-2.32	2.74E-11
ENSDARG00000100598	CDH19	-2.32	1.34E-06
ENSDARG00000019274	rasd1	-2.32	1.10E-06
ENSDARG00000102671	dpyda.1	-2.32	0.00033996
ENSDARG00000055075	svila	-2.32	5.38E-10
ENSDARG00000037116	cxcl12a	-2.32	4.65E-09
ENSDARG00000035649	ext1c	-2.32	1.08E-09
ENSDARG00000079079	sult1st7	-2.32	6.15E-06
ENSDARG00000097535	si:ch211-252f13.5	-2.32	1.22E-11
ENSDARG00000103286	kcnk4a	-2.32	0.00026007
ENSDARG00000036895	dap1b	-2.32	8.68E-12
ENSDARG00000006849	asic2	-2.32	1.49E-05
ENSDARG00000060862	atxn1b	-2.32	4.65E-09
ENSDARG00000070620	grin2db	-2.32	0.00150615
ENSDARG00000105274	CABZ01074130.1	-2.33	4.92E-11
ENSDARG00000077907	si:dkey-183p4.10	-2.33	7.26E-08
ENSDARG00000101095	cpne4a	-2.33	0.00241529
ENSDARG00000022810	fzr1b	-2.33	4.01E-08
ENSDARG00000020114	slc20a1a	-2.33	8.21E-08
ENSDARG00000020761	arrdc2	-2.33	8.36E-06
ENSDARG00000062217	kcnj3b	-2.33	4.82E-06
ENSDARG00000079917	rassf7a	-2.34	1.75E-07
ENSDARG00000027017	ppp2r5a	-2.34	6.81E-08
ENSDARG00000097239	si:ch73-31d8.2	-2.34	0.0006884
ENSDARG00000071460	si:ch211-234p6.5	-2.34	6.80E-09
ENSDARG00000099390	lama2	-2.34	7.47E-05
ENSDARG00000030975	ccdc80l1	-2.34	6.68E-09
ENSDARG00000060410	thbs2a	-2.34	4.11E-08
ENSDARG00000053152	pcmtd1	-2.34	3.73E-08
ENSDARG00000075222	amer2	-2.35	1.04E-08

ENSDARG00000004724	tcea3	-2.35	5.95E-10
ENSDARG00000004177	fam169ab	-2.35	2.64E-08
ENSDARG00000073695	mamdc2b	-2.36	4.35E-11
ENSDARG00000018382	prkcha	-2.36	1.46E-07
ENSDARG00000005648	olfml2a	-2.36	4.15E-09
ENSDARG00000001710	flot1a	-2.36	1.25E-07
ENSDARG00000059473	kank4	-2.36	4.82E-08
ENSDARG00000023768	mfsd4aa	-2.36	3.12E-06
ENSDARG00000086842	dap1b	-2.36	2.81E-12
ENSDARG00000059391	gyg1b	-2.36	2.55E-10
ENSDARG00000044803	dhrs3b	-2.36	4.79E-08
ENSDARG00000102687	MINOS1-NBL1	-2.37	1.51E-09
ENSDARG00000071230	lrfn5a	-2.37	0.00011098
ENSDARG00000075161	defbl1	-2.37	3.49E-06
ENSDARG00000037390	gsg1l	-2.37	2.90E-06
ENSDARG00000052361	il15	-2.37	1.12E-05
ENSDARG00000055498	si:ch1073-184j22.1	-2.37	2.62E-09
ENSDARG00000070857	si:dkey-32e6.6	-2.38	4.90E-08
ENSDARG00001104811	cyp2aa2	-2.38	1.27E-05
ENSDARG00000075054	rasgrf2a	-2.38	2.23E-05
ENSDARG00000077400	rbm10	-2.38	1.41E-10
ENSDARG00000042055	fam129aa	-2.38	4.12E-09
ENSDARG00000092898	si:ch211-157j23.3	-2.39	0.00106201
ENSDARG00000094511	ccl20b	-2.39	8.40E-07
ENSDARG00000062278	C1GALT1 (1 of many)	-2.39	2.94E-05
ENSDARG00000070597	prelp	-2.39	1.86E-10
ENSDARG00000073883	clstn3	-2.39	0.00010486
ENSDARG00000044532	nr4a2b	-2.39	4.80E-09
ENSDARG00000101816	col5a3b	-2.40	1.79E-11
ENSDARG00000069048	serpinf1	-2.40	2.90E-12
ENSDARG00000007220	ncam1b	-2.40	1.89E-06
ENSDARG00000101964	CTRL (1 of many)	-2.40	0.00385864
ENSDARG00000074341	hykk.2	-2.40	7.50E-09
ENSDARG00000040944	ntd5	-2.40	1.28E-10
ENSDARG00000087087	col28a1b	-2.40	9.49E-09
ENSDARG00000101951	CABZ01079721.1	-2.40	7.98E-09
ENSDARG00000101609	si:dkey-109a10.2	-2.40	3.13E-05
ENSDARG00000010294	fmodb	-2.40	0.00041108
ENSDARG00000102495	CT573234.4	-2.41	0.00123538
ENSDARG00000074633	gpr35.1	-2.41	8.38E-07
ENSDARG00000069100	aldh9a1a.1	-2.41	2.12E-11
ENSDARG00000045580	lum	-2.41	1.89E-11
ENSDARG00000055722	bco2a	-2.41	5.46E-10
ENSDARG00000005943	htra4	-2.41	3.74E-09
ENSDARG00000104083	adgre5b.2	-2.41	1.35E-05
ENSDARG00000079336	si:ch211-150j10.4	-2.41	0.00016422
ENSDARG00000025320	col21a1	-2.42	1.96E-09
ENSDARG00000099634	elna	-2.42	7.04E-07
ENSDARG00000088906	CABZ01059404.1	-2.42	1.69E-06
ENSDARG00000053241	sts	-2.42	1.65E-10
ENSDARG00000087120	slc5a8	-2.42	2.04E-07
ENSDARG00000102777	thbs4a	-2.43	1.28E-09
ENSDARG00000099098	C1GALT1 (1 of many)	-2.43	1.69E-07
ENSDARG00000100320	BX005329.4	-2.43	7.85E-05
ENSDARG00000074231	SLC9A3R2 (1 of many)	-2.43	5.60E-08
ENSDARG00000004291	hecw1b	-2.43	5.76E-06
ENSDARG00000015495	klf3	-2.43	5.49E-06
ENSDARG00000035544	etnppl	-2.43	4.12E-06
ENSDARG00000075600	si:dkeyp-41f9.3	-2.43	6.03E-07
ENSDARG00000073850	hdac7b	-2.43	1.34E-07
ENSDARG00000056021	sostdc1b	-2.44	0.00052349
ENSDARG00000009764	srek1	-2.44	2.90E-08
ENSDARG00000071586	tgfbi	-2.44	4.42E-12

ENSDARG00000095132	si:dkey-51d8.2	-2.44	1.07E-05
ENSDARG00000070025	dchs1a	-2.45	3.08E-07
ENSDARG00000078828	npb	-2.45	2.60E-05
ENSDARG00000007349	dmrt1	-2.45	4.28E-07
ENSDARG00000056024	eva1c	-2.45	1.03E-06
ENSDARG00000103666	dapk2b	-2.45	7.64E-11
ENSDARG00000077231	vwf	-2.45	5.14E-06
ENSDARG00000036424	pcdh20	-2.46	0.000648
ENSDARG00000078915	mmp17a	-2.46	1.35E-10
ENSDARG00000039145	plaub	-2.46	8.53E-11
ENSDARG00000104555	sh2d3cb	-2.46	2.91E-05
ENSDARG00000091306	kcnn1a	-2.46	0.00111353
ENSDARG00000092976	si:ch211-127i16.2	-2.46	7.93E-05
ENSDARG00000017369	sema3d	-2.47	4.79E-09
ENSDARG00000076119	emid1	-2.47	2.08E-12
ENSDARG00000038561	klf6b	-2.47	6.56E-05
ENSDARG00000057751	zbtb47a	-2.47	6.76E-08
ENSDARG00000087387	znf1038	-2.47	6.18E-06
ENSDARG00000002758	dedd1	-2.47	1.15E-11
ENSDARG00000086853	dpyda.3	-2.48	1.88E-05
ENSDARG00000087386	pcp4b	-2.48	7.56E-06
ENSDARG00000099727	ssbp2	-2.48	2.06E-07
ENSDARG00000020795	rac3b	-2.48	7.98E-09
ENSDARG00000079248	mn1b	-2.48	4.17E-08
ENSDARG00000077245	si:dkey-225n22.4	-2.49	1.20E-10
ENSDARG00000013174	nkd3	-2.49	1.88E-07
ENSDARG00000060526	bmp3	-2.49	2.48E-12
ENSDARG00000053684	aldob	-2.49	2.12E-11
ENSDARG00000086576	si:cabz01069012.2	-2.49	5.46E-10
ENSDARG00000094996	sult1st9	-2.49	9.31E-06
ENSDARG00000061255	dusp3a	-2.49	0.00131724
ENSDARG00000076623	col14a1b	-2.50	2.74E-11
ENSDARG00000059826	crtac1a	-2.50	5.17E-06
ENSDARG00000076044	trhde.1	-2.50	1.43E-05
ENSDARG00000069402	lrrc4.1	-2.50	2.18E-07
ENSDARG00000073757	pdzrn3a	-2.50	0.00010176
ENSDARG00000024195	znf395b	-2.50	2.14E-08
ENSDARG00000068745	map4l	-2.51	5.87E-06
ENSDARG00000102825	olfm2b	-2.51	2.33E-09
ENSDARG00000036481	tcn2	-2.51	1.38E-05
ENSDARG00000034956	myclb	-2.51	4.44E-11
ENSDARG00000074680	rims1a	-2.51	0.00089994
ENSDARG00000039881	cemip	-2.51	5.73E-10
ENSDARG00000075779	ppp1r12b	-2.52	7.84E-08
ENSDARG00000060578	si:dkey-226m8.10	-2.53	8.97E-08
ENSDARG00000089920	mlip	-2.53	7.37E-06
ENSDARG00000052748	capn1b	-2.53	9.21E-09
ENSDARG00000101112	DRAP1 (1 of many)	-2.54	7.13E-07
ENSDARG00000088514	and1	-2.54	2.52E-07
ENSDARG00000052783	cdc42ep3	-2.54	2.48E-09
ENSDARG00000078060	syt7b	-2.54	1.48E-06
ENSDARG00000100691	prss35	-2.54	1.37E-10
ENSDARG00000040741	kcnab1b	-2.55	0.00125963
ENSDARG00000007184	zbtb16a	-2.55	2.39E-05
ENSDARG00000069518	aqp3b	-2.55	7.97E-08
ENSDARG00000042980	cyp2p7	-2.55	5.63E-08
ENSDARG00000101767	si:dkey-183i3.6	-2.55	2.58E-06
ENSDARG00000095259	tmem119a	-2.55	7.46E-10
ENSDARG00000077878	FBXL7 (1 of many)	-2.55	6.84E-05
ENSDARG00000005154	aspa	-2.55	0.00021007
ENSDARG00000074607	unm_sa1506	-2.56	1.32E-05
ENSDARG00000061454	nrxn2a	-2.56	2.39E-07
ENSDARG00000079713	ccl27b	-2.56	2.04E-11

ENSDARG00000035796	cdh31	-2.56	1.09E-08
ENSDARG00000103092	grem2b	-2.56	5.97E-05
ENSDARG00000037646	rgs11	-2.56	0.00238233
ENSDARG00000067984	gas1b	-2.57	2.80E-08
ENSDARG00000013125	dlx1a	-2.57	5.46E-10
ENSDARG00000079985	nrip2	-2.57	8.53E-11
ENSDARG00000038682	MFAP4 (1 of many)	-2.57	0.00055704
ENSDARG00000074275	limch1a	-2.57	3.54E-07
ENSDARG00000068967	zgc:153372	-2.57	8.74E-06
ENSDARG00000029402	sort1a	-2.57	3.53E-08
ENSDARG00000089338	si:ch211-110e21.3	-2.57	2.33E-09
ENSDARG00000077341	ppp1r14c	-2.57	7.70E-07
ENSDARG00000075557	apcdd1l	-2.58	6.09E-12
ENSDARG00000060871	mctp1b	-2.58	8.53E-11
ENSDARG00000010425	scara5	-2.58	2.33E-08
ENSDARG00000098652	pcdh11	-2.58	4.12E-06
ENSDARG00000077542	si:dkeyp-75b4.8	-2.59	1.44E-05
ENSDARG00000042677	cadm1b	-2.59	6.81E-06
ENSDARG00000087764	ponzr10	-2.59	1.00E-07
ENSDARG00000079570	rspo2	-2.59	3.63E-07
ENSDARG00000059081	PRSS35 (1 of many)	-2.60	0.00031322
ENSDARG00000099031	scn4ba	-2.61	0.00011321
ENSDARG00000045749	ppfibp1a	-2.61	2.23E-09
ENSDARG00000035695	scxa	-2.61	1.39E-07
ENSDARG00000052905	zgc:165423	-2.62	2.81E-08
ENSDARG00000058658	si:dkey-178e17.3	-2.62	7.65E-08
ENSDARG00000057652	dbpb	-2.62	0.00031035
ENSDARG00000070868	cfap126	-2.62	2.45E-06
ENSDARG00000103774	limch1b	-2.62	1.37E-11
ENSDARG00000076274	tnfsf14	-2.62	1.23E-06
ENSDARG00000089078	si:ch211-160j14.3	-2.62	6.94E-07
ENSDARG00000005739	gpm6ba	-2.63	5.70E-05
ENSDARG00000098720	LPL (1 of many)	-2.63	1.04E-05
ENSDARG00000075397	cipca	-2.64	9.00E-07
ENSDARG00000069540	si:dkey-30c15.2	-2.64	4.78E-06
ENSDARG00000054754	hs6st1a	-2.64	1.13E-05
ENSDARG00000034801	mylka	-2.64	8.00E-12
ENSDARG00000020219	dld	-2.65	1.04E-07
ENSDARG00000002760	gdf5	-2.65	1.67E-06
ENSDARG00000019396	rergla	-2.65	0.00052685
ENSDARG00000099137	LTBP4	-2.66	2.67E-12
ENSDARG00000101172	CABZ01089030.1	-2.66	0.00012116
ENSDARG00000098588	gchfr	-2.66	1.44E-08
ENSDARG00000092067	atn1	-2.67	2.47E-08
ENSDARG00000002945	bgnb	-2.67	4.33E-08
ENSDARG00000093549	sepp1a	-2.67	5.33E-11
ENSDARG00000071709	ppp1r9bb	-2.67	2.83E-05
ENSDARG00000100946	si:ch211-212k18.9	-2.67	3.84E-10
ENSDARG00000102556	nfat5b	-2.68	0.00108155
ENSDARG00000038305	vgll3	-2.68	3.84E-06
ENSDARG00000052470	igfbp2a	-2.69	1.78E-07
ENSDARG00000004789	lrp1ba	-2.69	0.02584051
ENSDARG00000071673	ctdspla	-2.69	4.59E-11
ENSDARG00000069282	bbc3	-2.69	0.00017878
ENSDARG00000098836	myocd	-2.69	8.14E-09
ENSDARG00000069978	si:ch211-67e16.2	-2.69	7.74E-10
ENSDARG00000087745	lrrc38b	-2.70	0.00123663
ENSDARG00000040928	CABZ01059391.1	-2.70	2.00E-06
ENSDARG00000075450	mkxa	-2.70	4.44E-09
ENSDARG00000042877	heca	-2.71	1.86E-06
ENSDARG00000058414	bglap	-2.71	1.14E-08
ENSDARG00000002330	lhx8a	-2.71	2.28E-05
ENSDARG00000104442	aatkb	-2.71	3.04E-09

ENSDARG00000093600	omd	-2.72	3.18E-07
ENSDARG00000034300	sema3c	-2.72	7.65E-09
ENSDARG00000056178	dpt	-2.72	7.64E-11
ENSDARG00000021584	cntn5	-2.72	4.14E-06
ENSDARG00000041715	bco2b	-2.72	1.40E-05
ENSDARG00000041747	sspn	-2.73	3.60E-08
ENSDARG00000079515	ptx3b	-2.73	2.68E-07
ENSDARG00000099446	slit1b	-2.73	3.24E-07
ENSDARG00000104358	CLASP1 (1 of many)	-2.73	1.81E-07
ENSDARG00000105441	pcdh11	-2.73	3.26E-05
ENSDARG00000024829	tnw	-2.75	4.57E-11
ENSDARG00000045071	chad	-2.75	5.06E-10
ENSDARG00000045517	itih5	-2.75	4.20E-07
ENSDARG00000063011	antxr2b	-2.75	1.41E-06
ENSDARG00000089791	slc25a32a	-2.75	1.43E-07
ENSDARG00000043446	efhd1	-2.76	2.04E-07
ENSDARG00000103937	ndrg4	-2.77	1.50E-12
ENSDARG00000069334	zgc:114045	-2.77	1.55E-09
ENSDARG00000062494	OLFML1	-2.77	1.43E-09
ENSDARG00000073891	gdf10b	-2.78	9.29E-09
ENSDARG00000055510	ypel3	-2.78	2.41E-08
ENSDARG00000013430	bhmt	-2.79	1.08E-10
ENSDARG00000007129	slc6a16a	-2.79	2.17E-08
ENSDARG00000015164	mknk2b	-2.79	3.14E-06
ENSDARG00000005453	foxp2	-2.79	0.00029667
ENSDARG00000053509	kazald3	-2.79	2.09E-09
ENSDARG00000017884	bgna	-2.80	8.82E-11
ENSDARG00000075833	lyve1a	-2.80	1.63E-05
ENSDARG00000078527	lingo4b	-2.80	9.98E-06
ENSDARG00000077817	cxxc4	-2.80	3.31E-05
ENSDARG00000020979	fam65c	-2.81	3.45E-09
ENSDARG00000087523	BX470224.2	-2.82	2.29E-05
ENSDARG00000100832	CABZ01009451.1	-2.82	8.08E-07
ENSDARG00000043514	si:dkey-239i20.4	-2.82	9.87E-07
ENSDARG00000045747	cped1	-2.82	3.49E-11
ENSDARG00000060264	si:dkey-37g12.1	-2.83	1.04E-07
ENSDARG00000040277	fbxo32	-2.83	3.52E-06
ENSDARG00000088157	smoc2	-2.83	1.52E-09
ENSDARG00000041691	bhlhe41	-2.83	5.91E-07
ENSDARG00000100560	zfpm2b	-2.83	7.65E-05
ENSDARG00000039964	fgfbp2a	-2.84	1.81E-06
ENSDARG00000071005	ppp1r3ca	-2.84	2.46E-06
ENSDARG00000036152	gas2b	-2.84	7.89E-08
ENSDARG00000087188	nfil3-6	-2.84	0.0008578
ENSDARG00000078964	esyt2b	-2.84	5.59E-09
ENSDARG00000087601	gpr153	-2.85	9.39E-08
ENSDARG00000076332	si:ch211-159i8.4	-2.85	5.99E-11
ENSDARG00000024847	col5a2b	-2.86	2.87E-12
ENSDARG00000069834	pnpla4	-2.87	2.88E-08
ENSDARG00000075189	cntnap5b	-2.87	2.57E-09
ENSDARG00000002336	dlc	-2.87	2.23E-09
ENSDARG00000027744	gadd45ba	-2.87	2.30E-07
ENSDARG00000039579	cfd	-2.87	1.18E-09
ENSDARG00000063631	ch1073-291c23.1	-2.88	1.16E-12
ENSDARG00000098226	smpd3	-2.88	1.52E-09
ENSDARG00000076351	brinp3a.1	-2.89	2.53E-05
ENSDARG00000051896	fbn2a	-2.89	5.45E-07
ENSDARG00000089271	si:dkey-114c15.7	-2.89	2.23E-05
ENSDARG00000096380	defbl2	-2.90	8.03E-07
ENSDARG00000035569	cyp1d1	-2.90	4.52E-06
ENSDARG00000076269	zgc:172131	-2.90	2.02E-06
ENSDARG00000105263	ccl36.1	-2.90	2.51E-06
ENSDARG00000040985	itgbl1	-2.90	1.47E-09

ENSDARG00000035253	npr3	-2.90	3.29E-09
ENSDARG00000011929	plp1b	-2.90	2.63E-07
ENSDARG00000044600	plppr2b	-2.90	4.00E-07
ENSDARG00000099985	cyr61l2	-2.90	1.45E-10
ENSDARG00000039959	gdnfa	-2.90	0.00067201
ENSDARG00000058154	znf385c	-2.90	2.38E-07
ENSDARG00000025089	loxl4	-2.91	6.41E-13
ENSDARG00000063097	scube1	-2.91	1.12E-08
ENSDARG00000044982	dhrs3a	-2.92	5.66E-07
ENSDARG00000069953	kcnq5b	-2.92	2.97E-10
ENSDARG00000026925	nos2a	-2.92	2.03E-06
ENSDARG00000018065	ntm	-2.93	5.14E-06
ENSDARG00000042122	acot11b	-2.93	1.67E-07
ENSDARG00000079977	nhsb	-2.93	9.68E-08
ENSDARG00000063577	klhl35	-2.93	1.96E-07
ENSDARG00000079522	si:ch211-184m13.4	-2.94	8.21E-06
ENSDARG00000062936	ndnf	-2.94	2.90E-12
ENSDARG00000074526	zbtb16b	-2.94	2.64E-08
ENSDARG00000012013	cpa6	-2.94	1.80E-08
ENSDARG00000101510	cetn2	-2.95	5.54E-07
ENSDARG00000004627	panx3	-2.95	1.08E-10
ENSDARG00000004880	acsm3	-2.96	5.47E-08
ENSDARG00000079872	rapgef4	-2.96	0.00547981
ENSDARG00000022650	cyp2ad3	-2.97	6.32E-06
ENSDARG00000020239	lpin1	-2.97	3.67E-05
ENSDARG00000011257	enpp2	-2.97	6.61E-12
ENSDARG00000043009	fam43a	-2.98	8.71E-06
ENSDARG00000018383	frzb	-2.98	4.79E-09
ENSDARG00000012422	col11a2	-2.98	1.71E-11
ENSDARG00000078416	zeb2b	-2.98	0.00032408
ENSDARG00000037099	irs2a	-2.98	2.53E-05
ENSDARG00000053186	vstm4b	-2.98	4.87E-09
ENSDARG00000014554	ppp1r3cb	-3.00	1.52E-05
ENSDARG00000086585	nrg2b	-3.00	4.04E-05
ENSDARG00000087782	rnf152	-3.00	1.15E-08
ENSDARG00000062106	klf5b	-3.01	1.77E-05
ENSDARG00000100795	timp4.3	-3.01	4.50E-07
ENSDARG00000075191	oacyl	-3.02	2.07E-10
ENSDARG00000005343	ccdc85al	-3.02	3.09E-07
ENSDARG00000077424	rassf10a	-3.02	5.26E-08
ENSDARG00000096755	si:ch211-202p1.5	-3.03	3.70E-08
ENSDARG00000090346	zmp:0000000991	-3.03	1.10E-09
ENSDARG00000033296	gpr37b	-3.03	1.53E-08
ENSDARG00000017329	cdkl1	-3.04	9.27E-07
ENSDARG00000096804	si:dkey-219e21.4	-3.04	5.12E-09
ENSDARG00000101199	rbp4	-3.04	2.79E-09
ENSDARG00000086189	mgp	-3.06	8.25E-11
ENSDARG00000020982	prickle2a	-3.06	1.89E-07
ENSDARG00000020493	lgi1a	-3.06	1.04E-09
ENSDARG00000103297	FO704607.1	-3.06	2.14E-05
ENSDARG00000014796	wnt11r	-3.06	5.97E-12
ENSDARG00000099961	bnip3	-3.07	5.08E-09
ENSDARG00000103641	CABZ01085241.1	-3.07	9.97E-11
ENSDARG00000094171	lrp1ba	-3.08	2.93E-09
ENSDARG00000015123	dnase1l4.1	-3.08	7.74E-10
ENSDARG00000037845	col9a3	-3.08	0.00010907
ENSDARG00000094990	si:dkey-91f15.1	-3.08	2.17E-11
ENSDARG00000025847	sox12	-3.09	1.68E-07
ENSDARG00000079198	usp13	-3.09	2.98E-06
ENSDARG00000027963	camkva	-3.09	3.11E-06
ENSDARG00000079781	slitrk4	-3.10	8.81E-05
ENSDARG00000090738	mylka	-3.10	4.11E-07
ENSDARG00000103124	slc35f4	-3.10	2.77E-07

ENSDARG00000097065	si:ch73-223p23.2	-3.11	0.00020864
ENSDARG00000020693	sesn1	-3.11	7.74E-10
ENSDARG00000044935	hpdb	-3.11	1.22E-11
ENSDARG00000042069	pebp1	-3.11	9.83E-08
ENSDARG00000011583	cry1ab	-3.12	4.30E-05
ENSDARG00000012776	smarca1	-3.12	3.12E-11
ENSDARG00000105153	ifitm5	-3.12	3.15E-11
ENSDARG00000020143	pah	-3.12	2.42E-11
ENSDARG00000105450	si:ch211-63p21.1	-3.12	2.56E-05
ENSDARG00000098161	cntn4	-3.13	6.25E-07
ENSDARG00000104340	rspo1	-3.14	8.46E-08
ENSDARG00000059944	c1qtnf2	-3.14	9.23E-08
ENSDARG00000101167	chst3b	-3.14	2.11E-09
ENSDARG00000003281	pik3ip1	-3.15	3.82E-07
ENSDARG00000101777	pdlim5a	-3.16	3.06E-08
ENSDARG00000008133	foxl1	-3.16	2.37E-06
ENSDARG00000074772	ccl44	-3.17	2.28E-08
ENSDARG00000077826	efcc1	-3.17	5.31E-10
ENSDARG00000030844	klf11a	-3.17	4.44E-09
ENSDARG00000092920	si:ch211-106h4.12	-3.17	5.25E-12
ENSDARG00000037145	slc8a4b	-3.17	2.37E-08
ENSDARG00000058005	hgd	-3.20	2.01E-12
ENSDARG00000003181	sult1st4	-3.20	5.00E-07
ENSDARG00000090690	nell2a	-3.21	2.09E-09
ENSDARG00000090170	rab11fip4a	-3.21	1.62E-07
ENSDARG00000093453	ahdc1	-3.23	3.21E-08
ENSDARG00000070710	prss60.3	-3.23	1.04E-08
ENSDARG00000043806	postna	-3.24	1.55E-10
ENSDARG00000022509	cox4i2	-3.25	3.18E-09
ENSDARG00000076056	IYD	-3.25	0.00058922
ENSDARG00000098989	CU459012.1	-3.26	1.15E-08
ENSDARG00000038794	zgc:113531	-3.27	4.17E-12
ENSDARG00000054916	eif4ebp3	-3.28	2.00E-10
ENSDARG00000010154	vstm4a	-3.28	1.96E-11
ENSDARG00000057687	sbk3	-3.29	3.13E-07
ENSDARG00000035655	rad21b	-3.29	2.24E-07
ENSDARG00000039647	slc6a1b	-3.30	2.91E-06
ENSDARG00000027394	si:ch211-150g13.3	-3.30	5.85E-08
ENSDARG00000092458	si:dkey-282h22.5	-3.31	1.48E-08
ENSDARG00000079752	col6a4a	-3.31	1.23E-08
ENSDARG00000056248	si:dkey-183i3.5	-3.32	2.58E-07
ENSDARG00000074746	kcnd1	-3.32	4.67E-07
ENSDARG00000078605	ptger1a	-3.32	7.98E-06
ENSDARG00000074582	graf4b	-3.33	1.02E-05
ENSDARG00000089885	slc16a12b	-3.33	8.63E-05
ENSDARG00000053362	cilp	-3.33	5.82E-08
ENSDARG00000095861	si:ch1073-441p17.1	-3.34	1.17E-11
ENSDARG00000005716	olfml2ba	-3.34	1.23E-10
ENSDARG00000008697	epas1a	-3.35	1.26E-11
ENSDARG00000091211	adh8a	-3.35	4.05E-07
ENSDARG00000097897	sgip1a	-3.35	4.47E-11
ENSDARG00000008329	asic1a	-3.35	0.00020765
ENSDARG00000089066	nhsl2	-3.35	7.07E-09
ENSDARG00000011673	si:ch211-246m6.5	-3.35	4.24E-07
ENSDARG00000079165	galr1b	-3.37	0.00029278
ENSDARG00000013210	htr2cl2	-3.37	3.61E-07
ENSDARG00000016439	slc7a1	-3.41	5.23E-05
ENSDARG00000063433	atp2b2	-3.41	4.37E-08
ENSDARG00000076299	EMILIN3	-3.41	1.17E-08
ENSDARG00000039665	zmp:0000001074	-3.42	1.36E-08
ENSDARG00000014670	colgalt2	-3.42	4.65E-11
ENSDARG00000052615	tnmd	-3.44	1.96E-11
ENSDARG00000100128	CU861477.1	-3.44	3.47E-05

ENSDARG00000101535	col10a1b	-3.46	8.11E-11
ENSDARG00000008407	tspan7b	-3.47	3.39E-08
ENSDARG00000054753	col10a1a	-3.47	3.88E-10
ENSDARG00000075015	soul5	-3.47	4.19E-08
ENSDARG00000060471	gcnt3	-3.47	2.58E-08
ENSDARG00000079283	si:ch211-247j9.1	-3.49	2.20E-07
ENSDARG00000022437	cd81b	-3.49	7.28E-12
ENSDARG00000023759	zgc:73226	-3.50	2.92E-05
ENSDARG00000003533	col8a1b	-3.51	4.64E-07
ENSDARG00000099776	glula	-3.52	2.72E-05
ENSDARG00000076820	xkr8.2	-3.52	6.99E-08
ENSDARG00000053820	pcmtd2	-3.55	2.73E-06
ENSDARG00000019692	colq	-3.55	4.94E-05
ENSDARG00000075301	gsdf	-3.57	1.91E-09
ENSDARG00000092087	si:ch211-240b21.5	-3.58	2.30E-05
ENSDARG00000011869	galnt8a.2	-3.59	1.10E-08
ENSDARG00000021789	myoc	-3.59	1.37E-08
ENSDARG00000027088	ptgdsb.1	-3.60	2.64E-11
ENSDARG00000091277	adra2da	-3.60	1.57E-06
ENSDARG00000015156	fbln2	-3.61	7.39E-12
ENSDARG00000075817	mettl24	-3.61	1.25E-11
ENSDARG00000037748	slc43a1b	-3.62	5.12E-08
ENSDARG00000105568	si:ch211-194p6.10	-3.63	2.75E-08
ENSDARG00000062030	gpr17	-3.63	4.17E-06
ENSDARG00000057419	slc44a5b	-3.64	1.54E-06
ENSDARG00000074949	c1qtnf7	-3.65	1.19E-08
ENSDARG00000070423	zgc:153157	-3.66	4.82E-06
ENSDARG00000079364	CR377211.1	-3.68	1.24E-06
ENSDARG00000025914	si:dkey-190g11.3	-3.68	7.66E-07
ENSDARG00000078250	zgc:194398	-3.68	5.70E-08
ENSDARG00000030632	ccdc3b	-3.68	2.04E-13
ENSDARG00000103750	si:ch211-246m6.5	-3.69	5.34E-11
ENSDARG00000098070	CABZ01085140.1	-3.71	0.0002213
ENSDARG00000096927	si:ch211-210b2.3	-3.72	1.16E-05
ENSDARG00000078847	si:dkey-238o13.4	-3.72	6.41E-13
ENSDARG00000070011	si:ch211-167j6.4	-3.73	3.35E-05
ENSDARG00000027799	ucmaa	-3.73	5.25E-12
ENSDARG00000103650	si:ch73-329n5.1	-3.75	0.00105269
ENSDARG00000045788	avpr1ab	-3.75	4.11E-07
ENSDARG00000098256	CU914622.1	-3.75	1.83E-07
ENSDARG00000090268	krtt1c19e	-3.76	2.01E-12
ENSDARG00000024032	coch	-3.77	1.10E-06
ENSDARG00000060893	col8a2	-3.78	2.07E-11
ENSDARG00000040610	si:ch73-352p4.8	-3.79	5.82E-07
ENSDARG00000009402	si:ch211-210b2.2	-3.81	3.01E-12
ENSDARG00000055192	zgc:136930	-3.82	6.69E-09
ENSDARG00000061479	thsd7aa	-3.82	1.05E-09
ENSDARG00000104914	muc5f	-3.83	8.45E-08
ENSDARG00000079107	clec11a	-3.83	3.16E-09
ENSDARG00000074205	si:dkey-1c7.3	-3.84	1.34E-06
ENSDARG00000059054	pdk2b	-3.84	0.00024126
ENSDARG00000058969	cntnap2a	-3.86	1.87E-05
ENSDARG00000010132	dacha	-3.87	1.67E-10
ENSDARG00000012060	thbs3b	-3.88	3.40E-12
ENSDARG00000068726	masp1	-3.88	4.06E-11
ENSDARG00000096242	si:ch211-76l23.4	-3.88	2.03E-13
ENSDARG00000094973	wnt16	-3.89	4.47E-11
ENSDARG00000030263	mfsd2b	-3.91	1.04E-09
ENSDARG00000052520	sgms2	-3.93	1.34E-08
ENSDARG00000056633	fgf13b	-3.93	4.08E-07
ENSDARG00000015947	matn4	-3.94	7.84E-10
ENSDARG00000078842	tns1a	-3.94	2.24E-06
ENSDARG00000053481	entpd5a	-3.94	8.07E-09

ENSDARG00000069630	tat	-3.94	1.21E-07
ENSDARG00000002847	fndc1	-3.96	3.10E-13
ENSDARG00000059121	EFEMP1 (1 of many)	-3.97	3.03E-11
ENSDARG00000010029	spon1a	-3.98	8.89E-06
ENSDARG00000068397	tns2b	-3.98	2.23E-11
ENSDARG00000019025	podn	-3.98	4.33E-08
ENSDARG00000059139	wfikkn2b	-3.99	9.22E-13
ENSDARG00000070206	si:busm1-160c18.6	-3.99	2.10E-05
ENSDARG00000089172	PTPRM	-4.00	0.00013317
ENSDARG00000069133	mstnb	-4.01	1.27E-09
ENSDARG00000098315	cyp1a	-4.01	3.16E-09
ENSDARG00000052633	si:ch211-106n13.3	-4.02	4.39E-09
ENSDARG00000044433	sned1	-4.03	6.06E-10
ENSDARG00000100480	si:ch73-364h19.2	-4.04	0.0002247
ENSDARG00000076848	LGALS3BP (1 of many)	-4.08	6.82E-07
ENSDARG00000092419	vtg7	-4.08	1.26E-09
ENSDARG00000052057	pcolceb	-4.08	1.22E-13
ENSDARG00000071626	ptgdsb.2	-4.09	6.86E-11
ENSDARG00000060584	kank1b	-4.10	3.32E-11
ENSDARG00000058252	adamts15b	-4.11	3.81E-09
ENSDARG00000104084	si:dkey-191g9.7	-4.14	2.26E-08
ENSDARG00000091723	si:ch211-202f3.4	-4.15	5.63E-08
ENSDARG00000091398	CABZ01065684.1	-4.16	9.33E-09
ENSDARG00000074600	gpr78a	-4.19	0.02159542
ENSDARG00000075183	rnf220b	-4.19	3.56E-05
ENSDARG00000098058	im:7150988	-4.21	2.35E-08
ENSDARG00000088878	c1qtnf1	-4.28	2.92E-11
ENSDARG00000055395	foxq1b	-4.34	3.83E-07
ENSDARG00000030176	ITGB1BP2	-4.35	1.88E-08
ENSDARG00000089887	mmp20a	-4.35	1.16E-08
ENSDARG00000007436	avpr2aa	-4.36	2.91E-07
ENSDARG00000036086	itga11a	-4.37	2.16E-09
ENSDARG00000079347	zgc:194659	-4.43	3.02E-07
ENSDARG00000075393	spock2	-4.44	1.47E-07
ENSDARG00000013522	pck1	-4.54	8.74E-06
ENSDARG00000044894	zgc:113307	-4.63	4.28E-10
ENSDARG00000005526	igfn1.1	-4.63	3.37E-08
ENSDARG00000056587	cyp2r1	-4.64	1.21E-10
ENSDARG00000095212	si:ch211-210b2.4	-4.72	2.01E-12
ENSDARG00000105048	CABZ01084447.1	-4.85	3.41E-06
ENSDARG00000011879	foxn1	-4.87	1.47E-10
ENSDARG00000074033	adamtsl2	-5.00	3.24E-06
ENSDARG00000062262	ednrab	-5.09	7.95E-07
ENSDARG00000104216	CU929368.1	-5.17	2.34E-12
ENSDARG00000019686	fgl2b	-5.27	1.89E-07
ENSDARG00000100772	si:ch211-154c21.1	-5.30	4.77E-06
ENSDARG00000056873	and3	-5.44	2.33E-08
ENSDARG00000058819	nog1	-5.56	9.38E-07
ENSDARG00000101012	CABZ01051600.1	-5.98	2.16E-05
ENSDARG00000044895	fmoda	-6.39	1.88E-06
ENSDARG00000040278	klhl38b	-6.80	0.00176406
ENSDARG00000079302	and2	-7.57	2.38E-11
ENSDARG00000077275	crispld1a	-8.63	4.59E-08

Table A.2. Select predicted miRNA-mRNA interactions predicted by only one database. MicroCosm threshold cutoff for significance was p < 0.01. TargetScan threshold for significance was ≥ 50 percentile. MicroCosm and TargetScan based significance off p-value and percentile, respectively.

miRNA	Target	MicroCosm	TargetScan
miR-132-3p	c1qtnf12	-	54
miR-132-3p	dvl1b	-	77
miR-132-3p	fzd7a	-	85
miR-132-3p	rspo1	-	68
miR-132-3p	fgf10b	-	91
miR-132-3p	fgfrl1b	-	62
miR-132-3p	ptk2bb	-	84
miR-132-3p	EFEMP1 (1 of many)	-	82
miR-132-3p	tob1a	-	88
miR-132-3p	scube1	-	77
miR-132-3p	smad3a	-	72
miR-132-3p	nog1	-	69
miR-132-3p	kazald3	-	99
miR-132-3p	igfbp2a	-	66
miR-132-3p	cxcl12a	-	77
miR-132-3p	epha4b	-	93
miR-132-3p	ephb3a	-	84
miR-132-3p	hdac5	-	65
miR-132-3p	sema3c	-	88
miR-132-3p	sema6e	-	78
miR-132-3p	bnip3	-	95
miR-132-3p	aatkb	-	81
miR-132-3p	arhgap25	-	100
miR-132-3p	arl4d	-	95
miR-132-3p	celsr1b	-	76
miR-132-3p	rab33a	-	87
miR-132-3p	rgs4	-	97
miR-132-3p	anos1a	-	73
miR-132-3p	bcan	-	99
miR-132-3p	col8a2	-	70
miR-132-3p	itgb3a	-	67
miR-132-3p	itih5	-	92
miR-132-3p	serpi-10a	-	71
miR-132-3p	tgfbi	-	89
miR-132-3p	zgc:172271	-	99
miR-132-3p	vhl	6.32E-03	-

miR-132-3p	il2rb	-	99
miR-132-3p	cyp2u1	-	98
miR-132-3p	stat4	-	95
miR-132-3p	chad	-	94
miR-132-3p	UTS2R	-	81
miR-132-3p	apln	-	80
miR-132-3p	dio1	-	73
miR-132-3p	ptger1a	-	69
miR-132-3p	edn2	-	53
miR-132-3p	bcorl1	-	79
miR-132-3p	dmrt1	-	68
miR-132-3p	ebf1a	-	64
miR-132-3p	elk1	-	79
miR-132-3p	epas1a	-	65
miR-132-3p	epas1b	-	71
miR-132-3p	foxo3b	-	63
miR-132-3p	foxp2	-	85
miR-132-3p	hey1	-	74
miR-132-3p	hlfa	-	88
miR-132-3p	irf4a	-	84
miR-132-3p	klf2b	-	94
miR-132-3p	maml3	-	84
miR-132-3p	meox2a	-	70
miR-132-3p	pbx1a	-	78
miR-132-3p	satb1b	-	90
miR-132-3p	smad3a	-	72
miR-132-3p	tefb	-	95
miR-132-3p	thraa	-	81
miR-132-3p	zbtb16a	-	73
miR-132-3p	zbtb47a	-	93
miR-132-5p	tgfb3	6.92E-03	-
miR-145-5p	hsd17b12b	-	96
miR-146a	dixdc1b	-	91
miR-146a	dvl1b	-	96
miR-146a	wnt7bb	-	93
miR-146a	fgfr1a	-	66
miR-146a	hhip	-	68
miR-146a	hdac5	-	88
miR-146a	kat7a	-	94
miR-146a	sema4e	-	61
miR-146a	zgc:114045	-	67
miR-146a	cib2	-	75

miR-146a	crispld1a	-	98
miR-146a	serpi-10a	-	59
miR-146a	sostdc1b	-	96
miR-146a	ednrba	-	69
miR-146a	alx4a	-	75
miR-146a	maml3	-	86
miR-146a	runx3	-	96
miR-146a	zbtb47a	-	97
miR-146b	dixdc1b	-	91
miR-146b	dvl1b	-	96
miR-146b	wnt7bb	-	91
miR-146b	fgfr1a	-	66
miR-146b	hhip	-	59
miR-146b	hdac5	-	86
miR-146b	kat7a	-	94
miR-146b	sema4e	-	63
miR-146b	zgc:114045	-	67
miR-146b	cib2	-	75
miR-146b	crispld1a	-	98
miR-146b	serpi-10a	-	60
miR-146b	sostdc1b	-	96
miR-146b	bgnb	-	97
miR-146b	ednrba	-	65
miR-146b	alx4a	-	76
miR-146b	atf7b	-	51
miR-146b	maml3	-	86
miR-146b	runx3	-	97
miR-146b	zbtb47a	-	96
miR-21	amer2	-	62
miR-21	dkk2	-	84
miR-21	ndrg2	-	93
miR-21	fgfr1b	-	98
miR-21	fgfr1a	-	73
miR-21	ptk2bb	-	92
miR-21	cd248a	-	85
miR-21	bmper	-	72
miR-21	htra4	-	97
miR-21	ephb3a	-	91
miR-21	smarca2	-	97
miR-21	sema3b	-	86
miR-21	sema3bl	-	82
miR-21	bnip3la	-	97

miR-21	adgrg1	8.92E-03	-
miR-21	adgrg1	-	75
miR-21	arl4ab	-	83
miR-21	arl4d	-	77
miR-21	dgkaa	-	85
miR-21	rac3b	-	66
miR-21	rapgef4	-	95
miR-21	si:ch211-184m13.4	-	99
miR-21	tie1	-	96
miR-21	zgc:92360	-	71
miR-21	cd59	-	70
miR-21	mxra5a	-	70
miR-21	wfikkn2b	-	75
miR-21	lhcgr	5.63E-03	-
miR-21	apln	-	85
miR-21	ptn	-	53
miR-21	alx4a	-	53
miR-21	bcorl1	-	66
miR-21	bhlhe40	-	53
miR-21	bhlhe41	-	83
miR-21	cipca	-	82
miR-21	dlx1a	-	83
miR-21	epas1b	-	67
miR-21	foxd2	-	70
miR-21	foxn1	-	97
miR-21	foxo3a	-	78
miR-21	foxo3b	-	97
miR-21	foxp2	-	66
miR-21	hey1	-	67
miR-21	hlfa	-	74
miR-21	irf4a	-	66
miR-21	nr1i2	-	87
miR-21	per3	-	77
miR-21	plag1	-	86
miR-21	pparaa	-	61
miR-21	rfx7	-	75
miR-21	satb1b	-	84
miR-21	sox3	-	75
miR-21	sox5	-	51
miR-21	tbx18	-	78
miR-21	tp53inp1	-	67
miR-21	zbtb4	-	99

miR-21	zic3	-	57
miR-21	dpep2	-	94
miR-21	GGT5 (1 of many)	-	80
miR-31	nkd1	-	82
miR-31	fgfr1b	-	73
miR-31	cxcl12a	-	96
miR-31	epha4b	-	89
miR-31	smarca2	-	62
miR-31	tox2	-	63
miR-31	sema3bl	-	79
miR-31	cdc14ab	-	89
miR-31	adgrg1	-	66
miR-31	prex2	-	80
miR-31	rasef	-	91
miR-31	zgc:92360	-	88
miR-31	col11a1a	-	83
miR-31	crispld1a	-	88
miR-31	dpt	-	99
miR-31	frem1b	-	73
miR-31	glipr2	-	88
miR-31	itgb1a	-	92
miR-31	itgb1b.1	7.61E-03	74
miR-31	thy1	7.00E-03	97
miR-31	zgc:113307	4.22E-03	-
miR-31	ntf3	3.25E-03	-
miR-31	calcrla	-	77
miR-31	cyp2u1	-	57
miR-31	bhlhe40	-	50
miR-31	cbfa2t3	-	66
miR-31	crtc3	-	79
miR-31	dlx1a	-	91
miR-31	ebf1a	-	91
miR-31	hbp1	-	70
miR-31	hoxa4a	-	55
miR-31	klf15	-	70
miR-31	klf3	-	63
miR-31	klf6b	-	80
miR-31	nr1i2	-	73
miR-31	plag1	-	62
miR-31	rorca	-	94
miR-31	runx3	4.30E-02	70
miR-31	zbtb4	-	65

miR-489	tgfb2	-	75
miR-489	lemd3	-	62
miR-489	gatad1	-	87
miR-489	prmt3	-	86
miR-489	top1l	-	65
miR-489	cdk2	5.13E-03	-
miR-489	asap2a	-	81
miR-489	ERAS	-	90
miR-489	hcar1-4	-	97
miR-489	ipo13	2.86E-03	-
miR-489	ralaa	-	92
miR-489	ERAS	0.00E+00	1
miR-489	ctsz	-	66
miR-489	fn1a	-	73
miR-489	hapln1a	-	62
miR-489	m17	-	79
miR-489	arntl2	-	54
miR-489	atf3	-	94
miR-489	e2f3	-	57
miR-489	junbb	-	98
miR-489	zgc:153115	-	52
miR-489	med24	-	70
miR-489	mycn	-	79
miR-489	sall1a	-	76
miR-489	sp3a	-	89
miR-489	spi1a	-	92
miR-489	tgif1	-	85
miR-489	zgc:113363	-	87
miR-489	ankib1a	-	98
miR-489	bop1	-	61
miR-489	coil	-	67
miR-489	d-jb1a	-	80
miR-489	d-jc21	-	80
miR-489	d-jc25	-	92
miR-489	grpel1	-	99
miR-489	hspa4b	3.71E-03	-
miR-489	gar1	-	78
miR-722	sytl2b	-	97
miR-724	fgf20a	-	57
miR-92b-3p	inhbaa	-	75
miR-92b-3p	igf2b	-	86
miR-92b-3p	prmt1	-	92

miR-92b-3p	sema6dl	-	61
miR-92b-3p	bub1bb	-	91
miR-92b-3p	ccnjl	-	94
miR-92b-3p	cdk1	-	60
miR-92b-3p	arfgap2	-	89
miR-92b-3p	cpa5	-	82
miR-92b-3p	ctsba	-	92
miR-92b-3p	ctsla	3.36E-02	84
miR-92b-3p	fn1b	-	63
miR-92b-3p	frem2a	-	66
miR-92b-3p	itga5	-	95
miR-92b-3p	itgb8	-	72
miR-92b-3p	hsd17b12b	-	99
miR-92b-3p	hsd17b2	-	79
miR-92b-3p	atf3	-	83
miR-92b-3p	e2f3	-	62
miR-92b-3p	fosl2	-	58
miR-92b-3p	foxm1	-	57
miR-92b-3p	foxp4	-	77
miR-92b-3p	zgc:153115	-	60
miR-92b-3p	nono	-	66
miR-92b-3p	nr2c1	-	75
miR-92b-3p	pprc1	-	75
miR-92b-3p	prmt1	-	92
miR-92b-3p	sall1b	-	86
miR-92b-3p	sox11a	-	99
miR-92b-3p	tgif1	-	80
miR-92b-3p	vezf1a	-	64
miR-92b-3p	ankzf1	-	99
miR-92b-3p	d-jc10	-	88
miR-92b-3p	fkbp1ab	-	76
miR-92b-3p	hspa14	-	52
miR-92b-3p	tsr1	7.20E-03	-
miR-92b-3p	pomp	3.65E-03	-

Appendix B – Supplemental Data for Chapter 3

Table B.1 Classification of transcripts altered by BDP exposure according to function. Human orthologs of transcripts altered greater than 2-fold by BDP exposure were analyzed by Ingenuity software and grouped according to their respective biological function(s).

Genes	Fold change		Genes	Fold change	
Cell Death			**Cell-To-Cell Signaling and Interaction**		
SOCS3	2.03	UP	TYMS	2.05	DOWN
CA2	2.57	DOWN	DLL1	2.00	UP
ANGPT2	2.46	UP	ANGPT2	2.46	UP
CDC20	2.12	DOWN	SLC4A2	2.04	DOWN
DLX4b	2.06	DOWN	UCP2	2.57	UP
BCL2L13	2.26	UP	DKK3	4.33	DOWN
ATP1A1	2.50	UP	ANXA1	6.44	DOWN
DKK3	4.33	DOWN	GFAP	2.04	UP
ANXA1	6.44	DOWN	GPM6A	2.13	UP
HSD11B2	14.36	UP	DCT	2.05	UP
GFAP	2.04	UP	ADCYAP1	2.03	UP
FKBP5	6.33	UP			
SNCB	2.18	UP	**Inflammatory Response**		
TYMS	2.05	DOWN	SOCS3	2.03	UP
DLL1	2.00	UP	ANGPT2	2.46	UP
UCP2	2.57	UP	UCP2	2.57	UP
RRM2	2.09	DOWN	DUSP1	3.87	UP
TDGF1	8.53	UP	ANXA1	6.44	DOWN
ANXA4	3.13	UP	ADCYAP1	2.03	UP
PLK1	2.08	DOWN	GSN	2.25	DOWN
GSN	2.25	DOWN			
XIAP	2.41	UP	**Cell Cycle**		
PFKM	2.43	UP	TYMS	2.05	DOWN
DUSP1	3.87	UP	KIF23	2.29	DOWN
DCT	2.05	UP	NUSAP1	2.01	DOWN
ADCYAP1	2.03	UP	CDC20	2.01	UP
HMGB2	2.18	DOWN	ORC6L	2.33	DOWN
			PLK1	2.08	DOWN
Connective Tissue Development and Function			PTGES3 (includes EG:10728)	2.04	UP
SOCS3	2.03	UP	SMC2	2.49	DOWN

ANGPT2	2.46	UP
SLC4A2	2.04	DOWN
ANXA1	6.44	DOWN
HMX3	2.04	UP
HSD11B2	14.36	UP
ADCYAP1	2.03	UP
GSN	2.25	DOWN

Cellular Growth and Proliferation

KIF23	2.29	DOWN
TYMS	2.05	DOWN
SOCS3	2.03	UP
ANGPT2	2.46	UP
DLL1	2.00	UP
SLC4A2	2.04	DOWN
TDGF1	8.53	UP
PLK1	2.08	DOWN
XIAP	2.41	UP
DUSP1	3.87	UP
DKK3	4.33	DOWN
ANXA1	6.44	DOWN
HSD11B2	14.36	UP
FKBP5	6.33	UP
ADCYAP1	2.03	UP

Cell Signaling

SOCS3	2.03	UP
SYT4	2.52	UP
ANGPT2	2.46	UP
UCP2	2.57	UP
DUSP1	3.87	UP
CPLX2	3.44	UP
ANXA1	6.44	DOWN
GSN	2.25	DOWN
ADCYAP1	2.03	UP
XIAP	2.41	UP

Connective Tissue Disorders

SOCS3	2.03	UP
SLC4A2	2.04	DOWN

Gene Expression

DUSP1	3.87	UP
ASPM	2.09	DOWN
ANXA1	6.44	DOWN
ADCYAP1	2.03	UP
KIF11	2.25	DOWN

Cellular Movement

KIF23	2.29	DOWN
SOCS3	2.03	UP
SYT4	2.52	UP
NUSAP1	2.01	DOWN
ANGPT2	2.46	UP
DLL1	2.00	UP
UCP2	2.57	UP
CDC20	2.12	DOWN
TDGF1	8.53	UP
PLK1	2.08	DOWN
GSN	2.25	DOWN
DKK3	4.33	DOWN
DUSP1	3.87	UP
CPLX2	3.44	UP
ANXA1	6.44	DOWN
GFAP	2.04	UP
HMGB2	2.18	DOWN

Tissue Morphology

TYMS	2.05	DOWN
SOCS3	2.03	UP
CA2	2.57	DOWN
ANGPT2	2.46	UP
SLC4A2	2.04	DOWN
TDGF1	8.53	UP
GSN	2.25	DOWN
XIAP	2.41	UP
DKK3	4.33	DOWN
ANXA1	6.44	DOWN
HSD11B2	14.36	UP
GFAP	2.04	UP
ADCYAP1	2.03	UP

Tissue Development

SOCS3	2.03	UP

SOCS3	2.03	UP	CA2	2.57	DOWN
PTGES3 (includes EG:10728)	2.04	UP	ANGPT2	2.46	UP
SMC2	2.49	DOWN	DLL1	2.00	UP
DLX4	2.06	DOWN	DKK3	4.33	DOWN
ADCYAP1	2.03	UP	TDGF1	8.53	UP
HMGB2	2.18	DOWN	HMX3	2.04	UP
			PLK1	2.08	DOWN
			GSN	2.25	DOWN
			ADCYAP1	2.03	UP

Table B.2. Transcription factors (TFs) that increased or decreased expression in the microarray data and were used for downstream promoter analysis of zebrafish *cripto-1*.

TFs with increased expression (Affymetrix ID)		TFs with decreased expression (Affymetrix ID)	
KLF9	(Dr.16174.1.A1_at)	RUNX3	(Dr.10668.1.S2_at)
ISL1	(Dr.12208.1.S1_s_at)	DLX4B	(Dr.153.1.S1_at)
POU3F1	(Dr.57.1.S1_at)	WHSC1	(Dr.2130.1.A1_at)
HMX3	(Dr.10448.1.S1_at)	MYBL2	(Dr.17421.1.A1_at)
POU3F3	(Dr.21068.1.S1_s_at)	FOXM1	(Dr.17623.1.S1_at)
CEBPD	(Dr.1280.1.A1_at)	EPAS1	(Dr.12182.1.A1_at)
MAF	(Dr.10168.2.S1_at)	VOX	(Dr.10458.1.S1_at)
FOSA	(Dr.12986.1.A1_at)		
MYT1	(Dr.25176.2.A1_at)		
EN1	(Dr.2794.1.A1_at)		
HIF1AL	(Dr.11978.1.A1_at)		
FOXD3	(Dr.590.1.S1_at)		
KLF2	(Dr.3448.1.S1_at)		
HOXD11	(Dr.5759.1.A1_at)		

Table B.3 Results from promoter analysis of zebrafish *cripto-1* using MatInspector v8.4.1. Weight matrices of the glucocorticoid receptor and TFs from Table B.2 were searched against the genomic sequence 3000 base pairs upstream of the transcriptional start site. In the Sequence column, capital letters indicate core sequence used by MatInspector. Red letters indicate where the matrix has a high conservation profile.

Matrix	Detailed Matrix Information	from	to	anchor	Strand	Matrix sim.	Sequence
V$IR2_NGRE.01	Repressive binding sites for glucocorticoid receptor (IR2)	230	244	237	(+)	0.886	ctCTCCcgggacagc
V$ISL1.01	Pancreatic and intestinal lim-homeodomain factor	1383	1405	1394	(-)	0.866	atgttatagTAATgaaccaaata
V$ISL1.01	Pancreatic and intestinal lim-homeodomain factor	1464	1486	1475	(+)	0.836	acaatagacTAATgttttaaaag
V$ISL1.01	Pancreatic and intestinal lim-homeodomain factor	2549	2571	2560	(+)	0.82	tattttgcaTAATgttgggaaat
V$HMX3.02	Hmx3/Nkx5-1 homeodomain transcription factor	347	365	356	(-)	0.982	ttcacagcacTTAAatgac
V$HMX3.02	Hmx3/Nkx5-1 homeodomain transcription factor	342	360	351	(+)	0.977	ctgtggtcatTTAAgtgct
V$HMX3.02	Hmx3/Nkx5-1 homeodomain transcription factor	2679	2697	2688	(-)	0.968	ttactcacccTTAAgtgat
V$HMX3.02	Hmx3/Nkx5-1 homeodomain transcription factor	2674	2692	2683	(+)	0.967	ttggaatcacTTAAgggtg
V$HMX3.02	Hmx3/Nkx5-1 homeodomain transcription factor	1402	1420	1411	(-)	0.932	tagaattcacTTAAaatgt
V$HMX3.02	Hmx3/Nkx5-1 homeodomain transcription factor	2792	2810	2801	(-)	0.924	aatgatttcaTTAAttgat
V$HMX3.02	Hmx3/Nkx5-1 homeodomain transcription factor	1397	1415	1406	(+)	0.922	ctataacattTTAAgtgaa

V$HMX3.01	H6 homeodomain HMX3/Nkx5.1 transcription factor	270	288	279	(+)	0.921	acatatctAAGTgggaact
V$HMX3.01	H6 homeodomain HMX3/Nkx5.1 transcription factor	1747	1765	1756	(+)	0.898	gaaattctAAGTggtggat
V$HMX3.03	H6 homeodomain HMX3/Nkx5.1 transcription factor	346	364	355	(+)	0.878	ggtcattTAAGtgctgtga
V$POU3F3.01	POU class 3 homeobox 3 (POU3F3), OTF8	2550	2564	2557	(+)	0.932	attttGCATaatgtt
V$POU3F3.01	POU class 3 homeobox 3 (POU3F3), OTF8	2955	2969	2962	(+)	0.875	tgtatGAATaaatga
V$POU3F3.01	POU class 3 homeobox 3 (POU3F3), OTF8	1445	1459	1452	(+)	0.872	tgtatGAATaacttt
V$POU3F3.01	POU class 3 homeobox 3 (POU3F3), OTF8	2000	2014	2007	(-)	0.872	aatatGTATaagttg
V$POU3F3.01	POU class 3 homeobox 3 (POU3F3), OTF8	2827	2841	2834	(+)	0.859	cacttGCATaaatgc
V$POU3F3.01	POU class 3 homeobox 3 (POU3F3), OTF8	2003	2017	2010	(+)	0.836	cttatACATattaga
V$POU3F3.01	POU class 3 homeobox 3 (POU3F3), OTF8	2161	2175	2168	(+)	0.83	tatatGTATactcaa
V$POU3F3.01	POU class 3 homeobox 3 (POU3F3), OTF8	170	184	177	(-)	0.829	aataaGCATataagg
V$POU3F3.01	POU class 3 homeobox 3 (POU3F3), OTF8	2158	2172	2165	(-)	0.825	agtatACATataaat
V$POU3F3.01	POU class 3 homeobox 3 (POU3F3), OTF8	2816	2830	2823	(+)	0.817	taaatGCATgacact
V$POU3F3.01	POU class 3 homeobox 3 (POU3F3), OTF8	1442	1456	1449	(-)	0.812	gttatTCATacaata
V$MAFK.01	V-maf musculoaponeurotic fibrosarcoma oncogene homolog K (half site)	543	567	555	(+)	0.829	aatactttttattAGCAttttttt
V$MYT1.02	MyT1 zinc finger transcription factor involved in primary neurogenesis	2667	2679	2673	(+)	0.987	aaaAAGTttggaa
V$MYT1L.01	Myelin transcription factor 1-like, neuronal	760	772	766	(+)	0.958	tgagAGTTcctca

	C2HC zinc finger factor 1						
V$MYT1L.01	Myelin transcription factor 1-like, neuronal C2HC zinc finger factor 1	2721	2733	2727	(-)	0.945	ggatAGTTcacac
V$MYT1L.01	Myelin transcription factor 1-like, neuronal C2HC zinc finger factor 1	2569	2581	2575	(-)	0.925	cgatAGTTacatt
V$MYT1.02	MyT1 zinc finger transcription factor involved in primary neurogenesis	1481	1493	1487	(+)	0.901	taaAAGTtcttga
V$MYT1.02	MyT1 zinc finger transcription factor involved in primary neurogenesis	1567	1579	1573	(-)	0.895	cagAAGTttaaaa
V$MYT1.02	MyT1 zinc finger transcription factor involved in primary neurogenesis	621	633	627	(+)	0.889	aggAAGTttaaat
V$MYT1.02	MyT1 zinc finger transcription factor involved in primary neurogenesis	1279	1291	1285	(-)	0.889	aggAAGTttaaga
V$MYT1.02	MyT1 zinc finger transcription factor involved in primary neurogenesis	2046	2058	2052	(+)	0.887	ctcAAGTtttta
V$MYT1.02	MyT1 zinc finger transcription factor involved in primary neurogenesis	1449	1461	1455	(-)	0.886	ttaAAGTtattca
V$MYT1.02	MyT1 zinc finger transcription factor involved in primary neurogenesis	571	583	577	(-)	0.883	aaaAAGTtaggat
V$MYT1.02	MyT1 zinc finger transcription factor involved in primary neurogenesis	395	407	401	(-)	0.88	ctaAAGTtggaac
V$MYT1.01	MyT1 zinc finger transcription factor involved in primary neurogenesis	696	708	702	(+)	0.799	caaAAGCgtactt

V$MYT1.01	MyT1 zinc finger transcription factor involved in primary neurogenesis	2058	2070	2064	(-)	0.799	gtaATGTatactt
V$MYT1.01	MyT1 zinc finger transcription factor involved in primary neurogenesis	699	711	705	(-)	0.758	tcaAAGTacgctt
V$MYT1.01	MyT1 zinc finger transcription factor involved in primary neurogenesis	598	610	604	(-)	0.756	ataAAGCtgattt
V$MYT1.01	MyT1 zinc finger transcription factor involved in primary neurogenesis	1414	1426	1420	(-)	0.756	aaaAAGTagaatt
V$EN1.02	Engrailed homeobox 1	2788	2806	2797	(+)	0.904	tgcaatcAATTaatgaaat
V$EN1.01	Homeobox protein engrailed (en-1)	1398	1416	1407	(+)	0.893	tataacatTTTAagtgaat
V$EN1.01	Homeobox protein engrailed (en-1)	1346	1364	1355	(+)	0.867	ttatacagTTTAagtgcaa
V$EN1.01	Homeobox protein engrailed (en-1)	343	361	352	(+)	0.834	tgtggtcaTTTAagtgctg
V$EN1.01	Homeobox protein engrailed (en-1)	395	413	404	(+)	0.827	gttccaacTTTAgttgaaa
V$EN1.01	Homeobox protein engrailed (en-1)	1348	1366	1357	(-)	0.809	ccttgcacTTAAactgtat
V$EN1.01	Homeobox protein engrailed (en-1)	1259	1277	1268	(+)	0.795	atgtcggaTTTAaatcaaa
V$EN1.01	Homeobox protein engrailed (en-1)	372	390	381	(+)	0.794	tggcaacaTTAAaatgctt
V$EN1.01	Homeobox protein engrailed (en-1)	1400	1418	1409	(-)	0.792	gaattcacTTAAaatgtta
V$EN1.01	Homeobox protein engrailed (en-1)	602	620	611	(+)	0.787	cagctttaTTTAatttcac
V$EN1.01	Homeobox protein engrailed (en-1)	1449	1467	1458	(+)	0.775	tgaataacTTTAagtacaa
V$MYBL2.01	v-myb myeloblastosis viral oncogene homolog (avian)-like 2 (BMYB), dimeric binding site	912	932	922	(-)	0.816	taaccgccgAAACcctaaagt
V$MYBL2.01	v-myb myeloblastosis viral oncogene	1469	1489	1479	(-)	0.789	gaacttttaAAACattagtct

homolog (avian)-like 2
(BMYB), dimeric
binding site

	v-myb myeloblastosis viral oncogene homolog (avian)-like 2 (BMYB), dimeric							ttactgttcCAACtttagttg
V$MYBL2.01	binding site	390	410	400	(+)	0.78		
	v-myb myeloblastosis viral oncogene homolog (avian)-like 2 (BMYB), dimeric							aatccgggcTAACagtgtgga
V$MYBL2.01	binding site	1315	1335	1325	(-)	0.769		
	v-myb myeloblastosis viral oncogene homolog (avian)-like 2 (BMYB), dimeric							ttactatccTAACttttttgg
V$MYBL2.01	binding site	566	586	576	(+)	0.757		
	v-myb myeloblastosis viral oncogene homolog (avian)-like 2 (BMYB), dimeric							caactatatTCACtgtaaaaa
V$MYBL2.01	binding site	1080	1100	1090	(+)	0.755		

Table B.4 Results from promoter analysis of mouse *cripto-1* using MatInspector v8.4.1. Weight matrices of the glucocorticoid receptor and TFs from Table B.2 were searched against the genomic sequence 3000 base pairs upstream of the transcriptional start site. In the Sequence column, capital letters indicate core sequence used by MatInspector. Red letters indicate where the matrix has a high conservation profile.

Matrix	Detailed Matrix Information	from	to	anchor	Strand	Matrix sim.	Sequence
V$IR2_NGRE.01	Repressive binding sites for glucocorticoid receptor (IR2)	252	266	259	(-)	0.887	gaCTCCcaggagtta
	Repressive binding sites for glucocorticoid receptor (IR2)	253	267	260	(+)	0.883	aaCTCCtgggagtct
V$IR2_NGRE.01	Repressive binding sites for glucocorticoid receptor (IR2)	407	421	414	(-)	0.862	ccCTCCcccgagata
	Pancreatic and intestinal lim-homeodomain factor	2871	2893	2882	(+)	0.863	ttgggtggaTAATgcttccgcag
V$IR2_NGRE.01	Pancreatic and intestinal lim-homeodomain factor	2551	2573	2562	(+)	0.861	ttgataaaaTAATgtatactatg
	Hmx3/Nkx5-1 homeodomain transcription factor	505	523	514	(-)	0.938	tttttttcaaTTAAattca
V$ISL1.01	Hmx3/Nkx5-1 homeodomain transcription factor	2829	2847	2838	(+)	0.92	cagaaagccaTTAActtgt
	H6 homeodomain HMX3/Nkx5.1 transcription factor	2353	2371	2362	(+)	0.891	accaactcAAGGgggaggg
V$ISL1.01	POU class 3 homeobox 3 (POU3F3), OTF8	2039	2053	2046	(-)	0.82	tcactGCATatatat
	V-maf musculoaponeurotic fibrosarcoma oncogene homolog K (half site)	2716	2740	2728	(-)	0.826	tgcattcaaaaatcTGCAatttcag
V$HMX3.02	Myelin transcription factor 1-like, neuronal C2HC zinc finger factor 1	2338	2350	2344	(-)	0.922	tgagAGCTtatct
	MyT1 zinc finger transcription factor involved in primary neurogenesis	922	934	928	(+)	0.777	tcaAAATtatctt
V$HMX3.02	MyT1 zinc finger transcription factor involved in primary neurogenesis	1327	1339	1333	(+)	0.758	tcaAATTtgtctt
	MyT1 zinc finger transcription factor involved in primary neurogenesis	2155	2167	2161	(-)	0.758	ccaAATTtcattt
V$HMX3.01	Homeobox protein engrailed (en-1)	501	519	510	(+)	1	ttgttgaaTTTAattgaaa
	Engrailed homeobox 1	515	533	524	(+)	0.873	tgaaaaaAATTaagatttt
V$POU3F3.01	v-myb myeloblastosis viral oncogene homolog (avian)-like 2 (BMYB), dimeric binding site	868	888	878	(-)	0.767	aatctgattTAACcttttttt

Table B.5 Results from promoter analysis of human *cripto-1* using MatInspector v8.4.1. Weight matrices of the glucocorticoid receptor and TFs from Table B.2 were searched against the genomic sequence 3000 base pairs upstream of the transcriptional start site. In the Sequence column, capital letters indicate core sequence used by MatInspector. Red letters indicate where the matrix has a high conservation profile.

Matrix	Detailed Matrix Information	from	to	anchor	Strand	Matrix sim.	Sequence
V$IR2_NGRE.01	Repressive binding sites for glucocorticoid receptor (IR2)	252	266	259	(-)	0.887	gaCTCCcaggagtta
V$IR2_NGRE.01	Repressive binding sites for glucocorticoid receptor (IR2)	253	267	260	(+)	0.883	aaCTCCtgggagtct
V$IR2_NGRE.01	Repressive binding sites for glucocorticoid receptor (IR2)	407	421	414	(-)	0.862	ccCTCCcccgagata
V$ISL1.01	Pancreatic and intestinal lim-homeodomain factor	2871	2893	2882	(+)	0.863	ttgggtggaTAATgcttccgcag
V$ISL1.01	Pancreatic and intestinal lim-homeodomain factor	2551	2573	2562	(+)	0.861	ttgataaaaTAATgtatactatg
V$HMX3.02	Hmx3/Nkx5-1 homeodomain transcription factor	505	523	514	(-)	0.938	tttttttcaaTTAAattca
V$HMX3.02	Hmx3/Nkx5-1 homeodomain transcription factor	2829	2847	2838	(+)	0.92	cagaaagccaTTAActtgt
V$HMX3.01	H6 homeodomain HMX3/Nkx5.1 transcription factor	2353	2371	2362	(+)	0.891	accaactcAAGGgggaggg
V$POU3F3.01	POU class 3 homeobox 3 (POU3F3), OTF8	2039	2053	2046	(-)	0.82	tcactGCATatatat
V$MAFK.01	V-maf musculoaponeurotic fibrosarcoma oncogene homolog K (half site)	2716	2740	2728	(-)	0.826	tgcattcaaaaatcTGCAatttcag
V$MYT1L.01	Myelin transcription factor 1-like, neuronal C2HC zinc finger factor 1	2338	2350	2344	(-)	0.922	tgagAGCTtatct
V$MYT1.01	MyT1 zinc finger transcription factor involved in primary neurogenesis	922	934	928	(+)	0.777	tcaAAATtatctt
V$MYT1.01	MyT1 zinc finger transcription factor involved in primary neurogenesis	1327	1339	1333	(+)	0.758	tcaAATTtgtctt
V$MYT1.01	MyT1 zinc finger transcription factor involved in primary neurogenesis	2155	2167	2161	(-)	0.758	ccaAATTtcattt
V$EN1.01	Homeobox protein engrailed (en-1)	501	519	510	(+)	1	ttgttgaaTTTAattgaaa
V$EN1.02	Engrailed homeobox 1	515	533	524	(+)	0.873	tgaaaaaAATTaagatttt
V$MYBL2.01	v-myb myeloblastosis viral oncogene homolog (avian)-like 2 (BMYB), dimeric binding site	868	888	878	(-)	0.767	aatctgattTAACcttttttt

Table B.6. Primer sequences (and their associated Affymetrix probe identifiers) used for qRT-PCR validation of differentially expressed genes from the microarray. Forward and reverse primers are designated F and R, respectively.

Target gene	Sequence 5' to 3'	Affymetrix probe set number
F β-*actin*	AAGCAGGAGTACGATGAGTC	Dr.1109.1.S1_at
R β-*actin*	TGGAGTCCTCAGATGCATTG	Dr.1109.1.S1_at
F *cripto-1*	CACAACTTTCATTTGCCGTG	Dr.581.1.S1_at
R *cripto-1*	CTGGGTTTTTGATGCGAGTT	Dr.581.1.S1_at
F *gilz*	CGACTTGTTTATATGGGCTG	Dr.12437.1.A1_at
R *gilz*	TCTTCAGACACCAACATGCC	Dr.12437.1.A1_at
F *fkbp506*	CACGTTCACAAACACACTGC	Dr.2675.1.A1_at
R *fkbp506*	ATCAAACGAACAAGCGGGTC	Dr.2675.1.A1_at
F *glula*	AAGGGTGGTTCTAACATGGC	Dr.4147.1.S1_at
R *glula*	TGGACTGCGACTTTGTACCG	Dr.4147.1.S1_at

Appendix C – Supplemental Data for Chapter 4

Table C.1 48 hpf significantly differentially expressed transcripts following exposure to BkF (q ≤ 0.05, FC > 2)

ENSEMBLE ID	Symbol	log2FoldChange	padj
ENSDARG00000018298	cyp1c2	9.05	0
ENSDARG00000026039	cyp1a	8.99	1.76E-229
ENSDARG00000068934	cyp1b1	8.75	0
ENSDARG00000058980	cyp1c1	7.14	5.27E-241
ENSDARG00000059387	fgf7	5.29	2.44E-165
ENSDARG00000070925	EDN3 (1 of 2)	4.81	2.18E-53
ENSDARG00000097080	si:ch73-181m17.1	4.39	3.09E-46
ENSDARG00000091116	pkhd1l1	4.35	7.61E-176
ENSDARG00000097491	ugt1b1	4.11	5.16E-149
ENSDARG00000055643	cyb5a	3.83	0
ENSDARG00000078617	CABZ01048958.1	3.78	1.62E-33
ENSDARG00000089507	ugt1b5	3.72	9.88E-101
ENSDARG00000052618	ahrrb	3.68	1.07E-41
ENSDARG00000005141	camkvb	3.55	1.23E-33
ENSDARG00000010376	SLC5A3 (1 of 2)	3.54	8.21E-28
ENSDARG00000007356	fgf20a	3.47	1.60E-45
ENSDARG00000097716	si:dkey-86k10.8	3.42	3.04E-68
ENSDARG00000074683	CABZ01048960.1	3.40	1.44E-29
ENSDARG00000035677	bmp8a	3.36	2.66E-36
ENSDARG00000076933	aldh1a3	3.29	1.86E-33
ENSDARG00000092704	BX072532.3	3.24	9.73E-28
ENSDARG00000095409	si:ch211-226h7.8	3.11	1.34E-20
ENSDARG00000030896	foxq1a	3.07	1.44E-29
ENSDARG00000019492	shbg	2.94	8.06E-14
ENSDARG00000094120	BX548047.2	2.86	7.69E-15
ENSDARG00000020086	NUAK1 (1 of 2)	2.86	1.77E-60
ENSDARG00000056057	GREM2 (2 of 2)	2.85	7.47E-23
ENSDARG00000079221	si:ch211-162k9.6	2.82	4.96E-15
ENSDARG00000055081	si:dkey-285b23.3	2.80	1.99E-14
ENSDARG00000052949	BX548047.1	2.77	9.95E-13
ENSDARG00000079296	gcga	2.70	2.36E-16
ENSDARG00000036767		2.68	5.08E-18
ENSDARG00000087020		2.67	2.60E-118
ENSDARG00000051876	ush1c	2.64	1.16E-31
ENSDARG00000057338	gstp2	2.64	1.02E-10

ENSDARG00000052626	si:ch211-226h7.7	2.62	6.49E-13
ENSDARG00000056654	gna15.2	2.59	1.16E-20
ENSDARG00000006207	gpx1b	2.59	2.96E-51
ENSDARG00000022570	BX248318.1	2.57	1.37E-11
ENSDARG00000086826	sult6b1	2.55	6.15E-290
ENSDARG00000088595	CRISPLD2	2.50	9.07E-30
ENSDARG00000061841	tiparp	2.50	3.30E-57
ENSDARG00000070929	sox14	2.49	2.32E-32
ENSDARG00000093365	si:ch211-226h7.3	2.49	2.25E-16
ENSDARG00000045371	prdm14	2.47	1.59E-19
ENSDARG00000026611	socs3b	2.47	1.47E-42
ENSDARG00000079199	megf6a	2.46	1.22E-27
ENSDARG00000075891	sall1b	2.46	9.15E-47
ENSDARG00000061896	slco2a1	2.45	3.49E-15
ENSDARG00000035852		2.43	3.80E-15
ENSDARG00000088371	junbb	2.43	5.54E-19
ENSDARG00000039957	rspo1	2.41	3.37E-56
ENSDARG00000006427	fabp2	2.34	6.33E-17
ENSDARG00000068180	bmp16	2.34	3.61E-13
ENSDARG00000078749	b4galnt3a	2.33	1.50E-10
ENSDARG00000077151	cbln2b	2.32	4.05E-23
ENSDARG00000097991	si:dkey-86k10.14	2.30	7.26E-10
ENSDARG00000074642	BX072532.1	2.29	9.12E-12
ENSDARG00000070546	msgn1	2.29	1.14E-10
ENSDARG00000090530	LAMB3	2.28	4.52E-11
ENSDARG00000094158	si:dkey-285b23.4	2.28	3.17E-09
ENSDARG00000058570	ccl1	2.28	8.75E-11
ENSDARG00000070710	si:dkeyp-41g9.6	2.27	1.01E-10
ENSDARG00000091572	BX005234.1	2.26	2.68E-08
ENSDARG00000090776	SEMA7A (2 of 2)	2.26	1.90E-10
ENSDARG00000037859	il11a	2.24	6.87E-14
ENSDARG00000094815	si:ch73-49p17.1	2.24	7.65E-18
ENSDARG00000038634	CCK (1 of 2)	2.23	4.52E-18
ENSDARG00000042470	s1pr3a	2.20	1.37E-46
ENSDARG00000059369		2.17	3.40E-21
ENSDARG00000055278	cfb	2.15	3.40E-11
ENSDARG00000059340	dlgap2a	2.14	1.97E-12
ENSDARG00000089205	BX927064.1	2.12	2.88E-24
ENSDARG00000016479	ugt5a1	2.12	1.28E-08
ENSDARG00000096156		2.11	4.88E-07
ENSDARG00000040623	fosl2	2.10	2.46E-19

ENSDARG00000043448	itm2ca	2.09	8.94E-32
ENSDARG00000093101	BX005305.7	2.09	2.75E-08
ENSDARG00000017860	rgs5b	2.09	7.88E-12
ENSDARG00000079227	plekhs1	2.08	5.23E-07
ENSDARG00000079290	si:ch211-162k9.5	2.06	2.16E-10
ENSDARG00000022303	hig1	2.06	8.24E-36
ENSDARG00000092719	si:ch211-226h7.4	2.05	1.38E-08
ENSDARG00000056074	fgf22	2.05	1.76E-09
ENSDARG00000089131	il17rel	2.05	3.06E-07
ENSDARG00000003902	ctsl.1	2.02	1.31E-07
ENSDARG00000036569	bach2a	2.01	6.45E-38
ENSDARG00000091792	akap12a	-2.00	3.02E-11
ENSDARG00000077505	rbp4	-2.03	2.04E-14
ENSDARG00000070331	muc5ac	-2.04	3.17E-12
ENSDARG00000055192	zgc:136930	-2.08	1.25E-07
ENSDARG00000003395	col4a3	-2.09	4.02E-62
ENSDARG00000055172	si:ch211-256m1.8	-2.14	4.01E-09
ENSDARG00000030632	zgc:110191	-2.19	7.70E-20
ENSDARG00000062477	kiaa1549la	-2.21	1.76E-14
ENSDARG00000087375	zgc:66473	-2.24	1.48E-09
ENSDARG00000007490	adrb1	-2.25	6.29E-14
ENSDARG00000075600	si:dkeyp-41f9.3	-2.25	4.47E-14
ENSDARG00000052279	osgn1	-2.26	5.21E-17
ENSDARG00000078962	DUOXA1	-2.27	2.99E-08
ENSDARG00000086805	ccdc129	-2.27	4.64E-15
ENSDARG00000088116	gstm3	-2.33	2.93E-50
ENSDARG00000062688	gpnmb	-2.34	4.35E-15
ENSDARG00000068910	nos1	-2.36	2.31E-09
ENSDARG00000090268	si:dkeyp-113d7.4	-2.43	7.50E-26
ENSDARG00000060345	apod	-2.58	4.95E-16
ENSDARG00000070919	cpne5	-2.65	5.95E-17
ENSDARG00000002847	fndc1	-2.66	1.16E-26
ENSDARG00000052470	igfbp2a	-2.68	3.13E-119
ENSDARG00000056938	kera	-2.70	6.97E-26
ENSDARG00000096762	si:dkey-61p9.11	-2.79	1.21E-15
ENSDARG00000058462	zgc:158846	-2.94	2.10E-14

Table C.2 60 hpf significantly differentially expressed transcripts following exposure to BkF (q ≤ 0.05, FC > 2)

ENSEMBLE ID	Symbol	log2FoldChange	padj
ENSDARG00000068934	cyp1b1	8.90	0
ENSDARG00000018298	cyp1c2	8.74	0
ENSDARG00000026039	cyp1a	8.45	7.33E-204
ENSDARG00000058980	cyp1c1	6.01	5.79E-179
ENSDARG00000059387	fgf7	5.39	5.56E-181
ENSDARG00000070925	EDN3 (1 of 2)	4.74	2.19E-52
ENSDARG00000052618	ahrrb	4.43	9.95E-61
ENSDARG00000091116	pkhd1l1	4.42	1.04E-182
ENSDARG00000097491	ugt1b1	4.24	1.14E-159
ENSDARG00000097080	si:ch73-181m17.1	4.20	6.11E-45
ENSDARG00000055643	cyb5a	4.19	0
ENSDARG00000056057	GREM2 (2 of 2)	4.00	3.68E-48
ENSDARG00000089507	ugt1b5	3.96	2.74E-113
ENSDARG00000005141	camkvb	3.78	2.44E-40
ENSDARG00000078617	CABZ01048958.1	3.76	8.07E-35
ENSDARG00000007356	fgf20a	3.70	9.09E-56
ENSDARG00000074683	CABZ01048960.1	3.69	6.01E-38
ENSDARG00000035677	bmp8a	3.67	3.70E-49
ENSDARG00000097716	si:dkey-86k10.8	3.61	3.06E-80
ENSDARG00000076933	aldh1a3	3.51	2.56E-41
ENSDARG00000020086	NUAK1 (1 of 2)	3.47	1.46E-88
ENSDARG00000090530	LAMB3	3.46	8.79E-24
ENSDARG00000010376	SLC5A3 (1 of 2)	3.43	2.27E-27
ENSDARG00000052626	si:ch211-226h7.7	3.18	1.78E-19
ENSDARG00000012395	mmp13a	3.16	9.13E-25
ENSDARG00000078749	b4galnt3a	3.15	5.68E-19
ENSDARG00000039957	rspo1	3.08	6.52E-96
ENSDARG00000055278	cfb	3.06	1.83E-21
ENSDARG00000035852		3.04	1.72E-23
ENSDARG00000022570	BX248318.1	3.02	3.53E-16
ENSDARG00000045371	prdm14	3.02	4.02E-31
ENSDARG00000052895	htra3a	3.01	1.48E-22
ENSDARG00000091380		3.01	2.44E-18
ENSDARG00000087020		3.00	2.58E-150
ENSDARG00000051876	ush1c	2.95	2.34E-41
ENSDARG00000095409	si:ch211-226h7.8	2.95	6.10E-19
ENSDARG00000059369		2.94	2.06E-39
ENSDARG00000037859	il11a	2.84	5.86E-22

ENSDARG00000079296	gcga	2.82	7.27E-17
ENSDARG00000045548	lepb	2.80	1.11E-15
ENSDARG00000094951	BX072532.5	2.79	4.31E-20
ENSDARG00000057338	gstp2	2.75	7.63E-12
ENSDARG00000026611	socs3b	2.75	8.65E-53
ENSDARG00000070710	si:dkeyp-41g9.6	2.71	1.60E-15
ENSDARG00000089706	BX005410.2	2.71	2.32E-27
ENSDARG00000040623	fosl2	2.66	3.96E-31
ENSDARG00000052329	CD200 (2 of 3)	2.65	9.25E-20
ENSDARG00000056654	gna15.2	2.64	1.69E-25
ENSDARG00000077580	tspeara	2.62	3.47E-24
ENSDARG00000019492	shbg	2.60	5.33E-11
ENSDARG00000069335	BCL6B	2.60	2.89E-60
ENSDARG00000017860	rgs5b	2.59	1.31E-25
ENSDARG00000092719	si:ch211-226h7.4	2.58	6.83E-16
ENSDARG00000003902	ctsl.1	2.57	2.18E-12
ENSDARG00000074150	si:ch211-226h7.5	2.56	2.64E-11
ENSDARG00000056077	dcst1	2.56	1.73E-12
ENSDARG00000094815	si:ch73-49p17.1	2.53	1.04E-21
ENSDARG00000022303	hig1	2.53	3.38E-54
ENSDARG00000086826	sult6b1	2.50	1.25E-279
ENSDARG00000088371	junbb	2.50	2.79E-20
ENSDARG00000030896	foxq1a	2.50	4.62E-20
ENSDARG00000075829	kiss1	2.47	1.68E-10
ENSDARG00000033684	oxgr1a.1	2.47	1.39E-10
ENSDARG00000076797		2.47	5.20E-11
ENSDARG00000097435	si:dkey-31i7.1	2.46	1.51E-10
ENSDARG00000054324	rerglb	2.45	1.49E-54
ENSDARG00000061841	tiparp	2.44	2.76E-55
ENSDARG00000079221	si:ch211-162k9.6	2.44	9.17E-12
ENSDARG00000014031	abcc2	2.42	4.29E-25
ENSDARG00000087359	c3b	2.41	9.96E-12
ENSDARG00000097539	si:ch211-39f2.3	2.41	9.60E-13
ENSDARG00000079199	megf6a	2.39	3.14E-28
ENSDARG00000074642	BX072532.1	2.38	7.53E-15
ENSDARG00000053493	aldh1a2	2.37	1.43E-21
ENSDARG00000008305	hand2	2.36	2.53E-10
ENSDARG00000056324	zgc:123295	2.34	1.22E-53
ENSDARG00000016750	abcc6a	2.33	3.67E-70
ENSDARG00000079765	AL929022.2	2.29	7.02E-26
ENSDARG00000097991	si:dkey-86k10.14	2.29	2.56E-10

			2.29	6.91E-09
ENSDARG00000035632			2.29	6.91E-09
ENSDARG00000070929	sox14		2.27	1.20E-29
ENSDARG00000036767			2.26	3.16E-13
ENSDARG00000031588	si:dkey-239b22.1		2.25	6.55E-09
ENSDARG00000079227	plekhs1		2.24	2.59E-08
ENSDARG00000093101	BX005305.7		2.23	1.74E-10
ENSDARG00000055705	f5		2.23	2.06E-08
ENSDARG00000092704	BX072532.3		2.22	1.73E-14
ENSDARG00000038025	cbx7a		2.19	1.13E-23
ENSDARG00000093365	si:ch211-226h7.3		2.19	1.08E-13
ENSDARG00000060471	gcnt3		2.17	5.18E-12
ENSDARG00000041382	si:dkey-283b15.2		2.16	9.36E-13
ENSDARG00000079191	CD200 (3 of 3)		2.16	7.81E-16
ENSDARG00000055081	si:dkey-285b23.3		2.16	3.58E-09
ENSDARG00000043448	itm2ca		2.15	6.45E-37
ENSDARG00000003303	stc1		2.09	7.52E-08
ENSDARG00000058730	rdh10a		2.08	1.20E-15
ENSDARG00000070546	msgn1		2.08	3.58E-08
ENSDARG00000071560	dlx4b		2.08	3.89E-35
ENSDARG00000092778	BX072532.4		2.08	1.47E-07
ENSDARG00000092170	apoc1l		2.07	1.22E-16
ENSDARG00000088283	si:ch73-248e21.5		2.06	3.13E-14
ENSDARG00000089131	il17rel		2.04	1.91E-07
ENSDARG00000006220	ugt1a7		2.03	3.69E-25
ENSDARG00000036900	CFI		2.03	1.74E-12
ENSDARG00000075891	sall1b		2.01	6.82E-40
ENSDARG00000069559	muc13a		2.01	3.60E-15
ENSDARG00000055186	ccr9a		2.01	1.42E-10
ENSDARG00000038634	CCK (1 of 2)		2.01	1.77E-15
ENSDARG00000077151	cbln2b		2.00	1.43E-19
ENSDARG00000095002	TNNC2 (2 of 2)		-2.02	3.08E-10
ENSDARG00000087318	zgc:174688		-2.02	1.24E-13
ENSDARG00000097032	si:ch211-256a21.4		-2.03	6.11E-20
ENSDARG00000090292	CABZ01071757.1		-2.03	2.19E-21
ENSDARG00000074772	ccl-c11b		-2.05	2.91E-18
ENSDARG00000002847	fndc1		-2.06	2.21E-16
ENSDARG00000043923	sox9b		-2.08	4.32E-59
ENSDARG00000088116	gstm3		-2.09	1.29E-41
ENSDARG00000036832	cyt1l		-2.09	2.83E-30
ENSDARG00000077216	wu:fc51h05		-2.10	5.96E-11
ENSDARG00000031952	mb		-2.11	1.05E-12

ENSDARG00000077505	rbp4	-2.11	6.65E-16
ENSDARG00000075038	CABZ01058371.1	-2.12	1.03E-25
ENSDARG00000023768	mfsd4a	-2.15	2.97E-24
ENSDARG00000077084	col28a1	-2.16	1.35E-10
ENSDARG00000030632	zgc:110191	-2.20	2.93E-22
ENSDARG00000060345	apod	-2.21	1.57E-12
ENSDARG00000039579	cfd	-2.21	1.08E-08
ENSDARG00000091792	akap12a	-2.24	1.28E-14
ENSDARG00000097513	si:ch211-84k18.3	-2.24	2.37E-08
ENSDARG00000003395	col4a3	-2.25	2.94E-71
ENSDARG00000028878	vipr1a	-2.26	1.31E-11
ENSDARG00000005943	htra4	-2.32	6.36E-23
ENSDARG00000062632	duox	-2.38	2.32E-10
ENSDARG00000035791	si:busm1-71b9.3	-2.38	7.13E-15
ENSDARG00000036830	KRT23 (1 of 2)	-2.45	7.04E-50
ENSDARG00000086805	ccdc129	-2.48	6.01E-19
ENSDARG00000062688	gpnmb	-2.49	2.73E-17
ENSDARG00000075865	CABZ01076351.1	-2.51	1.17E-11
ENSDARG00000097804	si:ch73-156o22.2	-2.52	1.94E-13
ENSDARG00000007490	adrb1	-2.55	7.16E-17
ENSDARG00000090268	si:dkeyp-113d7.4	-2.55	1.08E-28
ENSDARG00000096381	neu3.4	-2.56	1.16E-10
ENSDARG00000078962	DUOXA1	-2.58	1.13E-10
ENSDARG00000087375	zgc:66473	-2.63	1.52E-13
ENSDARG00000056938	kera	-2.68	1.10E-25
ENSDARG00000052279	osgn1	-2.71	3.24E-24
ENSDARG00000068910	nos1	-2.73	1.36E-12
ENSDARG00000070919	cpne5	-2.74	3.56E-17
ENSDARG00000096762	si:dkey-61p9.11	-2.84	1.04E-16
ENSDARG00000075600	si:dkeyp-41f9.3	-2.96	2.97E-25
ENSDARG00000056248	KRT78	-3.02	1.14E-14
ENSDARG00000052470	igfbp2a	-3.07	1.18E-155
ENSDARG00000055192	zgc:136930	-3.16	2.67E-17

Table C.3 72 hpf significantly differentially expressed transcripts following exposure to BkF (q ≤ 0.05, FC > 2)

ENSEMBLE ID	Symbol	log2FoldChange	padj
ENSDARG00000068934	cyp1b1	8.68	0
ENSDARG00000026039	cyp1a	8.52	6.24E-207
ENSDARG00000018298	cyp1c2	8.40	0
ENSDARG00000058980	cyp1c1	5.65	1.31E-157
ENSDARG00000059387	fgf7	5.61	4.66E-177
ENSDARG00000091116	pkhd1l1	4.82	3.94E-216
ENSDARG00000070925	EDN3 (1 of 2)	4.44	3.99E-46
ENSDARG00000055643	cyb5a	4.40	0
ENSDARG00000052618	ahrrb	4.34	5.26E-61
ENSDARG00000045371	prdm14	4.25	7.80E-57
ENSDARG00000097491	ugt1b1	4.19	1.61E-153
ENSDARG00000045548	lepb	4.16	1.96E-34
ENSDARG00000090530	LAMB3	4.14	2.53E-34
ENSDARG00000097716	si:dkey-86k10.8	3.94	5.98E-93
ENSDARG00000010376	SLC5A3 (1 of 2)	3.79	3.33E-33
ENSDARG00000076933	aldh1a3	3.73	2.30E-45
ENSDARG00000089507	ugt1b5	3.72	2.05E-99
ENSDARG00000056057	GREM2 (2 of 2)	3.68	2.70E-43
ENSDARG00000078617	CABZ01048958.1	3.61	5.77E-33
ENSDARG00000078749	b4galnt3a	3.58	1.85E-25
ENSDARG00000097080	si:ch73-181m17.1	3.51	6.62E-32
ENSDARG00000059369	si:ch1073-15f12.3	3.48	3.07E-55
ENSDARG00000035677	bmp8a	3.46	1.35E-43
ENSDARG00000005141	camkvb	3.43	1.69E-34
ENSDARG00000052895	htra3a	3.42	2.92E-29
ENSDARG00000020086	NUAK1 (1 of 2)	3.41	1.30E-85
ENSDARG00000007356	fgf20a	3.39	1.14E-51
ENSDARG00000037859	il11a	3.38	6.48E-31
ENSDARG00000055278	cfb	3.37	1.85E-25
ENSDARG00000097435	si:dkey-31i7.1	3.37	1.63E-20
ENSDARG00000035632		3.34	4.16E-19
ENSDARG00000074683	CABZ01048960.1	3.34	1.58E-33
ENSDARG00000074150	si:ch211-226h7.5	3.34	4.10E-19
ENSDARG00000052626	si:ch211-226h7.7	3.30	1.03E-21
ENSDARG00000079296	gcga	3.30	3.40E-24
ENSDARG00000094951	BX072532.5	3.26	6.69E-29
ENSDARG00000051876	ush1c	3.25	1.98E-50
ENSDARG00000095409	si:ch211-226h7.8	3.23	1.45E-23

ENSDARG00000069335	BCL6B		3.22	5.05E-90
ENSDARG00000039957	rspo1		3.16	2.64E-105
ENSDARG00000091380			3.15	2.71E-21
ENSDARG00000012395	mmp13a		3.12	2.02E-24
ENSDARG00000079191	CD200 (3 of 3)		3.08	9.15E-28
ENSDARG00000041382	si:dkey-283b15.2		3.08	2.35E-24
ENSDARG00000092719	si:ch211-226h7.4		3.08	3.34E-24
ENSDARG00000092170	apoc1l		3.02	1.26E-34
ENSDARG00000033684	oxgr1a.1		3.00	1.03E-15
ENSDARG00000035852			2.99	7.44E-23
ENSDARG00000079199	megf6a		2.99	1.21E-43
ENSDARG00000087020			2.98	1.29E-148
ENSDARG00000060471	gcnt3		2.98	1.56E-21
ENSDARG00000040623	fosl2		2.96	1.27E-38
ENSDARG00000026611	socs3b		2.93	4.78E-60
ENSDARG00000089706	BX005410.2		2.93	7.14E-32
ENSDARG00000068580	glis1a		2.90	4.65E-20
ENSDARG00000075829	kiss1		2.89	1.90E-14
ENSDARG00000070929	sox14		2.87	1.66E-41
ENSDARG00000088283	si:ch73-248e21.5		2.82	3.48E-26
ENSDARG00000016750	abcc6a		2.80	2.05E-104
ENSDARG00000053493	aldh1a2		2.79	3.07E-30
ENSDARG00000052329	CD200 (2 of 3)		2.78	1.31E-21
ENSDARG00000097991	si:dkey-86k10.14		2.78	2.70E-16
ENSDARG00000054324	rerglb		2.78	3.08E-73
ENSDARG00000055638	ankrd33aa		2.76	5.63E-21
ENSDARG00000097726	si:ch211-149e23.4		2.72	1.15E-27
ENSDARG00000087832	bcl3		2.69	4.92E-27
ENSDARG00000022570	BX248318.1		2.68	8.53E-13
ENSDARG00000078847	si:dkey-238o13.4		2.66	5.29E-15
ENSDARG00000015273	alpi.1		2.63	1.94E-53
ENSDARG00000091085	lepa		2.63	1.27E-11
ENSDARG00000061419	zmat4b		2.62	1.91E-26
ENSDARG00000093101	BX005305.7		2.59	1.62E-14
ENSDARG00000055081	si:dkey-285b23.3		2.59	5.60E-13
ENSDARG00000003303	stc1		2.57	9.40E-12
ENSDARG00000006220	ugt1a7		2.57	3.15E-39
ENSDARG00000059891			2.55	3.48E-14
ENSDARG00000006526	fn1b		2.55	8.81E-26
ENSDARG00000094158	si:dkey-285b23.4		2.55	1.15E-11
ENSDARG00000056654	gna15.2		2.54	2.22E-24

ENSDARG00000077580	tspeara		2.53	4.44E-21
ENSDARG00000086826	sult6b1		2.49	4.37E-276
ENSDARG00000092521	CR382283.2		2.49	4.01E-25
ENSDARG00000087359	c3b		2.47	1.71E-12
ENSDARG00000094815	si:ch73-49p17.1		2.45	1.16E-20
ENSDARG00000079221	si:ch211-162k9.6		2.44	1.00E-11
ENSDARG00000061841	tiparp		2.42	2.57E-54
ENSDARG00000092250	BX072532.2		2.42	1.14E-09
ENSDARG00000074642	BX072532.1		2.42	6.88E-16
ENSDARG00000095022	thsd7ba		2.41	6.73E-11
ENSDARG00000074363	TTC9		2.41	8.01E-30
ENSDARG00000022303	hig1		2.40	1.88E-48
ENSDARG00000056324	zgc:123295		2.40	1.43E-54
ENSDARG00000079765	AL929022.2		2.40	1.88E-28
ENSDARG00000088371	junbb		2.38	1.20E-18
ENSDARG00000030896	foxq1a		2.38	1.71E-18
ENSDARG00000008305	hand2		2.37	1.60E-10
ENSDARG00000055186	ccr9a		2.36	4.37E-15
ENSDARG00000071560	dlx4b		2.35	1.37E-41
ENSDARG00000073912	si:ch211-202h22.7		2.35	6.88E-38
ENSDARG00000035768	pltp		2.32	1.66E-95
ENSDARG00000014277	vox		2.32	3.89E-20
ENSDARG00000056077	dcst1		2.31	3.44E-10
ENSDARG00000014031	abcc2		2.31	1.28E-22
ENSDARG00000093365	si:ch211-226h7.3		2.30	2.34E-15
ENSDARG00000076797			2.30	9.93E-10
ENSDARG00000034559	srpx2		2.29	1.70E-22
ENSDARG00000036900	CFI		2.27	3.27E-15
ENSDARG00000060434	MAP1B		2.24	1.85E-17
ENSDARG00000057040	tmprss13a		2.24	1.43E-33
ENSDARG00000042816	mmp9		2.23	1.50E-18
ENSDARG00000092704	BX072532.3		2.23	6.82E-15
ENSDARG00000075487	si:ch211-267e7.3		2.22	1.96E-23
ENSDARG00000073970	mctp2b		2.22	2.99E-27
ENSDARG00000089697	nfe2l2b		2.22	5.13E-48
ENSDARG00000077938	cd248b		2.22	3.05E-39
ENSDARG00000040314	psph		2.21	4.12E-31
ENSDARG00000008249	ptchd4		2.21	2.94E-10
ENSDARG00000070683	dkk3b		2.20	4.22E-55
ENSDARG00000007950	itga11b		2.19	2.40E-16
ENSDARG00000074656	ctssb.1		2.18	3.91E-29

ENSDARG00000001452	adam8a		2.18	1.73E-35
ENSDARG00000086028	IGFN1 (3 of 4)		2.16	5.45E-11
ENSDARG00000056795	serpine1		2.16	2.40E-25
ENSDARG00000097539	si:ch211-39f2.3		2.15	1.70E-10
ENSDARG00000076196	si:ch211-226h7.6		2.15	5.35E-11
ENSDARG00000042470	s1pr3a		2.13	1.93E-58
ENSDARG00000016718	mmp11b		2.13	2.09E-58
ENSDARG00000017489	zgc:123068		2.13	1.20E-23
ENSDARG00000093381	tgm2l		2.13	4.65E-17
ENSDARG00000092778	BX072532.4		2.12	5.43E-08
ENSDARG00000079570	rspo2		2.11	3.96E-23
ENSDARG00000017860	rgs5b		2.09	2.39E-19
ENSDARG00000003902	ctsl.1		2.09	1.73E-08
ENSDARG00000090444	ponzr1		2.08	6.88E-25
ENSDARG00000070491	hpcal4		2.08	1.38E-16
ENSDARG00000074677	frem3		2.08	2.53E-14
ENSDARG00000045316	map7d2b		2.08	9.69E-11
ENSDARG00000055705	f5		2.08	1.72E-07
ENSDARG00000075891	sall1b		2.07	7.40E-45
ENSDARG00000094648			2.06	4.59E-16
ENSDARG00000069559	muc13a		2.06	2.58E-16
ENSDARG00000077151	cbln2b		2.04	1.86E-21
ENSDARG00000070710	si:dkeyp-41g9.6		2.04	3.15E-09
ENSDARG00000086391	cald1		2.04	2.36E-41
ENSDARG00000055226	slc7a7		2.03	9.15E-27
ENSDARG00000033567	fkbp1ab		2.00	1.85E-14
ENSDARG00000026766	bcl2l10		2.00	4.91E-28
ENSDARG00000068180	bmp16		2.00	1.71E-13
ENSDARG00000044827	wnt7aa		-2.00	9.18E-42
ENSDARG00000021720	col7a1		-2.01	1.02E-33
ENSDARG00000092064	si:dkey-117n7.4		-2.02	1.23E-46
ENSDARG00000017624	krt4		-2.03	1.49E-39
ENSDARG00000018351	hpda		-2.03	2.14E-09
ENSDARG00000074772	ccl-c11b		-2.03	3.89E-18
ENSDARG00000075038	CABZ01058371.1		-2.04	8.40E-25
ENSDARG00000032246	tmtopsb		-2.04	3.76E-11
ENSDARG00000087289	zgc:66473		-2.06	2.40E-12
ENSDARG00000077084	col28a1		-2.06	6.93E-10
ENSDARG00000090468	ppp1r3aa		-2.07	5.34E-11
ENSDARG00000068812	tlr7		-2.08	9.87E-14
ENSDARG00000018382	prkcha		-2.09	1.24E-11

ENSDARG00000016695	p2rx1	-2.09	1.52E-43
ENSDARG00000034808	kcnip1b	-2.09	3.61E-17
ENSDARG00000002831	col4a4	-2.10	1.16E-51
ENSDARG00000088116	gstm3	-2.11	1.17E-42
ENSDARG00000092450	si:dkey-173l11.3	-2.12	1.31E-07
ENSDARG00000075865	CABZ01076351.1	-2.12	9.15E-09
ENSDARG00000004396	b3gnt5b	-2.14	6.10E-11
ENSDARG00000055926	foxi3a	-2.14	1.47E-07
ENSDARG00000074988	si:ch211-209n20.1	-2.15	1.05E-11
ENSDARG00000009550	foxi3b	-2.18	1.60E-08
ENSDARG00000052905	zgc:165423	-2.18	3.10E-08
ENSDARG00000028878	vipr1a	-2.19	1.20E-11
ENSDARG00000005943	htra4	-2.22	1.09E-21
ENSDARG00000090292	CABZ01071757.1	-2.23	2.95E-27
ENSDARG00000097032	si:ch211-256a21.4	-2.25	4.22E-24
ENSDARG00000095002	TNNC2 (2 of 2)	-2.28	1.37E-13
ENSDARG00000031952	mb	-2.29	1.72E-15
ENSDARG00000007912	si:ch211-196i2.2	-2.30	4.95E-17
ENSDARG00000043923	sox9b	-2.35	6.36E-75
ENSDARG00000037861	slc2a3b	-2.37	1.90E-22
ENSDARG00000062632	duox	-2.39	1.35E-10
ENSDARG00000078962	DUOXA1	-2.40	1.78E-09
ENSDARG00000074403	PEX5L (2 of 2)	-2.41	7.86E-20
ENSDARG00000030632	zgc:110191	-2.43	2.74E-27
ENSDARG00000077505	rbp4	-2.45	2.38E-21
ENSDARG00000014939	KCNN2	-2.46	4.14E-10
ENSDARG00000097513	si:ch211-84k18.3	-2.48	2.81E-10
ENSDARG00000068910	nos1	-2.51	8.44E-11
ENSDARG00000056938	kera	-2.54	2.06E-23
ENSDARG00000052279	osgn1	-2.58	5.49E-22
ENSDARG00000036832	cyt1l	-2.59	1.23E-46
ENSDARG00000007490	adrb1	-2.60	5.64E-16
ENSDARG00000014091	osr1	-2.62	1.52E-11
ENSDARG00000096762	si:dkey-61p9.11	-2.64	3.96E-15
ENSDARG00000087375	zgc:66473	-2.65	2.64E-14
ENSDARG00000096242	si:ch211-76l23.4	-2.65	1.86E-64
ENSDARG00000090268	si:dkeyp-113d7.4	-2.66	2.84E-31
ENSDARG00000003395	col4a3	-2.68	5.62E-99
ENSDARG00000023768	mfsd4a	-2.75	1.24E-34
ENSDARG00000023151	ucp1	-2.76	6.28E-12
ENSDARG00000036830	KRT23 (1 of 2)	-2.81	5.34E-66

ENSDARG00000070919	cpne5		-2.83	1.00E-18
ENSDARG00000035791	si:busm1-71b9.3		-2.85	2.01E-21
ENSDARG00000086805	ccdc129		-2.90	2.55E-26
ENSDARG00000094990	si:dkey-91f15.1		-2.91	4.54E-17
ENSDARG00000052470	igfbp2a		-3.08	2.90E-156
ENSDARG00000056248	KRT78		-3.25	4.57E-17
ENSDARG00000075600	si:dkeyp-41f9.3		-3.29	1.07E-31
ENSDARG00000039579	cfd		-3.30	5.86E-19
ENSDARG00000055192	zgc:136930		-3.42	1.99E-20

Table C.4 96 hpf significantly differentially expressed transcripts following exposure to BkF (q ≤ 0.05, FC > 2)

ENSEMBL ID	Symbol	log2FoldChange	padj
ENSDARG00000018298	cyp1c2	9.03	0
ENSDARG00000026039	cyp1a	8.49	2.16E-205
ENSDARG00000068934	cyp1b1	8.27	0
ENSDARG00000059387	fgf7	5.78	2.18E-191
ENSDARG00000058980	cyp1c1	5.44	1.74E-146
ENSDARG00000052618	ahrrb	4.84	1.28E-70
ENSDARG00000091116	pkhd1l1	4.83	1.31E-216
ENSDARG00000045548	lepb	4.78	3.95E-49
ENSDARG00000097491	ugt1b1	4.42	1.12E-169
ENSDARG00000070925	EDN3 (1 of 2)	4.42	1.40E-45
ENSDARG00000056057	GREM2 (2 of 2)	4.24	3.54E-56
ENSDARG00000079296	gcga	4.13	1.32E-39
ENSDARG00000089507	ugt1b5	4.09	1.73E-116
ENSDARG00000055643	cyb5a	4.03	0
ENSDARG00000010376	SLC5A3 (1 of 2)	4.01	4.03E-38
ENSDARG00000087017	PTGR1 (2 of 2)	3.90	2.92E-25
ENSDARG00000055186	ccr9a	3.88	2.92E-38
ENSDARG00000097716	si:dkey-86k10.8	3.76	1.25E-84
ENSDARG00000005141	camkvb	3.75	1.35E-38
ENSDARG00000012395	mmp13a	3.71	1.56E-34
ENSDARG00000059369	si:ch1073-15f12.3	3.71	2.79E-63
ENSDARG00000055638	ankrd33aa	3.65	2.12E-32
ENSDARG00000039957	rspo1	3.64	2.15E-139
ENSDARG00000074150	si:ch211-226h7.5	3.58	4.62E-22
ENSDARG00000097435	si:dkey-31i7.1	3.56	7.46E-23
ENSDARG00000094951	BX072532.5	3.56	2.67E-34
ENSDARG00000089706	BX005410.2	3.50	7.77E-46
ENSDARG00000045371	prdm14	3.49	2.68E-40
ENSDARG00000090530	LAMB3	3.47	6.65E-27
ENSDARG00000033684	oxgr1a.1	3.43	8.37E-21
ENSDARG00000068580	glis1a	3.38	3.64E-26
ENSDARG00000041382	si:dkey-283b15.2	3.38	4.09E-30
ENSDARG00000060471	gcnt3	3.37	2.18E-27
ENSDARG00000052626	si:ch211-226h7.7	3.37	1.20E-22
ENSDARG00000007356	fgf20a	3.36	1.01E-48
ENSDARG00000059891		3.34	2.48E-24
ENSDARG00000007950	itga11b	3.31	4.21E-37
ENSDARG00000078847	si:dkey-238o13.4	3.28	2.33E-22

ENSDARG00000074683	CABZ01048960.1	3.27	2.97E-32
ENSDARG00000053493	aldh1a2	3.27	2.10E-41
ENSDARG00000097726	si:ch211-149e23.4	3.21	1.53E-43
ENSDARG00000092719	si:ch211-226h7.4	3.20	6.77E-26
ENSDARG00000070683	dkk3b	3.20	1.33E-118
ENSDARG00000078617	CABZ01048958.1	3.16	6.24E-26
ENSDARG00000095409	si:ch211-226h7.8	3.13	1.32E-22
ENSDARG00000094815	si:ch73-49p17.1	3.10	1.04E-31
ENSDARG00000087020		3.10	2.10E-159
ENSDARG00000078622	scpp5	3.06	1.65E-18
ENSDARG00000061419	zmat4b	3.03	4.45E-33
ENSDARG00000052895	htra3a	2.98	2.17E-24
ENSDARG00000069335	BCL6B	2.98	3.40E-78
ENSDARG00000078749	b4galnt3a	2.97	1.43E-17
ENSDARG00000092521	CR382283.2	2.96	1.86E-35
ENSDARG00000097991	si:dkey-86k10.14	2.95	8.37E-18
ENSDARG00000073912	si:ch211-202h22.7	2.95	3.96E-61
ENSDARG00000056795	serpine1	2.92	1.03E-46
ENSDARG00000056654	gna15.2	2.91	3.27E-32
ENSDARG00000016750	abcc6a	2.91	4.21E-113
ENSDARG00000088283	si:ch73-248e21.5	2.90	3.78E-27
ENSDARG00000008249	ptchd4	2.90	3.15E-17
ENSDARG00000077151	cbln2b	2.90	2.16E-41
ENSDARG00000097080	si:ch73-181m17.1	2.88	7.10E-22
ENSDARG00000030896	foxq1a	2.84	5.35E-26
ENSDARG00000070622	CABZ01064972.1	2.81	3.57E-22
ENSDARG00000015273	alpi.1	2.81	3.33E-61
ENSDARG00000055081	si:dkey-285b23.3	2.79	6.85E-15
ENSDARG00000092170	apoc1l	2.77	7.62E-30
ENSDARG00000088371	junbb	2.76	5.28E-25
ENSDARG00000097527	si:ch73-56d11.3	2.75	1.59E-22
ENSDARG00000022303	hig1	2.74	4.15E-64
ENSDARG00000003902	ctsl.1	2.74	2.51E-14
ENSDARG00000075891	sall1b	2.69	2.65E-74
ENSDARG00000055226	slc7a7	2.69	2.03E-47
ENSDARG00000078280	nkx3-1	2.66	4.25E-34
ENSDARG00000006220	ugt1a7	2.64	2.39E-42
ENSDARG00000076933	aldh1a3	2.61	5.88E-22
ENSDARG00000042470	s1pr3a	2.59	6.92E-83
ENSDARG00000076797		2.59	1.08E-12
ENSDARG00000020086	NUAK1 (1 of 2)	2.58	1.87E-49

ENSDARG00000093546	ms4a17a.2		2.57	1.62E-20
ENSDARG00000061841	tiparp		2.55	2.73E-60
ENSDARG00000068126	NPPC (1 of 2)		2.55	2.73E-15
ENSDARG00000079199	megf6a		2.55	6.22E-32
ENSDARG00000025921	runx1		2.54	4.47E-11
ENSDARG00000016713	dhrs13l1		2.53	1.70E-49
ENSDARG00000035677	bmp8a		2.52	5.20E-22
ENSDARG00000026611	socs3b		2.49	7.66E-44
ENSDARG00000091380			2.49	2.93E-14
ENSDARG00000091085	lepa		2.47	1.71E-10
ENSDARG00000008305	hand2		2.43	2.09E-11
ENSDARG00000040623	fosl2		2.43	2.46E-26
ENSDARG00000025428	socs3a		2.43	1.63E-19
ENSDARG00000074656	ctssb.1		2.43	6.34E-38
ENSDARG00000057029	htr2a		2.42	8.73E-10
ENSDARG00000093101	BX005305.7		2.42	7.58E-13
ENSDARG00000003303	stc1		2.42	3.52E-10
ENSDARG00000079221	si:ch211-162k9.6		2.41	1.67E-11
ENSDARG00000010276	ptgs2b		2.41	7.76E-21
ENSDARG00000029482	ush2a		2.40	5.66E-14
ENSDARG00000074971	CU638740.1		2.39	3.15E-21
ENSDARG00000096156			2.37	3.36E-09
ENSDARG00000017860	rgs5b		2.36	3.12E-24
ENSDARG00000075985	FP243385.1		2.36	6.44E-10
ENSDARG00000038634	CCK (1 of 2)		2.36	1.28E-21
ENSDARG00000070401	MAL (3 of 3)		2.35	5.89E-32
ENSDARG00000086826	sult6b1		2.35	9.61E-244
ENSDARG00000035632			2.34	1.99E-09
ENSDARG00000054324	rerglb		2.32	7.69E-51
ENSDARG00000095022	thsd7ba		2.31	2.31E-10
ENSDARG00000096047			2.31	4.79E-09
ENSDARG00000088285	CABZ01079296.1		2.30	5.04E-36
ENSDARG00000036912	edn1		2.30	1.74E-18
ENSDARG00000056324	zgc:123295		2.30	6.77E-55
ENSDARG00000070586	ctgfb		2.29	6.36E-20
ENSDARG00000042983	has1		2.29	4.57E-09
ENSDARG00000070389	foxf2b		2.29	1.04E-22
ENSDARG00000092704	BX072532.3		2.29	1.08E-15
ENSDARG00000040314	psph		2.28	3.23E-33
ENSDARG00000036900	CFI		2.28	1.57E-15
ENSDARG00000073970	mctp2b		2.28	1.04E-28

ENSDARG00000069559	muc13a		2.28	6.92E-20
ENSDARG00000070929	sox14		2.27	1.65E-27
ENSDARG00000015797	mmp13b		2.26	2.03E-47
ENSDARG00000089131	il17rel		2.25	3.65E-09
ENSDARG00000035942	hrh3		2.25	2.88E-11
ENSDARG00000020031	cldn11a		2.24	4.39E-10
ENSDARG00000037859	il11a		2.24	6.44E-15
ENSDARG00000015626	pglyrp6		2.22	1.32E-08
ENSDARG00000074363	TTC9		2.22	3.17E-28
ENSDARG00000051876	ush1c		2.22	2.44E-25
ENSDARG00000068141	tnfsf11		2.22	1.51E-17
ENSDARG00000074642	BX072532.1		2.21	1.50E-13
ENSDARG00000077938	cd248b		2.21	3.48E-39
ENSDARG00000095475	si:ch211-196j1.2		2.21	1.85E-17
ENSDARG00000086391	cald1		2.20	1.72E-48
ENSDARG00000022570	BX248318.1		2.17	1.65E-08
ENSDARG00000094158	si:dkey-285b23.4		2.17	1.06E-08
ENSDARG00000075265	plaua		2.16	8.77E-08
ENSDARG00000074378	junba		2.14	1.52E-09
ENSDARG00000070710	si:dkeyp-41g9.6		2.13	1.63E-10
ENSDARG00000020544	rem1		2.11	1.63E-29
ENSDARG00000042816	mmp9		2.11	8.90E-17
ENSDARG00000087646	RUNX1 (2 of 2)		2.11	8.13E-08
ENSDARG00000093365	si:ch211-226h7.3		2.11	4.79E-13
ENSDARG00000015399	foxf1		2.10	3.57E-49
ENSDARG00000088261	CABZ01052953.2		2.10	2.94E-08
ENSDARG00000076794	STAG3		2.10	2.24E-19
ENSDARG00000088693	dcst2		2.08	1.04E-08
ENSDARG00000068460	OTOG		2.08	5.02E-17
ENSDARG00000016718	mmp11b		2.07	3.47E-55
ENSDARG00000057678	sfrp1b		2.06	3.16E-20
ENSDARG00000055669	NCAM2 (2 of 2)		2.05	3.19E-07
ENSDARG00000076050	TMEM255B		2.04	2.41E-21
ENSDARG00000087832	bcl3		2.04	5.11E-17
ENSDARG00000088988	CABZ01079804.1		2.03	5.77E-07
ENSDARG00000039269	arg2		2.03	2.04E-10
ENSDARG00000070792	lrrc15		2.03	3.46E-16
ENSDARG00000055751	fosb		2.02	6.34E-14
ENSDARG00000068180	bmp16		2.02	2.84E-12
ENSDARG00000019861	fgl2		2.01	6.75E-13
ENSDARG00000077882	wisp2		2.01	1.17E-08

ENSDARG00000086102	NOX4 (1 of 2)	2.01	1.30E-31
ENSDARG00000035891	acana	-2.00	1.88E-12
ENSDARG00000055527	cmn	-2.00	7.16E-20
ENSDARG00000043198	si:rp71-1i20.2	-2.01	1.37E-15
ENSDARG00000040118	zgc:113232	-2.01	1.28E-10
ENSDARG00000011879	foxn1	-2.03	5.60E-14
ENSDARG00000075865	CABZ01076351.1	-2.05	3.11E-08
ENSDARG00000023151	ucp1	-2.05	5.19E-07
ENSDARG00000034808	kcnip1b	-2.05	5.48E-16
ENSDARG00000093135	si:dkey-117n7.2	-2.07	3.78E-35
ENSDARG00000028878	vipr1a	-2.07	3.05E-10
ENSDARG00000062487	si:dkey-6n6.1	-2.07	5.03E-27
ENSDARG00000086669	edn3b	-2.08	4.18E-09
ENSDARG00000044290	rph3al	-2.08	6.49E-19
ENSDARG00000022689	itgb1b.2	-2.09	5.23E-45
ENSDARG00000020758	tmem178	-2.09	8.99E-16
ENSDARG00000021720	col7a1	-2.09	2.71E-36
ENSDARG00000076332		-2.10	4.84E-29
ENSDARG00000006456	pdgfrl	-2.10	2.07E-23
ENSDARG00000078250	zgc:194398	-2.10	9.22E-49
ENSDARG00000095002	TNNC2 (2 of 2)	-2.10	3.54E-11
ENSDARG00000078518	kazald2	-2.10	4.89E-18
ENSDARG00000042899	si:ch211-163l21.8	-2.10	7.48E-10
ENSDARG00000014321	eng1a	-2.11	3.42E-16
ENSDARG00000090419	CABZ01078499.2	-2.12	8.11E-08
ENSDARG00000018351	hpda	-2.13	2.17E-10
ENSDARG00000068947	si:ch211-264e16.1	-2.13	1.41E-07
ENSDARG00000015073	eng1b	-2.14	4.17E-24
ENSDARG00000075026	mkxb	-2.14	3.67E-11
ENSDARG00000052279	osgn1	-2.17	8.16E-16
ENSDARG00000070873	ccl25b	-2.17	2.30E-21
ENSDARG00000034070	cyp2aa3	-2.17	7.83E-10
ENSDARG00000037861	slc2a3b	-2.19	5.22E-20
ENSDARG00000087289	zgc:66473	-2.19	2.31E-13
ENSDARG00000087641	si:ch73-96b22.1	-2.19	2.69E-20
ENSDARG00000037598	prf1.5	-2.20	5.55E-27
ENSDARG00000090598	pkp1a	-2.20	8.85E-34
ENSDARG00000088411	notum2	-2.21	8.09E-66
ENSDARG00000035562	mpdu1a	-2.22	9.70E-54
ENSDARG00000002847	fndc1	-2.26	9.28E-20
ENSDARG00000078299	COLGALT2 (2 of 2)	-2.29	6.03E-14

ENSDARG00000005716	olfml2ba	-2.30	1.04E-44
ENSDARG00000091378	CABZ01068473.1	-2.32	1.85E-22
ENSDARG00000003395	col4a3	-2.32	8.55E-75
ENSDARG00000094973	wnt16	-2.34	8.03E-11
ENSDARG00000092947	cyt1	-2.35	1.18E-119
ENSDARG00000096381	neu3.4	-2.36	2.88E-09
ENSDARG00000038232	zgc:112964	-2.36	3.22E-11
ENSDARG00000002722	ankrd2	-2.38	5.16E-11
ENSDARG00000070331	muc5ac	-2.40	1.14E-16
ENSDARG00000045139	ca7	-2.41	8.80E-11
ENSDARG00000006901	AEBP1 (1 of 2)	-2.41	2.26E-19
ENSDARG00000069983	scinla	-2.44	2.29E-18
ENSDARG00000043923	sox9b	-2.52	2.88E-84
ENSDARG00000016695	p2rx1	-2.52	3.54E-56
ENSDARG00000007490	adrb1	-2.52	6.68E-14
ENSDARG00000091639	scinla	-2.58	4.33E-17
ENSDARG00000068812	tlr7	-2.59	2.74E-20
ENSDARG00000023768	mfsd4a	-2.60	1.74E-28
ENSDARG00000003181	sult1st4	-2.63	3.30E-13
ENSDARG00000076830	si:dkey-65b12.6	-2.63	6.01E-13
ENSDARG00000070919	cpne5	-2.63	8.38E-17
ENSDARG00000092567	si:dkey-61l1.4	-2.65	9.97E-31
ENSDARG00000077505	rbp4	-2.66	3.29E-25
ENSDARG00000078962	DUOXA1	-2.66	1.55E-11
ENSDARG00000074772	ccl-c11b	-2.67	2.19E-26
ENSDARG00000037278	lrata	-2.67	6.20E-20
ENSDARG00000094990	si:dkey-91f15.1	-2.68	1.02E-14
ENSDARG00000017624	krt4	-2.69	3.65E-69
ENSDARG00000036834	zgc:109868	-2.77	1.48E-38
ENSDARG00000056938	kera	-2.77	1.01E-27
ENSDARG00000075600	si:dkeyp-41f9.3	-2.78	1.15E-22
ENSDARG00000086805	ccdc129	-2.85	3.63E-25
ENSDARG00000026403	HEPHL1 (1 of 3)	-2.93	1.05E-25
ENSDARG00000077216	wu:fc51h05	-3.02	3.43E-21
ENSDARG00000087375	zgc:66473	-3.04	3.06E-18
ENSDARG00000035791	si:busm1-71b9.3	-3.05	3.51E-24
ENSDARG00000096762	si:dkey-61p9.11	-3.11	3.79E-20
ENSDARG00000062632	duox	-3.14	6.57E-18
ENSDARG00000069478	slc13a3	-3.15	3.30E-46
ENSDARG00000036830	KRT23 (1 of 2)	-3.15	4.04E-83
ENSDARG00000090268	si:dkeyp-113d7.4	-3.23	3.60E-46

|			
ENSDARG00000056248	KRT78	-3.26	2.58E-17
ENSDARG00000068910	nos1	-3.40	2.28E-19
ENSDARG00000052470	igfbp2a	-3.45	9.17E-172
ENSDARG00000055192	zgc:136930	-3.53	9.83E-22
ENSDARG00000036832	cyt1l	-3.61	1.65E-90
ENSDARG00000039579	cfd	-3.62	9.22E-23
ENSDARG00000096242	si:ch211-76l23.4	-3.90	4.92E-119
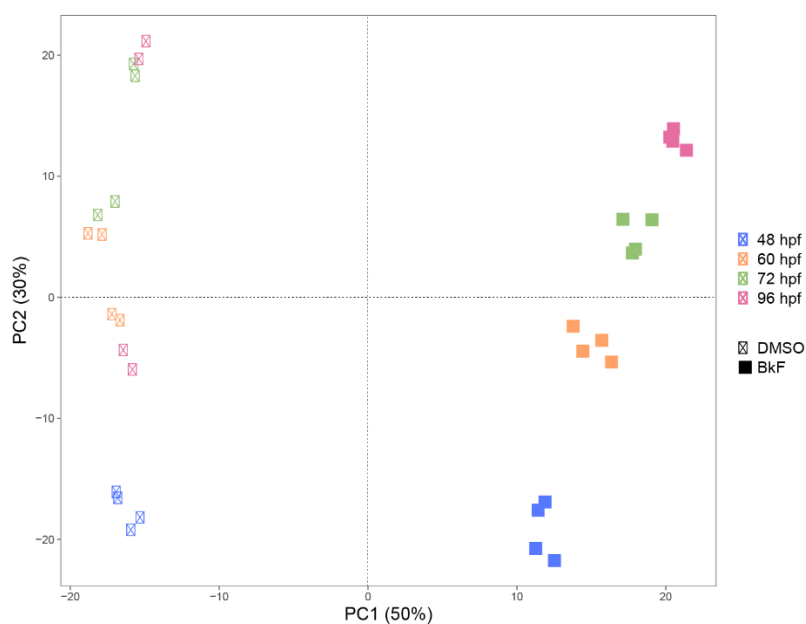
Figure C.1 Principal components analysis (PCA) of the 500 genes with the greatest differential expression in larvae exposed to 12 μM. benzo[k]fluoranthene (BkF). BkF vs vehicle (1% DMSO) is indicated by filed vs. non-filled squares. Age condition is indicated by color: blue = 48 hpf; orange = 60 hpf; green = 72 hpf; red = 96 hpf.